

**Biomarker discovery for psychiatric disorders:
Insights from quantitative proteomics studies
in animal models**

Dissertation
der Fakultät für Biologie
der Ludwig-Maximilians-Universität München

vorgelegt von
Michaela Filiou

München, Juli 2010

Λέω τις ζωές που δόθηκαν στο φως..

**Που διάβηκαν αμφίβολα, θαμπά
σαν άστρα κάποιας ώρας αυγινής..**

Κώστας Καρυωτάκης

Ο Πόνος του Ανθρώπου και των Πραμάτων

To my beloved parents

Erstgutachter: Prof. Dr. Rainer Landgraf

Zweitgutachter: Prof. Dr. George Boyan

Tag der mündlichen Prüfung: 15 Dezember 2010



Abstract

Although psychiatric disorders are among the leading causes of disability in modern societies, no molecular biomarkers exist for their accurate diagnosis, classification and treatment efficacy assessment. Proteomics technologies provide useful tools for identifying protein markers related to disease pathophysiology. To unravel the neurobiological underpinnings and identify candidate biomarkers for anxiety disorders, we interrogated the mouse model of high (HAB), normal (NAB) and low (LAB) anxiety-related behavior by a combined quantitative proteomics and metabolomics approach. The cingulate cortex synaptosome proteomes of HAB and LAB mice were compared by *in vivo* ^{15}N metabolic labeling and quantitative proteomics. In addition, the cingulate cortex metabolomes of HAB/NAB/LAB mice were quantified, and altered protein and metabolite networks were identified by *in silico* pathway analysis. Differential expression of sideroflexin-5 (Sfxn5), carbonic anhydrase 2 (Car2), myosin, heavy polypeptide 10 (Myh10) and succinate dehydrogenase, subunit b (Sdhb) in HAB and LAB mice was validated by Western blot in an independent HAB/NAB/LAB population, providing a set of candidate biomarkers for anxiety-related behavior. Proteomics, metabolomics and *in silico* analyses revealed pronounced mitochondrial pathway alterations, suggesting previously not highlighted roles of the organelle in modulating anxiety-related behavior by affecting energy metabolism, oxidative stress and neurotransmission processes.

To allow an accurate characterization of the HAB/NAB/LAB mouse model, proteomics tools were established and optimized. Mouse synaptosome proteome profiling was carried out to create a reference map for quantitative proteomics experiments. Furthermore, the quantitative proteomics platform based on metabolic labeling of the HAB/NAB/LAB mouse model with the ^{15}N heavy isotope was established, and the ^{15}N isotope effect on the proteome during metabolic labeling was investigated.

To elucidate the role of the G72 protein in schizophrenia, the G72/G30 transgenic mouse model of schizophrenia-like symptoms was studied with traditional, gel-based proteomics approaches. The cerebellar proteomes of G72/G30 transgenic mice were compared with wild type (WT)



controls, revealing differential expression of proteins involved in mitochondrial function and oxidative stress.

Taken together, quantitative proteomics approaches were applied to identify disease-specific differences in animal models of psychiatric disorders. Our data provide the basis for the establishment of a biomarker panel for anxiety disorders and schizophrenia and offer insights toward a systemic understanding of mental disease and discovery of novel therapeutic targets.



Table of contents

Abstract	i
Table of contents	iii
Abbreviations	viii
Protein names	x
1 Introduction	1
1.1 Psychiatric disorders	1
1.1.1 Anxiety and depression	1
1.1.2 Schizophrenia	2
1.2 Biomarkers for psychiatric disorders	3
1.2.1 What is a biomarker?	3
1.2.2 The quest for biomarkers in psychiatric research	3
1.3 Mouse models for psychiatric disorders	4
1.3.1 Advantages of mouse models in psychiatric research	4
1.3.2 The HAB/NAB/LAB mouse model of trait anxiety	4
1.3.2.1 Bidirectional selective breeding	4
1.3.2.2 Behavioral and molecular characteristics	5
1.3.3 The G72/G30 transgenic mouse model of schizophrenia-like symptoms	6
1.4 Biomarker discovery platforms	7
1.4.1 Quantitative proteomics	7
1.4.1.1 Advantages of studying the proteome	7
1.4.1.2 Mass spectrometry	7
1.4.1.3 Mass spectrometry instrumentation	9
1.4.1.4 Mass spectrometry-based proteomics	10
1.4.1.5 Quantitative proteomics methodologies	10
1.4.2 Quantitative metabolomics	12
1.5 Biomarker discovery in the HAB/NAB/LAB mouse model of trait anxiety	13
2 Aim of the thesis	15



3	Material and methods	16
3.1	Animals, equipment and standard procedures	16
3.2	Profiling of mouse synaptosome proteome and phosphoproteome	17
3.2.1	Synaptosome enrichment from CD1 mouse whole brain	17
3.2.2	Western blot analysis of selected synaptosomal proteins	17
3.2.3	Isoelectric focusing-proteomics sample preparation	18
3.2.4	LC-ESI-MS/MS	19
3.2.5	Proteomics data analysis	19
3.3	¹⁵N metabolic labeling of the HAB/NAB/LAB mouse model of trait anxiety	20
3.3.1	¹⁵ N metabolic labeling breeding and feeding scheme	20
3.3.2	Behavioral testing	22
3.3.2.1	Ultrasonic vocalization test	22
3.3.2.2	Elevated plus-maze test	22
3.3.2.3	Tail suspension test	23
3.3.3	Tissue acquisition	24
3.3.4	¹⁵ N metabolic labeling efficiency estimation	24
3.3.4.1	Proteomics sample preparation	24
3.3.4.2	MALDI-TOF/TOF MS-relative quantification	25
3.4	Biomarker and pathway discovery in the HAB/NAB/LAB mouse model of trait anxiety	25
3.4.1	Animals	25
3.4.2	Synaptosome enrichment from HAB/NAB/LAB cingulate cortices	26
3.4.3	Proteomics sample preparation from HAB/NAB/LAB synaptosomes	26
3.4.4	Mass spectrometry-relative quantification-data analysis	26
3.4.5	HAB/NAB/LAB cingulate cortex metabolome comparison	27
3.4.6	Western blot validation of selected differentially expressed proteins	28
3.4.7	<i>In silico</i> pathway analysis	28
3.5	¹⁵N isotope effect investigation in HAB mice and <i>Escherichia coli</i>	29
3.5.1	Animals	29



3.5.2	<i>Escherichia coli</i> culture	29
3.5.3	<i>Escherichia coli</i> proteomics sample preparation-mass spectrometry	30
3.5.4	<i>Escherichia coli</i> proteomics data analysis	30
3.5.5	Western blot validation of selected differentially expressed proteins	31
3.5.6	Pyruvate assay of $^{14}\text{N}/^{15}\text{N}$ <i>Escherichia coli</i> cytoplasm	31
3.5.7	<i>In silico</i> pathway analysis	31
3.6	Biomarker discovery in the G72/G30 transgenic mouse model of schizophrenia-like symptoms	32
3.6.1	Animals	32
3.6.2	Sample preparation from G72/G30 transgenic and wild type cerebella	32
3.6.3	Two-dimensional Western blot	32
3.6.4	Two-dimensional polyacrylamide gel electrophoresis	33
3.6.5	Identification of differentially expressed proteins	33
4	Profiling of mouse synaptosome proteome and phosphoproteome	34
4.1	Introduction	34
4.2	Results	35
4.2.1	Western blot analysis of selected synaptosomal proteins	35
4.2.2	Synaptosome proteome	37
4.2.3	Synaptosome phosphoproteome	39
4.3	Discussion	42
5	^{15}N metabolic labeling of the HAB/NAB/LAB mouse model of trait anxiety	45
5.1	Introduction	45
5.2	Results	45
5.2.1	Behavioral characteristics of bacteria-fed HAB/NAB/LAB mice	45
5.2.1.1	Anxiety-related behavior	46
5.2.1.2	Depression-like behavior	47
5.2.2	^{15}N metabolic labeling efficiency estimation	47
5.3	Discussion	49



6	Biomarker and pathway discovery in the HAB/NAB/LAB mouse model of trait anxiety	52
6.1	Introduction	52
6.2	Results	54
6.2.1	HAB/LAB cingulate cortex synaptosome proteome comparison	54
6.2.2	HAB/NAB/LAB cingulate cortex metabolome comparison	55
6.2.3	Western blot validation of selected differentially expressed proteins	56
6.2.3.1	Sideroflexin-5 (Sfxn5)	57
6.2.3.2	Carbonic anhydrase 2 (Car2)	57
6.2.3.3	Myosin, heavy polypeptide 10 (Myh10)	58
6.2.3.4	Succinate dehydrogenase, subunit b (Sdhb)	59
6.2.4	<i>In silico</i> analysis of altered pathways in HAB and LAB mice	60
6.2.5	Altered networks in HAB and LAB mice	65
6.2.5.1	Glycolysis	65
6.2.5.2	Neurotransmission	66
6.2.5.3	Mitochondrial function	67
6.3	Discussion	69
7	¹⁵N isotope effect investigation in HAB mice and <i>Escherichia coli</i>	74
7.1	Introduction	74
7.2	Results	76
7.2.1	Investigation of the ¹⁵ N isotope effect in HAB mice	76
7.2.1.1	¹⁴ N HAB/ ¹⁵ N HAB cingulate cortex synaptosome proteome comparison	76
7.2.1.2	Western blot validation of selected differentially expressed proteins	76
7.2.1.3	<i>In silico</i> analysis of altered pathways in ¹⁴ N HAB and ¹⁵ N HAB mice	78
7.2.1.4	Altered networks in ¹⁴ N HAB and ¹⁵ N HAB mice	80
7.2.2	Investigation of the ¹⁵ N isotope effect in <i>Escherichia coli</i>	80
7.2.2.1	¹⁴ N/ ¹⁵ N <i>Escherichia coli</i> cytoplasmic proteome comparison	80
7.2.2.2	Western blot validation of beta galactosidase	82
7.2.2.3	Pyruvate metabolism alterations in ¹⁴ N and ¹⁵ N <i>Escherichia coli</i>	83
7.2.2.4	<i>In silico</i> analysis of altered pathways in ¹⁴ N and ¹⁵ N <i>Escherichia coli</i>	86



7.3	Discussion	86
8	Biomarker discovery in the G72/G30 transgenic mouse model of schizophrenia-like symptoms	90
8.1	Introduction	90
8.2	Results	90
8.2.1	Detection of the G72 protein in G72/G30 transgenic mice	90
8.2.2	Protein expression differences between G72/G30 transgenic and wild type mice	91
8.3	Discussion	93
9	Outlook and perspectives	95
9.1	Biomarker discovery in psychiatric disorders	95
9.2	Proteomics technologies	96
10	References	97
11	Appendixes	111
12	Acknowledgments	125
13	Curriculum vitae	127
14	Publications	128



Abbreviations

1D	One-dimensional
2D	Two-dimensional
2D-PAGE	Two-dimensional polyacrylamide gel electrophoresis
ABC	ATP-binding cassette
BAC	Bacterial artificial chromosome
CI	Confidence interval
CID	Collision-induced dissociation
EP	Enolase phosphatase
EPM	Elevated plus-maze
ESI	Electrospray ionization
ETC	Electron transport chain
FDA	Food and Drug Administration
GABA	Gamma-aminobutyric acid
GC-TOF-MS	Gas chromatography-time of flight-mass spectrometry
GnRH	Gonadotropin-releasing hormone
GO	Gene Ontology
HAB	High anxiety-related behavior
IEF	Isoelectric focusing
IPG	Immobilized pH gradient
IPI	International protein index
KEGG	Kyoto encyclopedia of genes and genomes
LAB	Low anxiety-related behavior
LC-ESI-MS/MS	Liquid chromatography-electrospray-tandem mass spectrometry
LTD	Linear-trap quadrupole
MALDI	Matrix-assisted laser desorption ionization
MANOVA	Multivariate analysis of variance
mRNA	Messenger ribonucleic acid
MS	Mass spectrometry
MS/MS	Tandem mass spectrometry
m/z	Mass-to-charge ratio
NAB	Normal anxiety-related behavior
NADPH	Nicotinamide adenine dinucleotide phosphate
NMDA	N-methyl-D-aspartate
PAGE	Polyacrylamide gel electrophoresis
PND	Post-natal day
RF	Random forest



ROS	Reactive oxygen species
RP-HPLC	Reversed-phase high performance liquid chromatography
S	Serine
SAM	S-adenosyl-L-methionine
SDS	Sodium dodecyl sulfate
SEM	Standard error of the mean
SILAC	Stable isotope labeling by amino acids in cell culture
SNP	Single-nucleotide polymorphism
SNARE	Soluble N-ethylmaleimide sensitive fusion protein attachment protein receptors
T	Threonine
TBS	Tris buffered saline
TBS-T	Tris buffered saline buffer containing 0.05% Tween 20
TFFBS	Test- and functional-free biomarker searching
TOF	Time of flight
TST	Tail suspension test
USV	Ultrasonic vocalization test
UV	Ultra-violet
WT	Wild type
XIC	Extracted ion chromatogram
Y	Tyrosine



Protein names

Atcay	Caytaxin
Cadps	Calcium-dependent secretion activator 1 (Caps1)
CaMKII	Calcium/calmodulin-dependent protein kinase type II
Car2	Carbonic anhydrase 2
Cartpt	Cocaine- and amphetamine-regulated transcript protein
Cend1	Cell cycle exit and neuronal differentiation protein 1
Cfl1	Cofilin-1 (COF1)
Cltb	Clathrin light chain B
Cltc	Clathrin heavy chain
Crym	Mu-crystallin
DAO	D-amino acid oxidase
Dld	D-lactate dehydrogenase
Dlg 1-4	Discs large homologs 1-4
EP	Enolase phosphatase
G72	D-amino acid oxidase activator (or DAOA)
Gad2	Glutamate decarboxylase 2
Gap43	Neuromodulin
Gdi1	Rho GDP dissociation inhibitor (GDIR)
Glo1	Glyoxalase 1
Glud1	Mitochondrial glutamate dehydrogenase 1
Glul	Glutamine synthetase (Q91VC6)
Gphn	Gephyrin
Gria2	Glutamate receptor 2 (GluR2)
Gria3	Glutamate receptor 3
Grm3	Metabotropic glutamate receptor 3
Gstm1	Glutathione S-transferase M1
Gstp1	Glutathione S-transferase P1
Homer 1-3	Homer protein homologs 1-3
Idh1	Isocitrate dehydrogenase
Kcnc3	Isoform Kv3.3B of potassium voltage-gated channel subfamily C member 3
Kpyk2	Pyruvate kinase II
LacZ	Beta galactosidase
LG72	Longest G72 splice variant
MAPK	Mitogen-activated protein kinase
Marcks	Myristoylated alanine-rich C-kinase substrate
Mbp	Myelin basic protein



Mdh	Malate dehydrogenase (Q9K2L4, Q9ETZ1, Q9KH77, Q9KH79 variants)
Myh10	Myosin, heavy polypeptide 10, non-muscle
Nefm	Neurofilament medium polypeptide
Odp2	Dihydrolipoyllysine-residue acetyltransferase component of pyruvate dehydrogenase complex
Pcsk1n	Proprotein convertase 1 inhibitor ProSAAS
PflB	Formate acetyltransferase 1
Pgam1	Phosphoglycerate mutase 1
Ppcl	Phosphoenolpyruvate carboxylase mutant (Q47521)
PpsA	Phosphoenolpyruvate synthase
Prdx2	Peroxiredoxin-2
Prkc	Protein kinase C family
Prkcb1	Protein kinase C beta type
Prkcc	Protein kinase C gamma type
Prkce	Protein kinase C epsilon type
PSD95	Discs large homolog 4 or post-synaptic density protein 95 (Dlg4)
Pta	Phosphate acetyltransferase
Rgs6	Regulator of G-protein signaling 6
Sdh	Succinate dehydrogenase
Sdha	Succinate dehydrogenase [ubiquinone] flavoprotein subunit, mitochondrial precursor
Sdhb	Succinate dehydrogenase [ubiquinone] iron-sulfur subunit, mitochondrial precursor
Sdhc	Succinate dehydrogenase cytochrome b560 subunit, mitochondrial precursor
Sfxn1	Sideroflexin-1
Sfxn3	Sideroflexin-3
Sfxn5	Sideroflexin-5
Shank1	SH3 and multiple ankyrin repeat domains 1
Slc17a7	Brain-specific sodium-dependent inorganic phosphate co-transporter (VGlut1)
Slc1a1	Solute carrier family 1 (Neuronal/epithelial high affinity glutamate transporter, system Xag), member 1
Slc1a2	Isoform Glt-1A of excitatory amino acid transporter 2
Slc1a3	Excitatory amino acid transporter 1
Slc25a3	Phosphate carrier protein, mitochondrial precursor
Slc25a4	ADP/ATP translocase 1
Slc25a5	ADP/ATP translocase 2
Slc25a11	Mitochondrial 2-oxoglutarate/malate carrier protein
Slc25a12	Calcium-binding mitochondrial carrier protein Aralar1
Slc25a18	Mitochondrial glutamate carrier 2 (33kDa protein)



Slc25a22	Mitochondrial glutamate carrier 1
Slc6a1	Sodium- and chloride-dependent GABA transporter 1
Slc6a11	Sodium- and chloride-dependent GABA transporter 4
Slc7a8	Large neutral amino acids transporter small subunit 2
Snap91	Isoform long of clathrin coat assembly protein AP180
Sod1	Superoxide dismutase
Stx1a	Syntaxin-1A
Syt 1-3	Synaptotagmin 1-3
TIM	Translocase of the inner mitochondrial membrane
TnR	Tenascin-R precursor
TOM	Translocase of the outer mitochondrial membrane
Tuba1a	Tubulin alpha 1A chain (Q3TGF0)
Tubb2c	Tubulin beta 2C chain (Q99JZ6)
Vamp 1-4	Vesicle-associated membrane proteins 1-4
Vdac 1-3	Voltage-dependent anion-selective channels 1-3
VEGF	Vascular endothelial growth factor.

Where applicable, additional common protein names or accession IDs are included. A detailed list of proteins mentioned in the text is also provided in Appendixes 3, 4 and 5.



1 Introduction

1.1 Psychiatric disorders

Although over the last century tremendous progress has been made in the therapy and mortality decrease of devastating conditions such as cancer and cardiopathies, no decrease has been observed in mortality rates or overall prevalence of psychiatric disorders (Kessler et al., 2005). It is therefore not surprising that according to the World Health Organization, psychiatric disorders are one of the leading causes of disease burden and disability worldwide (World Health Organization, 2008).

1.1.1 Anxiety and depression

Anxiety can be conceptualized as the emotional anticipation of an aversive situation, which is likely to occur and difficult to predict and control (Landgraf, 2001). In its non-pathological form, anxiety can be classified into state anxiety, referring to the acute or immediate level of anxiety and trait anxiety, which reflects the long-term tendency of an individual to show an increased anxiety response (Leonardo and Hen, 2006). It is believed that pathological anxiety evolves from normal anxiety behavior along a continuum from physiology to psychopathology (Landgraf et al., 2007; Rosen and Schulkin, 1998). In its pathological form, anxiety encompasses a wide spectrum of conditions, including panic disorder, agoraphobia, social phobia, obsessive-compulsive disorder, generalized anxiety disorder, post-traumatic stress disorder and acute stress disorder (American Psychiatric Association, 2000). Anxiety disorders constitute the most common psychiatric disorders in the industrialized world with an estimated lifetime prevalence ranging from 14.5% to 28.8% in Europe and in the USA (Jacobi et al., 2004; Kessler et al., 2005). Twin and family studies have revealed a 30-40% heritability of anxiety disorders (Hettema et al., 2001), suggesting a considerable genetic contribution. Remarkably, there is an up to 60% co-morbidity with depression. Depression, one of the most debilitating psychiatric disorders, is highly heritable (Fava and Kendler, 2000) and shares common symptoms with anxiety, making mild versions of both disorders difficult to distinguish (Kalueff et al., 2007). Antidepressants are also used for the treatment of anxiety disorders, indicating convergent underlying pathways (Gorman, 1996; Levine et al., 2001; Nutt, 2005).



Within the spectrum of anxiety disorders, the facts that they often co-occur (Hettema et al., 2005), and most of them respond to a similar spectrum of pharmacological treatments (Gross and Hen, 2004; Kent et al., 2002) indicates that they share common neurobiological and physiological characteristics, as well. At the neuroanatomical level, the amygdala and the limbic system are the key players involved in processing anxiogenic stimuli, which are in turn linked to cortex, hypothalamus and hippocampus, comprising the neural circuit involved in anxiety. At the synaptic level, imbalance between excitatory and inhibitory neurotransmission in these brain areas has been proposed to be responsible for the manifestation of anxiety-like behavior (McNaughton, 1997; Wu et al., 2008). At the neuroendocrine level, the hypothalamic-pituitary-adrenal axis as well as neuropeptides (e.g., vasopressin) have been suggested to play a role in the mediation and modulation of anxiety symptomatology. Yet, the exact molecular mechanisms of anxiety pathogenesis remain elusive.

1.1.2 Schizophrenia

Auditory hallucinations, delusions, thought disorder and cognitive deficits are the main symptoms of schizophrenia, which affects ~1% of the general population (Freedman, 2003) with disease onset appearing in late adolescence. Evidence from genetics, neuroimaging and pharmacology suggests that schizophrenia is a heterogeneous group of disorders (Harrison and Weinberger, 2005; Kirkpatrick et al., 2001). Currently, schizophrenia is viewed as a subtle disorder of brain development and synaptic plasticity with a complex contribution from genetic and environmental factors (Arnold et al., 2005; Harrison and Weinberger, 2005; Rapoport et al., 2005). As there is up to 80% heritability in schizophrenia (Cardno and Gottesman, 2000), useful information concerning the underlying disease mechanisms has been derived from association and linkage genetic studies. Contributing genes include among others G72 (D-amino acid oxidase activator or DAOA) (Abou Jamra et al., 2006), neuregulin 1 (Li et al., 2006), disrupted-in-schizophrenia-1 (Schumacher et al., 2009) and dysbindin (Straub et al., 2002). Insights from antipsychotic drug action have implicated dopamine neurotransmission (Carlsson, 1978) and hypofunction of the glutamate N-methyl-D-aspartate (NMDA) receptor (Coyle, 2006) in the pathophysiology of schizophrenia. However, as is the case for anxiety disorders, the exact etiology of schizophrenia is not fully understood.



1.2 Biomarkers for psychiatric disorders

1.2.1 What is a biomarker?

According to the National Institutes of Health, a biomarker is a characteristic that is objectively measured and evaluated as an indicator of normal biological processes, pathogenic processes, or pharmacological responses to a therapeutic intervention (Biomarkers Definitions Working Group, 2001). Biomarkers are critical to differentiate between distinct biological states. Representative biomarkers routinely used in modern biology and medicine include human chorionic gonadotropin to detect pregnancy, serum ferritin to assess anemia and cholesterol to predict cardiovascular disease risk.

1.2.2 The quest for biomarkers in psychiatric research

To date, no molecular biomarker exists for any psychiatric disorder. No prognostic test is available that could reliably identify individuals at risk of developing psychopathologies due to genetic predisposition or vulnerability to relevant environmental stimuli. Diagnosis and disease categorization are symptomatic and mainly rely on a subjective, interview-based communication with the patient (Turck et al., 2005). Current medication is not without side-effects and/or requires weeks to work, while not all patients respond to existing drug treatment (Bystritsky, 2006). Taken together, reliable molecular biomarkers in psychiatry are of paramount importance for identification of at risk individuals, premorbid diagnosis, patient stratification, disease monitoring and effective, personalized treatment.

Besides clinical practice, biomarkers can accelerate drug discovery by being used as surrogate markers of drug efficacy and hence reduce production costs and pipeline development time (Schwarz and Bahn, 2008). In basic research, biomarkers can contribute to the elucidation of molecular mechanisms of disease pathogenesis. However, because of the complex nature and the increased intra-heterogeneity of psychiatric disorders, a single biomarker will not be able to unequivocally distinguish between clinical phenotypes. A panel of biomarkers, which depict more accurately a disease state is required to significantly represent complex traits like anxiety disorders or schizophrenia (Turck et al., 2005). In this context, animal models and novel -omics technologies promise to be useful tools for biomarker discovery.



1.3 Mouse models for psychiatric disorders

1.3.1 Advantages of mouse models in psychiatric research

Mental disorder research on human subjects is problematic not only due to ethical issues but also due to increased intra-individual heterogeneity unrelated to disease pathology, restricted access to human material (e.g., cerebrospinal fluid) and limited control of retrieval protocols consistency (Ditzen et al., 2010). Studies on human *post-mortem* tissue have been informative, but largely unreliable due to *post-mortem* delay-derived changes, confounding clinical conditions, previous drug treatment and unavailability of suitable controls. In this respect, the use of model organisms represents the best possible alternative to investigate psychiatric disorders. Mice constitute a valuable model organism because they can be cost-effectively bred, housed and maintained in large numbers under standardized laboratory conditions. They have a short life span and can be quickly reproduced, enabling long-term studies of a stimulus effect. Advantageously, inbred mouse lines have limited heterogeneity relative to human populations, and material acquisition and *post-mortem* tissue preparation can be performed in a consistent manner. A plethora of tools (information resources, molecular technologies, genetic manipulation methods, behavioral tests) is now available for mice, facilitating the application of diverse experimental approaches. Obviously, psychiatric disorders cannot be fully recapitulated in mice given that certain manifestations of disease symptomatology (e.g., low self esteem, suicidal ideation) cannot be modeled (Cryan and Holmes, 2005). Nevertheless, there is significant similarity between humans and mice since they share 99% of their genes (Mouse Genome Sequencing Consortium, 2002), whereas brain structural organization and certain neural circuit interconnections, physiological parameters and behavioral responses are widely conserved across mammals (Ohl, 2005). While caution should be taken in extrapolating conclusions from animal studies to humans, a great amount of our current understanding of psychopathologies is derived from mouse models (Landgraf et al., 2007).

1.3.2 The HAB/NAB/LAB mouse model of trait anxiety

1.3.2.1 Bidirectional selective breeding

Following the same breeding strategy previously applied to rats (Landgraf and Wigger, 2002; Liebsch et al., 1998a; Liebsch et al., 1998b), Prof. Rainer Landgraf and colleagues in the group of



Behavioral Neuroendocrinology at the Max Planck Institute of Psychiatry in Munich have established the HAB/NAB/LAB mouse model of trait anxiety. Outbred CD1 mice were used for selective and bidirectional breeding based on their performance on the elevated plus-maze (EPM) (Fig. 1.1). The method of bidirectional selective breeding enhances the representation of genetic material associated with a specific trait, thus shifting the animals' phenotype from the population mean (Falconer and Mackay, 1996). The EPM is a physiologically and pharmacologically validated behavioral test that assesses anxiety in rodents in a spontaneous and unconditioned manner. The EPM principle is based on generating an approach-avoidance conflict between the exploratory drive of mice and their innate fear of illuminated, unprotected and heightened areas (Lister, 1987; Pellow et al., 1985). It consists of an elevated plus-shaped apparatus with two aversive open arms, two dark arms with protecting walls and a neutral zone (see 3.3.2.2 and Fig. 1.1B). The amount of time spent on the EPM open arms is considered to indicate genetic predisposition for trait anxiety and is predictive for stress coping (Ducottet and Belzung, 2004). According to the % test time spent on the open arms, mice were bred with the corresponding partners to generate the behavioral extreme phenotypes. Mice spending less than 10% of the test time on the open arms gave rise to the high anxiety-related behavior (HAB) line, whereas mice spending most of the test time on the open arms (~50% or more) gave rise to the low anxiety-related behavior (LAB) line. Normal anxiety-related behavior (NAB) mice display an intermediate phenotype (time spent on open arms ~30%) (Fig. 1.1A).

1.3.2.2 Behavioral and molecular characteristics

The HAB/NAB/LAB mouse model has been extensively studied, revealing behavioral, cognitive and molecular alterations in HAB and LAB mice. Apart from the EPM, HAB and LAB lines show differences in a battery of behavioral paradigms assessing anxiety-related behavior including the ultrasonic vocalization (USV, see 3.3.2.1) and the dark-light avoidance test, with HAB mice exhibiting increased anxiety levels (Krömer et al., 2005). In behavioral tests measuring depression-like phenotype such as the forced swim and the tail suspension test (TST, see 3.3.2.2), LAB animals exhibit decreased immobility, indicating a reduced depression-like behavior (Krömer et al., 2005). At the cognitive level, HAB exhibit superior performance compared to LAB mice in the social recognition test (Bunck, 2008). At the molecular level, vasopressin SNPs and decreased vasopressin mRNA expression have been reported in LAB mice (Bunck et al., 2009;



Kessler et al., 2007). Additional gene expression differences between HAB and LAB mice have been found in a number of brain regions by microarray analysis (Czibere, 2009).

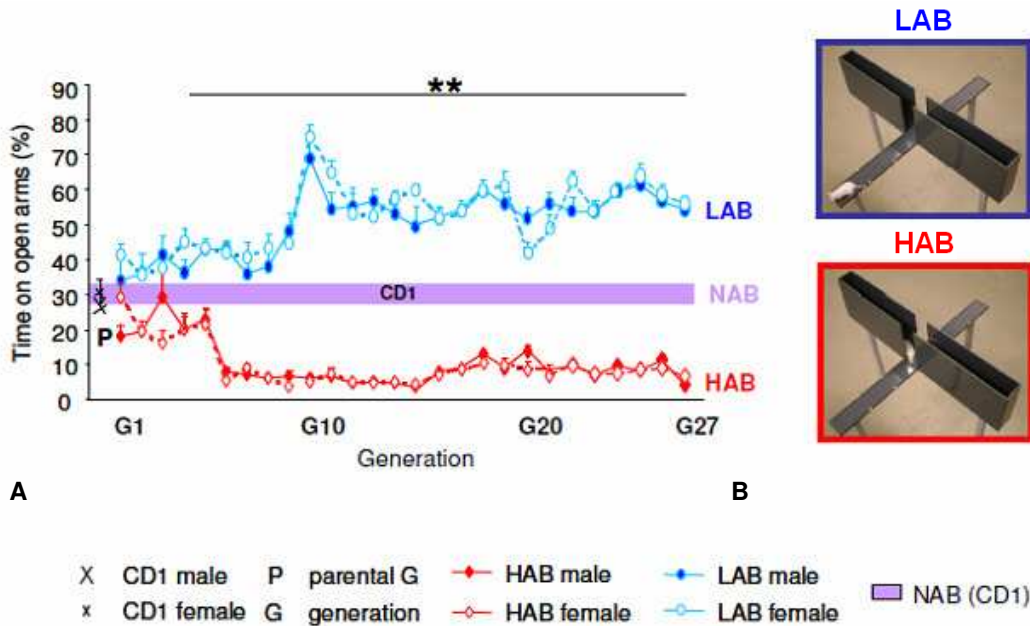


Figure 1.1 Breeding scheme of the HAB/NAB/LAB mouse model of trait anxiety

A. EPM data (% time spent on the open arms) of the parental generation P and generations G1 to G27 of HAB and LAB mice, with CD1 (NAB) mice as controls. From the fourth generation on, HAB and LAB animals differ significantly in their anxiety-related behavior independent of gender (** $p < 0.01$, $n = 40-80$ per line and generation). **B.** Characteristic behavior of HAB and LAB mice on the EPM. LAB mice explore the a priori aversive open arms (blue square), while HAB animals spend more time in the protective closed arms (red square) (figure kindly provided by Dr. Ludwig Czibere).

1.3.3 The G72/G30 transgenic mouse model of schizophrenia-like symptoms

There is accumulating evidence from linkage and association studies that the G72/G30 region on chromosome 13q32-q33 is a strong susceptibility locus for schizophrenia (reviewed in Abou Jamra et al., 2006; Detera-Wadleigh et al., 2006). The G72 and G30 genes are transcribed from overlapping opposite DNA strands, with only G72 appearing to be actively translated (Chumakov et al., 2002). G72 is a primate-specific gene with a complex alternative splicing pattern



(Chumakov et al., 2002), whose exact function is largely unknown. To elucidate the functional role of the G72 protein and its involvement in schizophrenia, Prof. Andreas Zimmer and colleagues at the Institute of Molecular Psychiatry at the University of Bonn generated a G72/G30 transgenic mouse model by injecting bacterial artificial chromosome (BAC) plasmids containing the G72/G30 genomic region into pronuclei of fertilized oocytes from CD1 mice. The G72/G30 transgenic mice display behavioral phenotypes relevant to psychiatric disorders, including impaired motor coordination, sensorimotor gating and olfactory discrimination as well as increased compulsive behavior (Otte et al., 2009).

1.4 Biomarker discovery platforms

1.4.1 Quantitative proteomics

1.4.1.1 Advantages of studying the proteome

Although genomics have provided useful insights into genes conferring susceptibility to complex diseases, many disease-related genes have low penetrance and do not exhibit an effect on the phenotype in a predictable and quantifiable manner (Schwarz and Bahn, 2008). Moreover, in a given disease state, multiple lesions occur at the gene level that vary across the individuals. On the other hand, altered protein signatures have the potential to reflect disease states. Disease-related changes are depicted at the proteome level, thus relating proteome alterations to the disease phenotype. Consequently, interrogation of the proteome can result into an accurate and unbiased investigation of disease pathophysiology and drug action mechanisms (Turck et al., 2005).

1.4.1.2 Mass spectrometry

Mass spectrometry (MS) -based techniques are powerful tools in proteomics research enabling protein identification and quantification in complex mixtures. MS determines the molecular weight of chemical compounds, which is characteristic for every molecule, by separating molecular ions based on their mass-to-charge ratio (m/z) in a mass spectrometer. The main components of a mass spectrometer are an ionization source, a mass analyzer and an ion detector (Fig. 1.2A).

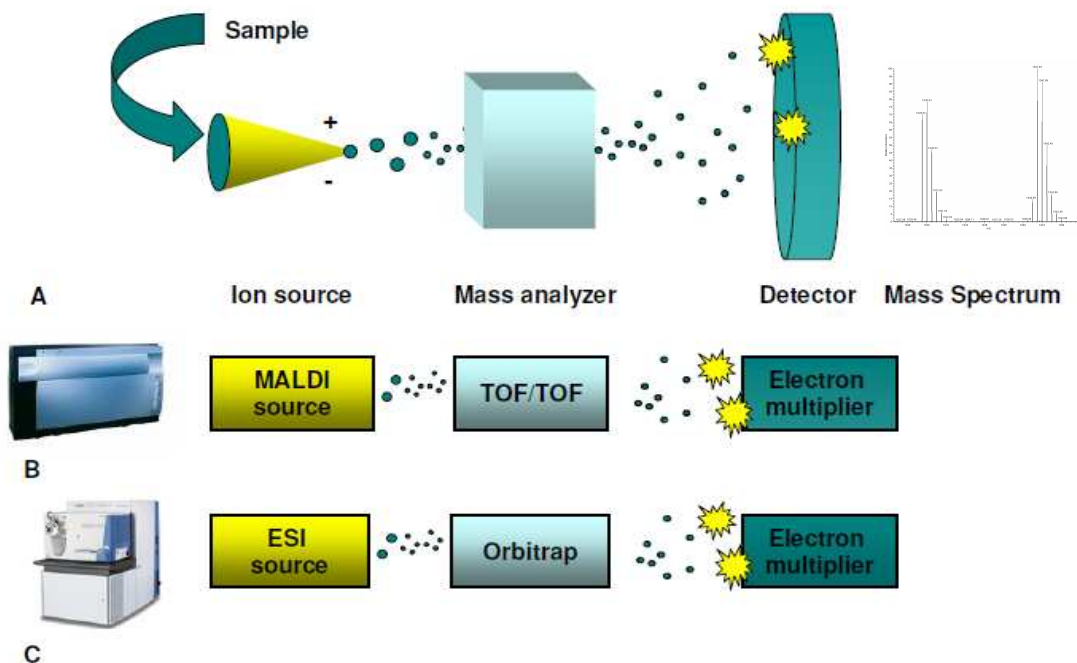


Figure 1.2 Components of a mass spectrometer

A. Generic components of a mass spectrometer. The output of the measurement is a mass spectrum, where intensities of different m/z peaks are plotted (figure adapted from www.magnet.fsu.edu). **B.** Simplified set-up of the Ultraflex MALDI-TOF/TOF instrument. **C.** Simplified set-up of the LTQ-Orbitrap instrument.

Once a sample is introduced into the mass spectrometer, it undergoes ionization in the ionization source. The charged ions are then electrostatically propelled into the mass analyzer, where they are separated according to their m/z ratio and detected by the ion detector (Siuzdak, 1996). The output is a mass spectrum (ion intensity at different m/z values) that provides molecular weight information of the measured compounds (Fig. 1.2A). Different ion sources and ionization techniques can be combined with mass analyzers giving rise to different mass spectrometers (see 1.4.1.3). In tandem mass spectrometry (MS/MS), the separation of ions according to their m/z is used as a preparative step to isolate an ion with a desired m/z . The selected ion is then fragmented, and the m/z of the fragment ions is defined in a second stage of analysis. As a result, selected ions in a complex mixture can be studied, and their amino acid sequence can be determined (Kinter and Sherman, 2000).



1.4.1.3 Mass spectrometry instrumentation

Ultraflex MALDI-TOF/TOF

Matrix-assisted laser desorption ionization (MALDI) was first developed by Karas and colleagues (Karas et al., 1985). The sample to be analyzed is dissolved in a solid, non-volatile, ultra-violet (UV) absorbing material (matrix) and co-crystallizes with it. The mixture is then irradiated with a short-pulsed UV laser resulting in matrix ionization, followed by energy and proton transfer to the sample. The ionized sample molecules are then directed to a time of flight (TOF) mass analyzer (Siuzdak, 1996). In the TOF mass analyzer, the ion population coming from the ion source is accelerated by an electrical potential. After acceleration, the ions pass through a field-free region, where each ion is traveling with a speed characteristic of its m/z value. At the end of the field-free region, the detector measures the flight time (Matthiesen and Mutenda, 2007). In MALDI-TOF/TOF MS, two TOF analyzers are used consecutively (Fig. 1.2B). The first TOF mass analyzer isolates the precursor ions of choice using a velocity filter, and the second analyzes the selected ions (Vestal and Cambell, 2005).

LTQ-Orbitrap

Electrospray ionization (ESI) was first developed by Yamashita and Fenn (Yamashita and Fenn, 1984). The sample is dissolved in a polar, volatile solvent; the sample solution passes through a needle and is sprayed from a strong electric field region. The highly charged droplets are electrostatically attracted to the mass spectrometer inlet, and ions are then generated during droplet evaporation (Siuzdak, 1996). After ionization, ions are entering a linear-trap quadrupole (LTQ) mass analyzer, which is linked to an Orbitrap mass analyzer via a C-trap. From LTQ, ions are axially injected in the C-trap and in addition in the Orbitrap mass analyzer, where they are electrostatically trapped while rotating around the central electrode performing axial oscillation (Fig. 1.2C). The oscillation frequencies are determined using a Fourier transform and are converted to masses (Makarov, 2000). For higher analytical sensitivity, samples are first separated with reversed-phase high performance liquid chromatography (RP-HPLC), and the eluents are directly infused to the mass spectrometer. This set-up [referred to from now on as liquid chromatography-electrospray-tandem mass spectrometry (LC-ESI-MS/MS), see 3.1] ensures high mass accuracy and resolution, making it the method of choice for quantitative proteomics experiments.



1.4.1.4 Mass spectrometry-based proteomics

In a typical proteomics workflow, a protein population is extracted from the material under investigation (tissue, cells, etc.) (Fig. 1.3A), and the subproteome of interest is enriched (Fig. 1.3B). To reduce complexity, extracted proteins are separated by gel-based approaches (i.e. 1D- or 2D-gel electrophoresis) and digested with trypsin to generate peptides (Fig. 1.3C). Peptides are then extracted (Fig. 1.3D) and analyzed by MS (Fig. 1.3E). The corresponding fragment masses are searched against protein databases and are used for protein identification and/or quantification (Fig. 1.3F).

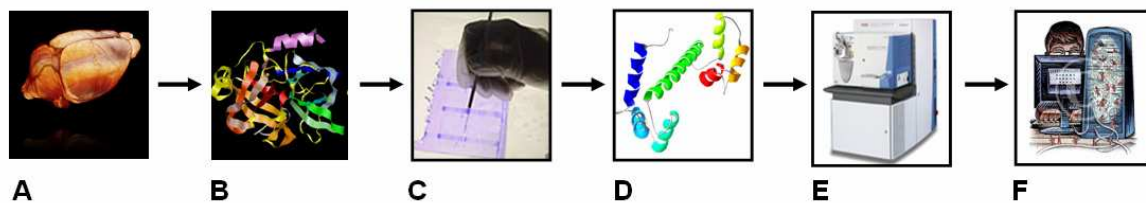


Figure 1.3 Proteomics workflow scheme

A. Protein extraction. **B.** Subproteome enrichment. **C.** Gel electrophoresis and in gel tryptic digestion. **D.** Peptide extraction. **E.** MS. **F.** Database search and data analysis.

1.4.1.5 Quantitative proteomics methodologies

Two-dimensional polyacrylamide gel electrophoresis

Until recently, two-dimensional polyacrylamide gel electrophoresis (2D-PAGE) was the main proteomics approach for comparing two different states (i.e. disease, control), being based on the bidimensional separation of proteins in a complex mixture. In the first dimension, proteins are separated according to their isoelectric point by isoelectric focusing (IEF) using immobilized pH gradient (IPG) strips. In the second dimension, proteins are separated according to their molecular weight on polyacrylamide gels (O'Farrell, 1975). The 2D-gels are then stained, and spot signal intensities are compared across the samples. Spots with different intensities between the groups under study are excised from the 2D-gels, and the corresponding proteins are identified by MS. Although 2D-PAGE is a well-established quantitative approach, the analysis of hydrophobic, membrane, extreme pH and high or low molecular weight proteins remains challenging. Furthermore, expression of low abundant proteins can be masked by high abundant proteins, while reproducibility issues concerning intra-gel variability and sample pre-fractionation



yeast (Oda et al., 1999), bacteria (Conrads et al., 2001; Pan et al., 2008), *Drosophila melanogaster* (Krijgsveld et al., 2003), *Caenorhabditis elegans* (Dong et al., 2007; Krijgsveld et al., 2003) and plants (Bindschedler et al., 2008; Huttlin et al., 2007; Kierszniowska et al., 2009a; Kierszniowska et al., 2009b; Lanquar et al., 2007; Palmblad et al., 2007; Schaff et al., 2008). Recently, rodents fed with ^{15}N -labeled algae (Huttlin et al., 2009; McClatchy et al., 2007a; Wu et al., 2004) were metabolically labeled with ^{15}N for quantitative proteomics experiments.

^{15}N isotope effect on the proteome

The use of stable isotopes in proteomics is based on the isotope dilution theory (De Leenheer and Thienpont, 1992) according to which, a stable isotope labeled peptide is chemically identical to its unlabeled counterpart and therefore the behavior of the two peptides is identical during chromatographic and MS workflows. However, in most quantitative proteomics studies where ^{15}N metabolic labeling was used, control strategies for the ^{15}N isotope effect were employed either by reciprocal labeling of the two states to be compared (Huttlin et al., 2009; Kierszniowska et al., 2009b; Krijgsveld et al., 2003; Lanquar et al., 2007; Oda et al., 1999) or by the use of a ^{15}N -labeled internal standard (Dong et al., 2007; Liao et al., 2008; McClatchy et al., 2007a; Pan et al., 2008; Wu et al., 2004). These measures were introduced to avoid potential confounding ^{15}N -derived artifacts. Yet to date, no study has examined the actual effects of the ^{15}N isotope introduction on a given proteome *per se*.

1.4.2 Quantitative metabolomics

The repertoire of small molecules present in cells, tissues and body fluids is known as the metabolome. Metabolomics (the study of the metabolome) have emerged to be the newest member of the -omics family. Metabolomics reflect the status of diverse biochemical pathways in a given metabolic state in health or disease. MS-based metabolomics enable the identification and quantification of known as well as new metabolites (Dettmer et al., 2007). In particular, gas chromatography (GC) coupled with MS has been used for metabolomics quantification in psychiatric and neurodegenerative disorders (Paige et al., 2007; Underwood et al., 2006) due to its high sensitivity, quantitative precision and chromatographic resolution and wide dynamic range (Quinones and Kaddurah-Daouk, 2009). Altered metabolic signatures can provide useful information about disease pathophysiology and together with proteomics information can



contribute to a systemic approach for the study of disease pathogenesis and biomarker discovery (Kaddurah-Daouk et al., 2008).

1.5 Biomarker discovery in the HAB/NAB/LAB mouse model of trait anxiety

2D-PAGE in amygdala, hypothalamus and motor cortex of HAB, NAB and LAB mice revealed differences in two proteins, glyoxalase 1 (Glo1) and enolase phosphatase (EP). Glo1 expression was significantly higher in LAB compared to HAB mice in all brain areas examined, with NAB animals exhibiting intermediate Glo1 levels (Fig. 1.5). The same pattern was shown by Western blot analysis in red blood mouse cells (Ditzen et al., 2006; Krömer et al., 2005). Glo1 is a cytosolic enzyme that detoxifies dicarbonyl metabolites, such as methylglyoxal (Thornalley, 1993). In mice, Glo1 gene copy number has been associated with anxiety-related behavior (Williams et al., 2009), whereas Glo1 and glutathione reductase 1 have been reported to play a causal role in anxiety (Hovatta et al., 2005). In humans, a Glo1 single-nucleotide polymorphism (SNP) has been associated with panic disorder without agoraphobia (Politi et al., 2006). Furthermore, Glo1 mRNA levels in white blood cells have been suggested to be a state-dependent marker of mood disorders (Fujimoto et al., 2008). Notably, the predictive validity of Glo1 as a biomarker for the HAB/NAB/LAB mouse model has been demonstrated by identifying HAB or LAB in a blind manner based on Glo1 expression levels (Krömer et al., 2005).

EP showed a different motility pattern between HAB, NAB and LAB mice in the second dimension of 2D-PAGE in all areas examined (Fig. 1.5) (Ditzen et al., 2006). EP is a member of methionine salvage pathway, where methionine is metabolized to S-adenosyl-L-methionine (SAM), a natural antidepressant and mood stabilizer also involved in polyamine biosynthesis (Papakostas, 2009). Differential expression of polyamines has been repeatedly reported in mental disorders (Fiori and Turecki, 2008). Further analyses revealed the presence of line-specific EP SNPs, altered EP enzymatic activity in HAB and LAB mice as well as increased polyamine expression in HAB mice (Ditzen et al., 2010). Importantly, Glo1 and EP are detectable by Western blot in human red and white blood cells, respectively, illustrating their applicability as markers for non-invasive patient screening (Ditzen et al., 2006). However, taking into account the multifactorial and polygenic nature of anxiety psychopathology, a considerable number of proteins that remain to be identified are likely to contribute to anxiety manifestation.

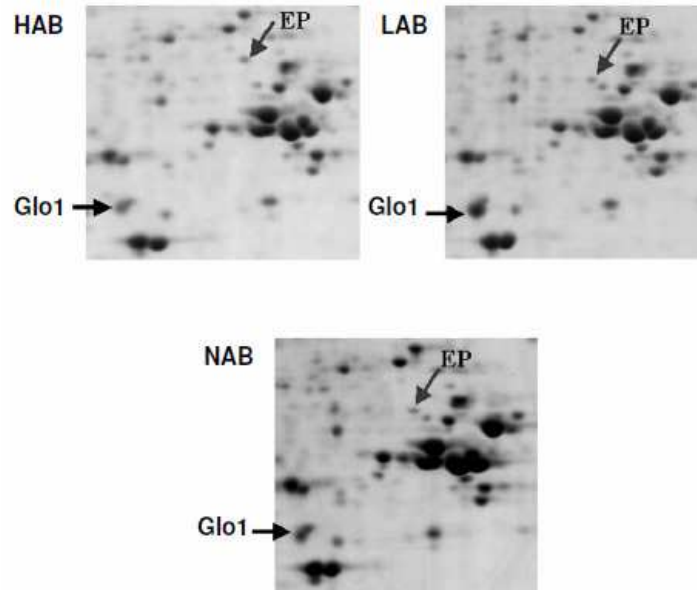


Figure 1.5 Two-dimensional polyacrylamide gel electrophoresis-based biomarker discovery in HAB/NAB/LAB mice

Representative 2D-PAGE of amygdala protein extracts from male HAB/NAB/LAB mice (n=12 per line). Differences in Glo1 and EP are pointed with arrows (Ditzen et al., 2006).



2 Aim of the thesis

The aim of the present study was to identify brain biomarkers and affected pathways in mouse models of psychiatric disorders by establishing and employing quantitative proteomics platforms. Specifically, the following subjects were addressed:

1. To establish and optimize proteomics tools for accurate characterization of the HAB/NAB/LAB mouse model of trait anxiety, a protein profiling of mouse synaptosomes was performed to generate a synaptic protein reference map for quantitative studies (Chapter 4). Furthermore, a quantitative proteomics platform was established based on ^{15}N metabolic labeling of the HAB/NAB/LAB mouse model (Chapter 5), and the effect of the ^{15}N isotope introduction on the proteome during ^{15}N metabolic labeling was investigated (Chapter 7).
2. To identify candidate biomarkers and altered pathways in the HAB/NAB/LAB mouse model of trait anxiety, the cingulate cortex synaptosome proteomes of HAB and LAB mice were compared by the ^{15}N metabolic labeling quantitative proteomics platform. Differences between the HAB, NAB and LAB mouse lines were also investigated by quantitative metabolomics, *in silico* pathway analyses and immuno-based methods (Chapter 6).
3. To elucidate the functional role of G72 in schizophrenia, the cerebellar proteomes of G72/G30 transgenic mice of schizophrenia-like symptoms and wild type (WT) counterparts were compared by 2D-gel-based proteomics (Chapter 8).



3 Materials and methods

3.1 Animals, equipment and standard procedures

All animal studies performed were approved by local authorities and conducted according to current regulations for animal experimentation in Germany and the European Union (European Communities Council Directive 86/609/EEC). Unless otherwise stated, animals were kept in the animal facility of the Max Planck Institute of Psychiatry under standard housing conditions (room temperature $23\pm 2^{\circ}\text{C}$, air humidity 60%, food and tap water *ad libitum*) in groups of 2-4 animals per cage. Tissue acquisition and behavioral testing were performed between 8a.m and 1p.m. Dissection of the desired brain areas was performed according to the mouse brain atlas (Paxinos and Franklin, 2001). Only male animals were studied. Quantitative MS measurements were performed with a nanoflow HPLC-2D system (Eksigent, Dublin, CA, USA) coupled online to a LTQ-Orbitrap mass spectrometer (Thermo Fisher Scientific, Bremen, Germany) via a nanoelectrospray ion source (Thermo Fisher Scientific) (referred to as LC-ESI-MS/MS). For sample infusion into the mass spectrometer, in-house packed, fused silica, $3\mu\text{m}$ RP-C18 (Maisch, Monheim, Germany), $0.075\text{mm} \times 15\text{cm}$ columns connected to distal coated silica tips (New Objective, Ringoes, NJ, USA) were used. ^{15}N incorporation calculation and 2D-PAGE spot identification MS measurements were performed with an Ultraflex MALDI-TOF/TOF mass spectrometer (Bruker Daltonik, Bremen, Germany) equipped with a nitrogen laser operating at 50Hz (referred to as MALDI-TOF/TOF MS). For pipeting volumes up to 1ml, Gilson pipets (Pipetman, Gilson, Middleton, WI) were used. Pipet tips and tubes were purchased from Eppendorf (Eppendorf, Hamburg, Germany). For centrifugation steps, a 5804R centrifuge (Eppendorf) was used. Ultracentrifugation steps were performed in a L8-70M Ultracentrifuge (Beckman Coulter, Krefeld, Germany). Samples were lyophilized in a Savant Speed Vac plus SC210A concentrator (Thermo Fisher Scientific). Unless otherwise stated, 12.5% polyacrylamide, sodium dodecyl sulfate (SDS) -containing mini gels with ten 1.5mm wells were used for 1D-gel electrophoresis. Electrophoretic equipment was purchased from BioRad (BioRad, Hercules, CA, USA). Protein content was estimated by the Bradford Assay (BioRad). Absorption at 595nm was measured by a DU-640 spectrophotometer (Beckman Coulter). Gels and Western blot autoradiographs were scanned by a GS-800 Calibrated Densitometer (BioRad). All commercially



available antibodies used for Western blot analysis are listed in Appendix 1. GraphPad Prism was used for statistical analysis (v5.03, GraphPad Software, San Diego, CA, USA). Unless otherwise specified, statistical significance was accepted for p values <0.05 , determined as follows: * $p<0.05$, ** $p<0.01$, *** $p<0.001$. Data are presented in mean+SEM (standard error of the mean).

3.2 Profiling of mouse synaptosome proteome and phosphoproteome

3.2.1 Synaptosome enrichment from CD1 mouse whole brain

Synaptosomes are artificially isolated synapses produced by mild disruption of brain tissue (see 4.1). Synaptosomes were purified according to Gray and Whittaker (Gray and Whittaker, 1962) with slight modifications (Filiou et al., 2010a). The whole brain of a CD1 adult mouse was homogenized in ten volumes (w/v) of 0.32M sucrose (Sigma Aldrich, St. Louis, MO, USA) and 4mM HEPES (Sigma Aldrich) buffer (pH 7.4). Cocktail inhibitor tablets (Roche Diagnostics, Indianapolis, IN, USA) were used to inhibit phosphatase activity. The homogenate was centrifuged twice at 1000g for 10min to pellet the nuclei (nuclear fraction N), the two supernatants were combined (supernatant S1) and centrifuged at 17000g for 55min. Supernatant was removed (supernatant S2), and the pellet was resuspended in 0.32M sucrose, followed by sucrose gradient ultracentrifugation at 64000g for 2h (0.32M/0.8M/1.2M sucrose gradient). The interface of 0.8M/1.2M sucrose gradient (containing crude synaptosomes) was collected and centrifuged at 164000g for 60min. The supernatant was removed (supernatant S3), and the resulting pellet (synaptosomal fraction, Syn) was dissolved in distilled water. All steps were performed at 4⁰C.

3.2.2 Western blot analysis of selected synaptosomal proteins

To investigate the expression of selected identified proteins in different fractions of the synaptosomal protocol as well as in cytosolic fraction C, a Western blot analysis was performed. The cytosolic fraction C of a whole mouse brain was isolated according to Cox and Emili (Cox and Emili, 2006). In addition, five μ g of nuclear fraction N, cytosolic fraction C, supernatants S1, S2, S3 and synaptosomal fraction Syn (see 3.2.1) were resolved by 1D-gel electrophoresis, and proteins were electrotransferred to Immobilon PVDF membranes (Millipore, Bellerica, MA, USA) at 100V for 1h. Membranes were blocked overnight with 5% (w/v) Carnation instant non-fat dry milk in Tris buffered saline (TBS) buffer containing 0.05% Tween 20 (TBS-T) (GE Healthcare,



Piscataway, NJ, USA) and incubated with anti-Slc17a7 (NeuroMab, Davis, CA, USA, mouse monoclonal, 1:1100), anti-Gria2 (NeuroMab, mouse monoclonal, 1:1100), anti-PSD95 (Genetex, Irvine, CA, USA, goat polyclonal, 1:3000), anti-Gap43 (Abcam, Cambridge, UK, rabbit polyclonal, 1:6000), anti-Prkc (Santa Cruz Biotechnology, Santa Cruz, CA, USA, rabbit polyclonal, 1:1000), anti-Crym (Santa Cruz Biotechnology, goat polyclonal, 1:1000) and anti-Mbp (Abcam, rabbit monoclonal, 1:2000) primary antibodies for 1.5-2h at room temperature. Membranes were incubated for 1h at room temperature with the corresponding anti-rabbit (GE Healthcare), anti-mouse (GE Healthcare) and anti-goat (Santa Cruz Biotechnology) secondary antibodies. Immune complexes were detected by the ECLplus reagent kit (GE Healthcare), membranes transferred to a Hypercassette (GE Healthcare) and exposed to Hyperfilm (GE Healthcare) for the required amount of time. Equal loading amounts were ensured by staining transfer membranes with Coomassie brilliant blue R-250 (BioRad) and comparing signal intensities.

3.2.3 Isoelectric focusing-proteomics sample preparation

Isoelectric focusing (IEF) is an electrophoretic method, where proteins or peptides are separated according to their isoelectric point on an IPG strip. Because of the negative charge of the phosphogroup, phosphopeptides have lower isoelectric points compared to non-phosphorylated peptides and therefore they migrate to the acidic part of the IPG strip. Due to phosphopeptide enrichment at the acidic part of the strip, IEF can be employed as a separation method to simultaneously interrogate the proteome and phosphoproteome of mouse synaptosomes. In the present study, 1.2mg of whole mouse brain synaptosomal proteins in 100 μ l distilled water were dissolved in 200mM ammonium bicarbonate (Merck, Darmstadt, Germany), pH 8.5 (10 μ g/ μ l) and 8M urea (Genaxxon, Ulm, Germany). After reduction with 10mM dithiothreitol (BioRad) and alkylation with 50mM iodoacetamide (BioRad), the urea concentration was reduced by ultrafiltration to 2M and a final sample volume of 100 μ l. One hundred μ l of distilled water were added, and the sample was digested first with 24 μ g endoproteinase Lys-C (Wako, Neuss, Germany) overnight at room temperature, followed by 24 μ g trypsin (Promega, Madison, WI, USA) overnight at 37⁰C. To the digests, distilled water and urea were added to a final volume of 300 μ l and a final urea concentration of 2.5M. The digest solution was applied to a pH 3.5-4.5, 18cm, non-linear IPG strip (GE Healthcare). After 10h of active rehydration at 50V, IEF was carried out in an IEF Cell (BioRad) until 60kVh were reached. The IPG strip was then cut into 47 4mm pieces.



For each gel piece, peptide extraction was performed three times with 5% formic acid. Oil extraction of the combined peptide fraction was performed three times with 150 μ l hexane (VWR, Darmstadt, Germany). The organic phase was discarded and the aqueous fraction lyophilized. The resulting pellet was again oil extracted with 10 μ l hexane (VWR) and air-dried overnight. Pellets were dissolved in 25 μ l 5% formic acid and lyophilized. Samples were redissolved in 6 μ l 1% formic acid, and 3 μ l were used for MS analysis. Desalting with OMIX tips (Varian, Palo Alto, CA, USA) was performed according to manufacturer's instructions.

3.2.4 LC-ESI-MS/MS

For LC-ESI-MS/MS, 3 μ l from each IPG fraction were loaded onto a fused silica column, washed with 0.1% formic acid for 20min and eluted with a gradient of 95% acetonitrile/0.1% formic acid from 2% to 45% over 90min at a flow rate of 200nl/min. The mass spectrometer was operated in the positive ion mode applying a data-dependent automatic scan switch between MS and MS/MS acquisition. Full scans were recorded in the Orbitrap mass analyzer at a mass range of m/z 380-1600 and a resolution of R=60000 (m/z 400) in profile mode. The MS/MS analysis of the five most intense peptide ions for each scan was recorded in the LTQ mass analyzer in centroid mode (top5 method). Fragmentation in the LTQ was induced by collision-induced dissociation (CID) with a target value of 10000 ions. Ion selection threshold was 500 ions, and the selected sequenced ions were dynamically excluded for 120s. Other MS conditions were as follows: Spray voltage 1.9-2.1kV, no sheath and auxiliary gas flow, ion transfer tube temperature 190-200⁰C and normalized collision energy 35%. An activation q=0.25 and activation time of 30ms were applied for MS/MS acquisitions.

3.2.5 Proteomics data analysis

MS raw files were searched against a concatenated, forward/reverse decoy, international protein index (IPI) mouse database (v3.29) utilizing BioWorks (v3.3.1, Thermo Fischer Scientific) and SEQUEST (v28, Thermo Fischer Scientific) softwares. Precursor and fragment ion tolerance was set to 5ppm and 1Da, respectively. Trypsin was chosen as enzyme, and up to two missed cleavage sites were allowed. Cysteine carboxyamidomethylation was used as static modification. Methionine oxidation and serine, threonine and tyrosine phosphorylation were used as variable modifications. Filtering parameters for peptide identifications were minimum Delta Cn: 0.08 and



Xcorr: 1.90 ($z=1+$), 2.70 ($z=2+$), 3.50 ($z=3+$), 3.00 ($z\geq 4+$). Due to the isoelectric point-based separation at the peptide level, peptides belonging to the same protein can migrate in different parts of the strip according to their amino acid composition. Therefore, peptide identifications from all IPG fractions were merged with an in-house developed Perl script. Keratin and hemoglobin proteins were excluded. Proteins identified by only one peptide sequence in a single fraction were removed. Proteins identified by one peptide sequence present in more than one fraction were considered for further analysis. Phosphorylated proteins identified by one peptide sequence both in its modified and unmodified forms or by more than two phosphopeptides were included. All phosphopeptide spectra were manually confirmed. Due to the low phosphorylation stoichiometry, phosphopeptides with a low SEQUEST score were also manually validated. Functional annotation was performed according to Gene Ontology (GO) using the FatiGO online tool (Al-Shahrour et al., 2005; <http://babelomics3.bioinfo.cipf.es>). GO annotations were then grouped into ten broader categories.

3.3 ^{15}N metabolic labeling of the HAB/NAB/LAB mouse model of trait anxiety

3.3.1 ^{15}N metabolic labeling breeding and feeding scheme

To enable an accurate quantitative proteomics comparison, mice were labeled with the ^{15}N isotope through a ^{15}N bacterial protein-based diet (U-15N-SILAM-Mouse, Silantes, Munich, Germany). To avoid any diet-specific effects on the proteome, the unlabeled mice that were used for the $^{14}\text{N}/^{15}\text{N}$ comparison received a ^{14}N (unlabeled) bacterial protein-based diet (U-14N-SILAM-Mouse, Silantes) with the same composition as the ^{15}N diet (Table 3.1) following the same feeding protocol as the ^{15}N bacteria-fed mice. To achieve high ^{15}N incorporation rates, the ^{15}N feeding started *in utero* according to the breeding and feeding protocol shown in Fig. 3.1. In detail, females were mated one-to-one to a male. After pregnancy detection, males were separated from the dams, and pregnant dams were fed for a four day period *ad libitum* with both standard food (Altromin, Lage, Germany) and the respective ^{15}N or ^{14}N bacteria-based food so as to habituate to the new diet. Dams were then fed exclusively with the bacteria-based diet. For the offspring, gender detection was performed on post-natal day (PND) 2. On PND 5, USV was tested, and litters got culled to a usual litter size number. On PND 28, animals were weaned and group-housed (2-4 animals per cage). Groups were composed of mice deriving evenly from all litters so



as to minimize cage effects. Each cage was supplied with the ¹⁴N or ¹⁵N bacterial diet according to the diet that the dam received. All animals were tested on PND 49 on the EPM and on PND 51 in the TST. On PND 5, 14, 28 and 56, animal sampling was performed for ¹⁵N metabolic labeling efficiency calculation. On PND 56, material from all animals (10 ¹⁵N HAB, 24 ¹⁵N NAB, 10 ¹⁴N HAB, 13 ¹⁴N NAB and 12 ¹⁴N LAB mice, all males) was acquired.

Bacterial diet composition
20% <i>Ralstonia eutropha</i> [Lyophilized, ¹⁵ N-labeled (isotope enrichment >98%) or ¹⁴ N bacterial hydrolysate]
35% Sucrose
13% Maltodextrin
10% Corn Starch
0.3% L-Cystine
8% Soybean Oil
7.2% Cellulose
0.3% Calcium Phosphate, dibasic
0.025% Ferric Citrate
1.4% Vitamin Mix, AIN-93-VX (94047)
0.25% Choline Bitartrate
0.0024% Tert-butylhydroquinone, antioxidant
4.5% Mineral Mix, AIN-93M-MX (94049)

Table 3.1 Composition of the bacteria-based diet

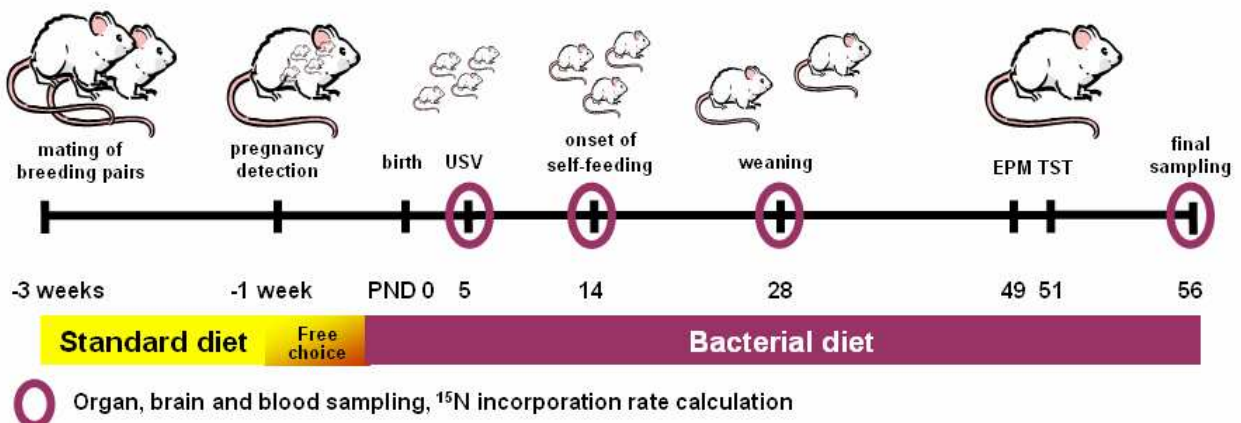


Figure 3.1 Bacterial diet breeding and feeding protocol



3.3.2. Behavioral testing

3.3.2.1 Ultrasonic vocalization test

It has been proposed that the number of USV calls induced by separation and isolation of the offspring from the dam can be considered as a measure of separation anxiety and is indicative of adult emotionality (Brunelli, 2005). Therefore, USV can be used to monitor anxiety-related behavior at an early developmental stage (Krömer et al., 2005). On PND 5, each pup was separated from its mother and was placed onto a Petri dish (diameter: 15cm, wall height: 1.5cm, temperature: 23°C kept constant by a water bath below the dish) having no olfactory or auditory contact to its litter (Fig. 3.2). USV was recorded for 5min using a Mini-3 Bat detector (Ultrasonic Advice, London, UK), fixed about 10cm above the pup and a WM-D6C tape recorder (Sony Professional, Cologne, Germany). The number of vocalization calls at 70kHz was quantified by Eventlog (v1.0, EMCO Software, Reykjavik, Iceland). Before the introduction of each pup, the dish was cleaned with a 70% alcohol solution.

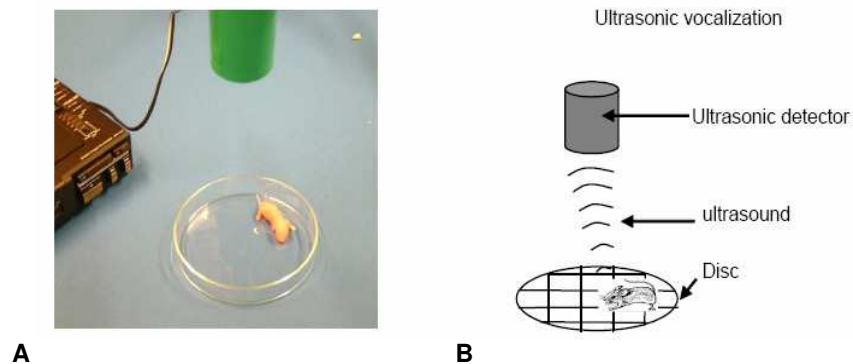


Figure 3.2 Ultrasonic vocalization test

A. Experimental set-up. **B.** Schematic overview of ultrasound recording by the ultrasonic detector (figure kindly provided by Dr. Mirjam Bunck).

3.3.2.2 Elevated plus-maze test

The EPM testing apparatus consists of a plus-shaped platform, 37cm elevated above the floor, with two open (30 x 5cm) and two closed (30 x 5 x 15cm) arms with a connecting central zone (5 x 5cm). The open arms were lit by white light of 300lux, the neutral zone by 60lux and the closed arms by 5lux. The EPM apparatus was surrounded by a black curtain to limit visual or auditory cues for the tested subject. Mice were transferred from their cage to the EPM apparatus and placed on the central part, facing one of the closed arms (Fig. 3.3). The % time spent on the open



arms (ratio of time spent on the open arms to total time spent on closed and open arms) and the total number of entries into all arms were recorded during a 5min exposure by Plus-maze (v2.0, Ernst Fricke, Munich, Germany). For all animals tested, EPM was performed on PND 49. Before the introduction of each mouse, the maze was cleaned with water containing detergent and 70% alcohol.

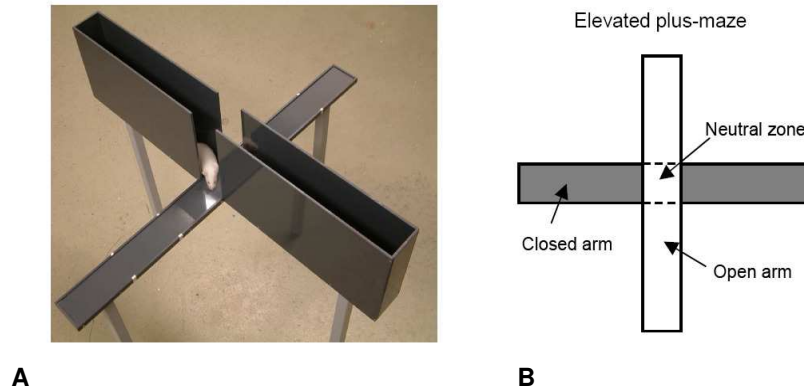


Figure 3.3 Elevated plus-maze test

A. Experimental set-up. **B.** Schematic overview of the different areas of the maze (figure kindly provided by Dr. Mirjam Bunck).

3.3.2.3 Tail suspension test

The TST is based on the fact that mice subjected to the short-term, inescapable stress of being suspended by their tail, immediately engage in active, escape-oriented behavior, followed progressively by increasing periods of immobility. Immobility is indicative of a passive, depression-like behavior (Cryan et al., 2005).

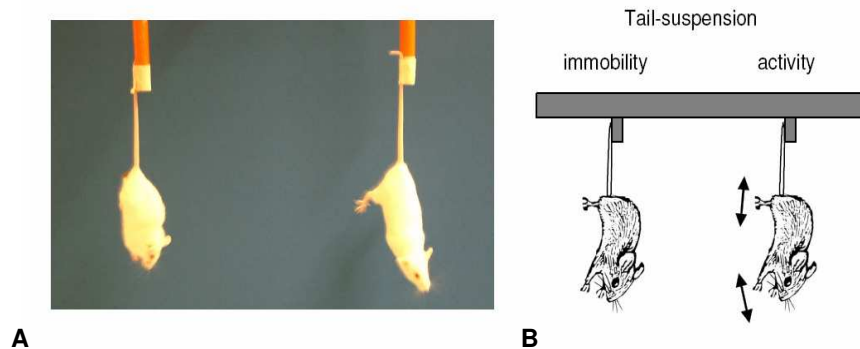


Figure 3.4 Tail suspension test

A. Experimental set-up. **B.** Schematic overview of the behavioral parameters assessed (figure kindly provided by Dr. Mirjam Bunck).



The TST experimental set-up consists of a horizontal plastic rod (length 75cm) at a height of 75cm with four vertical rods (15cm). Mice were suspended by their tails at a height of 35cm above the ground by an adhesive autoclave tape for 6min (Fig. 3.4). Four animals were tested simultaneously, and each trial was videotaped. Animal behavior (total immobility time) was analyzed using Eventlog (v1.0, EMCO Software). For behavioral test data analysis, data dependent on two or more variables were compared using univariate analysis of a general linear model, subsequently split and further analyzed by Student's t test (two tailed, unpaired). Bonferroni correction was applied to adjust for multiple comparisons (Frank et al., 2009).

3.3.3 Tissue acquisition

For tissue acquisition on PND 5, 14, 28 and 56, animals were anesthetized and perfused with 0.9% saline. Whole brain was extracted and cingulate cortex, cerebellum and hippocampus were dissected. Pituitary, thymus, heart, lung, liver, spleen, pancreas, adrenals, kidney and muscle were also harvested. Prior to perfusion, blood was collected and centrifuged at 13000g for 10min at 4°C to separate plasma from red blood cells. All samples were snap frozen in liquid nitrogen and stored at -80°C.

3.3.4 ¹⁵N metabolic labeling efficiency estimation

3.3.4.1 Proteomics sample preparation

¹⁵N metabolic labeling efficiency was monitored throughout the breeding protocol in brain and plasma at different time points (PND 5, 14, 28 and 56). Up to four ¹⁴N/¹⁵N mouse pairs were assessed per time point (cerebellum and plasma). Equal tissue weights of ¹⁴N/¹⁵N mouse cerebella pairs and equal volumes of ¹⁴N/¹⁵N plasma pairs were mixed. Brain samples were then homogenized in 250mM sucrose (Sigma Aldrich) buffer containing 50mM Tris-HCl (BioRad), 5mM MgCl₂ (Sigma Aldrich), 1mM dithiothreitol (BioRad), spermine (25µg/ml, Sigma Aldrich), spermidine (25µg/ml, Sigma Aldrich) and cocktail inhibitor tablets (Roche Diagnostics) and centrifuged at 25000g for 1h at 4°C. The supernatant was concentrated at 13000g, for 30min at 20°C using 3kDa cut off spin filters (Millipore). Plasma samples were diluted 1:10 (v/v) with 0.9% saline. Extracted protein mixtures from brain and plasma were resolved by 1D-gel electrophoresis and the gel stained with Coomassie brilliant blue R-250 (BioRad). Several gel bands were chosen, cut into small pieces, washed twice with 25mM ammonium bicarbonate (Merck)/50%



acetonitrile and digested with trypsin (5ng/μl, Promega) overnight at 37°C. Peptides were extracted with 50% acetonitrile/2% formic acid, lyophilized, redissolved in 10μl 0.5% trifluoroacetic acid (Sigma Aldrich) and desalted by OMIX tips (Varian).

3.3.4.2 MALDI-TOF/TOF MS-relative quantification

Samples were diluted 1:1 (v/v) with a saturated matrix solution of 4-hydroxy-alpha-cyanocinnamic acid (Bruker Daltonik), spotted onto an AnchorChip 600m target (Bruker Daltonik), air-dried at room temperature and then analyzed by MALDI-TOF/TOF MS. Ions were accelerated at +25kV with 0 nsec of pulsed ion extraction delay. Each spectrum was acquired in reflector positive mode summing 100 laser shots and externally calibrated by a peptide mixture standard (Bruker Daltonik). MS data were processed using the Flex analysis software (v3.0, Bruker Daltonik), and MS/MS data were searched against a Swissprot (v51.6) mouse database by the MASCOT software (v2.2, Matrix Science, London, UK). Dynamic oxidation of methionine and static carboxyamidomethylation of cysteine were set as amino acid modifications. Precursor and fragment ion tolerance was set to 150ppm and 0.7Da, respectively, allowing one missed cleavage for the tryptic digestion. MALDI MS raw spectra and MASCOT result files were exported to .dat and .xml formats, respectively and submitted to the in-house developed *QuantiSpec* software (Haegler et al., 2009) for calculation of ¹⁵N incorporation rates.

3.4 Biomarker and pathway discovery in the HAB/NAB/LAB mouse model of trait anxiety

3.4.1 Animals

¹⁴N bacteria-fed HAB and LAB mice were indirectly compared by using ¹⁵N NAB mice as internal standards (see Fig. 6.1). For the ¹⁴N HAB/¹⁴N LAB indirect line comparison, three ¹⁴N HAB/¹⁵N NAB and three ¹⁵N NAB/¹⁴N LAB bacteria-fed, PND 56 mouse pairs were analyzed by LC-ESI-MS/MS. Selection was based on the EPM performance (% time spent on the open arms), ensuring that the chosen mice accurately represent the HAB, NAB and LAB behavioral phenotype. The individual data of the animals studied with quantitative MS are given in Appendix 2. Western blot validation of selected differentially expressed proteins in ¹⁴N HAB and ¹⁴N LAB mice was conducted in an independent population of standard diet-fed (Altromin), HAB/NAB/LAB



animals of similar age as the bacteria-fed animals (n=8 per line). For quantitative MS and Western blot analyses, synaptosomes from cingulate cortices were studied. For quantitative metabolomics analysis, cingulate cortices from standard-fed HAB/NAB/LAB animals of similar age as the bacteria-fed animals were compared (n=6 per line).

3.4.2 Synaptosome enrichment from HAB/NAB/LAB cingulate cortices

Synaptosome enrichment and protein content estimation from HAB, NAB and LAB cortices were performed as described in 3.2.1 with slight modifications. For the bacteria-fed animals analyzed with MS, the ^{14}N and ^{15}N samples were processed separately until generation of the S1 supernatant. The S1 fractions from ^{14}N and ^{15}N cortices were then mixed 1:1 (w/w) based on protein content, and the combined fraction was used for synaptosome enrichment, as in 3.2.1. For the standard-fed animals used for Western blot analysis, synaptosome enrichment was performed as in 3.2.1.

3.4.3 Proteomics sample preparation from HAB/NAB/LAB synaptosomes

For quantitative MS, three ^{14}N HAB/ ^{15}N NAB and three ^{15}N NAB/ ^{14}N LAB animal pairs were compared. For each $^{14}\text{N}/^{15}\text{N}$ animal pair, 100 μg of the combined synaptosomal fraction from the corresponding $^{14}\text{N}/^{15}\text{N}$ cingulate cortices were resolved by 1D-gel electrophoresis, and the gel was stained with Coomassie brilliant blue R-250 (BioRad). Every gel lane was sliced into 25 fractions that were cut into small pieces and washed twice with 25mM ammonium bicarbonate (Merck)/50% acetonitrile, followed by reduction with 10mM dithiothreitol (BioRad) for 30min at 56 $^{\circ}\text{C}$ and carboxyamidomethylation with 50mM iodoacetamide (BioRad) for 30min at room temperature. Proteins were digested with trypsin (5ng/ μl , Promega) overnight at 37 $^{\circ}\text{C}$, and peptides were extracted twice with 50% acetonitrile/2% formic acid. For every fraction, peptides were lyophilized and dissolved in 10 μl 1% formic acid.

3.4.4 Mass spectrometry-relative quantification-data analysis

Five μl per fraction were analyzed by LC-ESI-MS/MS as described in 3.2.4. MS raw files were searched twice against a ^{14}N and a ^{15}N decoy IPI mouse database (v3.46), utilizing BioWorks (v3.3.1, Thermo Fisher Scientific) and SEQUEST (v28, Thermo Fisher Scientific) softwares. For both searches, precursor and fragment ion mass tolerance was set to 20ppm and 1Da,



respectively. Trypsin was chosen as enzyme and up to two missed cleavage sites and only fully tryptic peptides were allowed. Cysteine carboxyamidomethylation was used as static modification. Methionine oxidation was used as variable modification. Peptide identifications from both searches were exported as DTA files, combined and subsequently filtered and assembled into proteins by the DTASelect tool (v1.9, Tabb et al., 2002). To achieve a low false positive identification rate, the following filtering parameters were used: Minimum Delta Cn: 0.08; Xcorr: 1.90 ($z=1+$), 2.70 ($z=2+$), 3.50 ($z\geq 3+$); purging duplicate spectra on basis of the Xcorr ($-t=2$); minimum charge state: 1; maximum charge state: 6 and a minimum of one identified peptide per protein. Extracted ion chromatogram (XIC) generation as well as peptide and protein abundance ratio estimation was performed by the ProRata software (v1.0) using default parameters (Pan et al., 2006a). $^{14}\text{N}/^{15}\text{N}$ peptide pairs were used for relative quantification. The sum of the areas under each peak of the isotopologue pattern of the corresponding ^{14}N and ^{15}N peptide spectra were compared. Briefly, the identified peptides for every $^{14}\text{N}/^{15}\text{N}$ replicate were filtered and quantified with a minimum profile signal-to-noise ratio cutoff of 2. Proteins with at least two quantified peptides were evaluated for quantification. For the ^{14}N HAB/ ^{14}N LAB indirect comparison, the two ^{14}N HAB/ ^{15}N NAB and ^{15}N NAB/ ^{14}N LAB direct comparisons were combined, and proteins were further filtered with a maximum confidence interval (CI) width cutoff of 3. Quantification results were manually evaluated, and inaccurate quantifications due to incorrect isotopologue pattern assignment as well as quantified protein contaminants (e.g., keratin, hemoglobin) were excluded. To correct for potential mixing errors during sample preparation, quantification results were normalized by subtracting the median from all \log_2 ratios of the quantified proteins. Only proteins quantified in at least two out of three biological replicates per $^{14}\text{N}/^{15}\text{N}$ comparison were included for further analysis. Quantified proteins were considered to be differentially expressed when their ^{14}N HAB/ ^{14}N LAB protein abundance ratio was >1.3 fold, and the corresponding 95% CI did not contain 0.

3.4.5 HAB/NAB/LAB cingulate cortex metabolome comparison

For quantitative metabolomics analysis, lysates from cingulate cortices ($n=6$ per line) were compared. Samples were measured at the Metabolomics Core, UC Davis Genome Center, CA, USA by gas chromatography-time of flight-mass spectrometry (GC-TOF-MS), using a 6890 N gas chromatograph (Agilent Technologies, Palo Alto, CA, USA) interfaced to a TOF Pegasus III mass



spectrometer (Leco, St. Joseph, MI, USA). GC-TOF-MS was performed according to standard operation procedures, as previously described (Zou and Tolstikov, 2009). To identify a set of the most informative metabolites (i.e. those metabolites that could contribute reasonably to the discrimination between the HAB/NAB/LAB lines), two exploratory statistical analyses, namely random forest analysis (RF; Díaz-Uriarte and Alvarez de Andrés, 2006) and the in-house developed test- and functional-free biomarker searching method (TFFBS; Yassouridis et al., in preparation), were applied. Using the maximum set of metabolites selected by both methods as dependent variables and the animal line (HAB/NAB/LAB) as independent variable, a multivariate analysis of variance (MANOVA, Wilks multivariate tests of significance) was performed to verify whether there is a significant line effect on these metabolites and on which of them the effect is more pronounced. Bonferroni *post-hoc* tests at a 0.05 significance level were then applied to localize the line pairs, where each metabolite contributes significantly to the observed line differences. Finally, a discriminant analysis was conducted with the maximum set of metabolites selected by the exploratory methods to assess the discrimination power of the identified metabolite candidates.

3.4.6 Western blot validation of selected differentially expressed proteins

To confirm quantitative MS results of the ¹⁴N HAB/¹⁴N LAB indirect comparison, Western blot analysis was performed as described in 3.2.2 for the following primary antibodies: Anti-Sfxn5 (Abnova, Taipei, Taiwan, rabbit polyclonal, 1:100), anti-Car2 (Santa Cruz Biotechnology, goat polyclonal, 1:500), anti-Myh10 (Santa Cruz Biotechnology, goat polyclonal, 1:200) and anti-Sdhd (Abcam, mouse monoclonal, 1:1100). After development, autoradiographs were scanned, and quantification of the signal intensities was performed using QuantityOne (v4.4.0, BioRad). Signal intensity was measured as optical density x surface (OD*mm²). Student's t test (two tailed, unpaired) was employed to assess signal intensity differences between the groups under comparison.

3.4.7 *In silico* pathway analysis

For literature data mining and pathway visualization, Pathway Studio (v7.1, Ariadne Genomics, Rockville, MD, USA) was used. To identify altered pathways in HAB and LAB mice based on proteomics and metabolomics data, the HAB/LAB log₂ ratios of all quantified proteins and



metabolites were plotted in a combined histogram. Quantified proteins and metabolites were then assigned according to their HAB/LAB \log_2 ratios to five continuous bins: $(-\infty, -0.8)$, $[-0.8, -0.4)$, $[-0.4, 0.4]$, $(0.4, 0.8]$, $(0.8, +\infty)$. The contents of each bin were compared to Kyoto encyclopedia of genes and genomes (KEGG; Kanehisa and Goto, 2000) to identify overrepresented pathways per bin. The hypergeometric test was calculated for each pathway per bin using the statistical language R (www.R-project.org). The p value threshold for significantly enriched pathways was set to 0.01. Pathways with significant enrichment in at least one bin were then hierarchically clustered.

3.5 ^{15}N isotope effect investigation in HAB mice and *Escherichia coli*

3.5.1 Animals

For the ^{14}N HAB/ ^{15}N HAB comparison, three bacteria-fed, PND 56 ^{14}N HAB/ ^{15}N HAB mouse pairs were compared by LC-ESI-MS/MS. Selection criterion was their TST performance (immobility time), with the average immobility time of the ^{14}N HAB being higher than the average immobility time of the ^{15}N HAB mice, depicting the antidepressant-like effect of ^{15}N on the behavioral phenotype of HAB mice (see 5.2.1.2). The individual data of the HAB mice studied with quantitative MS are shown in Appendix 2. Western blot validation of differentially expressed proteins was performed in an independent population of bacteria-fed, PND 56 ^{14}N HAB (n=4) and ^{15}N HAB (n=7) mice. Cingulate cortex synaptosomes were analyzed with quantitative MS. For Western blot analysis, the cingulate cortex cytoplasmic fraction (S1 supernatant from the synaptosome protocol, see 3.2.1) was used. For the ^{14}N HAB/ ^{15}N HAB MS comparison, synaptosome enrichment, proteomics sample preparation and quantitative MS were performed as described in 3.2.1, 3.4.3 and 3.4.4, respectively. Only proteins whose ^{15}N HAB/ ^{14}N HAB abundance ratio was >1.3 fold, and CI did not contain 0 both at the level of individual replicates and at the level of average CI of all replicates were considered to be differentially expressed.

3.5.2 *Escherichia coli* culture

E. coli BL21star strain (Invitrogen, San Diego, CA, USA) was taken from glycerol stocks, scraped with a sterile loop, streaked out on a LB-agar plate with 100 $\mu\text{g}/\text{ml}$ ampicillin (Sigma Aldrich) as selective marker and incubated overnight at 37 $^{\circ}\text{C}$. Single colonies were taken and inoculated in



2ml of either unlabeled ^{14}N (Spectra 9-U) or ^{15}N -enriched (Spectra 9-N, >98%) media (Cambridge Isotope Laboratories, Andover, MA, USA) with 100 $\mu\text{g/ml}$ ampicillin. The pre-cultures were incubated for 6h at 37 $^{\circ}\text{C}$ with shaking at 220rpm, inoculated into 100ml of the ^{14}N or ^{15}N media containing 100 $\mu\text{g/ml}$ ampicillin and incubated overnight at 37 $^{\circ}\text{C}$ with shaking at 220rpm. The cultures were then centrifuged at 5000rpm for 15min at 4 $^{\circ}\text{C}$, supernatants were discarded, and ^{14}N and ^{15}N *E. coli* pellets were frozen. For quantitative MS and Western blot analyses, the ^{14}N and ^{15}N pellets were dissolved in lysis buffer (1ml/100ml culture) consisting of 100mM Tris-HCl (BioRad) pH 8.0, 150mM NaCl (Merck), 1mM EDTA (Sigma Aldrich) and sonicated to break the *E. coli* cells. The lysates were centrifuged at 13000rpm for 12min at 4 $^{\circ}\text{C}$, and supernatants containing the cytoplasmic fraction were collected.

3.5.3 *Escherichia coli* proteomics sample preparation-mass spectrometry

The ^{14}N and ^{15}N *E. coli* cytoplasmic fractions were combined 1:1 (w/w) based on protein content, 100 μg of the $^{14}\text{N}/^{15}\text{N}$ mixture were resolved by 1D-gel electrophoresis, and the gel was stained with Coomassie brilliant blue R-250 (BioRad). In gel digestion and peptide extraction were performed as described in 3.4.3. For every fraction, extracted peptides were lyophilized and dissolved in 10 μl 1% formic acid. Five μl were then loaded onto an in-house packed column and analyzed by LC-ESI-MS/MS as described in 3.2.4. Two technical replicates were measured per fraction.

3.5.4 *Escherichia coli* proteomics data analysis

For protein identification, a concatenated, forward/reverse decoy MSDB (<ftp://ftp.ncbi.nih.gov/repository/MSDB>) *E. coli* database was used. Database search and relative quantification were performed as previously described (see 3.4.4). Per replicate, proteins with at least two quantified peptides were evaluated for quantification. Peptides with the same sequence but different charge states were quantified as different entities. Peptides with the same sequence and charge state were grouped, provided that their MS/MS scans were acquired within a 2min interval (Pan et al., 2006b). Quantification results were manually evaluated, and inaccurate quantifications due to incorrect isotopologue pattern assignment were excluded. In the quantified dataset, for protein IDs corresponding to the same protein name, the amino acid sequences were manually checked. In all cases, every protein ID corresponded to a different protein variant and



therefore was treated as a separate protein entity. For every protein variant, variant-specific peptides were identified by MS. Quantification results were normalized by subtracting the median from all \log_2 ratios of the quantified proteins. Proteins were considered to be differentially expressed when their $^{14}\text{N}/^{15}\text{N}$ abundance ratio was >1.3 fold, and their 95% CI did not contain 0 in both replicates. Proteins quantified only in one of the two replicates were not considered for further analysis. Quantification reproducibility between the two replicates was assessed by Pearson correlation analysis that measures linear dependence between two variables.

3.5.5 Western blot validation of selected differentially expressed proteins

Western blot analysis and signal intensity quantification were performed as in 3.2.2 and 3.4.6, respectively. For the ^{14}N HAB/ ^{15}N HAB comparison, the anti-TnR (Santa Cruz Biotechnology, goat polyclonal, 1:400) and anti-Nefm primary antibodies (Abcam, rabbit polyclonal, 1:1000) were used. For the $^{14}\text{N}/^{15}\text{N}$ *E. coli* comparison, five μg of ^{14}N and ^{15}N *E. coli* cytoplasmic fractions were resolved by 1D-gel electrophoresis. An anti-beta galactosidase (LacZ) primary antibody (Novus Biologicals, Littleton, CO, USA, chicken polyclonal, 1:10000) and a secondary anti-rabbit antibody (GE Healthcare) were used. Five technical replicates were evaluated per *E. coli* group.

3.5.6 Pyruvate assay of $^{14}\text{N}/^{15}\text{N}$ *Escherichia coli* cytoplasm

Pyruvate levels in the ^{14}N and ^{15}N *E. coli* cytoplasm were assessed using a pyruvate assay kit (Biovision, Mountain View, CA, USA). ^{14}N and ^{15}N *E. coli* culture pellets were dissolved in 1ml pyruvate assay buffer each, centrifuged, supernatant collected, and the colored product of pyruvate oxidation by pyruvate oxidase was measured in triplicate using a GENios Pro microplate reader (Tecan, Männedorf, Switzerland) according to manufacturer's instructions. ^{14}N and ^{15}N group differences were statistically evaluated by Student's t test (two tailed, unpaired).

3.5.7 *In silico* pathway analysis

For the ^{14}N HAB/ ^{15}N HAB comparison, the FatiGO online tool (<http://babelomics3.bioinfo.cipf.es>) was used to compare over- or underrepresented functional groups in the differentially expressed and all quantified proteins. Pathway Studio (Ariadne Genomics) was utilized for literature data mining and pathway visualization. For the $^{14}\text{N}/^{15}\text{N}$ *E. coli* comparison, the functional clustering annotation tool DAVID (Dennis et al., 2003; <http://david.abcc.ncifcrf.gov/home.jsp>) was used.



3.6 Biomarker discovery in the G72/G30 transgenic mouse model of schizophrenia-like symptoms

3.6.1 Animals

Two transgenic mouse lines, G72Tg1 and G72Tg2, were generated carrying four and six copies of the human BAC clone RP11-111A8 containing the whole G72/G30 genomic region, respectively (see 1.3.3; Otte et al., 2009). Dissected cerebella from transgenic (G72Tg1 and G72Tg2, heterozygotes) and WT CD1 adult mice, bred in the animal facility of the University of Bonn were received for analysis.

3.6.2 Sample preparation from G72/G30 transgenic and wild type cerebella

Mouse brain cerebella were homogenized to powder in liquid nitrogen with mortar and pestle, and homogenates were solubilized using the PlusOne sample grinding kit (GE Healthcare) in IEF rehydration buffer [7M urea (Genaxxon), 2M thiourea (Sigma Aldrich), 100 mM dithiothreitol (BioRad), 4% CHAPS (BioRad), 0.2% biolytes (BioRad), 0.001% bromophenol blue (BioRad), phosphatase inhibitors (Sigma Aldrich), protease inhibitors (Roche Diagnostics) and pepstatin (Roche Diagnostics)].

3.6.3 Two-dimensional Western blot

Cerebellar homogenates from G72Tg1 transgenic and WT mice were compared. Per sample, 150µg of cerebellar protein homogenates were applied on pH 3-10, 11cm, non-linear IPG strips (BioRad), followed by active rehydration for 12h at 50V and IEF until 35kVh were reached. IPG strips were then layered on top of 10-20% linear gradient Criterion Tris-HCl gels (BioRad). After electrophoresis, proteins were transferred for 1h at 100V to Immobilon PVDF membranes (Millipore), followed by overnight blocking with 5% (w/v) Carnation instant non-fat dry milk in TBS-T buffer at 4°C. Membranes were simultaneously incubated for 2h at room temperature with the 1410 (1:200) and 1411 (1:350) anti-G72, rabbit polyclonal antibodies (non-commercially available, provided by Dr. Isabel Benzel), followed by incubation with an anti-rabbit secondary antibody (GE Healthcare) for 45min at room temperature. After each incubation step, membranes were rinsed with TBS-T. Membranes were treated with ECLplus (GE Healthcare) for 5min, transferred to a Hypercassette (GE Healthcare) and exposed to Hyperfilm (GE Healthcare). Both 1410 and 1411



anti-G72 antibodies are directed against a peptide within G72 variant AY138546 (VTRKEGWKRRHEDGY). Generation, purification and validation of these antibodies are described elsewhere (Benzel et al., 2008).

3.6.4 Two-dimensional polyacrylamide gel electrophoresis

Three G72Tg1 and three G72Tg2 mice were compared to three WT per line. Per sample, 150 μ g cerebellar protein homogenates were applied on pH 3-10, 17cm, non-linear IPG strips (BioRad). IPG strips were actively rehydrated for 12h at 50V until 60kVh were reached. After equilibration for 15min in 2% dithiothreitol (BioRad) and 13min in 2.5% iodoacetamide (BioRad), IPG strips were layered on top of a 12.5% SDS polyacrylamide gel and run overnight at 150V. Gels were fixed in 10% acetic acid/50% methanol and treated with ProQ diamond fluorescent phosphoprotein stain (Invitrogen), followed by colloidal Coomassie brilliant blue G (Sigma Aldrich). ProQ and Coomassie stained gel images were acquired with a fluorescent Molecular Imager FX (BioRad) and a GS-800 Calibrated Densitometer (BioRad), respectively. Image analysis, spot intensity quantification and normalization were performed with the PDQuest Advanced 2D analysis software (v8.0, BioRad).

3.6.5 Identification of differentially expressed proteins

Gel spots representing protein expression differences between the G72/G30 transgenic and WT mice were excised, destained with 20mM ammonium bicarbonate (Merck)/acetonitrile 1:1 (v/v), air-dried overnight and digested with trypsin (5ng/ μ l, Promega) in 1mM ammonium bicarbonate (Merck, 15min at 40 $^{\circ}$ C, 5h at 37 $^{\circ}$ C). Peptides were extracted twice in 2% trifluoroacetic acid and acetonitrile/2% trifluoroacetic acid 1:1 (v/v), lyophilized and dissolved in 5 μ l 0.3% trifluoroacetic acid. MALDI-TOF/TOF MS was performed as described in 3.3.4.2. Only hits with confidential index >95% were considered significant. For the identified differentially expressed proteins, Pathway Studio (Ariadne Genomics) was utilized for literature data mining and pathway visualization.



4 Profiling of mouse synaptosome proteome and phosphoproteome

4.1 Introduction

Synapses are the main structures for inter-neuron communication. Neurotransmitter- and signal transduction-related events represent brain responses to behavioral experience (Bai and Witzmann, 2007). Since synapses constitute the fundamental information processing unit in the brain, synaptic dysfunction is believed to be an underlying mechanism for psychiatric and neurodegenerative disorders (Mohn et al., 1999; Snyder et al., 2005; Südhof, 2008). At the post-translational modification level, reversible synaptic phosphorylation is required for basal neurotransmission (Smart, 1997) and is involved in learning and memory (Sunyer et al., 2008). Protein kinases and phosphatases have been implicated in the regulation of neurotransmitter release (Takahashi et al., 2003), receptor trafficking (Braithwaite et al., 2006), long term potentiation (Malenka and Nicoll, 1999) and memory consolidation (Bozon et al., 2003). Therefore, a thorough characterization of the synaptic proteome and phosphoproteome is crucial for understanding the organization of the synaptic machinery and its role in health and disease.

Synaptosomes are artificially produced, isolated synapses. After mild disruption of brain tissue, nerve terminals detach from their axons and post-synaptic and glial cells to which they are connected. Subsequently, the pre-synaptic membranes reseal and enclose the nerve terminal contents to form synaptosomes. Synaptosomes are made up of the entire pre-synaptic terminal (mitochondria, cytoplasm, cytoskeleton, external membranes and synaptic vesicles) and often a part of the attached post-synaptic side (post-synaptic membrane and post-synaptic density) (Schrimpf et al., 2005). Under metabolizing conditions, synaptosomes respire, take up oxygen and glucose, maintain a normal membrane potential and release neurotransmitters in a calcium-dependent manner (Whittaker, 1993), thus retaining the molecular neurotransmission machinery and mimicking synaptic function *in vivo*.

The synaptic machinery is of paramount importance in anxiety pathophysiology. Anxiety disorders are associated with alterations in neurotransmission, including serotonin, dopamine and gamma-aminobutyric acid (GABA) neurotransmitter systems (Nemeroff, 2003; Stein et al., 2002).



Furthermore, current anxiolytic treatment regulates neurotransmission (Gorman, 2002), neurotransmitter modulators constitute potential therapeutic targets (Nemeroff, 2003), and neurotransmitter receptors modulate anxiety levels (Barkus et al., 2010). Conceptually, the equilibrium between excitatory and inhibitory neurotransmission is critical for physiological anxiety, and disturbances of this synaptic balance can lead to pathological anxiety (Wu et al., 2008). Due to the pivotal role of synaptic neurobiology in anxiety manifestation, synaptosomes were chosen to be studied for identifying disease-specific markers and elucidating the molecular mechanisms underlying anxiety-related behavior in the HAB/NAB/LAB mouse model (Chapter 6).

Before comparing the synaptosome proteomes of HAB/NAB/LAB mice in a quantitative manner, a profiling of the synaptosome proteome and phosphoproteome of a CD1 mouse was performed to get insights into the protein composition of synaptosomes, and create a reference protein map for the subsequent quantitative proteomics experiments. It has been previously shown in our group that IEF can be used for phosphopeptide enrichment (Maccarrone et al., 2006). To achieve a simultaneous, comprehensive analysis of the mouse synaptosome proteome and phosphoproteome, IEF was employed as a fractionation step, followed by LC-ESI-MS/MS.

4.2 Results

4.2.1 Western blot analysis of selected synaptosomal proteins

To evaluate the specificity of the synaptosome enrichment procedure and investigate the expression of selected identified proteins in synaptosomes, a Western blot analysis was performed using fractions from different steps of the synaptosome enrichment protocol. A cytosolic fraction of a whole mouse brain was additionally included. Antibodies for synaptic proteins (anti-Gria2, anti-PSD95 and anti-Slc17a7) were used to test for synaptosome enrichment specificity. Glutamate receptor 2 (Gria2 or GluR2) binds L-glutamate in excitatory synapses activating ion transport channels. Discs large homolog 4 (PSD95) is a post-synaptic density protein marker, whereas brain specific sodium-dependent inorganic phosphate co-transporter (Slc17a7 or VGlut1) takes up glutamate into synaptic vesicles at pre-synaptic nerve terminals. All three antibodies showed satisfactory enrichment in the synaptosomal fraction and were not present in nuclei or in the supernatants S2 and S3 that do not include the synaptosomal fraction (see 3.2.1). Cytosolic proteins such as mu-crystallin (Crym) and protein kinase C family members



(Prkcb1, Prkcc, Prkce) were present but not specific for the synaptosomal fraction, as expected. Neuromodulin (Gap43), a neuronal marker, was also present in the synaptosomal fraction. Myelin basic protein (Mbp), which is involved in axon myelination and is commonly present as impurity in synaptosome preparations, was not detected in the synaptosomal fraction (Fig. 4.1).

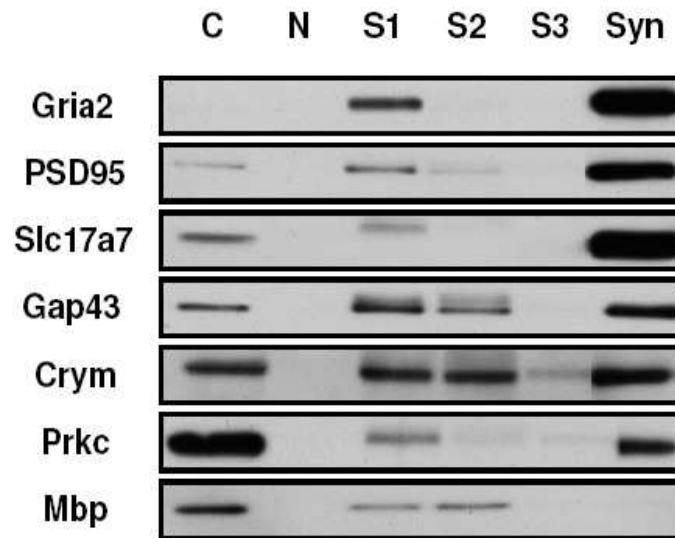


Figure 4.1 Western blot analysis of selected proteins in different steps of the synaptosome enrichment protocol

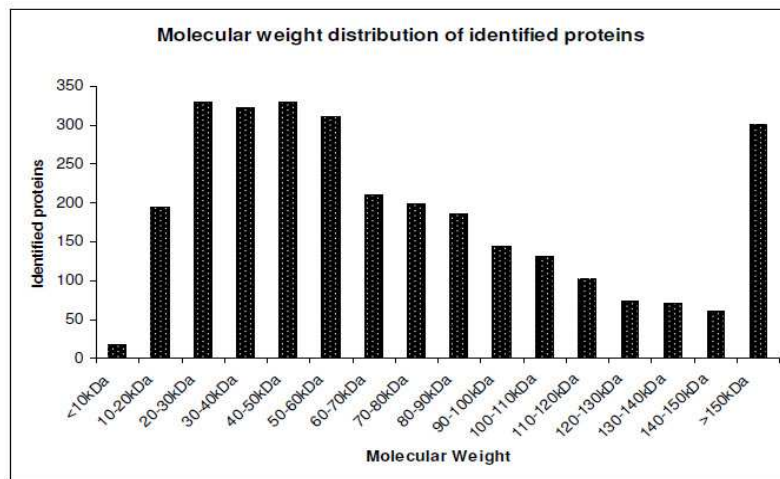
For the synaptosome-specific proteins *Gria2*, *PSD95* and *Slc17a7*, no signals in *N*, *S2* and *S3* fraction as well as enriched signals in *Syn* fraction were detected. The neuronal-specific protein *Gap43* and the cytosolic proteins *Crym* and *Prkc* exhibited a wide expression pattern including the *Syn* fraction. No detectable signal for *Mbp* was observed in *Syn* fraction. Nuclear fraction *N* was used as a negative control for non-nuclear proteins.

N: Nuclear fraction; *C*: Cytosolic fraction; *S1*, *S2*, *S3*: Successive supernatants in the synaptosome enrichment protocol (see 3.2.1); *Syn*: Synaptosomal fraction; *Slc17a7*: Brain-specific sodium-dependent inorganic phosphate co-transporter; *Gria2*: Glutamate receptor 2; *PSD95* (*Dlg4*): Post-synaptic density protein 95; *Gap43*: Neuromodulin; *Prkc*: Protein kinase C family; *Crym*: Mu-crystallin; *Mbp*: Myelin basic protein.

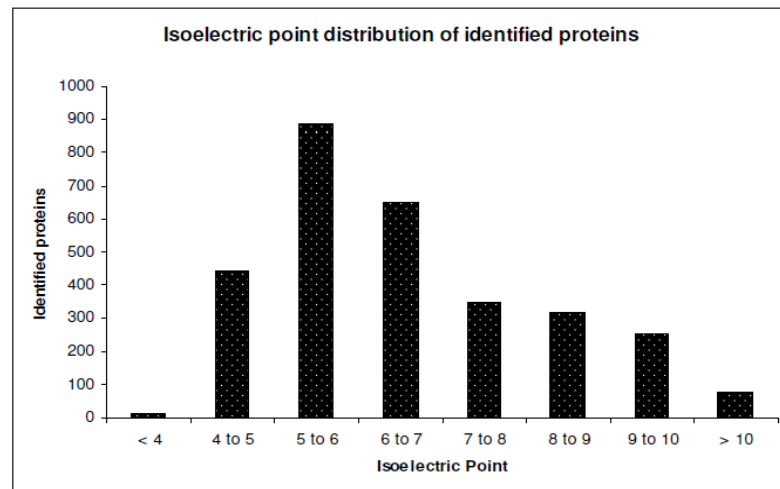


4.2.2 Synaptosome proteome

Analysis of whole mouse brain synaptosomes resulted in the identification of 4794 non-redundant protein hits, 2980 of which were identified with more than two peptides. False positive identification rate at the protein level was 0.35% after filtering and excluding one peptide hits using a decoy database. The identified proteins cover a wide range of molecular weights and isoelectric points (Fig. 4.2). The complete list of all identified proteins is available online (Filiou et al., 2010a; Table S1).



A



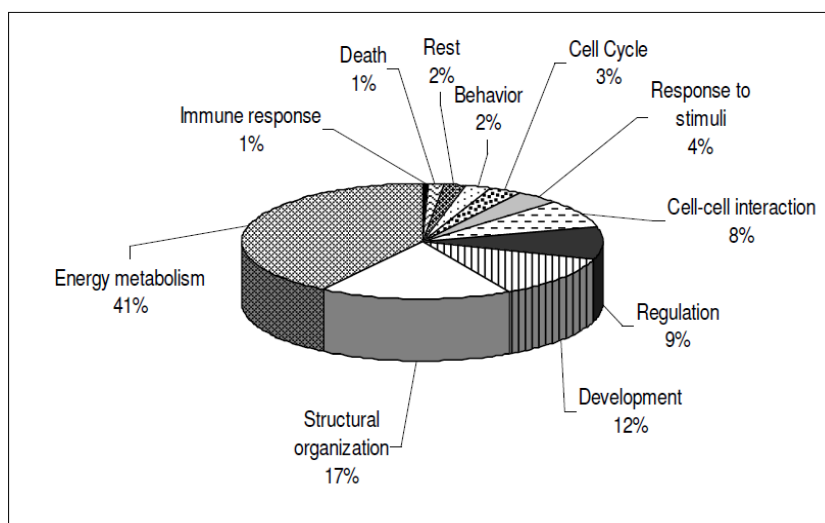
B

Figure 4.2 Physicochemical properties of synaptosomal proteins

A. Molecular weight distribution. **B.** Isoelectric point distribution.



Among the identified proteins were key components of synaptic function, including proteins involved in vesicle transport [synaptotagmin 1-3 (Syt1-3), vesicle-associated membrane proteins 1-4 (Vamp1-4)], clathrin-mediated endocytosis [clathrin light chain B (Cltb), clathrin heavy chain (Cltc), isoform long of clathrin coat assembly protein AP180 (Snap91)] and post-synaptic density components [discs large homologs 1-4 (Dlg1-4), homer protein homologs 1-3 (Homer1-3), gephyrin (Gphn), calcium/calmodulin-dependent protein kinase type II (CaMKII)]. In addition, cytoskeletal proteins and metabolic enzymes, including the complete list of enzymes that are part of the citric acid cycle as well as enzymes involved in glycolysis and fatty acid metabolism were detected. Potential therapeutic targets for brain disorders, such as sodium- and chloride-dependent GABA transporter 1 (Slc6a1) (LaRoche and Helmers, 2004), superoxide dismutase (Sod1) (Zhang et al., 2009a) and myristoylated alanine-rich C-kinase substrate (Marcks) (Watson et al., 1998) were also identified. GO analysis indicated that the majority of the annotated proteins are implicated in energy metabolism (41%), followed by structural organization (17%) and developmental processes (12%) (Fig. 4.3A). Enzyme/enzyme regulator activity characterizes 28% of the proteins, whereas 22% are involved in protein-protein interactions (Fig. 4.3B). Interestingly, many identified proteins participate in phosphorylation-related processes; 200 proteins exhibit kinase activity (GO: 0016301), 152 proteins phosphotransferase activity (GO: 0016773), 193 pyrophosphatase activity (GO: 0016462), while 18 proteins bind to kinases (GO: 0019900), and 493 proteins are involved in signal transduction (GO: 0007165).



A

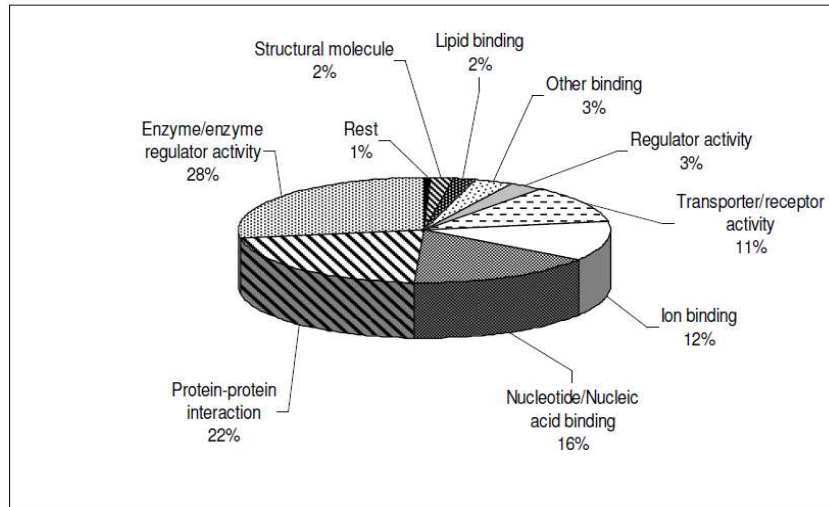
**B**

Figure 4.3 Gene Ontology analysis of the synaptosome proteome

A. Biological process annotation. **B.** Molecular function annotation.

4.2.3 Synaptosome phosphoproteome

The interrogation of mouse synaptosomes for phosphoproteins resulted in the identification of 264 phosphorylation sites, 205 of which were unambiguously assigned. Of the total phosphosites identified, 69% represent serine (S), 28% threonine (T) and 3% tyrosine (Y) modifications in accordance to the relative distribution of modified residues in other large scale mouse synaptic phosphoproteome studies (Collins et al., 2005; Trinidad et al., 2006). The identified phosphosites correspond to 133 unique phosphopeptides belonging to 118 phosphorylated proteins (Appendix 3). Intriguingly, eight identified proteins (Atcay, Cadps, Cartpt, Cend1, Kcnc3, Pcsk1n, Rgs6, Slc7a8) are reported for the first time to be phosphorylated (Table 4.1). In detail, calcium-dependent secretion activator 1 (Cadps or Caps1) is an essential component of the synaptic vesicle machinery (Jockusch et al., 2007). Cell cycle exit and neuronal differentiation protein 1 (Cend1) participates in cell cycle exit and differentiation coordination of neuronal precursors (Politis et al., 2007). Isoform Kv3.3B of potassium voltage-gated channel subfamily C member 3 (Kcnc3) is a potassium channel protein expressed in cerebellum (Goldman-Wohl et al., 1994). Regulator of G-protein signaling 6 (Rgs6) controls secondary messenger cascades and interacts with transcription regulatory proteins (Liu and Fisher, 2004). Caytaxin (Atcay) inhibits kidney-type glutaminase, an enzyme that converts glutamine to glutamate and may thus regulate glutamate synthesis in synapses during neurotransmission (Buschdorf et al., 2006). Furthermore, large

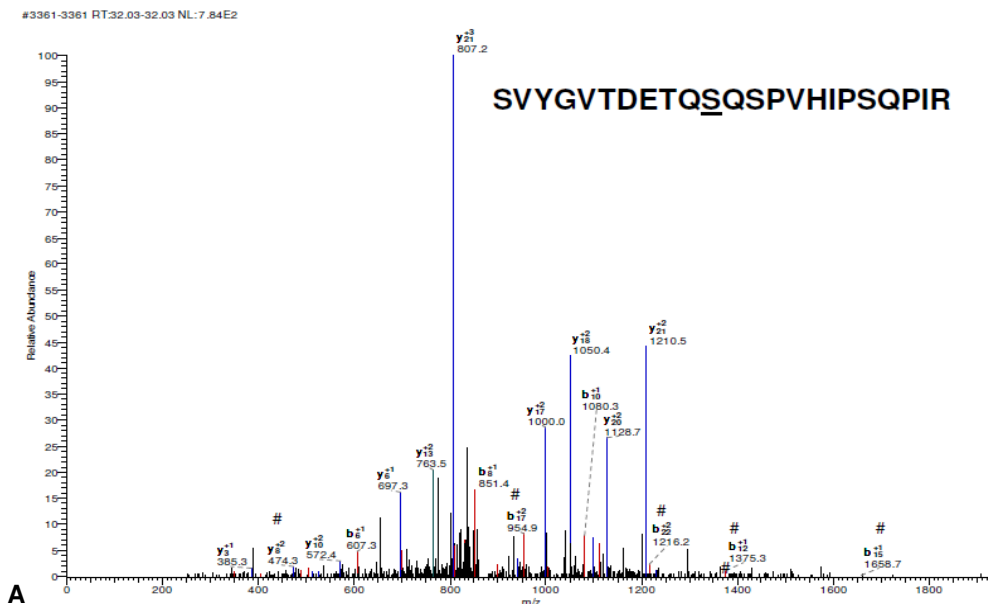


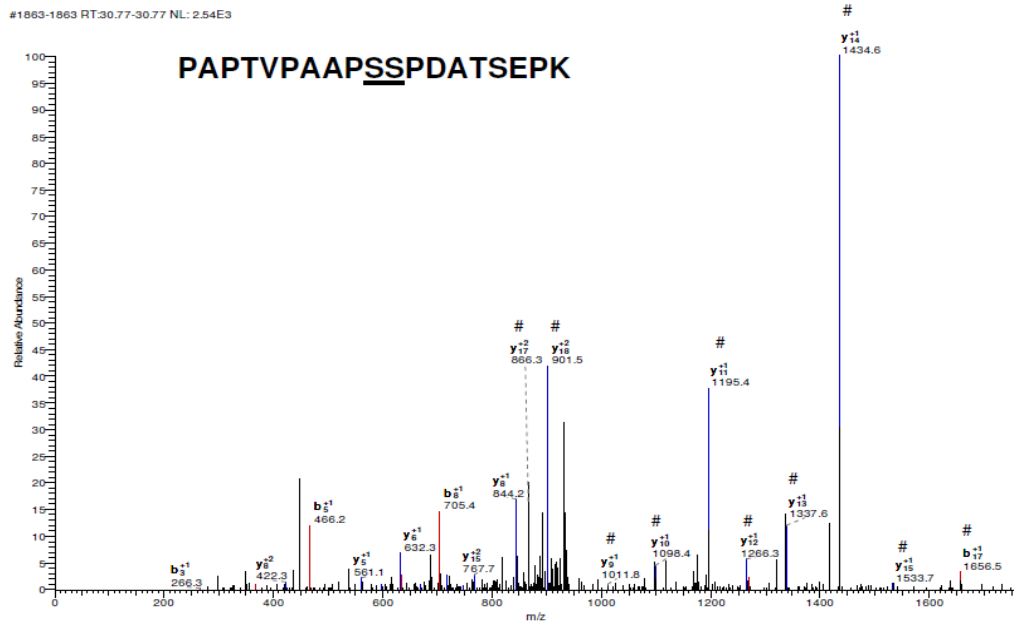
neutral amino acids transporter small subunit 2 (Slc7a8) is an amino acid transporter, whereas cocaine- and amphetamine-regulated transcript protein precursor (Cartpt) and proprotein convertase 1 inhibitor ProSAAS (Pcsk1n) are important neuropeptides for brain function. MS/MS spectra of novel phosphosites for the Rgs6 and Cend1 proteins are shown in Fig. 4.4. GO analysis of the phosphorylated dataset showed that major functional categories are energy metabolism (25%), structural organization (21%) and developmental processes (15%) (Fig. 4.5A). Moreover, 37% of the phosphorylated proteins are involved in protein-protein interactions, followed by enzyme/enzyme regulator activity (18%) (Fig. 4.5B).

Protein	Phosphorylated peptide	Phosphorylated residues
Atcay	LGGAVEDSSSPSTLNLSGAHR	<u>S8</u> S10
Cadps	PSSPSPSVVSEK	<u>S5 S7 S10</u>
Cartpt	ALDIYSAVDDASHEK	S6 <u>S12</u>
Cend1	PAPTVPAAAPSSPDATSEPK	<u>S10 S11 T15 S16</u>
Kcnc3	SLSSIVGLSGVSLR	<u>S1 S3</u>
Pcsk1n	ILTGSSEPEAAPAPR	T3
Rgs6	SVYGVTD <u>ET</u> QSQSPVHIPSQPIR	<u>T6 T9 S11</u>
Slc7a8	NHPGSDTSP <u>EA</u> EASSGGGGVALK	<u>S5 T7 S14</u> S15

Table 4.1 Novel phosphorylated synaptosomal proteins and their assigned sites of phosphorylation

Eight novel phosphorylated proteins were identified. Underlined residues indicate unambiguously assigned phosphosites.

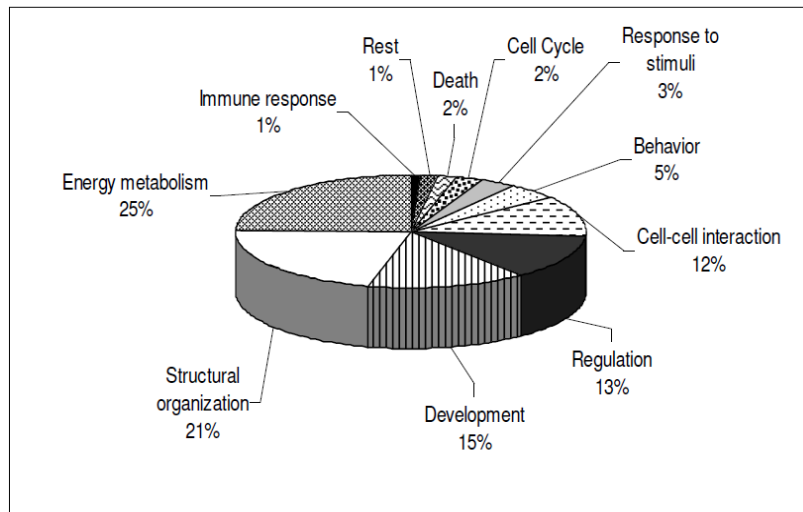




B

Figure 4.4 Representative MS/MS spectra of novel phosphosites

A. Phosphorylation at S11 for the *Rgs6* peptide SVYGVTD^{S11}EQSQSPVHIPSQPIR was unambiguously assigned. **B.** For the *Cend1* peptide PAPTVPAAAPSSPDATSEPK, phosphorylation at S10 and S11 could not be unambiguously assigned. In the MS/MS spectra, the mono, double and triple charged b and y ions identified are shown. Peaks marked by (#) in the ion superscript denote phosphorylated fragment ions. Underlined in the peptide sequence are the (potential) phosphorylation sites. Red and blue peaks correspond to b and y ions, respectively.



A

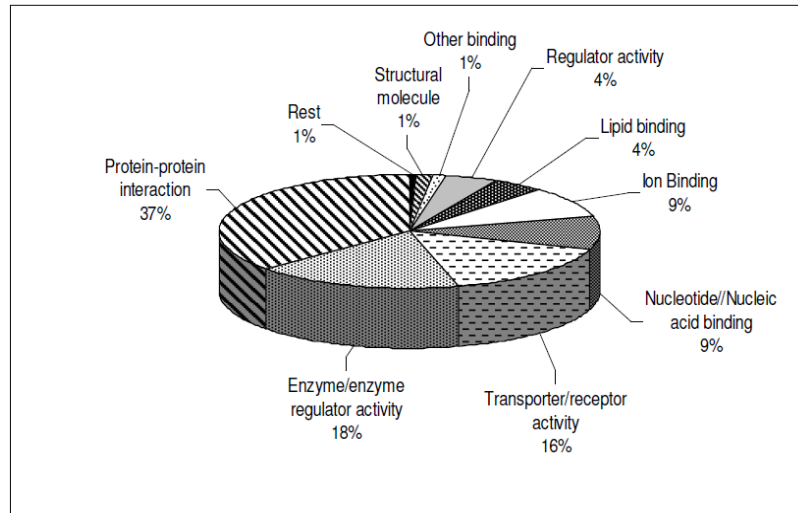
**B**

Figure 4.5 Gene Ontology analysis of the synaptosome phosphoproteome

A. Biological process annotation. **B.** Molecular function annotation.

4.3 Discussion

Although a number of studies have been performed to characterize the synaptic mouse proteome, comprehensive proteomics investigations of mouse synaptosomes have been rare. In the only study where the whole mouse brain synaptosome proteome was examined, Schrimpf and colleagues analyzed synaptosomes by isotope-coded affinity tags, strong cation exchange chromatography and LC-ESI-MS/MS and identified 1113 proteins (Schrimpf et al., 2005). Here, an in-depth analysis of the mouse synaptosome proteome and phosphoproteome is presented. We identified 2980 unique proteins with two or more peptides, including 118 phosphoproteins, which is the most detailed mouse synaptosome protein dataset described to date (Filiou et al., 2010a). IEF is an effective fractionation method at the peptide level compared to classical 1D-gel electrophoresis at the protein level (Filiou, unpublished observations), resulting in a comprehensive analysis of brain tissue subproteomes. IEF fractionation is a highly sensitive method for the detection of low stoichiometry proteins and significantly increases the dynamic range of the analysis. A substantial number of low abundant proteins identified by only two or few peptides are reported. For the synaptic proteome, the successful identification of such proteins is of major importance since the key components of the synaptic machinery that are responsible for



neurotransmission and synaptic plasticity (e.g., neurotransmitters and their receptors) are present in very low amounts.

GO analysis of the protein dataset showed that apart from neurotransmission and synaptic plasticity, synaptosomal proteins participate in a variety of biological processes, including metabolism and development (Fig. 4.3A). Interestingly, 109 proteins participate in response to stress (GO: 0006950) and 125 in apoptosis (GO: 0006915), indicating that the synapse itself has developed mechanisms to retain its homeostasis. Our data support the observation that the molecular complexity of the synaptic proteome is greater than expected (Pocklington et al., 2006). Isolation of synaptosomal proteins is innately demanding, since synaptosomes constitute no pre-existing subcellular organelle. Employing a well-established protocol, also used by others (Witzmann et al., 2005), only few protein identifications indicated contamination from astrocytes, myelin and serum (astrocytic phosphoprotein, myelin-forming proteins, albumin), whereas Western blot analysis showed satisfactory enrichment and specificity for synaptic proteins. No myelin basic protein, a myelin contamination marker, was detected (Fig. 4.1), thus ensuring the validity of the current protocol to study synaptosomes in an accurate manner and to be further used for quantitative studies of the synaptosome proteome (Chapter 6).

IPG-based fractionation was applied to analyze complex protein mixtures from mouse brain and investigate the synaptosome phosphoproteome without employing additional steps for phosphoprotein enrichment. To date, only one other study has employed IEF to analyze phosphopeptides in brain tissue (Beranova-Giorgianni et al., 2006). In that report, a human pituitary protein extract was analyzed by IEF, and peptide mixtures were enriched for phosphopeptides with immobilized metal affinity chromatography resulting in the identification of 73 phosphorylated peptides corresponding to 26 proteins. In the present study, 133 phosphopeptides corresponding to 118 phosphoproteins were identified using a comparable amount of tissue. Large scale synaptosome phosphoproteome studies (Collins et al., 2005; Munton et al., 2007) often employ additional steps such as immobilized metal affinity or strong cation exchange chromatography to specifically enrich for phosphopeptides. In the current study, no additional phosphoenrichment step was performed, and both the synaptic proteome and phosphoproteome were investigated. This accounts for the relatively lower number of identified phosphopeptides compared to studies focusing exclusively on the phosphoproteome. Due to the low stoichiometry and the reversible nature of phosphorylation, the presence of phosphoproteins



may be masked by the expression of high abundant synaptic proteins making their identification in a complex mixture challenging.

Taken together, a considerable percentage of the synaptosome proteome is involved in the regulation of phosphorylation and dephosphorylation events, suggesting that this post-translational modification is of major importance in synaptic terminals. We performed a detailed literature search of the phosphorylated dataset and found 33 proteins that are reported to be implicated in psychiatric/neurodegenerative disorders. Among these, 13 proteins have been shown to be associated with more than one disorder, suggesting a possible role in multiple disease pathways (Filiou et al., 2010a). Remarkably, phosphorylation events in eight neuronal-specific proteins are for the first time reported. Four of the novel phosphorylated proteins (Atcay, Carptp, Slc8a2, Pcsk1n) have been implicated in neuropsychiatric disorders. The novel phosphorylation sites found in the present study may point out relevant mechanisms involved in disease pathobiology and deserve further investigation.

In conclusion, the most comprehensive mouse synaptosome proteome analysis described to date was conducted. IEF coupled with LC-ESI-MS/MS is an effective proteomics platform that can be employed for the simultaneous analysis of the proteome and phosphoproteome of complex mixtures, such as brain synaptosome protein extracts. Synaptosomes are characterized by considerable functional diversity and the explicit investigation of the synaptosomal protein constituents and especially low abundant synaptic proteins will aid the further understanding of brain neurochemistry and synapse function, provide a reference map for synaptic large scale quantification studies in mouse models, reveal key components of neurotransmission and point to potential candidates for therapeutic intervention.



5 ¹⁵N metabolic labeling of the HAB/NAB/LAB trait anxiety mouse model

5.1 Introduction

In vivo ¹⁵N metabolic labeling has been applied so far to a wide range of organisms to address a variety of biological questions. In *Rhodospseudomonas palustris*, ¹⁵N metabolic labeling has been used to characterize *p*-coumarate anaerobic catabolism under different carbon sources (Pan et al., 2008). In *C. elegans*, ¹⁵N metabolic labeling has been employed to compare WT and germless strains (Krijgsveld et al., 2003) as well as to elucidate insulin signaling targets in insulin-receptor deficient mutants (Dong et al., 2007). In *Arabidopsis thaliana*, the effects of oxidative stress (Bindschedler et al., 2008), cadmium exposure (Lanquar et al., 2007) and sucrose resupply after carbon starvation (Kierszniowska et al., 2009b) have been investigated by ¹⁵N metabolic labeling. *In vivo* ¹⁵N metabolic labeling is a powerful technique that also holds great promise for the study of higher organisms, including mammals (McClatchy et al., 2007a; Wu et al., 2004). Recently, the ¹⁵N metabolic labeling approach was applied to an animal model of colon cancer in order to identify tumor-specific markers (Huttlin et al., 2009). To date, ¹⁵N metabolic labeling has not been yet applied to study animal models of psychopathologies. Here, the HAB/NAB/LAB mouse model was metabolically labeled with ¹⁵N via a bacterial, protein-based, ¹⁵N-labeled diet. The high ¹⁵N incorporation achieved *in vivo* provides ¹⁵N-labeled tissue to be used in quantitative proteomics experiments, ensuring an accurate relative quantification of ¹⁴N/¹⁵N material.

5.2 Results

5.2.1 Behavioral characteristics of bacteria-fed HAB/NAB/LAB mice

No physiological, morphological or developmental defects were observed in the bacteria-fed animals. No differences in overall food consumption before weaning were observed for any mouse line, ¹⁴N or ¹⁵N bacterial diet (Frank et al., 2009). At the behavioral phenotype level, anxiety-related and depression-like behaviors were examined.



5.2.1.1 Anxiety-related behavior

Anxiety-related behavior was assessed on PND 5 by USV (see 3.3.2.1) and on PND 49 by EPM (see 3.3.2.2). USV calls (Fig. 5.1A) and % time spent on the open EPM arms (Fig. 5.1B) were the main behavioral parameters examined. HAB, NAB and LAB animals showed the significant phenotypic divergence observed in the mice of the standard breeding both in USV and EPM tests (Frank et al., 2009, data not shown), indicating that the bacterial diet *per se* exerted no effect on anxiety-related behavior in all lines. In both tests, no significant difference was observed between ¹⁴N and ¹⁵N bacteria-fed animals of the same line, showing that the introduction of the ¹⁵N isotope did not influence anxiety-related behavior.

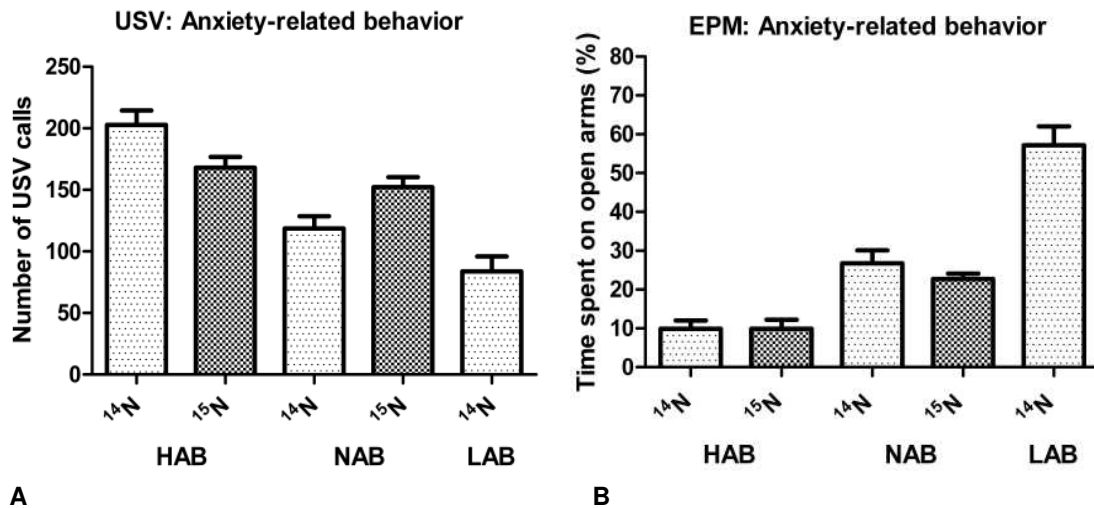


Figure 5.1 Anxiety-related behavior in the ultrasonic vocalization and the elevated plus-maze test

A. An increased number of USV calls during the test time were observed in bacteria-fed HAB compared to LAB mice, with NAB mice exhibiting an intermediate behavior, similar to the animals of the standard breeding. No significant difference in the number of USV calls was found between ¹⁴N and ¹⁵N bacteria-fed HAB or NAB animals. All available bacteria-fed animals on PND 5 were tested (27 ¹⁴N HAB, 29 ¹⁵N HAB, 46 ¹⁴N NAB, 83 ¹⁵N NAB, 29 ¹⁴N LAB). **B.** HAB, NAB and LAB animals exhibited the significant anxiety-related, line-specific phenotypic divergence, similar to the animals of the standard breeding. HAB spent less time on the EPM open arms compared to LAB mice, and NAB mice exhibited an intermediate behavior. No significant difference in % time spent on the open arms was observed between ¹⁴N and ¹⁵N bacteria-fed HAB or NAB animals. The ¹⁵N diet had no effect on locomotion as measured by the total number of entries into all arms



(Frank et al., 2009; data not shown). On the EPM, 10 ¹⁴N HAB, 10 ¹⁵N HAB, 13 ¹⁴N NAB, 24 ¹⁵N NAB and 12 ¹⁴N LAB mice were tested.

5.2.1.2 Depression-like behavior

Depression-like behavior was assessed on PND 51 by TST (see 3.3.2.3.). Total immobility time was the main behavioral parameter examined. The bacterial diet *per se* had no influence on the depression-like behavior compared to the animals of the standard breeding (Frank et al., 2009; data not shown). Intriguingly, a significant decrease in total immobility time in bacteria-fed ¹⁵N HAB compared to ¹⁴N HAB mice was observed, indicating a bacterial diet-independent, antidepressant-like effect of the ¹⁵N isotope in HAB mice (Fig. 5.2).

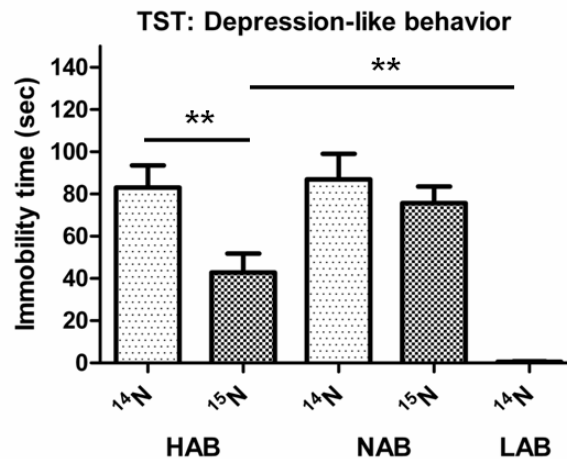


Figure 5.2 Depression-like behavior in the tail suspension test

Total immobility time indicative of depression-like behavior was significantly reduced in bacteria-fed ¹⁵N HAB compared to ¹⁴N HAB mice (** $p < 0.01$). Bacteria-fed ¹⁵N HAB still showed significantly increased total immobility time compared to ¹⁴N LAB mice (** $p < 0.01$). No significant difference in immobility time was observed between bacteria-fed ¹⁴N NAB and ¹⁵N NAB mice. The same animals that were tested on the EPM were also tested here.

5.2.2 ¹⁵N metabolic labeling efficiency estimation

¹⁵N incorporation efficiency was monitored at different developmental time points (PND 5, 14, 28 and 56) in cerebellum and plasma of ¹⁵N bacteria-fed mice. Already on PND 5, ¹⁵N incorporation was >50.0% both in cerebellum and plasma. At early developmental time points, ¹⁵N incorporation in cerebellum was lower than in plasma due to the slow protein turnover in the brain.



However, on PND 56, the ¹⁵N incorporation in brain increased, reaching up to 92.0% both in cerebellum and plasma (Fig. 5.3). Representative examples of ¹⁴N/¹⁵N peptide pairs throughout development are shown in Fig. 5.4.

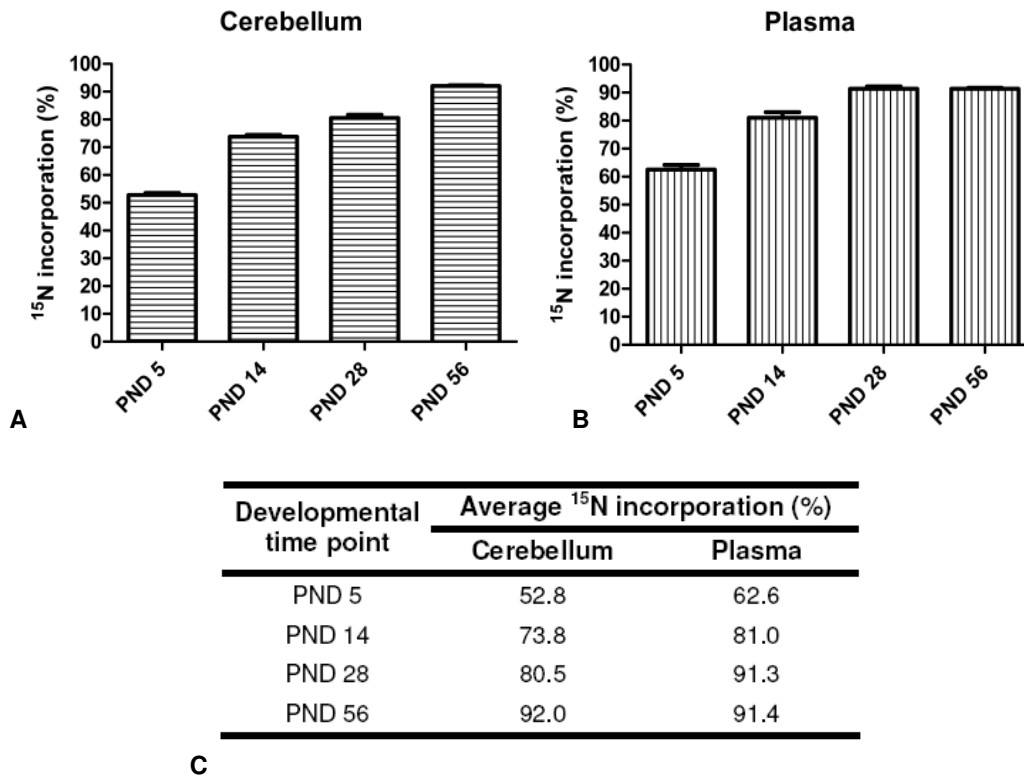
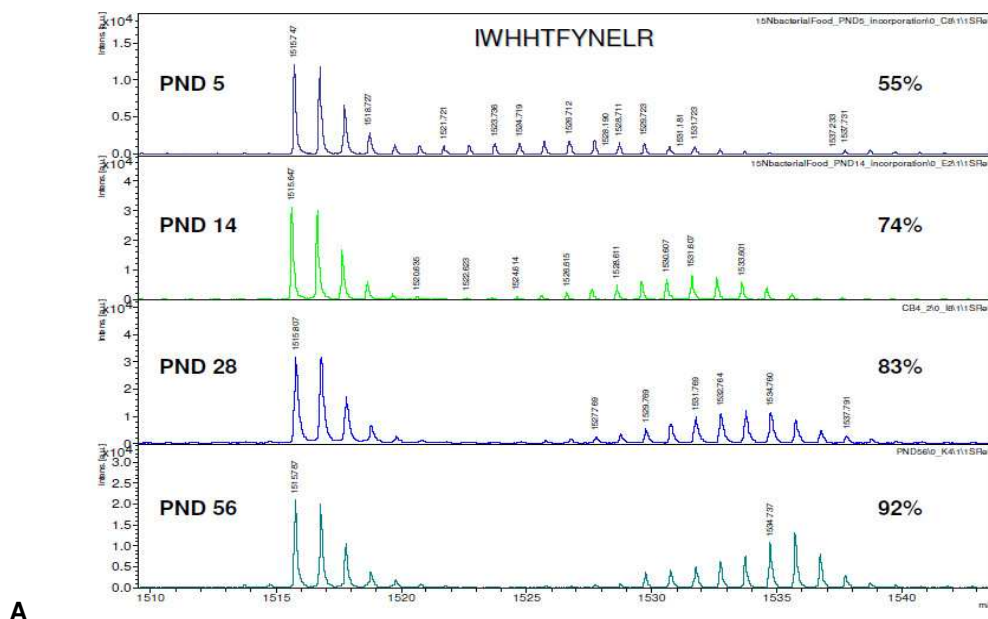
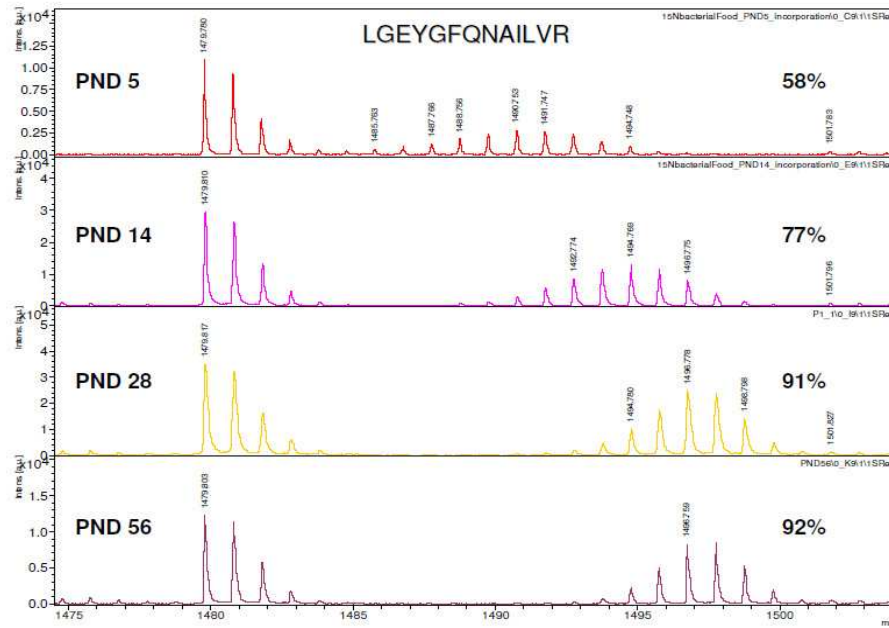


Figure 5.3 ¹⁵N metabolic labeling efficiency at different developmental time points
A. Cerebellum. **B.** Plasma. **C.** Table of average ¹⁵N incorporation rates at different PNDs.





B

Figure 5.4 Representative ¹⁴N/¹⁵N peptide spectra from different developmental time points and their corresponding ¹⁵N incorporation rates

A. Brain beta-actin peptide IWHHTFYNELR. **B.** Plasma serum albumin peptide LGEYGFQNAILVR. As ¹⁵N incorporation increases, the isotopologue pattern of the ¹⁵N-labeled peptide (on the right) is shifted towards higher m/z ratios due to the presence of more 'heavy' nitrogens in the peptide backbone.

5.3 Discussion

A breeding and feeding protocol was established for *in vivo* metabolic labeling of mice with ¹⁵N through a bacterial protein-based diet. The bacterial protein-based diet did not interfere with normal development, and no side-effects were observed apart from a slight body weight reduction of the bacteria- compared to standard-fed animals (Frank et al., 2009). To date, metabolic labeling of rodents has been performed using a ¹⁵N-labeled, blue-green algae diet (*Spirulina*) (Wu et al., 2004; McClatchy et al., 2007a; Huttlin et al., 2009). All published efforts to label rodents with ¹⁵N and relevant proteomics applications are summarized in Table 5.1. According to our experience, offspring fed exclusively with the *Spirulina*-based diet exhibited severe developmental problems (Frank et al., 2009). Therefore, the bacteria-based diet was chosen due to the lack of side-effects in normal development and its lower cost compared to the *Spirulina*-



based diet. Notably, a four day habituation period was introduced, during which mice had access *ad libitum* both to standard and bacterial food so as to ensure optimal transition to the new diet (Fig. 3.1). The bacterial diet did not influence anxiety-related behavior both at early and late developmental stages (as measured by USV and EPM, respectively), thus enabling proteomics analyses for identifying anxiety-related changes in an unbiased manner. Although the bacterial diet *per se* had no effect on the depression-like phenotype compared to the standard diet, an antidepressant-like effect of the ¹⁵N isotope was observed in HAB mice (see 5.2.1.2). This is the first time that the introduction of the ¹⁵N isotope has been reported to affect the behavioral characteristics of labeled organisms. Further investigation of this effect at the molecular level can shed light on pathways involved in the depression-like behavior in HAB (discussed in Chapter 7). For quantitative MS experiments, a satisfactory ¹⁵N incorporation is required to guarantee an accurate ¹⁴N/¹⁵N quantification. In the only study where mice have been metabolically labeled with ¹⁵N, ¹⁵N feeding started at the age of 3 weeks for 44 days, achieving an 82.8% ¹⁵N incorporation in brain. Here, a labeling protocol was established starting with ¹⁵N feeding *in utero* until early adulthood (8 weeks of age), achieving a 92.0% ¹⁵N incorporation in brain and 91.3% in plasma. By starting the ¹⁵N feeding *in utero*, high ¹⁵N incorporation was achieved already at early developmental time points (Fig. 5.3). In the future, this will enable MS-based quantitative studies to investigate the ontogenetic development of anxiety-related behavior.

Stable isotope labeling approaches have revolutionized the proteomics field and are to date the most sensitive quantitative proteomics approaches due to the ability of mixing the samples under comparison prior handling. Consequently, any error during experimental handling is introduced uniformly in both samples, and relative quantification accuracy is not affected (see 1.4.1.5). Although the generation of a ¹⁵N-labeled mouse is of considerable cost, all resulting ¹⁵N-labeled tissues can be used in a plethora of experimental workflows as internal standards, facilitating highly sensitive proteomics comparisons and providing an overall cost-effective, highly precise tool for quantitative proteomics. Incomplete labeling was until recently the main bottleneck for ¹⁵N metabolic labeling applications, as the complex nature of partially ¹⁵N-labeled spectra hindered accurate ¹⁴N/¹⁵N quantification. To address this issue, optimized *in silico* identification and quantification strategies for partially labeled peptides (Gouw et al., 2008; Zhang et al., 2009b) and several software solutions were developed to allow accurate ¹⁴N/¹⁵N quantification for partially



labeled material, both for MALDI (Haegler et al., 2009) and ESI instruments (Pan et al., 2006a; Park et al., 2008; Park and Yates, 2010).

Taken together, a novel ¹⁵N metabolic labeling workflow that does not interfere with normal mouse development and results in high ¹⁵N incorporation rates even in organs with slow protein turnover (i.e. brain) has been established. This is the first time that ¹⁵N metabolic labeling has been applied to a mouse model of psychopathology. ¹⁵N-labeled NAB mice can be used in quantitative proteomics experiments to investigate anxiety-related protein changes (Chapter 6). Furthermore, the investigation of the ¹⁵N antidepressant-like effect in HAB mice can shed light on pathways involved in depression manifestation (Chapter 7).

Organism	Diet	Labeling protocol	¹⁵ N brain incorporation (%)	Application
Rat	¹⁵ N labeled <i>Spirulina</i> ^a	From PND 21 for 44 days (Wu et al., 2004)	74.3	Protein synthesis inhibition in liver (Wu et al., 2004)
		<i>In utero</i> until PND 45 (McClatchy et al., 2007a)	87.0	-
		From weaning on (for dams) until PND 45 for pups (McClatchy et al., 2007a)	95.0	Developmental comparison of synaptosomal cerebellum proteome (McClatchy et al., 2007b) and nuclear cortex phosphoproteins (Liao et al., 2008)
Mouse	¹⁵ N labeled <i>Spirulina</i> ^a	From weaning on until PND 68 (Wu et al., 2004 adapted)	82.8	Colon cancer (Huttlin et al., 2009)
	¹⁵ N labeled <i>Ralstonia eutropha</i> ^b	<i>In utero</i> until PND 56, 4 day habituation period (Frank et al., 2009)	92.0	Anxiety disorders (Frank et al., 2009)

^a Spectra Stable Isotopes (now part of Cambridge Isotope Laboratories)

^b Silantes

Table 5.1 Published approaches for metabolically labeling rodents with ¹⁵N

¹⁵N-labeled rats have been used for developmental brain proteome and phosphoproteome comparisons. ¹⁵N metabolic labeling in mice has been applied to a model of colon cancer and the HAB/NAB/LAB model of trait anxiety.



6 Biomarker and pathway discovery in the HAB/NAB/LAB mouse model of trait anxiety

6.1 Introduction

Although anxiety disorders are the most common psychiatric disorders, no molecular markers exist for their prognosis, classification or treatment outcome. In our efforts to unravel the neurobiological underpinnings and identify candidate biomarkers for anxiety disorders, we interrogated the HAB/NAB/LAB mouse model of trait anxiety utilizing a quantitative multi-omics approach. As brain region of interest, the cingulate cortex was chosen. The cingulate cortex is in close connection to the amygdala, and its activation has been proposed to modulate amygdala's response to fear (Coplan and Lydiard, 1998; Milad and Rauch, 2007; Muigg et al., 2008). Neuroimaging studies in humans and lesion analyses in animal models have implicated cingulate cortex areas in the modulation of emotional behavior (Drevets and Savitz, 2008; Etkin and Wager, 2007; Hasler et al., 2007). Notably, alterations in cingulate cortex have been reported in panic disorder (Asami et al., 2008) as well as in other psychiatric conditions, including depression (Ballmaier et al., 2004) and schizophrenia (Carter et al., 1997). Furthermore, the cingulate cortex tissue amount obtained per animal allows proteomics interrogation of synaptosomes.

Due to the key role of the synaptic machinery in anxiety pathophysiology (summarized in 4.1), we focused our proteomics investigation on synaptosomes. The quantitative proteomics platform based on ^{15}N metabolic labeling (described in Chapter 5) and quantitative MS were applied to compare the cingulate cortex synaptosome proteomes of HAB and LAB mice. To circumvent ^{15}N isotope-derived alterations, an indirect comparison workflow was employed using ^{15}N -labeled NAB animals as internal standards (Fig. 6.1).

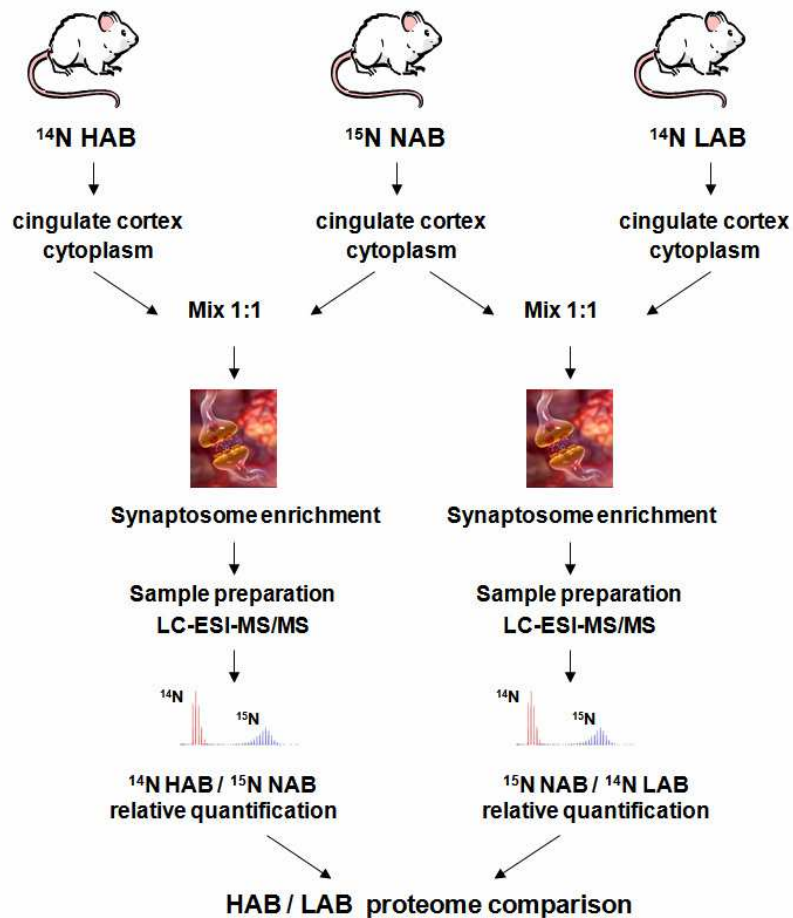


Figure 6.1 Proteomics strategy for HAB/LAB relative quantification

Cingulate cortices from ^{15}N bacteria-fed NAB as well as from ^{14}N bacteria-fed HAB and LAB mice were excised and cytoplasmic fractions were mixed 1:1 (w/w) based on protein content for every $^{14}\text{N}/^{15}\text{N}$ comparison. ^{15}N bacteria-fed NAB mice were compared pairwise with ^{14}N HAB and ^{14}N LAB mice in two parallel steps. Data from the ^{14}N HAB/ ^{15}N NAB and ^{15}N NAB/ ^{14}N LAB comparisons were combined to indirectly compare the ^{14}N HAB and ^{14}N LAB synaptosome proteomes.

In addition, the cingulate cortex metabolomes of HAB/NAB/LAB mice were quantified utilizing an established quantitative metabolomics platform in collaboration with the Metabolomics Core of UC Davis, CA, USA (Fig. 6.2). Moreover, differential expression of selected proteins was validated by Western blot in an independent, standard-fed HAB/NAB/LAB population and *in silico* pathway analyses based on proteomics and metabolomics data were performed to unravel altered networks in HAB and LAB animals.

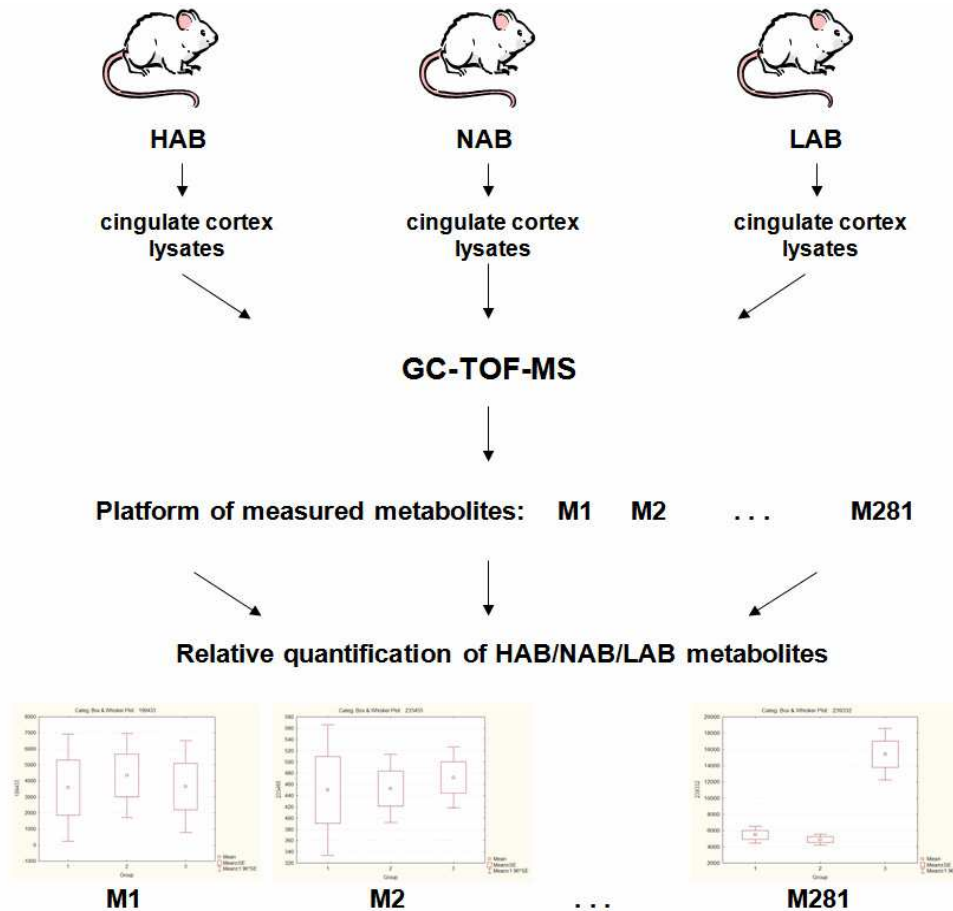


Figure 6.2 Metabolomics strategy for HAB/NAB/LAB relative quantification

Metabolite levels were quantified in cingulate cortex lysates of HAB/NAB/LAB mice employing a GC-TOF-MS-based quantitative platform.

GC-TOF-MS: Gas chromatography-time of flight-mass spectrometry.

6.2 Results

6.2.1. HAB/LAB cingulate cortex synaptosome proteome comparison

For quantitative MS analysis, three bacteria-fed ^{14}N HAB and three ^{14}N LAB mice were compared. In total, 2678 non-redundant proteins were quantified in all $^{14}\text{N}/^{15}\text{N}$ measured replicates. Of these, 1214 were quantified in at least two out of three biological replicates per $^{14}\text{N}/^{15}\text{N}$ direct comparison ($^{14}\text{HAB}/^{15}\text{NAB}$ and $^{15}\text{NAB}/^{14}\text{LAB}$) and were considered for further analysis. Among them, 273 were found differentially expressed in HAB and LAB synaptosomes >1.3 fold (listed in Appendix 4), with 92 proteins showing expression differences ≥ 2 fold. Intriguingly, Glo1 was the



protein with the highest expression difference in HAB and LAB animals, exhibiting a 6.25 fold increased expression in LAB mice, thus confirming previous findings (Ditzen et al., 2006; Krömer et al., 2005).

6.2.2 HAB/NAB/LAB cingulate cortex metabolome comparison

For quantitative metabolomics analysis, 281 chromatographic peaks were quantified in all replicates (n=6 per line), 129 of which were assigned to known metabolites. Two explorative statistical analyses (RF and TFFBS) were employed, revealing a maximum set of 11 metabolite entities that seemed to be the most informative and most capable to accurately discriminate between the HAB/NAB/LAB lines (Table 6.1). Multivariate analysis showed a significant effect of the set of the 11 metabolite entities [Wilks multivariate tests of significance; effect of group: $F(22,10)=10.71$, $f<0.0001$], which was also significant for xylose, dehydroascorbate 1, dehydroascorbate 3 and four other metabolites, whose identity is unknown (203235, 239332, 216860, 284389) (prime candidate metabolite biomarkers, univariate F-tests, $*p<0.05$). Subsequent Bonferroni *post-hoc* tests were used to localize in which of the line pairs HAB/LAB, HAB/NAB or NAB/LAB the selected metabolite entities show significant differences (arrows in Table 6.1).

Metabolites ^a	HAB/LAB		HAB/NAB		NAB/LAB	
	RF	TFFBS	RF	TFFBS	RF	TFFBS
Dehydroascorbate 1 ^{b*}	↓	↓	↓	↓		
Dehydroascorbate 3 ^{b*}	↓	↓	↓	↓		
Xylose*	↓	↓			↓	↓
203235*				↓		
216860*				↓		↑
239332*			↓	↓	↑	↑
284389*						↓
Adenosine-5-monophosphate ⁺						↑
Flavin-adenine dinucleotide ⁺				↓		
Succinate ⁺					↑	↑
234580 ⁺		↓		↓		

^a numerical IDs correspond to quantified metabolites of unknown identity

^b quantified chromatographic peaks that correspond to the same metabolite

* prime candidate metabolite biomarkers (univariate F-tests $*p<0.05$ at a corrected level of significance)

⁺ informative metabolites (metabolites identified as significant at the uncorrected level of significance only)

**Table 6.1: Metabolites with the best discrimination power between HAB/NAB/LAB lines**

List of metabolites that can discriminate between the HAB/NAB/LAB mouse lines (based on RF, TFFBS and MANOVA analyses). \downarrow : Ratio between the compared groups <1 ; \uparrow : Ratio between the compared groups >1 .

To assess the discrimination power of the set of the 11 metabolite entities, a discriminant analysis was performed resulting in an excellent overall classification rate of 100%. In a second discriminant analysis, the seven prime candidate metabolite biomarkers were used as discriminators, and excellent discrimination power (100%) was also achieved. To assess whether there is a subset of the prime candidate metabolite biomarkers that can discriminate between the three lines, all possible combinations of the prime candidate metabolite biomarkers as discriminators were considered. We found that dehydroascorbate 3, xylose and metabolite 239332 constitute the minimum set of metabolites that can discriminate between the HAB/NAB/LAB lines (discrimination power 100%). Both dehydroascorbate and xylose were found at elevated levels in LAB compared to HAB mice.

6.2.3 Western blot validation of selected differentially expressed proteins

To validate quantitative MS data, differential expression of selected proteins (Table 6.2) was confirmed by Western blot in cingulate cortex synaptosomes of an independent, standard-fed HAB/NAB/LAB population. Selection criteria for the proteins to be validated were the quality of MS raw data, the number of quantified peptides and antibody availability. Representative MS raw spectra and Western blot analysis are shown in the following sections.

Protein symbol	IPI Accession	Protein name	HAB/LAB abundance ratio	Quantified non-redundant peptides
Sfxn5	IPI00221602	Sideroflexin-5	2.14	9
Car2	IPI00121534	Carbonic anhydrase 2	1.87	13
Myh10	IPI00338604	Myosin, heavy polypeptide 10, non-muscle	0.76	36
Sdhb	IPI00338536	Succinate dehydrogenase [ubiquinone] iron-sulfur subunit	2.00	11

Table 6.2 Differentially expressed proteins in HAB and LAB synaptosomes confirmed by Western blot



6.2.3.1 Sideroflexin-5 (Sfxn5)

Sfxn5 belongs to the sideroflexin protein family of mitochondrial transmembrane transporters. Apart from Sfxn5 (Fig. 6.3), two other sideroflexin family members were expressed at higher levels in HAB mice (Sfxn1 and Sfxn3, both 1.74 fold).

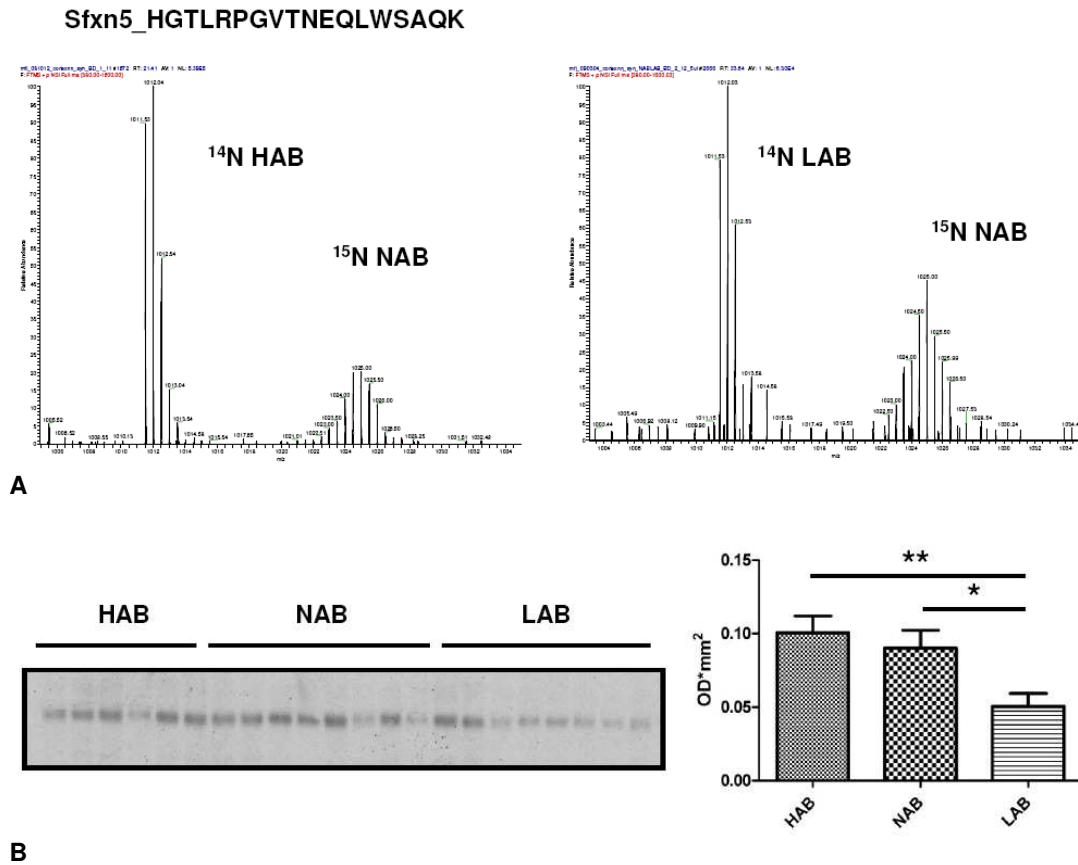


Figure 6.3 Increased Sfxn5 expression in HAB mice

A. Increased expression of the Sfxn5 peptide HGTLRPGVTNEQLWSAQK in bacteria-fed ^{14}N HAB compared to ^{15}N NAB mice (left) and in ^{15}N NAB compared to ^{14}N LAB mice (right). **B.** Significantly increased Sfxn5 expression in standard-fed HAB ($n=6$) and NAB ($n=8$) compared to LAB ($n=8$) mice (** $p=0.0043$ and * $p=0.0209$, respectively).

6.2.3.2 Carbonic anhydrase 2 (Car2)

Car2, expressed at higher levels in HAB mice (Fig. 6.4), is a cytosolic protein that belongs to the family of carbonic anhydrases, which catalyze the reversible conversion of carbon dioxide to



bicarbonate ions, facilitating the transport and elimination of carbon dioxide from tissues (Breton, 2001).

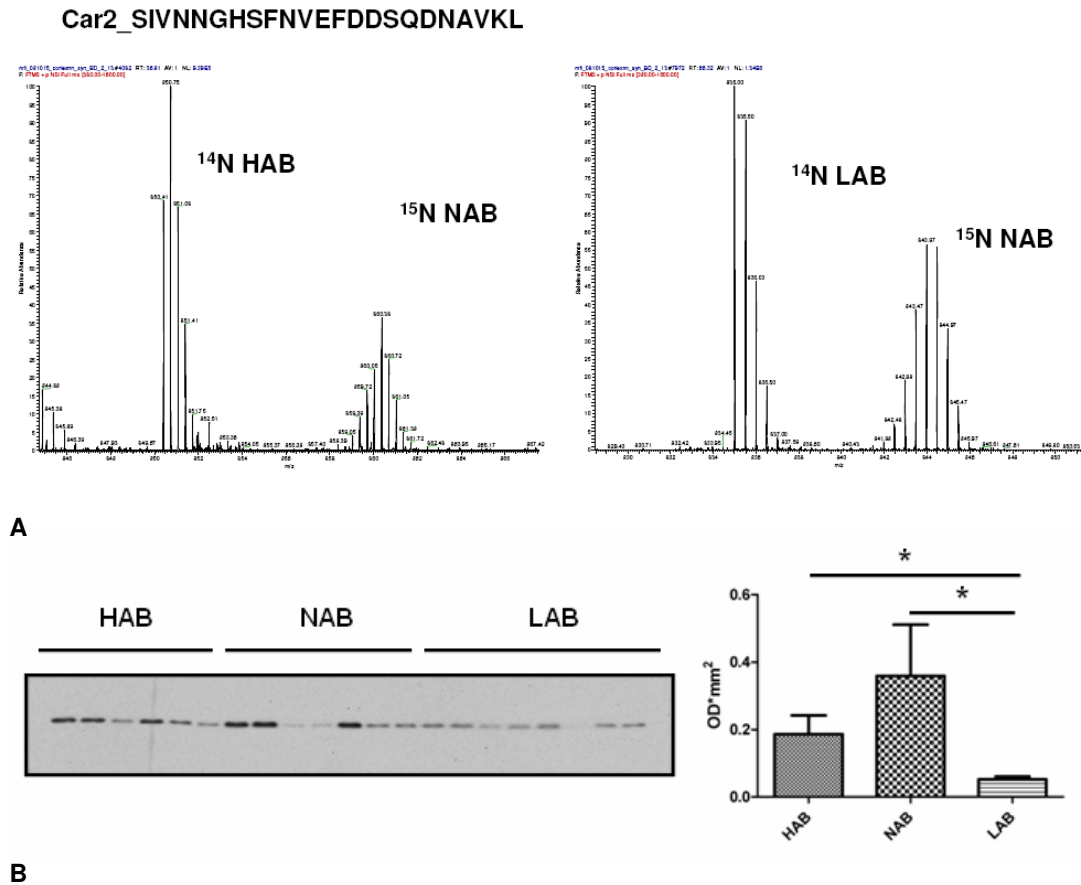


Figure 6.4 Increased Car2 expression in HAB mice

A. Increased expression of the Car2 peptide SIVNNGHSFNVEFDDSQDNAVKL in bacteria-fed ^{14}N HAB compared to ^{15}N NAB mice (left) and ^{15}N NAB compared to ^{14}N LAB mice (right). **B.** Significantly increased Car2 expression in standard-fed HAB ($n=6$) and NAB ($n=7$) compared to LAB ($n=8$) mice ($*p=0.0165$ and $*p=0.0491$, respectively).

6.2.3.3 Myosin, heavy polypeptide 10 (Myh10)

Myh10, expressed at higher levels in LAB mice (Fig. 6.5), belongs to the myosin family of motor proteins. Unlike conventional myosin family members, Myh10 localizes in filopodia tips (Berg and Cheney, 2002).

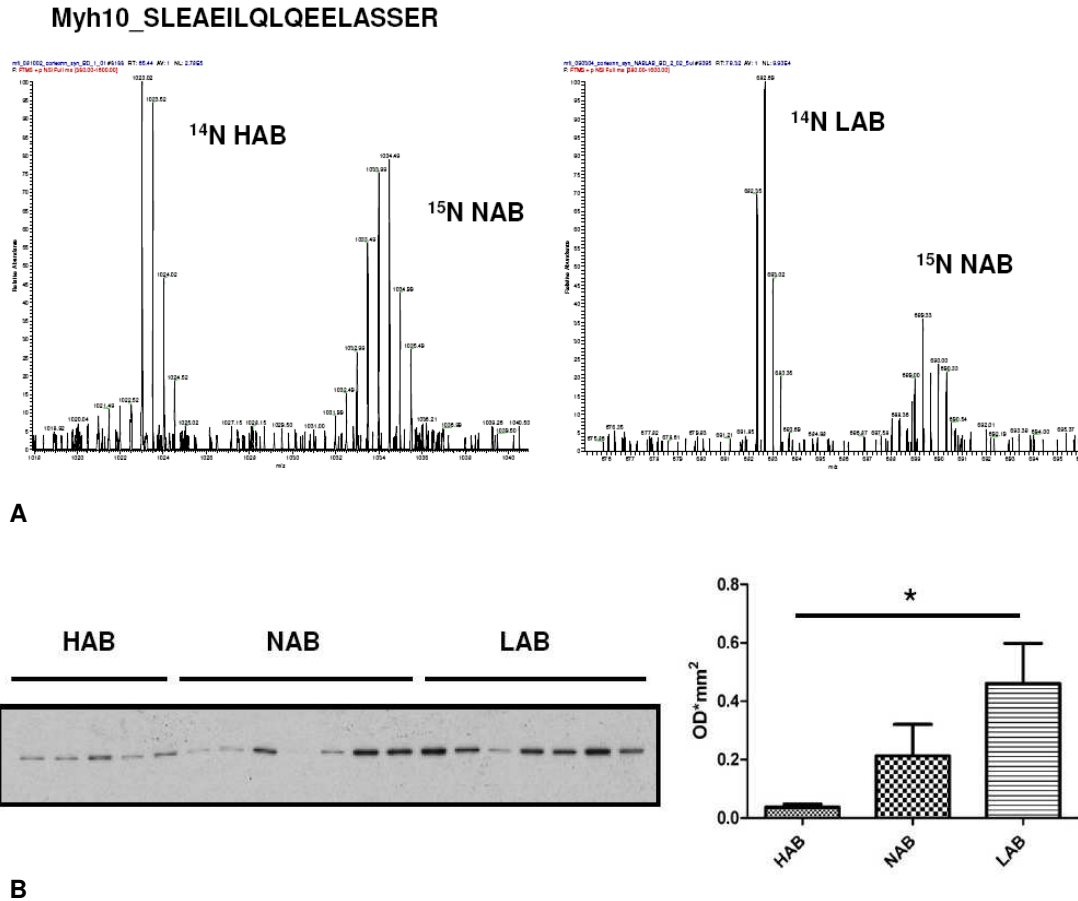


Figure 6.5 Increased Myh10 expression in LAB mice

A. Increased expression of the Myh10 peptide SLEAEILQLQEELASSER in bacteria-fed ^{15}N NAB compared to ^{14}N HAB (left) and ^{14}N LAB compared to ^{15}N NAB mice (right). **B.** Significantly increased Myh10 expression in standard-fed LAB ($n=7$) compared to HAB ($n=5$) mice ($*p=0.0289$), with NAB mice ($n=7$) exhibiting intermediate intensities.

6.2.3.4 Succinate dehydrogenase, subunit b (Sdhb)

Succinate dehydrogenase (Sdh) links the electron transport chain (ETC) and the citric acid cycle by catalyzing the reduction of ubiquinone to ubiquinol with the oxidation of succinate to fumarate. It consists of four subunits named a-d. Apart from Sdhb (Fig. 6.6), Sdha and Sdhc were also expressed at higher levels in HAB mice.

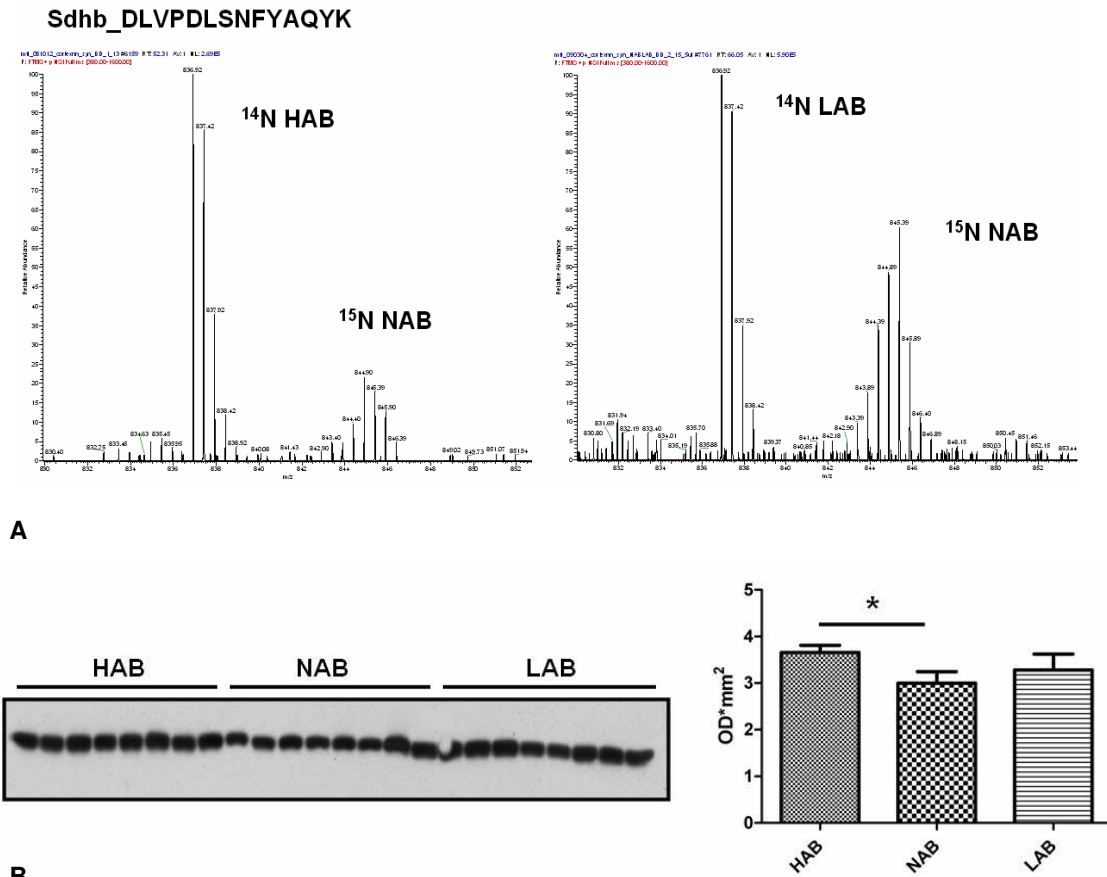


Figure 6.6 Increased Sdhb expression in HAB mice

A. Increased expression of the Sdhb peptide DLVPDLSNFYAQYK in bacteria-fed ¹⁴N HAB compared to ¹⁵N NAB mice (left) and ¹⁵N NAB compared to ¹⁴N LAB mice (right). **B.** Significantly increased expression of Sdhb in standard-fed HAB (n=8) compared to NAB (n=8) mice (*p=0.0398). Increased expression of HAB compared to LAB mice did not reach significance.

6.2.4 In silico analysis of altered pathways in HAB and LAB mice

Pathway Studio analysis was performed to search the literature and visualize inter-connections between proteins and metabolites with altered levels in HAB and LAB mice and cellular processes (Fig. 6.7) as well as major psychiatric disorders (Fig. 6.8).

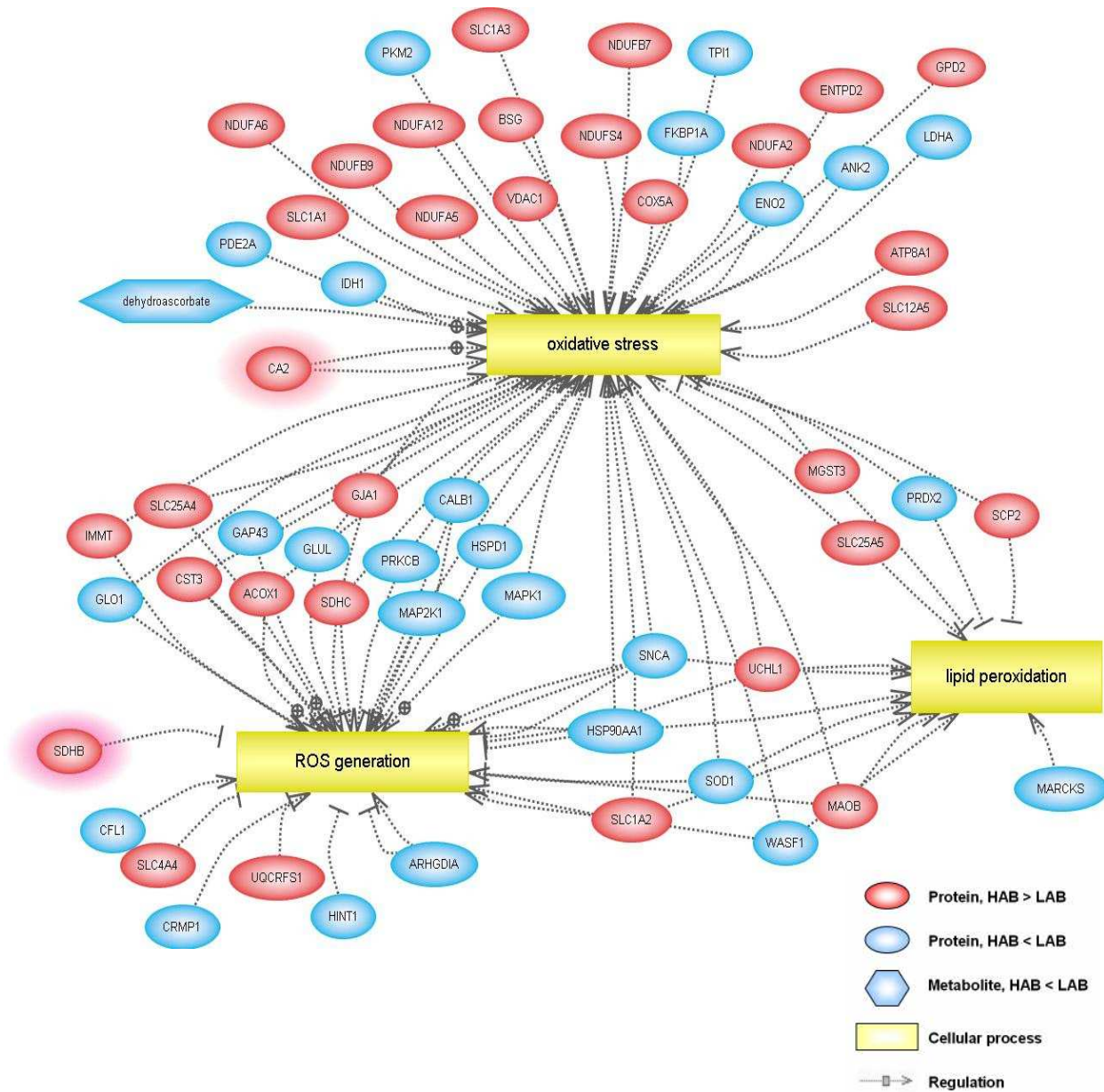


Figure 6.7 Differentially expressed proteins and metabolites pertinent to oxidative stress-related processes

A number of proteins and metabolites with altered levels in HAB and LAB animals have been implicated in oxidative stress-related processes in the literature. Highlighted proteins denote confirmed differential expression by Western blot (protein names corresponding to the abbreviations used here are given in Appendix 4).

ROS: Reactive oxygen species.

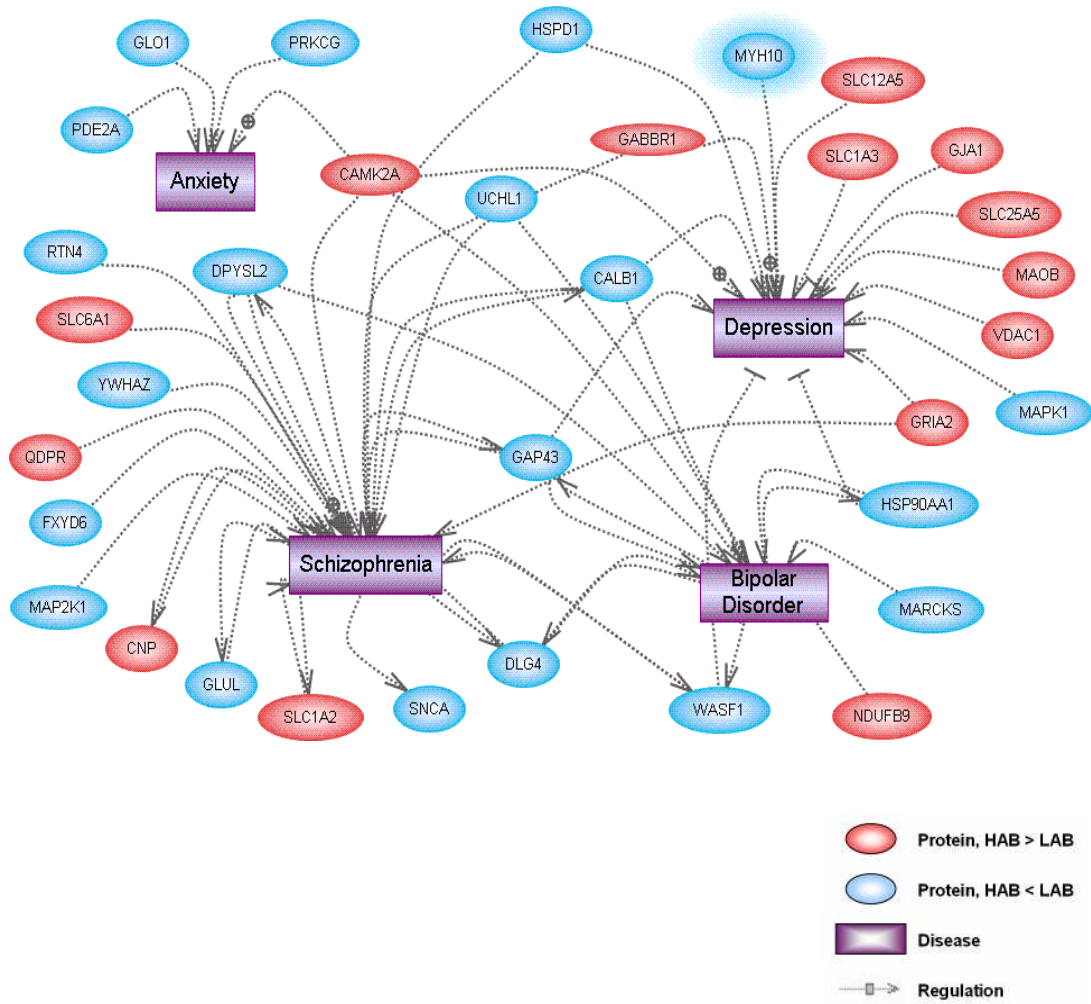


Figure 6.8 Differentially expressed proteins related to major psychiatric disorders

A number of differentially expressed proteins in HAB and LAB mice have been related to psychiatric disorders, although only few to anxiety. Highlighted proteins denote confirmed differential expression by Western blot (protein names corresponding to the abbreviations used here are given in Appendix 4).



In a second *in silico* pathway analysis approach, all quantified proteins and metabolites in HAB/LAB mice were plotted in a combined histogram according to their HAB/LAB \log_2 ratios and were then assigned to five continuous bins (based on their HAB/LAB \log_2 ratios), as shown in Fig. 6.9. Components of each bin were compared to the KEGG database in order to identify significantly overrepresented pathways (Fig. 6.10).

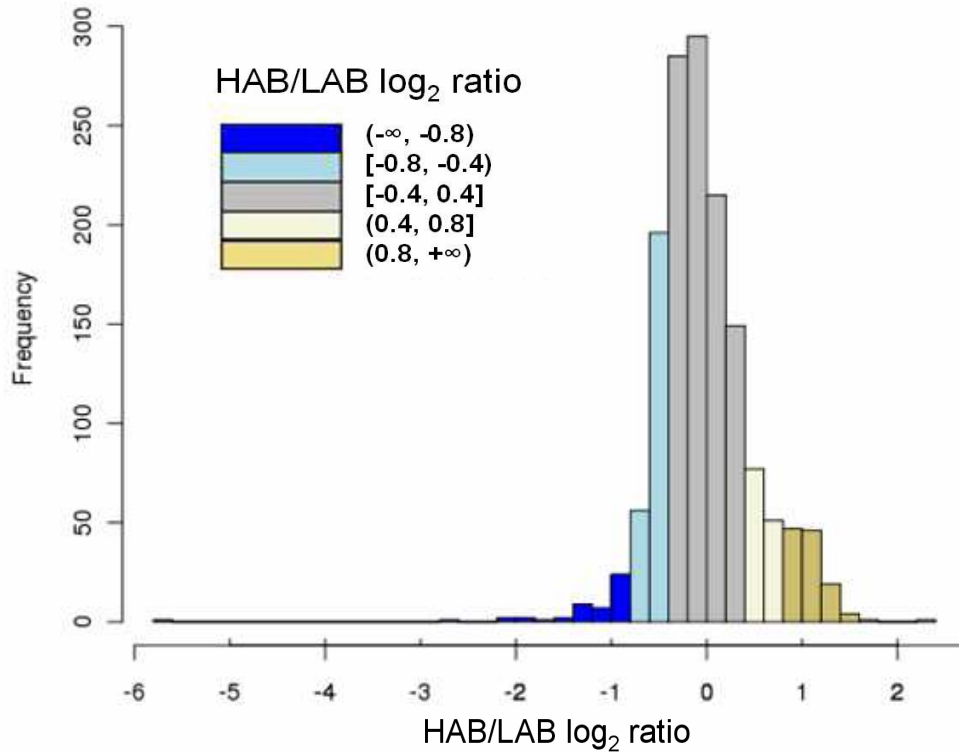


Figure 6.9 HAB/LAB \log_2 ratio distribution of all quantified proteins and metabolites

Quantified proteins and metabolites were assigned to five color-coded bins according to their HAB/LAB \log_2 ratios as follows: Dark blue, decreased HAB/LAB \log_2 ratio $(-\infty, -0.8)$; light blue, moderately decreased HAB/LAB \log_2 ratio $[-0.8, -0.4)$; grey, non-differential HAB/LAB \log_2 ratio $[-0.4, 0.4]$; white, moderately increased HAB/LAB \log_2 ratio $(0.4, 0.8]$; yellow, increased HAB/LAB \log_2 ratio $(0.8, +\infty)$. As expected, the majority of the quantified proteins and metabolites were not differentially expressed.

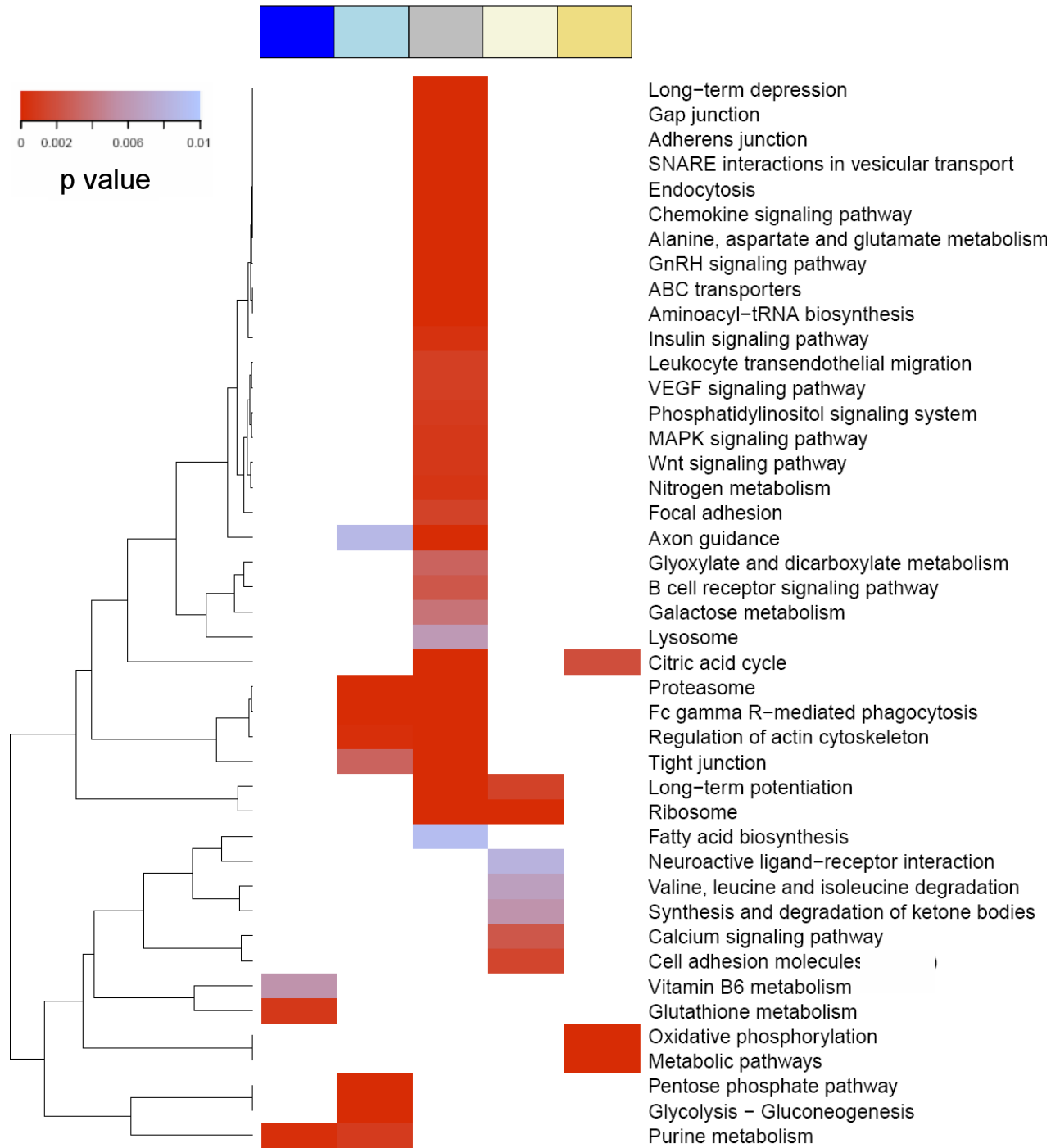


Figure 6.10 Significantly overrepresented pathways in the quantified proteins and metabolites dataset

Bins are color-coded according to Fig. 6.9 (center top). On the left, the hierarchical clustering of the significantly overrepresented pathways based on their p values is shown. Statistical significance for overrepresented pathways was accepted for $p < 0.01$.



ABC: ATP-binding cassette; GnRH: Gonadotropin-releasing hormone; MAPK: Mitogen-activated protein kinase; SNARE: Soluble N-ethylmaleimide sensitive fusion protein attachment protein receptors; VEGF: Vascular endothelial growth factor; Wnt: Wingless-type MMTV integration site family member.

Of interest are predominantly pathways that appear significantly overrepresented only in the increased or decreased HAB/LAB \log_2 ratio bins (indicating increased expression in HAB or LAB mice, respectively). Oxidative phosphorylation was the most significant overrepresented pathway ($p=2.04E-84$), exclusively appearing in the increased HAB/LAB \log_2 ratio bin (yellow). Overall, metabolic pathways were also significantly overrepresented in the increased HAB/LAB \log_2 ratio bin (yellow) although specific energy-related pathways such as glycolysis and pentose phosphate pathway were found significantly overrepresented in the moderately decreased HAB/LAB \log_2 ratio bin (light blue). Moreover, calcium signaling pathway and cell adhesion molecules were significantly overrepresented in the moderately decreased HAB/LAB \log_2 ratio bin (light blue). Significantly overrepresented in the decreased HAB/LAB \log_2 ratio bin (dark blue) were pathways involved in antioxidant defense (e.g., glutathione metabolism, vitamin B6 metabolism).

6.2.5 Altered networks in HAB and LAB mice

Having interrogated the HAB/NAB/LAB mouse model of trait anxiety at the proteome, metabolome and pathway levels, several altered systems in HAB and LAB mice emerged such as glycolysis, neurotransmission and mitochondrial function and are discussed below.

6.2.5.1 Glycolysis

Eight out of the ten enzymes catalyzing glycolysis pathway reactions, including the proteins that catalyze the three committed steps of the pathway (hexokinase, phosphofruktokinase and pyruvate kinase), were differentially expressed in HAB and LAB synaptosomes. Importantly, seven of those enzymes showed increased expression in LAB mice (Fig. 6.11).

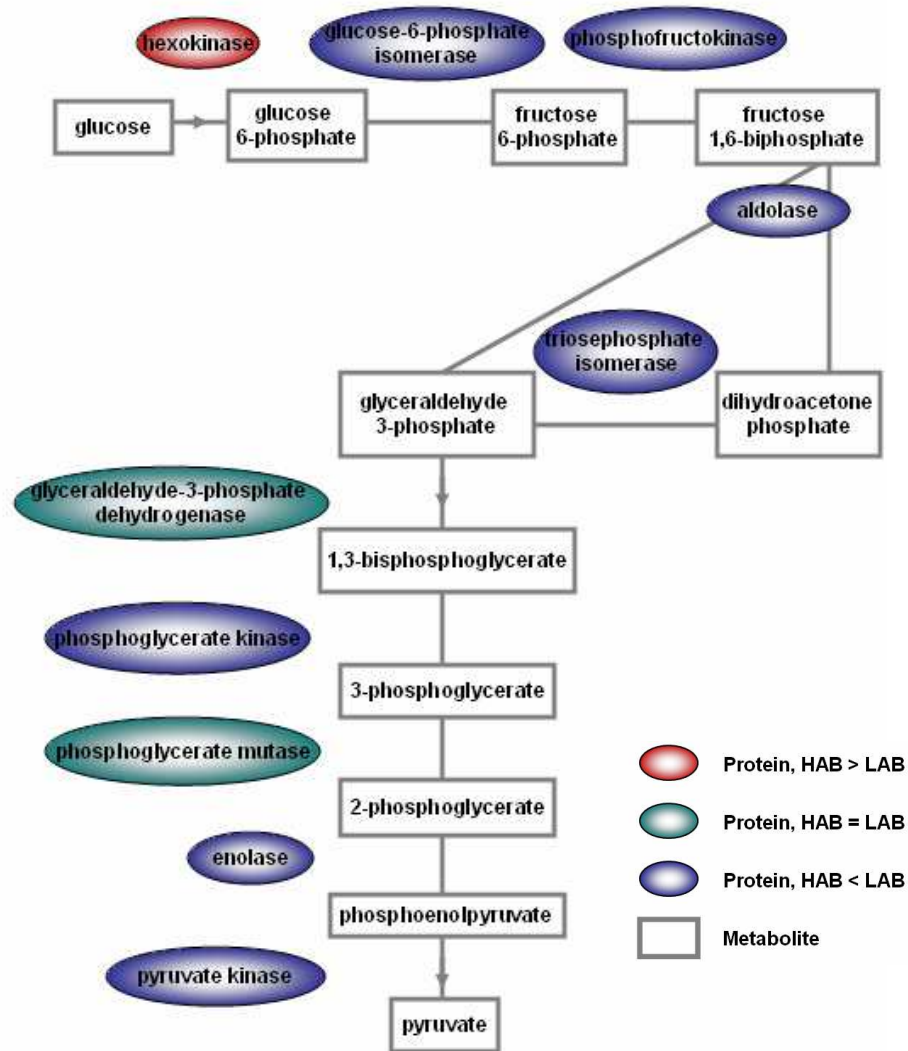


Figure 6.11 Glycolysis divergencies between HAB and LAB cingulate cortex synaptosomes

6.5.2.2 Neurotransmission

Glutamate and GABA are the main excitatory and inhibitory neurotransmitters, respectively. Increased expression of glutamate (Grm3, Gria2, Gria3) and GABA (Gabbr1) receptors as well as glutamate (Slc1a1, Slc1a2) and GABA (Slc6a1) transporters was found in HAB compared to LAB synaptosomes, suggesting an overall increased neurotransmission activity in HAB mice. In addition, proteins involved in glutamate metabolism, such as the mitochondrial glutamate dehydrogenase 1 (Glud1) and glutamate decarboxylase 2 (Gad2), were found differentially expressed in HAB and LAB synaptosomes. The calcium signaling pathway involved in



neurotransmission regulation was also overrepresented in the bin with a moderate increase in HAB mice (Fig. 6.10).

6.2.5.3 Mitochondrial function

Citric acid cycle and oxidative phosphorylation

Besides glycolysis, energy production takes place in mitochondria via the citric acid cycle and oxidative phosphorylation. Increased expression in LAB synaptosomes was observed for the citric acid cycle enzyme isocitrate dehydrogenase (Icdh1), which catalyzes the conversion of isocitrate to alpha-ketoglutarate, whereas increased expression of the Sdh subunits a, b and c was observed in HAB synaptosomes. As previously mentioned, Sdh couples the citric acid cycle and oxidative phosphorylation. Strikingly, subunits of all complexes participating in the ETC, including NADH dehydrogenase (complex I), Sdh (complex II), cytochrome bc1 (complex III), cytochrome c oxidase (complex IV) as well as ATP synthase showed higher expression in HAB compared to LAB synaptosomes, in most cases ≥ 2 fold (Fig. 6.12).

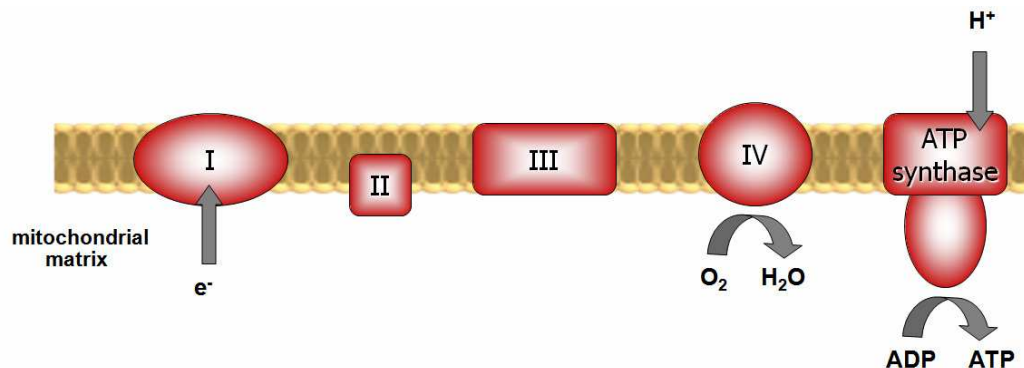


Figure 6.12 The electron transport chain in the inner mitochondrial membrane

The energy obtained through electron transfer down the ETC (complexes I to IV) creates an electrochemical proton gradient across the mitochondrial membrane, which allows ATP synthase to generate ATP. Red denotes increased expression in HAB mice.

Oxidative stress

Apart from producing ATP for energy metabolism, the ETC is one of the most prominent mechanisms of reactive oxygen species (ROS) generation that lead to oxidative stress. We found evidence for an increased antioxidant activity in LAB mice. At the proteome level, increased



expression of proteins with antioxidant properties, such as superoxide dismutase (Sod1) and peroxiredoxin-2 (Prdx2) was found in LAB mice. At the metabolome level, elevated levels of dehydroascorbate and xylose, two of the prime candidate metabolite biomarkers (see 6.2.2), were observed in LAB mice. Dehydroascorbate is the oxidized form of vitamin C (ascorbic acid), a known antioxidant (Sies et al., 1992). Unlike vitamin C, dehydroascorbate can cross the blood-brain barrier with the aid of glucose transporters, thus being the transportable form of vitamin C in the brain (Agus et al., 1997). Furthermore, the monosaccharide xylose can be converted to D-xylose-5-phosphate and enter the pentose phosphate pathway, an alternative pathway to glycolysis that generates NADPH, another key player in antioxidant defense. At the pathway level, overrepresentation of mechanisms involved in antioxidant defense, such as vitamin B6 and glutathione metabolism as well as the pentose phosphate pathway were found in the bins with increased expression in LAB mice (Fig. 6.10).

Mitochondrial import and transport

Increased expression of proteins participating in transport into and within mitochondria were observed in HAB synaptosomes. Among them were members of the translocases of the inner-outer mitochondrial membrane (TIM-TOM) complex (Tim16, Tim22, Tim23, Tom22), which constitute the molecular machinery for mitochondrial protein import (Neupert, 1997), metaxin 1 and 2, which participate in the pre-protein mitochondrial import complex (Armstrong et al., 1997; Armstrong et al., 1999) as well as the voltage-dependent anion-selective channel (Vdac) proteins 1, 2 and 3, which form pores in the outer mitochondrial membrane for diffusion of molecules in the mitochondrion (De Pinto and Palmieri, 1992). Notably, seven members of the mitochondrial membrane carrier family, which facilitate transport of molecules across mitochondrial membranes (Palmieri, 2004) were expressed at higher levels in HAB synaptosomes. These included ADP/ATP translocases (Slc25a4, Slc25a5) that assist the exchange of ADP and ATP between cytosol and mitochondria, glutamate carriers 1 and 2 (Slc25a22, Slc25a18), phosphate and oxoglutarate/malate carriers (Slc25a3, Slc25a11) as well as the calcium-binding protein Alalar 1 (Slc25a12). In addition, numerous proteins located in mitochondria showed increased expression in HAB synaptosomes. Apart from sideroflexins, prohibitins - proteins with multiple functions in mitochondrial senescence and dynamics (Artal-Sanz and Tavernarakis, 2009) - showed ≥ 2 fold increased expression in HAB synaptosomes.



6.3 Discussion

A multi-omics approach combined with *in silico* pathway analysis was applied to the HAB/NAB/LAB mouse model of trait anxiety to unravel the neurobiological underpinnings and identify candidate biomarkers for anxiety disorders. The cingulate cortex synaptosome proteomes of HAB and LAB mice were compared by *in vivo* ^{15}N metabolic labeling and quantitative proteomics. In addition, the cingulate cortex metabolome profiles of HAB/NAB/LAB mice were quantified. Selected differentially expressed candidates were validated by Western blot and affected pathways were identified by *in silico* analyses. Our data provide a panel of phenotype-specific markers, suggesting a key role for mitochondria in modulating anxiety-related behavior that has not been reported previously.

Differential expression of four proteins in HAB and LAB synaptosomes, namely Sfxn5, Car2, Myh10 and Sdhb, was confirmed in an independent HAB/NAB/LAB population. Sfxn5, a member of the sideroflexin family, showed increased expression in HAB mice. So far, limited information is available for sideroflexin functions (Fleming et al., 2001; Yoshikumi et al., 2005), and no association with psychiatric disorders has been reported. Sfxn1 mutations have been linked to abnormal iron deposition in mitochondria resulting in sideroblastic anemia in mice (Fleming et al., 2001). Interestingly, pre- and post-natal iron deficiency in rats led to increased anxiety-related behaviors (Beard et al., 2002; Eseh and Zimmerberg, 2005), suggesting a potential role of iron transport pathways in anxiety pathogenesis. Car2 was found expressed at higher levels in HAB compared to LAB mice. Increased Car2 expression has been also reported in a Down syndrome mouse model as well as in young Down syndrome patients (Palminiello et al., 2008). Carbonic anhydrases are ubiquitously expressed proteins, and carbonic anhydrase inhibitors have been used for the treatment of bipolar disorder (Brandt et al., 1998; Hayes, 1994) and atypical psychosis (Inoue et al., 1984). Myh10, with an increased expression in LAB mice, has been shown to promote filopodia extension by relocalizing integrins (Zhang et al., 2004) and to participate in axon path-finding by regulating netrin receptors (Zhu et al., 2007). Increased Myh10 expression in LAB mice may thus indicate implication of neuronal cell adhesion mechanisms in anxiety modulation. Notably, knock-out mice for cell adhesion-related molecules exhibited increased anxiety-related behavior (Blundell et al., 2009; Schmalzigaug et al., 2009). Taken together, these data point toward novel mechanisms for understanding anxiety pathobiology and



implicate proteins not previously reported in anxiety pathogenesis (i.e. Sfxn5, Myh10) that provide the basis for the establishment of a panel of candidate biomarkers for trait anxiety.

Due to the high costs involved in generating ^{15}N -labeled mice, the number of replicates used in the present study was limited. The animals used for the analyses were carefully chosen so as to accurately represent the phenotype of the individual mouse lines. The HAB and LAB mouse lines are inbred for many generations and therefore animal-to-animal variability is significantly lower compared to outbred animals. Furthermore, all validation assays were performed in a standard-fed, independent population so that any potential diet effect could be excluded, and results could be confirmed in a larger dataset. Due to the low amount of cingulate cortex synaptosomes obtained from a single mouse, using one ^{15}N NAB animal per ^{14}N HAB/ ^{14}N LAB pair was not feasible and thereby different ^{15}N NAB mice were used as internal labeled standards for HAB and LAB animals. Great care was taken in choosing NAB animals with the smallest possible variability with regard to phenotypic parameters as well as animal and cingulate cortex tissue weights.

Apart from single molecules, the biomarker discovery pipeline should extend to affected pathways, given that network dysfunctions rather than single molecular lesions are involved in the pathobiology of complex diseases such as anxiety disorders. Here, our proteomics, metabolomics and *in silico* analyses revealed pronounced alterations in mitochondrial functions, indicating a key role of mitochondria in anxiety-related behavior. In particular, decreased expression levels of glycolysis enzymes with simultaneous increased expression levels of ETC components were observed in HAB synaptosomes. Increased oxidative phosphorylation activity enhances ROS production and oxidative stress, which result in oxidative damage, lipid peroxidation and cell death. There is a mounting body of evidence that links oxidative stress to anxiety disorders. In human studies, increased ROS markers in patients with panic (Kuloglu et al., 2002b) and obsessive-compulsive (Behl et al., 2010; Kuloglu et al., 2002a) disorders have been reported. In mice, well-established anxiety-related behavior biomarkers, such as Glo1 and glutathione reductase 1 exert a neuroprotective role against oxidative damage (Ditzen et al., 2006; Gingrich, 2005; Hovatta et al., 2005; Krömer et al., 2005), and alterations in oxidative stress-related proteins have been described in a mouse model of anxiety (Szego et al., 2010). Moreover, anxiety-related behavior has been correlated with oxidative status in mouse brain (Rammal et al., 2008a) and blood (Bouayed et al., 2007; Rammal et al., 2008b). Remarkably, mitochondria-directed antioxidant treatment led to decreased anxiety-related behavior in rats (Stefanova et al.,



2010). In the present study, an increased expression of all ETC members that produce ROS and reduced levels of proteins and metabolites involved in antioxidant defense were found in HAB mice, implicating dysfunctional antioxidant protection in these animals.

Most cellular systems exhibit flexibility in shifting their metabolism between glycolysis and oxidative phosphorylation according to energetic demands or nutrient availability. Most importantly, the therapeutic potential of modulating this reallocation has been demonstrated in several diseases (Chen et al., 2007; Huber et al., 2004; Riepe et al., 1997). Shifting energy metabolism from oxidative phosphorylation to glycolysis can attenuate oxidative damage and suppress apoptosis (Hunter et al., 2007; Jeong et al., 2004; Vaughn and Deshmukh, 2008). Nutrient-sensitized screening has also revealed the ability of several Food and Drug Administration (FDA)-approved drugs to redirect oxidative phosphorylation to glycolysis (Gohil et al., 2010). This may provide a means for modulating high anxiety-related behavior that warrants further investigation.

An increased expression of proteins participating in mitochondrial import and transport was observed in HAB mice. Proteins such as the Vdac family or hexokinase have been proposed to participate or modulate the permeability transition pore complex, which regulates the exchange of small metabolites between the cytosol and the mitochondrial matrix. In response to ROS or calcium overload, the permeability transition pore complex allows a deregulated entry of small molecules into the mitochondrion, altering mitochondrial permeability and eventually leading to cell death (Kroemer et al., 2007). Interestingly, mice lacking members/modulators of the permeability transition pore complex exhibited alterations in anxiety-related behavior (Luvisetto et al., 2008).

Altered levels of proteins involved in neurotransmission were also observed in HAB mice. There is a close interplay between synapses and mitochondria. Mitochondria are located in synaptic terminals and tethered to sites where synaptic vesicle release occurs (Kageyama and Wongriley, 1982). In functional synapses, mitochondria supply ATP and regulate calcium levels, modulating neuronal polarity (Mattson and Partin, 1999), neurotransmission (Billups and Forsythe, 2002), receptor signaling (Kann et al., 2003) and synaptic plasticity (Vanden Berghe et al., 2002). An increased synaptic activity has been shown to induce mitochondrial-encoded gene expression (Williams et al., 1998). In particular, inhibition of mitochondrial Sdh that we have found to be differentially expressed in HAB and LAB synaptosomes resulted in altered NMDA-mediated



neurotransmission (Calabresi et al., 2001). Since neurotransmission disequilibrium is a hallmark of anxiety disorders (McNaughton, 1997), an altered activity of proteins involved in energy production and transport in mitochondria may in turn lead to neurotransmission perturbations and influence anxiety-related behavior.

Taken together, we submit a mitochondrion-centered hypothesis for the anxiety-related molecular alterations (Fig. 6.13) based on proteomics and metabolomics data and *in silico* pathway information (Filiou et al., 2009; Filiou et al., submitted). Although mitochondrial involvement has been suggested for other psychiatric disorders such as bipolar disorder (Kato, 2006; Stork and Renshaw, 2005) and schizophrenia (Ben-Shachar and Lainfenfeld, 2004), little is known about the role of mitochondria in anxiety disorders. In our dataset, mitochondria appear to be the common denominator of the energy metabolism, oxidative stress and neurotransmission divergencies observed between HAB and LAB mice. The shift from glycolysis to oxidative phosphorylation results in enhanced ROS production and consequently, increased oxidative stress and oxidative damage with an impact on anxiety-related behavior. On a second level, mitochondrial alterations affect the excitatory-inhibitory neurotransmission equilibrium modulating the processing of anxiogenic stimuli. Our hypothesis is further supported by increased anxiety-related behavior observed in mice deficient for mitochondrial proteins (Einat et al., 2005) as well as by the modulation of mitochondrial function by glucocorticoid stress hormones (Du et al., 2009). The structural and functional characteristics of mitochondria enable their selective targeting by drugs for therapeutic purposes. The therapeutic potential of selective mitochondrial targeting has already been demonstrated in cancer (Fulda et al., 2010) and neurodegenerative disorders (Armstrong, 2007) and may also provide a novel promising approach for the treatment of anxiety disorders.

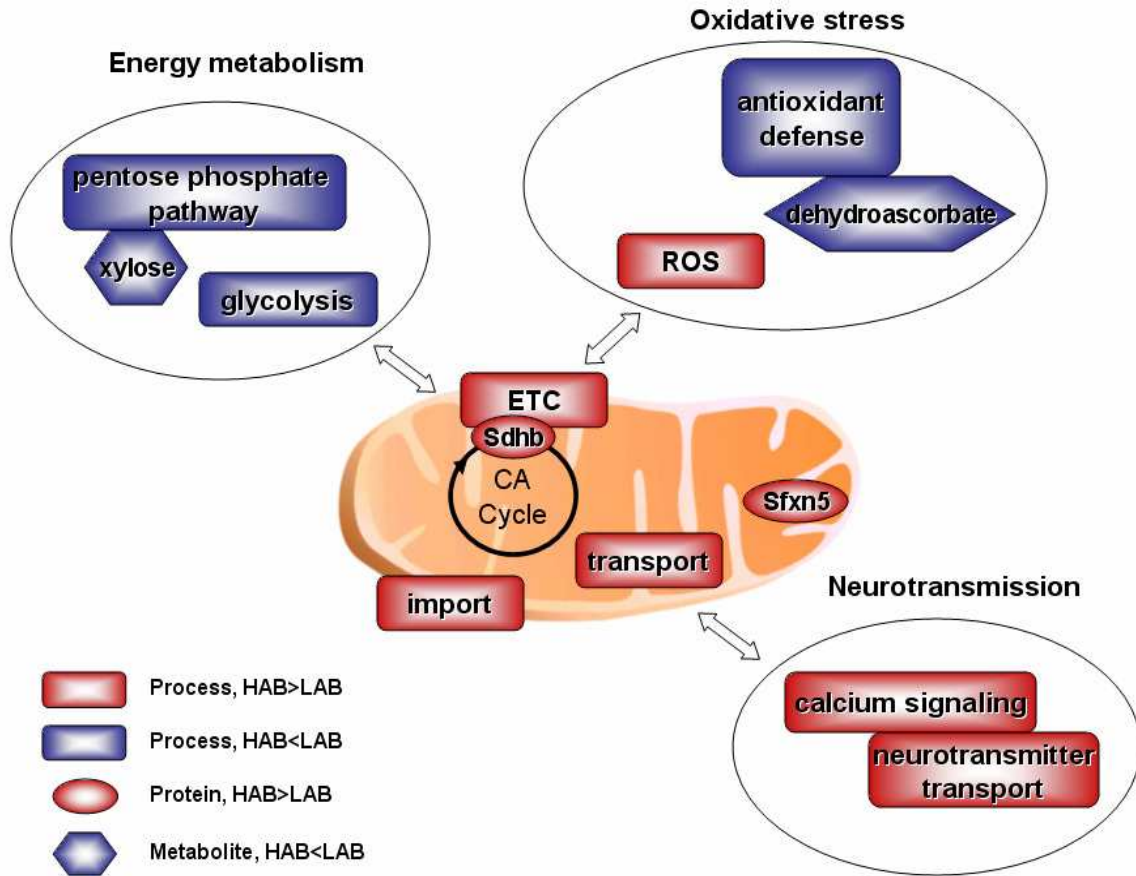


Figure 6.13 Mitochondria-modulated alterations in anxiety-related behavior

Divergencies in mitochondrial energy metabolism, import and transport processes are observed between HAB and LAB mice. HAB mice exhibit an increase in mitochondrial relative to non-mitochondrial energy metabolism and reduced levels of proteins and metabolites involved in antioxidant defense compared to LAB mice. An increase in ETC complexes leads to increased ROS production and oxidative stress. Mitochondrial alterations also have an impact on neurotransmission in the context of ATP supply and calcium regulation modulating anxiety-related behavior.

CA cycle: Citric acid cycle; ETC: Electron transport chain; ROS: Reactive oxygen species; Sdhb: Succinate dehydrogenase, subunit b; Sfxn5: Sideroflexin-5.



7 ¹⁵N isotope effect investigation in HAB mice and *Escherichia coli*

7.1 Introduction

The effect of the ¹⁵N introduction on the behavioral phenotype of HAB mice (see 5.2.1.2) raised the question whether the ¹⁵N introduction also exerts an effect on the HAB mouse proteome. To address this, we compared the cingulate cortex synaptosome proteomes of bacteria-fed ¹⁴N HAB and ¹⁵N HAB mice by employing the ¹⁴N/¹⁵N quantification platform (Fig. 7.1).

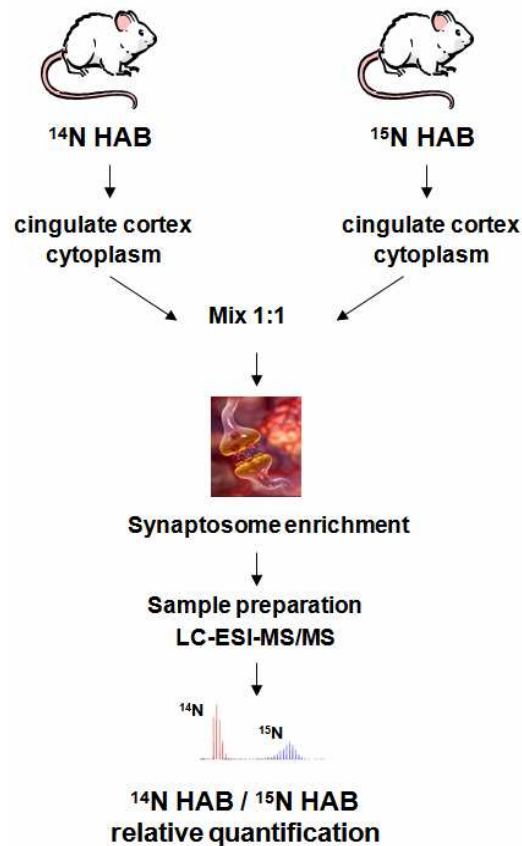


Figure 7.1 Proteomics strategy for ¹⁴N HAB/¹⁵N HAB relative quantification

Cingulate cortices from bacteria-fed ¹⁴N HAB and ¹⁵N HAB were excised and cytoplasmic fractions were mixed 1:1 (w/w) based on protein content for ¹⁴N/¹⁵N relative quantification.



In a second set of experiments, we examined whether the ¹⁵N introduction exerts an effect on the proteome of a different biological system. To investigate ¹⁵N isotope-derived changes, the cytoplasmic proteomes of *E. coli* grown in ¹⁴N (unlabeled) or ¹⁵N-enriched media were compared. Criteria for selecting *E. coli* were the ability to label bacteria in a fast and highly efficient manner via growing them in ¹⁵N-enriched media and their reduced complexity compared to mammals that eliminates the presence of ¹⁵N isotope-independent, confounding factors affecting protein expression levels (e.g., social stress, maternal care). To ensure an accurate proteomics comparison, the ¹⁴N and ¹⁵N media used had identical compositions (apart from the ¹⁵N isotope), and the ¹⁴N and ¹⁵N *E. coli* cultures were grown simultaneously under the same conditions. Relative quantification was performed employing the ¹⁴N/¹⁵N quantification platform (Fig. 7.2).

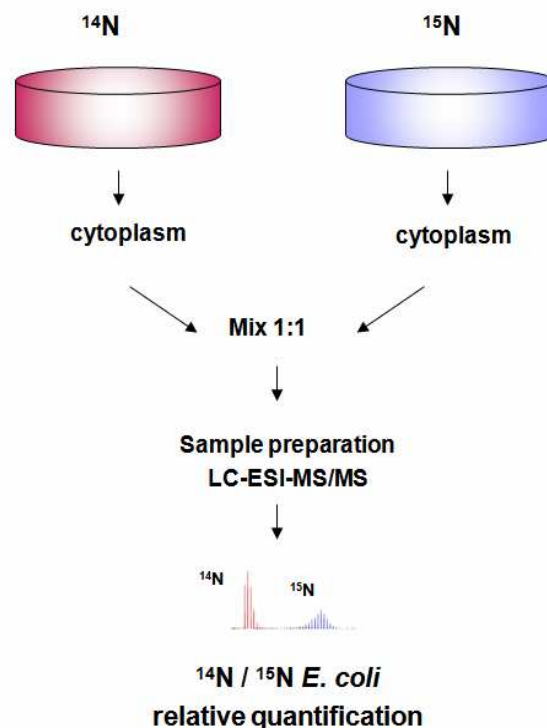


Figure 7.2 Proteomics strategy for ¹⁴N/¹⁵N *Escherichia coli* relative quantification

Cytoplasm from *E. coli* grown in ¹⁴N or ¹⁵N media were mixed 1:1 (w/w) based on protein content for subsequent ¹⁴N/¹⁵N relative quantification.



7.2 Results

7.2.1 Investigation of the ¹⁵N isotope effect in HAB mice

7.2.1.1 ¹⁴N HAB/¹⁵N HAB cingulate cortex synaptosome proteome comparison

Three bacteria-fed ¹⁴N HAB/¹⁵N HAB pairs were compared. In total, 1897 non-redundant proteins were quantified in at least two out of three ¹⁴N HAB/¹⁵N HAB pairs. Applying stringent criteria, we found 49 differentially expressed proteins >1.3 fold in at least two out of three ¹⁴N HAB/¹⁵N HAB pairs. A detailed list of differentially expressed proteins and their abundance ratios is given in Appendix 5.

7.2.1.2 Western blot validation of selected differentially expressed proteins

Differential expression of selected proteins was confirmed by Western blot in cingulate cortices of an independent, bacteria-fed ¹⁴N HAB and ¹⁵N HAB population (Table 7.1). Representative MS raw spectra and Western blot analysis are presented in the following sections.

Protein symbol	IPI Accession	Protein name	¹⁵ N HAB/ ¹⁴ N HAB abundance ratio	Quantified non-redundant peptides
TnR	IPI00227126	Tenascin-R precursor	0.31	11
Nefm	IPI00323800	Neurofilament medium polypeptide	0.47	4

Table 7.1 Differentially expressed proteins in ¹⁴N HAB and ¹⁵N HAB synaptosomes confirmed by Western blot

Tenascin-R (TnR)

TnR was the most highly differentially expressed protein in ¹⁴N HAB and ¹⁵N HAB mice (Fig. 7.3). TnR belongs to a family of extracellular matrix glycoproteins and is expressed in the central nervous system (Pesheva et al., 1989).

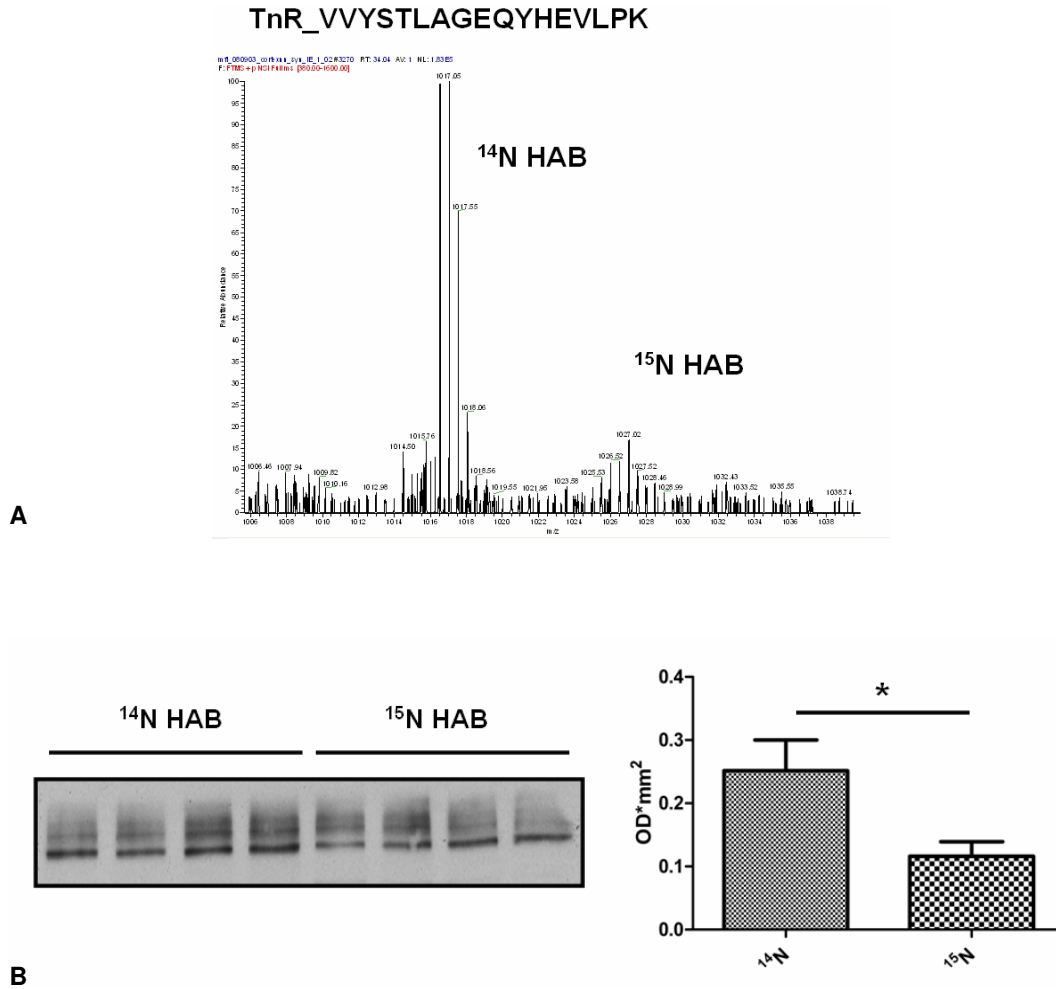


Figure 7.3 Decreased TnR expression in ¹⁵N HAB mice

A. Decreased expression of the TnR peptide VVYSTLAGEQYHEVLPK in bacteria-fed ¹⁵N HAB compared to ¹⁴N HAB mice. **B.** Significantly decreased TnR expression in bacteria-fed ¹⁵N HAB (n=4) compared to ¹⁴N HAB (n=4) mice (*p=0.0460).

Neurofilament medium polypeptide (Nefm)

Neurofilaments are structural parts of the neuronal cytoskeleton, classified in light, medium and heavy based on their molecular weight. Decreased Nefm expression was observed in ¹⁵N HAB compared to ¹⁴N HAB mice (Fig. 7.4).

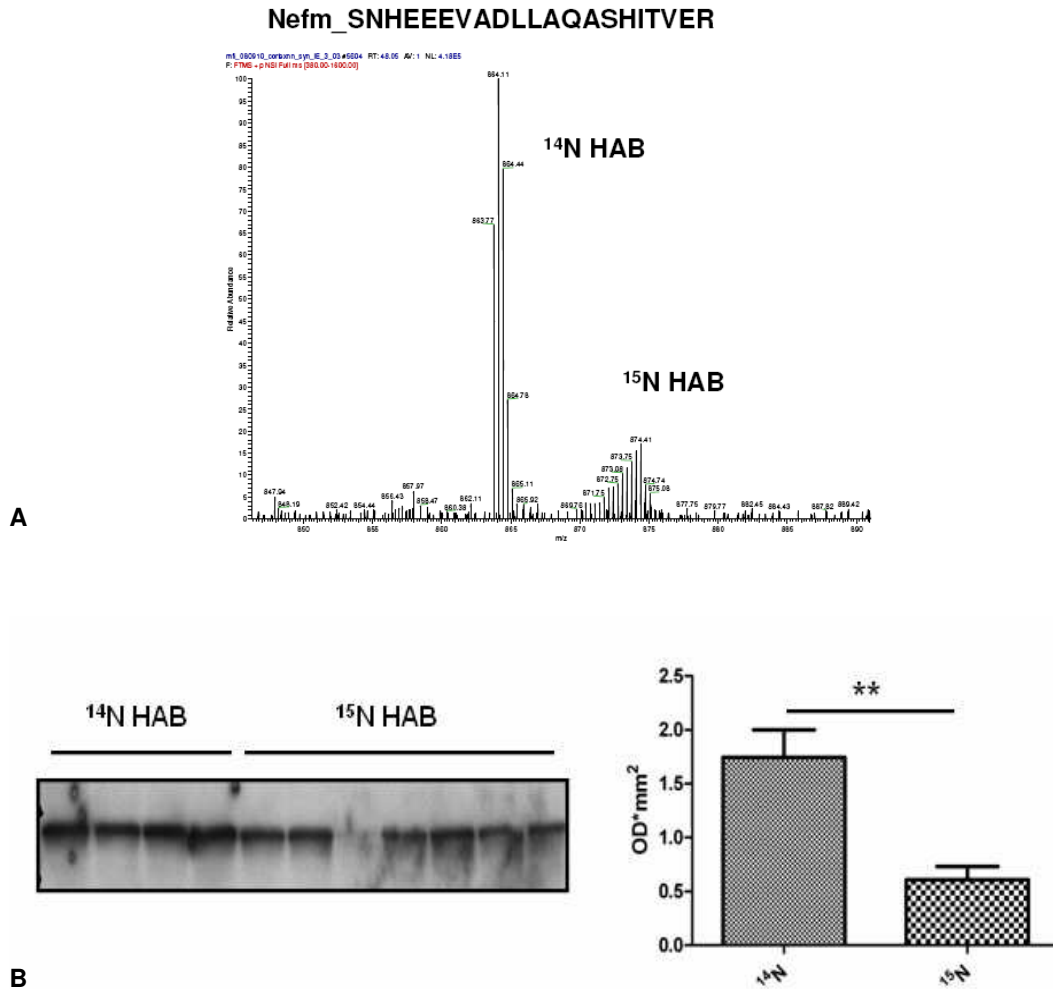


Figure 7.4 Decreased Nefm expression in ¹⁵N HAB mice

A. Decreased expression of the Nefm peptide SNHEEEVADLLAQASHITVER in bacteria-fed ¹⁵N HAB compared to ¹⁴N HAB mice. **B.** Significantly decreased Nefm expression in bacteria-fed ¹⁵N HAB (n=7) compared to ¹⁴N HAB (n=4) mice (**p=0.0018). Significance was retained after exclusion of the very low Nefm-expressing ¹⁵N HAB outlier (fifth from the right, **p=0.0031).

7.2.1.3 *In silico* analysis of altered pathways in ¹⁴N HAB and ¹⁵N HAB mice

Pathway Studio analysis revealed relevance of numerous differentially expressed proteins to depression (Fig. 7.5). Furthermore, the functional composition of the differentially expressed and all quantified proteins in ¹⁴N HAB/¹⁵N HAB animals was compared using FatiGO and significant differences in energy metabolism-related processes were found (Table 7.2).

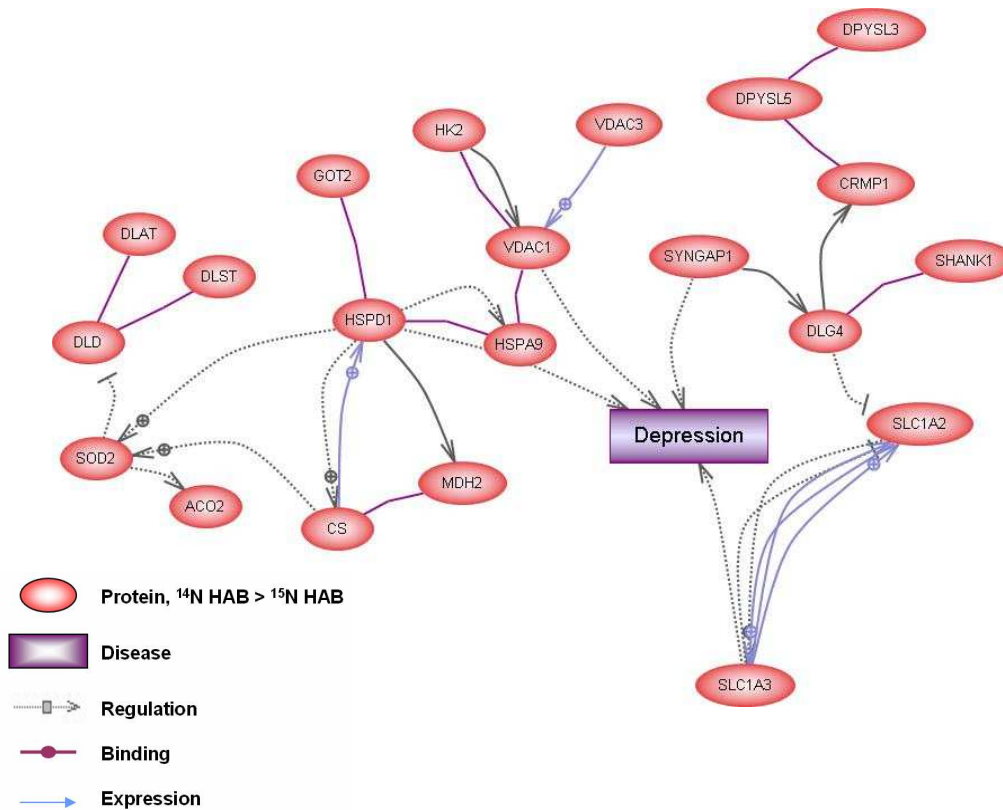


Figure 7.5 Differentially expressed proteins in ¹⁴N HAB and ¹⁵N HAB cingulate cortex synaptosomes and their relevance to depression

Twenty one of the differentially expressed proteins in ¹⁴N HAB and ¹⁵N HAB mice have been directly or indirectly related to depression in the literature (protein names corresponding to the abbreviations used here are given in Appendix 5).

Overrepresented GO terms in the differentially expressed dataset	GO ID	Adjusted p value
carbohydrate metabolic process	GO: 0005975	0.00463
cofactor metabolic process	GO: 0051186	0.00463
coenzyme metabolic process	GO: 0006732	0.00473
cofactor catabolic process	GO: 0051187	0.00473
energy derivation by oxidation of organic compounds	GO: 0015980	0.01490
acetyl-coenzyme A metabolic process	GO: 0006084	0.00059
coenzyme catabolic process	GO: 0009109	0.00270
cellular respiration	GO: 0045333	0.00321
cellular carbohydrate metabolic process	GO: 0044262	0.01220
acetyl-coenzyme A catabolic process	GO: 0046356	0.00962
aerobic respiration	GO: 0009060	0.00830
citric acid cycle	GO: 0006099	0.00710

Table 7.2 Overrepresented functional groups in the differentially expressed protein dataset compared to all quantified proteins in ¹⁴N HAB/¹⁵N HAB mice



7.2.1.4 Altered networks in ¹⁴N HAB and ¹⁵N HAB mice

Quantitative MS and *in silico* pathway analysis revealed protein expression differences predominantly related to energy metabolism. Strikingly, decreased expression of five enzymes catalyzing subsequent steps of the citric acid cycle was found in ¹⁵N HAB compared to ¹⁴N HAB mice (Fig. 7.6). Expression differences in synaptic proteins (Shank1, PSD95, Stx1a) and proteins involved in neurotransmitter transport (Slc6a11 and Slc1a3) were also observed in ¹⁴N HAB and ¹⁵N HAB mice.

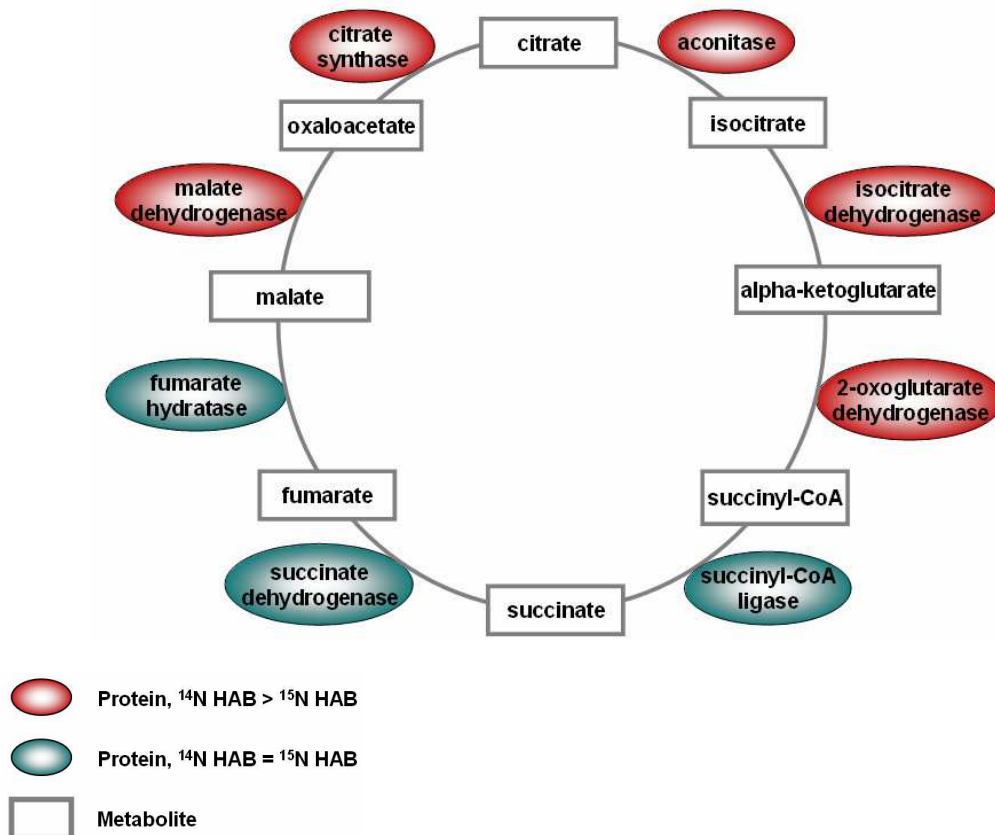


Figure 7.6 Citric acid cycle divergencies between ¹⁴N HAB and ¹⁵N HAB cingulate cortex synaptosomes

Decreased expression of five enzymes catalyzing subsequent steps of the citric acid cycle in ¹⁵N HAB compared to ¹⁴N HAB mice.

7.2.2 Investigation of the ¹⁵N isotope effect in *Escherichia coli*

7.2.2.1 ¹⁴N/¹⁵N *Escherichia coli* cytoplasmic proteome comparison

For relative quantification, two technical replicates of ¹⁴N/¹⁵N *E. coli* cytoplasmic fractions were measured. In total, 390 non-redundant proteins were identified by MS in both replicates. The false



positive identification rate was estimated to be 2% after filtering using a decoy database. Of the identified proteins, 166 were quantified in both replicates and were considered for further analysis. To assess quantification reproducibility between the two replicates, the protein ¹⁵N/¹⁴N log₂ ratios in both replicates were compared, indicating satisfactory quantification accuracy (r=0.93) (Fig. 7.7A). The average ¹⁵N/¹⁴N log₂ ratio distribution of the quantified proteins indicated that the majority of the proteins were not differentially expressed (Fig. 7.7B). However, 18 proteins were found to be consistently differentially expressed >1.3 fold in ¹⁵N compared to ¹⁴N *E. coli* cytoplasm in both replicates (Table 7.3).

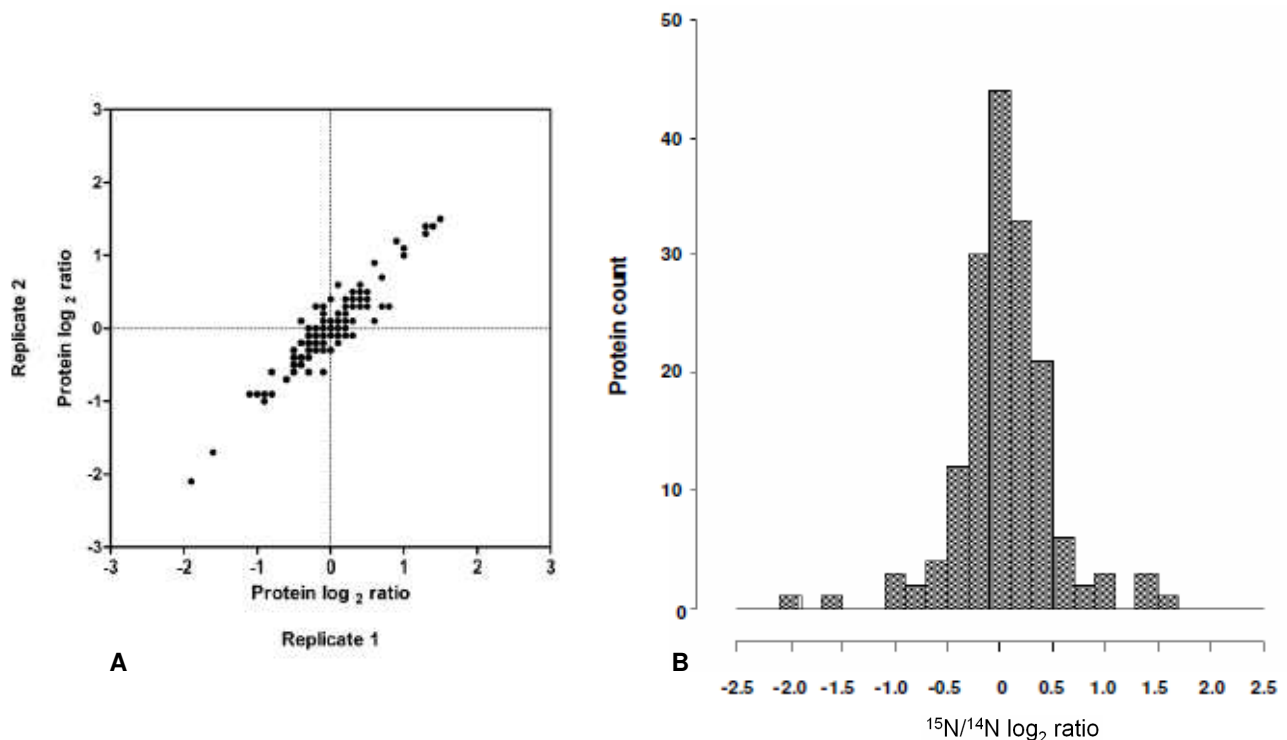


Figure 7.7 Quantification reproducibility of mass spectrometry measurements and ¹⁵N/¹⁴N log₂ ratio distribution of quantified proteins

A. Reproducibility of quantitative MS measurements as estimated by Pearson correlation analysis. The ¹⁵N/¹⁴N log₂ ratios of quantified proteins in both technical replicates were compared. Proteins with consistent ¹⁵N/¹⁴N log₂ ratios in both replicates are expected to distribute along the line $y=x$. The Pearson correlation coefficient showed satisfactory quantification reproducibility between the two measurements ($r=0.93$). **B.** Distribution of average ¹⁵N/¹⁴N log₂ ratios of the quantified proteins in both replicates.



Protein ID	¹⁵ N/ ¹⁴ N abundance ratio	Replicate 1			Replicate 2			Protein name
		¹⁵ N/ ¹⁴ N log ₂ ratio	CI	Pep No	¹⁵ N/ ¹⁴ N log ₂ ratio	CI	Pep No	
AZOR_ECOLI	4.00	1.9	[1.5, 2.2]	5	2.1	[1.5, 2.7]	3	FMN-dependent NADH-azoreductase
Q9R3B9_ECOLI	3.14	1.6	[1.1, 2.2]	4	1.7	[1.0, 2.4]	3	Iron-containing superoxide dismutase
YEBF_ECOLI	2.00	1.1	[0.5, 1.6]	2	0.9	[0.3, 1.4]	3	Protein yebF precursor
PFLB_ECOLI	1.93	1	[0.7, 1.2]	26	0.9	[0.6, 1.2]	14	Formate acetyltransferase 1
CYSJ_ECOLI	1.93	0.9	[0.6, 1.1]	20	1	[0.7, 1.3]	15	Sulfite reductase [NADPH] flavoprotein alpha-component (mutant Ppcl) ppc gene encoding a
Q47521_ECOLI	1.87	0.9	[0.3, 1.4]	6	0.9	[0.1, 1.6]	2	phosphoenolpyruvate carboxylase mutant
Q8VNN2_ECOLI	1.80	0.8	[0.5, 1.1]	14	0.9	[0.5, 1.4]	10	LacZ protein
AK2H_ECOLI	1.57	0.6	[0.3, 1.0]	14	0.7	[0.2, 1.2]	6	Bifunctional aspartokinase/homoserine dehydrogenase II
PPSA_ECOLI	1.37	0.4	[0.2, 0.6]	18	0.5	[0.1, 0.8]	7	Phosphoenolpyruvate synthase
Q2EVI1_ECOLI	1.37	0.4	[0.1, 0.8]	12	0.5	[0.1, 0.9]	11	PrsA
Q4JHR9_ECOLI	0.62	-0.7	[-1.2, -0.2]	4	-0.7	[-1.3, -0.1]	3	Ubiquinone synthesis-related protein
Q9F6G4_ECOLI	0.48	-0.9	[-1.2, -0.5]	11	-1.2	[-1.5, -0.8]	11	Threonine synthase
Q1PG46_ECOLI	0.50	-1	[-1.5, -0.5]	2	-1	[-1.6, -0.4]	2	CspC
Q6ITT5_ECOLI	0.48	-1	[-1.8, -0.2]	2	-1.1	[-1.9, -0.3]	2	MukE
Q6LELO_ECOLI ^a	0.39	-1.3	[-1.5, -1.1]	20	-1.4	[-1.6, -1.1]	15	Aspartokinase I-homoserine dehydrogenase I
Q8RMX0_ECOLI ^a	0.41	-1.3	[-1.7, -0.9]	6	-1.3	[-2.1, -0.5]	2	NADH-quinone oxidoreductase chain G
NUOG_ECOLI	0.38	-1.4	[-2.1, -0.7]	6	-1.4	[-2.3, -0.5]	2	Homoserine kinase
Q68QZ6_ECOLI	0.35	-1.5	[-2.1, -0.9]	4	-1.5	[-2.5, -0.5]	2	

^a different protein variants, treated as two different entities

Table 7.3 Differentially expressed proteins in ¹⁴N and ¹⁵N Escherichia coli cytoplasm

¹⁵N/¹⁴N abundance ratios were calculated from the average ¹⁵N/¹⁴N log₂ ratios of the two replicates. Pep No refers to unique quantified peptides. Proteins whose differential expression was validated by Western blot are indicated with a **bold italic** font.

7.2.2.2 Western blot validation of beta galactosidase

Beta galactosidase is an inducible hydrolytic enzyme that catalyzes the conversion of beta galactosides to monosaccharides. Increased expression of beta galactosidase was found in ¹⁵N compared to ¹⁴N *E. coli* cytoplasmic fraction (Q8VNN2_ECOLI or LacZ, 1.8 fold increase in ¹⁵N, 15 unique quantified peptides in both replicates). Selected beta galactosidase ¹⁴N/¹⁵N peptide pairs are shown in Fig. 7.8A. Increased expression of beta galactosidase in the ¹⁵N compared to the ¹⁴N *E. coli* cytoplasm was confirmed by Western blot (Fig. 7.8B). To assess biological variability, beta galactosidase expression was also investigated in different ¹⁴N and ¹⁵N *E. coli* cytoplasmic fraction preparations, revealing consistent increased expression in the ¹⁵N cytoplasm (data not shown).

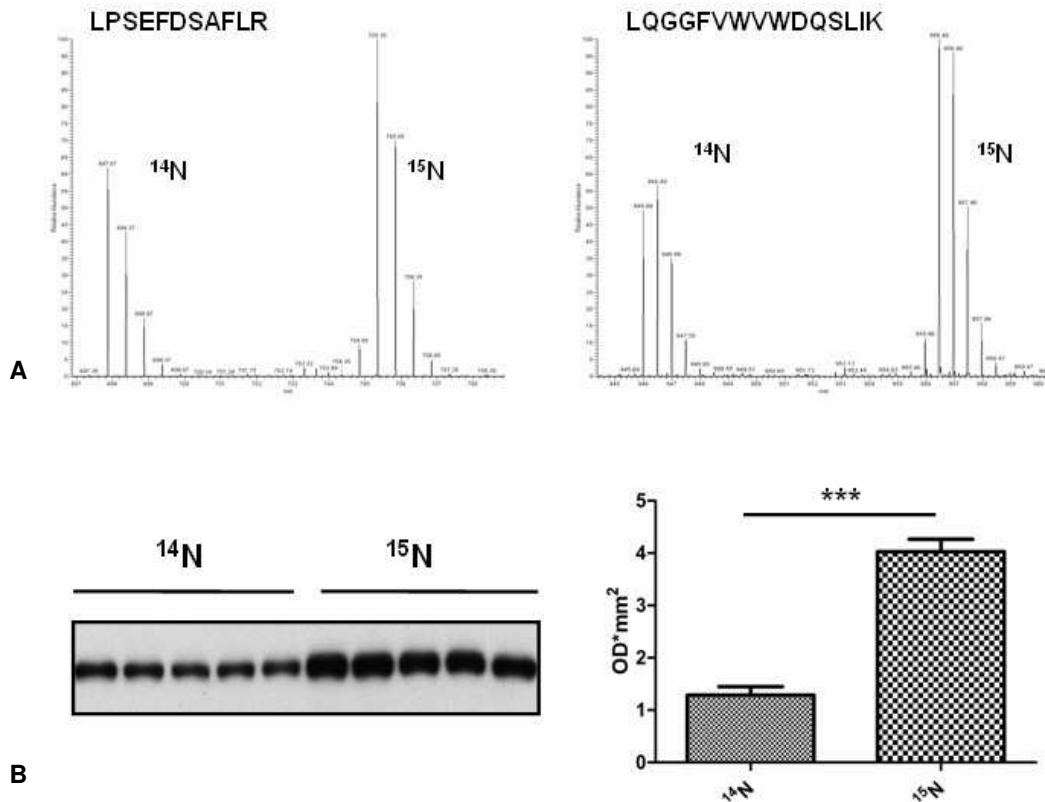


Figure 7.8 Increased beta galactosidase expression in ¹⁵N Escherichia coli cytoplasm
A. Increased expression of the beta galactosidase peptides LPSEFDSAFLR (left) and LQGGFVWVWDQSLIK (right) in the ¹⁵N compared to ¹⁴N E. coli cytoplasm. **B.** Significantly increased expression of beta galactosidase in ¹⁵N compared to ¹⁴N E. coli cytoplasm (***p*<0.0001). Five technical replicates were measured per group.

7.2.2.3 Pyruvate metabolism divergencies between ¹⁴N and ¹⁵N Escherichia coli

Increased expression of three enzymes implicated in pyruvate metabolism (PPSA_ECOLI, PFLB_ECOLI, Q47521_ECOLI) was found in the ¹⁵N E. coli cytoplasmic fraction in both replicates (Table 7.3). Phosphoenolpyruvate synthase (PPSA_ECOLI or PpsA, 1.37 fold increase in ¹⁵N, 20 unique peptides quantified in both replicates) catalyzes the reversible phosphorylation of pyruvate to phosphoenolpyruvate. Formate acetyltransferase 1 (PFLB_ECOLI or PflB, 1.93 fold increase in ¹⁵N, 31 unique peptides quantified in both replicates) catalyzes the reversible conversion of pyruvate and coenzyme A into formate and acetyl-coenzyme A and is involved in anaerobic glucose metabolism. In addition, 1.87 fold increased expression of a phosphoenolpyruvate carboxylase mutant (Q47521_ECOLI or PpcI mutant, six unique peptides quantified in both replicates) was observed in ¹⁵N cytoplasm. Phosphoenolpyruvate carboxylase



catalyzes the addition of carbon dioxide to phosphoenolpyruvate to form inorganic phosphate and oxaloacetate, an intermediate of the citric acid cycle. Unlike the WT variant, the phosphoenolpyruvate carboxylase mutant identified here, cannot be activated from the glycolysis intermediate fructose 1,6-biphosphate (Sutton et al., 1986). Selected quantified ¹⁴N/¹⁵N peptide signals of PPSA_ECOLI (PpsA) and PFLB_ECOLI (PflB) are shown in Fig. 7.9A. To further investigate the effect of the ¹⁵N isotope on pyruvate metabolism, pyruvate levels in ¹⁴N and ¹⁵N *E. coli* cytoplasmic fractions were assessed with a colorimetric-based assay and were found significantly higher in the ¹⁵N compared to the ¹⁴N cytoplasm (Fig. 7.9B). Pyruvate metabolism alterations in ¹⁵N *E. coli* cytoplasm are summarized in Fig. 7.10.

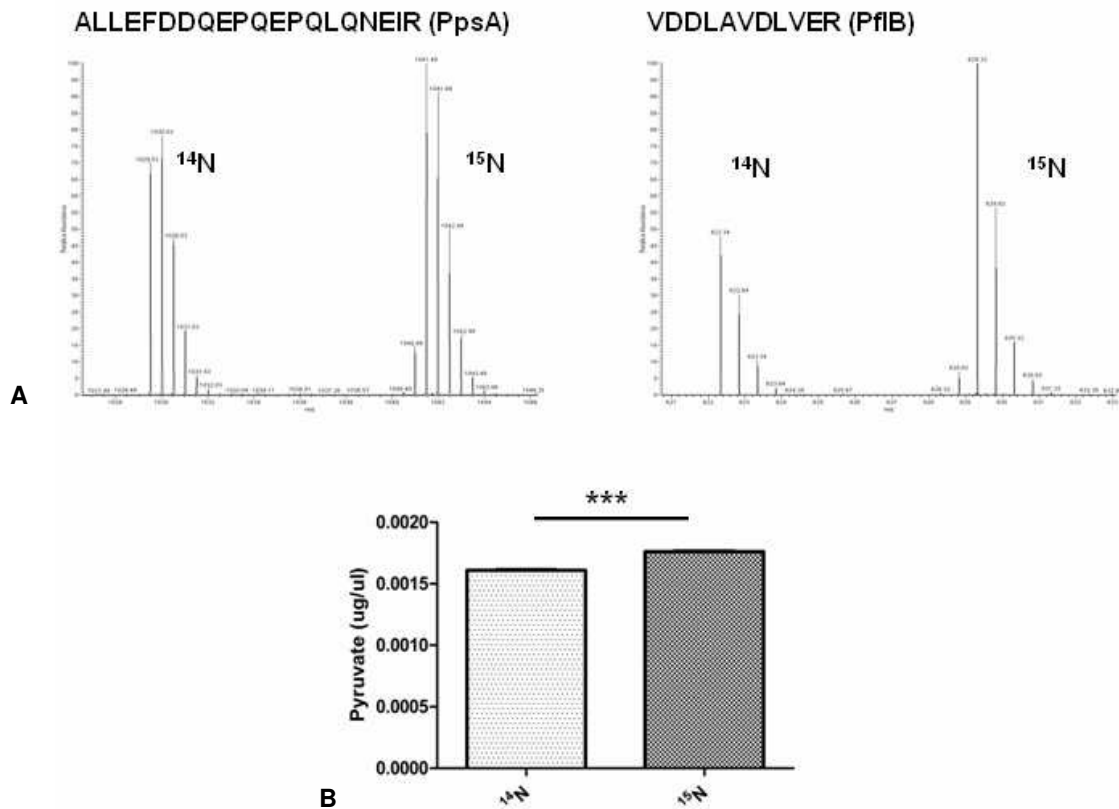


Figure 7.9 Relative quantification of pyruvate metabolism in ¹⁵N and ¹⁴N *Escherichia coli* cytoplasm

A. Increased expression of the phosphoenolpyruvate synthase (PpsA) peptide ALLEFDDQEPQEPQLQNEIR (left) and the formate acetyltransferase 1 (PflB) peptide VDDLAVDLVER (right) in ¹⁵N compared to ¹⁴N *E. coli* cytoplasm. **B.** Elevated levels of pyruvate (***) in ¹⁵N compared to ¹⁴N *E. coli* cytoplasm. Three technical replicates were measured per group.

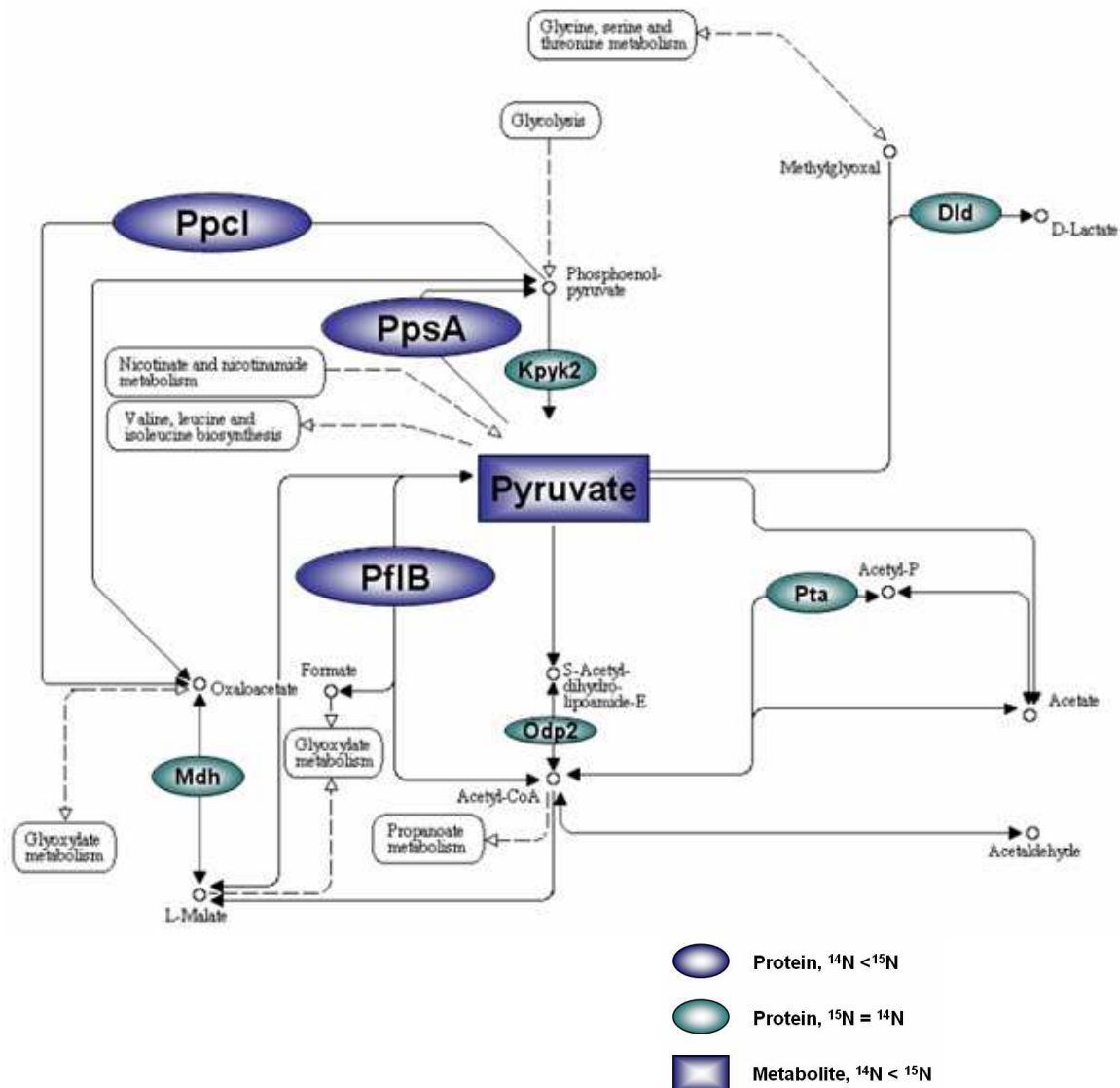


Figure 7.10 Pyruvate metabolism alterations in ¹⁵N Escherichia coli cytoplasm

Schematic representation of the pyruvate metabolism pathway (modified from the KEGG database). Reactions involved in the generation of phosphoenolpyruvate and oxaloacetate, intermediates of glycolysis and citric acid cycle, respectively were affected by the ¹⁵N introduction. Dld: D-lactate dehydrogenase; Kpyk2: Pyruvate kinase II; Mdh: Malate dehydrogenase (Q9KH79, Q9K2L4, Q9KH77, Q9ETZ1 variants); Odp2: Dihydrolipoalysine-residue acetyltransferase component of pyruvate dehydrogenase complex; PflB: Formate acetyltransferase 1; Ppcl: Phosphoenolpyruvate carboxylase mutant (Q47521); PpsA: Phosphoenolpyruvate synthase; Pta: Phosphate acetyltransferase.



7.2.2.4 *In silico* analysis of altered pathways in ¹⁴N and ¹⁵N *Escherichia coli*

GO analysis revealed that the differentially expressed proteins were predominantly involved in biosynthetic and metabolic processes (Filiou et al., in preparation). We compared the differentially expressed proteins and all quantified proteins and found that phosphorylation-related processes (phosphorylation, GO: 0016310; phosphorus metabolic process, GO: 0006793; phosphate metabolic process, GO: 0006796; *p=0.0240 for each) were significantly overrepresented in the group of differentially expressed proteins. The proteins with increased expression in ¹⁵N cytoplasm were then compared to all quantified proteins, and no significantly overrepresented groups were found. However, when comparing only the proteins with decreased expression in ¹⁵N cytoplasm to all quantified proteins, aspartate family amino acid metabolic process (GO: 0009066; *p=0.0450) was found significantly overrepresented in the group of proteins with decreased expression in ¹⁵N cytoplasm.

7.3 Discussion

Although ¹⁵N metabolic labeling in cell culture and live organisms is widely employed for quantitative proteomics experiments, the ¹⁵N isotope effect on protein expression during metabolic labeling has not been studied. After observing the effect of the ¹⁵N introduction on the behavioral phenotype of HAB mice, the ¹⁵N isotope effect on the HAB mouse synaptosome proteome was investigated. We found 49 differentially expressed synaptosomal proteins in three ¹⁴N HAB/¹⁵N HAB cingulate cortex pairs. Pronounced changes in the citric acid cycle (Fig. 7.6) as well as in other energy metabolism-related processes (Table 7.2) and alterations in synaptic proteins were observed in ¹⁵N HAB mice. Decreased expression of TnR and Nefm in ¹⁵N HAB mice was confirmed by Western blot in an independent ¹⁴N HAB/¹⁵N HAB population. Much of our knowledge concerning the role of TnR in the brain is derived from studies of TnR-deficient mice, where alterations in neurotransmission and synaptic plasticity (Bukalo et al., 2007; Gurevicius et al., 2004; Saghatelian et al., 2001) as well as increased anxiety-related behavior and impaired motor coordination (Freitag et al., 2003) have been reported. In addition, altered neurofilament levels have been found in depressed patients (Gudmundsson et al., 2010) and in a rat depression model (Reinés et al., 2004).



In HAB mice, ¹⁵N metabolic labeling resulted in the modulation of depression-like behavior assessed by the total immobility time in the TST. Many of the differentially expressed proteins caused by ¹⁵N metabolic labeling have been previously reported in the literature to be related to the depression phenotype (Fig. 7.5). However, this finding does not imply that the ¹⁵N incorporation has antidepressant, therapeutic properties and one has to be careful to not over-interpret the antidepressant-like effects of the ¹⁵N isotope in HAB mice. ¹⁵N incorporation to an organism can affect protein architecture (Hartmann et al., 2003) and as a result, enzymatic reactions and pathways can be altered in an unpredictable manner. Yet, the ¹⁵N isotope effect provides a means for studying affected pathways involved in depression-like behavior.

On a second level of analysis, the ¹⁵N isotope effect was studied in *E. coli* cultures. *E. coli* is an organism of lower complexity compared to mice, used both as a model organism for quantitative proteomics experiments and as a stable isotope source to metabolically label higher organisms (Krijgsveld et al., 2003). Strikingly, more than 10% of the quantified proteins were found to be differentially expressed in the ¹⁴N and ¹⁵N *E. coli* cytoplasm, demonstrating that the introduction of the ¹⁵N isotope on a proteome alters protein expression, a fact that needs to be taken into consideration when planning and executing quantitative proteomics experiments using ¹⁵N metabolic labeling. The 18 differentially expressed proteins in ¹⁴N and ¹⁵N *E. coli* cytoplasm were primarily involved in pyruvate metabolism, energy production and amino acid biosynthesis. Pyruvate is the endpoint of glycolysis, a central metabolic cascade conserved in all organisms. Via gluconeogenesis, pyruvate can be converted to carbohydrates, whereas through its conversion to oxaloacetate pyruvate can enter the citric acid cycle, thus being a key metabolite for major metabolic cascades. Increased expression of enzymes involved in pyruvate metabolism (PFLB_ECOLI, Q47521_ECOLI, PPSA_ECOLI) as well as elevated pyruvate levels were found in ¹⁵N cytoplasm. In addition, increased expression in ¹⁵N cytoplasm of beta galactosidase, an enzyme also involved in energy catabolism was demonstrated in ¹⁵N cytoplasm both by MS and Western blot analyses. Lactose catabolism by beta galactosidase leads to the production of galactose and glucose, the starting point of glycolysis. Apart from energy metabolism, alterations were observed in five proteins (AK2H_ECOLI, Q9F6G4_ECOLI, Q6LEL0_ECOLI, Q8RMX0_ECOLI, Q68QZ6_ECOLI, see Table 7.3) involved in aspartate amino acid family biosynthesis. Decreased expression in ¹⁵N *E. coli* cytoplasm was found for MukE (Q6ITT5_ECOLI) and CpsC (Q1PG46_ECOLI), proteins that participate in chromosome



segregation (Yamanaka et al., 1996) and transcription regulation (Bae et al., 2000), respectively. Enrichment analysis revealed that in the group of differentially expressed proteins phosphorylation-related processes were significantly overrepresented compared to all quantified proteins. Intriguingly, six of the differentially expressed proteins exhibit kinase activity (AK2H_ECOLI, PPSA_ECOLI, Q2EVI1_ECOLI, Q6LELO_ECOLI, Q8RMX0_ECOLI, Q68QZ6_ECOLI, see Table 7.3), whereas PPSA_ECOLI has recently been reported to be phosphorylated (Macek et al., 2008). In conclusion, the introduction of the ¹⁵N isotope in *E. coli* does not only affect essential metabolic pathways, such as glycolysis but also fundamental functions related to chromosome, transcription and post-translational modification regulation.

In the literature, the ¹⁵N isotope effect has been considered to be trivial since a substitution of ¹⁵N for ¹⁴N only results in a relatively small mass difference (Van Langenhove, 1986). To assess the effect of the ¹⁵N isotope, Bigeleisen (Bigeleisen, 1949) estimated the maximum ratio of the ¹⁴N and ¹⁵N specific rate constants (K_{14N}/K_{15N}) and found that it was within the error limits of normal measurements, concluding that the ¹⁵N isotope effect on a reaction process is insignificant. On the other hand, it is known that a chemical bond involving a heavy isotope is stronger and therefore more difficult to break than the same bond involving the corresponding light isotope of the same element (Melander and Saunders, 1980). If the cleavage of this bond is the rate-limiting step of a reaction, then the reaction will proceed slower for the molecule with the heavy isotope. We propose that minor synergistic changes introduced by the substitution of ¹⁴N for ¹⁵N may account for slight structural conformational changes in a protein. When these alterations occur in an enzyme's active site or in the peptide backbone of a rigid cluster, they could cause alterations in enzyme catalytic activity or distortions in spatial structure, respectively. As shown in our studies of HAB mice and *E. coli*, such alterations at the molecular level can affect biochemical reactions and pathways in an unpredictable manner. Our hypothesis is further supported by a study that compared ¹⁵N- or ¹³C-labeled to unlabeled Cu-thiolate cluster in yeast and found spectroscopic differences between the clusters, suggesting that stable isotope labeling can indeed affect the molecular architecture of a protein (Hartmann et al., 2003).

We show that the introduction of the ¹⁵N isotope affects evolutionary well-conserved pathways present in all organisms such as the glycolysis and the citric acid cycle as well as ubiquitous regulatory mechanisms such as phosphorylation. We have demonstrated the effect of the ¹⁵N incorporation at the proteome level both in low complexity organisms and mammals, where



additionally the behavioral phenotype was influenced. Future studies include validation of current findings in *E. coli* cultures grown in ¹⁴N and ¹⁵N media from other commercial sources, quantitative MS analyses of more biological replicates and assessment of metabolite levels by enzymatic methods. Preliminary data from *E. coli* grown in ¹⁴N and ¹⁵N media from another commercial source (Silantes) confirmed elevated pyruvate levels in ¹⁵N cytoplasm in different biological replicates, whereas reduced *E. coli* growth rates in ¹⁵N compared to ¹⁴N media were consistently observed (Filiou et al., in preparation).

To the best of our knowledge, this is the first time that alterations in protein expression due to the introduction of ¹⁵N isotope during metabolic labeling have been reported. Since ¹⁵N metabolic labeling is currently one of the most accurate quantitative MS methods with great potential for *in vivo* and *in vitro* studies (Filiou et al., accepted), the ¹⁵N isotope effect on the labeled proteome should be taken into consideration when planning quantitative proteomics experiments. The use of a labeling control strategy is therefore critical to avoid ¹⁵N isotope-derived, misleading analytical and biological information.



8 Biomarker discovery in the G72/G30 transgenic mouse model of schizophrenia-like symptoms

8.1 Introduction

Although a number of animal models of schizophrenia-like symptoms have been established, no mouse model addressing the molecular and behavioral effects of the G72 protein was up to now available since the G72/G30 locus that encodes for the G72 protein is primate-specific. The establishment of a transgenic mouse model for the G72/G30 locus (Otte et al., 2009) has enabled for the first time the examination of the G72 protein function at the level of a model organism. Due to the low G72 transcript expression in humans, only limited information is available on G72 tissue-specific expression patterns (Benzel et al., 2008). Increased expression of the G72 and G30 transcripts was found in mouse cerebella compared to other brain areas examined (Otte et al., 2009). Therefore, the cerebellum was selected to investigate proteome alterations caused by the introduction of the G72/G30 transgene in CD1 mice. However, unambiguous detection of the G72 protein in cerebellum with conventional Western blot analysis was not feasible due to the presence of confounding protein signals. To ensure optimal protein separation and G72 protein detection, a 2D-Western blot approach was employed. In addition, to achieve a molecular characterization of the G72/G30 transgenic animals, cerebellar proteomes of G72/G30 transgenic animals were compared to WT counterparts by 2D-PAGE. For all experiments, male animals heterozygous for the G72/G30 transgene were used.

8.2 Results

8.2.1 Detection of the G72 protein in G72/G30 transgenic mice

To ensure that the G72 protein was present in G72/G30 transgenic mice, a 2D-Western blot analysis was performed in cerebellar protein homogenates, revealing the presence of a protein with the physicochemical characteristics of the long splice variant LG72 in G72/G30 transgenic (G72Tg1) but not in WT mice (Fig. 8.1). This led to the conclusion that the transgenic G72/G30 animals produce the LG72 protein encoded by the longest G72 open reading frame.

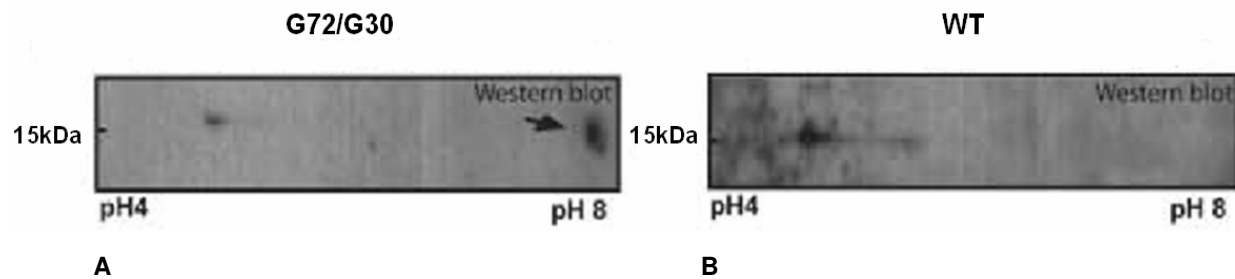


Figure 8.1 G72 protein detection in cerebella of G72/G30 transgenic mice by 2D-Western blot

A. The anti-G72 antibodies detected a protein signal corresponding to the LG72 molecular weight and isoelectric point in G72/G30 transgenic mice (arrow). **B.** This signal was not detected in WT mice.

8.2.2 Protein expression differences in G72/G30 transgenic and wild type mice

Cerebellar protein homogenates from both transgenic lines (G72tg1 and G72tg2, see 3.6.1) and WT mice were compared. 2D-PAGE analysis revealed a number of cerebellar protein expression differences between G72/G30 transgenic and WT animals (Table 8.1). Among the differentially expressed proteins, increased expression of glutathione transferase family members was observed. In particular, increased expression of glutathione S-transferase M1 (Gstm1) was consistently found in both transgenic lines (Fig. 8.2), whereas increased glutathione S-transferase P1 (Gstp1) expression was detected in G72Tg1 line. In addition, altered expression of cytoskeleton-related components, such as tubulins and the actin-binding protein cofilin-1 was observed in G72/G30 transgenic mice. Increased expression of phosphoglycerate mutase 1, rho GDP dissociation inhibitor and glutamine synthetase involved in glycolysis, signal transduction regulation and neurotransmitter biosynthesis, respectively, was found in the G72Tg2 line. Pathway Studio analysis indicated involvement of the differentially expressed proteins in oxidative stress and apoptosis, while implication of two proteins in schizophrenia has been previously reported in the literature (Fig. 8.3).



G72Tg1		
Protein ID	G72/G30 trasgenic/WT abundance ratio	Protein name
GSTP1_MOUSE	2.29	Glutathione S-transferase P1
GDIR_MOUSE	2.04	Rho GDP dissociation inhibitor
GSTM1_MOUSE	1.54	Glutathione S-transferase M1
Q3TGF0_MOUSE	0.42	Tubulin alpha 1A chain

G72Tg2		
Protein ID	G72/G30 trasgenic/WT abundance ratio	Protein name
Q91VC6_MOUSE	2.84	Glutamine synthetase
Q99JZ6_MOUSE	2.52	Tubulin beta 2C chain
PGAM1_MOUSE	2.41	Phosphoglycerate mutase 1
GSTM1_MOUSE	1.59	Glutathione S-transferase M1
COF1_MOUSE	1.45	Cofilin-1

Table 8.1 Protein expression differences in G72/G30 transgenic and wild type cerebella

Four and five differentially expressed proteins were found in the G72Tg1/WT and the G72Tg2/WT comparison, respectively.

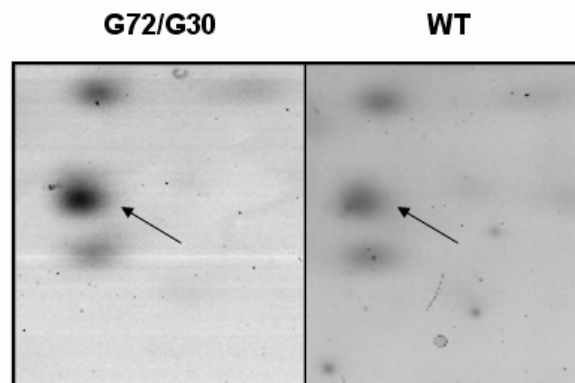


Figure 8.2 Increased Gstm1 expression in G72/G30 transgenic mice

Representative 2D-gel images indicating an increased signal intensity of the spot corresponding to Gsmt1 (arrows) in G72/G30 transgenic (G72Tg1) (left) compared to WT mice (right).

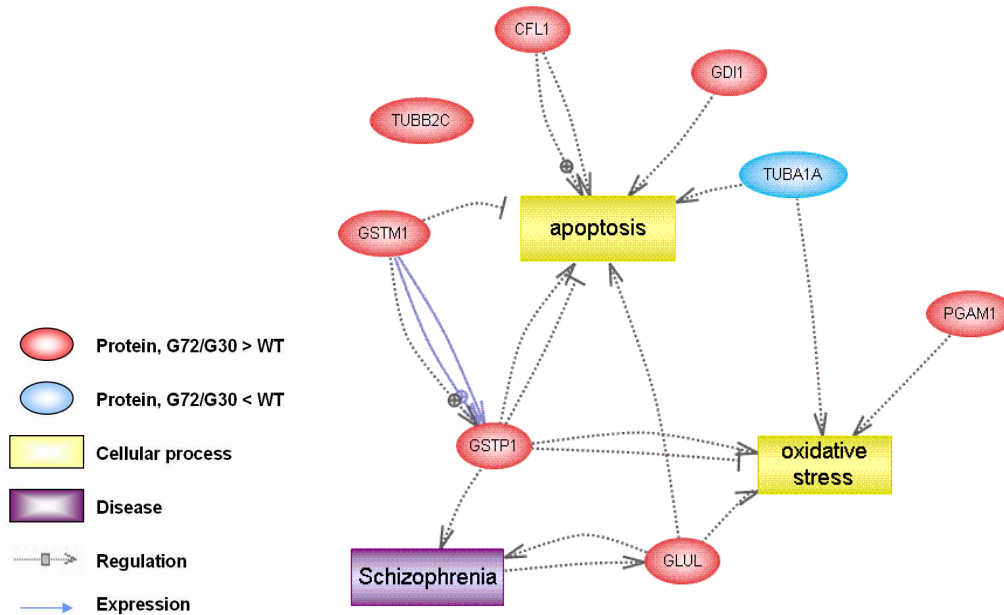


Figure 8.3 Pathway analysis of differentially expressed proteins in G72/G30 transgenic and wild type mice

Differentially expressed proteins have been related to oxidative stress and apoptosis (different nomenclature between pathway and proteomics analyses is due to different databases employed for data processing).

Cfl1: Cofilin-1; *Gdi1*: Rho GDP dissociation inhibitor; *Glul*: Glutamine synthetase; *Gstm1*: Glutathione S-transferase M1; *Gstp1*: Glutathione S-transferase P1; *Pgam1*: Phosphoglycerate mutase 1; *Tuba1a*: Tubulin alpha 1; *Tubb2c*: Tubulin beta 2.

8.3 Discussion

Although the G72/G30 locus is one of the most robust susceptibility regions for schizophrenia, the functional role of the G72 protein remains unclear. It has been reported that G72 binds to and activates *in vitro* D-amino acid oxidase (DAO) (Chumakov et al., 2002) which in turn oxidizes D-serine, an allosteric co-activator of glutamatergic NMDA (Mothet et al., 2000), in accordance with the NMDA hypofunction hypothesis of schizophrenia. However, G72 has been recently proposed to be a mitochondrial protein that promotes mitochondrial fragmentation, failing to show *in vivo* interaction with DAO (Kvajo et al., 2008). In the context of a potential G72 role in mitochondrial function, our 2D-PAGE analysis revealed expression differences in members of the glutathione



S-transferase family that are involved in detoxifying endogenous and xenobiotic compounds by catalyzing their conjugation to glutathione (Board, 2007). Because of the protective role of glutathione against ROS damage, a possible increase in oxidative stress due to G72 expression is suggested. Our data are further supported by altered activity of ETC complex I, accumulation of oxidized lipids in cerebellum and reduced glutathione activity in G72/G30 transgenic animals (Otte et al., in preparation). Taken together, an increased oxidative stress-related activity in G72/G30 transgenic mice is observed, pointing toward a mitochondrial role of G72, in accordance with oxidative stress and mitochondrial dysfunction reported in schizophrenia (Wood et al., 2009). The 2D-PAGE analysis performed revealed protein expression differences in G72/G30 transgenic and WT mice, thus providing useful insights into the functional role of the G72 protein. To achieve a more detailed characterization of the G72/G30 transgenic mouse model, future studies include brain tissue comparison of G72/G30 transgenic and WT animals by ¹⁵N metabolic labeling and quantitative MS using ¹⁵N-labeled CD1 mice as internal standards (similar to the quantitative proteomics platform used for the HAB/NAB/LAB trait anxiety mouse model).



9 Outlook and perspectives

9.1 Biomarker discovery in psychiatric disorders

The combination of powerful proteomics and metabolomics technologies and well-established rodent models of psychopathologies bridges behavioral biology, genetics, protein biochemistry and bioinformatics into a multidisciplinary approach to disentangle the pathobiology of psychiatric disorders. Here, we have thoroughly analyzed the HAB/NAB/LAB mouse model of trait anxiety and report altered proteins and pathways in HAB and LAB animals. We have confirmed differential expression of four selected proteins (Sfxn5, Car2, Myh10, Sdhd) identified by quantitative proteomics in an independent HAB/NAB/LAB population (Filiou et al., 2010b; Filiou et al., 2010c; Filiou et al., submitted), providing a panel of phenotype-specific markers. Most importantly, we highlight the role of mitochondria in modulating anxiety-related behavior by exerting an effect on energy metabolism, oxidative stress, molecular transport and neurotransmission pathways. Further investigation of the present findings in a larger population of HAB/NAB/LAB mice as well as assessment of the predictive validity of the identified candidate biomarkers are the next steps toward the establishment of anxiety-related behavior markers. Since the therapeutic potential of modulating mitochondrial energy metabolism (Gohil et al., 2010) and selectively targeting mitochondrial proteins (Fulda et al., 2010) has been demonstrated in disease, future work includes functional analyses to elucidate mitochondrial alterations in HAB and LAB mice (with special focus on oxidative stress and import/transport mechanisms) and pinpoint potential mitochondrial targets for therapeutic intervention. Moreover, the biomarker discovery pipeline based on ^{15}N metabolic labeling will be applied to other models of psychopathologies beginning with G72/G30 transgenic mice, thus expanding the findings acquired from the 2D-gel-based approach. Undoubtedly, there is a long way from animal models to the implementation of biomarkers for patient diagnosis. However, the data presented here aid significantly our understanding concerning protein networks implicated in the molecular neurobiology of trait anxiety at the synapse. The four validated candidates (Sfxn5, Car2, Myh10, Sdhd) share increased sequence similarity with the corresponding proteins in humans and are involved in well-conserved pathways, indicating their potential applicability for screening of human specimens. Eventually, a robust set of well-characterized biomarkers in HAB/NAB/LAB animals



will be tested in human samples in order to transfer the knowledge gained from animal models to humans. These candidate biomarkers in combination with affected pathways apart from advancing our understanding concerning the underlying mechanisms of anxiety-related behavior may also lead to novel therapeutic targets for anxiety disorders.

9.2 Proteomics technologies

The development of high-throughput methodologies to perform non-hypothesis driven research has revolutionized the biomedical field. Recent advances in establishing sophisticated proteomics platforms to quantify protein differences between two states have enabled the comparison of disease and control conditions at a holistic level. Consequently, large scale proteomics quantification studies can shed light on the molecular pathophysiology of psychiatric diseases in a way that has not been possible before. Yet, to benefit from the proteomics toolbox, fine-tuning of existing platforms for the material in question is of pivotal importance. In the present study, we optimized a previously reported IEF-based method for phosphopeptide analysis (Maccarrone et al., 2006) and applied it to brain tissue, resulting in the most detailed proteome and phosphoproteome synaptosome profiling described to date (Filiou et al., 2010a). At the quantitative level, we established an *in vivo* ^{15}N metabolic labeling strategy for mice, achieving high ^{15}N incorporation even in tissues with slow protein turnover (i.e. brain) without affecting normal development (Frank et al., 2009). ^{15}N -labeled WT mouse specimens can serve as internal standards for a battery of quantitative proteomics experiments and can be practically used to interrogate any disease animal model (Filiou et al., accepted). The use of stable isotope labeling is currently the state-of-the-art quantitative MS-based approach. For the first time, we showed that the introduction of the ^{15}N isotope can affect not only the labeled proteome but also the behavioral phenotype of the labeled organisms (Frank et al., 2009). This is of great importance to the field of quantitative proteomics because it demonstrates the indispensable need for employing a labeling control strategy when performing metabolic labeling experiments. Taken together, the proteomics technologies and relevant methodological considerations presented here shed light into proteomics platforms and provide robust and reliable tools that can be utilized in a wide range of applications in model organisms and human specimens for in-depth proteome profiling, accurate relative quantification and biomarker discovery.



10 References

Abou Jamra, R., Schmael, C., Cichon, S., Rietschel, M., Schumacher, J., Nothen, M.M., 2006. The G72/G30 gene locus in psychiatric disorders: A challenge to diagnostic boundaries? *Schizophr Bull* 32, 599-608.

Agus, D.B., Gambhir, S.S., Pardridge, W.M., Spielholz, C., Baselga, J., Vera, J.C., Golde, D.W., 1997. Vitamin C crosses the blood-brain barrier in the oxidized form through the glucose transporters. *J Clin Invest* 100, 2842-2848.

Al-Shahrour, F., Minguez, P., Vaquerizas, J.M., Conde, L., Dopazo, J., 2005. BABELOMICS: A suite of web tools for functional annotation and analysis of groups of genes in high-throughput experiments. *Nucleic Acids Res* 33, W460-464.

American Psychiatric Association, 2000. Diagnostic and statistical manual of mental disorders, 4th ed., text revision, American Psychiatric Association, Washington, DC, USA.

Armstrong, J.S., 2007. Mitochondrial medicine: Pharmacological targeting of mitochondria in disease. *Br J Pharmacol* 151, 1154-1165.

Armstrong, L.C., Komiya, T., Bergman, B.E., Mihara, K., Bornstein, P., 1997. Metaxin is a component of a preprotein import complex in the outer membrane of the mammalian mitochondrion. *J Biol Chem* 272, 6510-6518.

Armstrong, L.C., Saenz, A.J., Bornstein, P., 1999. Metaxin 1 interacts with metaxin 2, a novel related protein associated with the mammalian mitochondrial outer membrane. *J Cell Biochem* 74, 11-22.

Arnold, S.E., Talbot, K., Hahn, C.G., 2005. Neurodevelopment, neuroplasticity, and new genes for schizophrenia. *Prog Brain Res* 147, 319-345.

Artal-Sanz, M., Tavernarakis, N., 2009. Prohibitin and mitochondrial biology. *Trends Endocrinol Metab* 20, 394-401.

Asami, T., Hayano, F., Nakamura, M., Yamasue, H., Uehara, K., Otsuka, T., Roppongi, T., Nishihashi, N., Inoue, T., Hirayasu, Y., 2008. Anterior cingulate cortex volume reduction in patients with panic disorder. *Psychiatry Clin Neurosci* 62, 322-330.

Bae, W., Xia, B., Inouye, M., Severinov, K., 2000. *Escherichia coli* CspA-family RNA chaperones are transcription antiterminators. *Proc Natl Acad Sci U S A* 97, 7784-7789.

Bai, F., Witzmann, F.A., 2007. Synaptosome proteomics. *Subcell Biochem* 43, 77-98.

Ballmaier, M., Toga, A.W., Blanton, R.E., Sowell, E.R., Lavretsky, H., Peterson, J., Pham, D., Kumar, A., 2004. Anterior cingulate, gyrus rectus, and orbitofrontal abnormalities in elderly depressed patients: An MRI-based parcellation of the prefrontal cortex. *Am J Psychiatry* 161, 99-108.

Bantscheff, M., Schirle, M., Sweetman, G., Rick, J., Kuster, B., 2007. Quantitative mass spectrometry in proteomics: A critical review. *Anal Bioanal Chem* 389, 1017-1031.

Barkus, C., McHugh, S.B., Sprengel, R., Seeburg, P.H., Rawlins, J.N.P., Bannerman, D.M., 2010. Hippocampal NMDA receptors and anxiety: At the interface between cognition and emotion. *Eur J Pharmacol* 626, 49-56.

Beard, J.L., Erikson, K.M., Jones, B.C., 2002. Neurobehavioral analysis of developmental iron deficiency in rats. *Behav Brain Res* 134, 517-524.



- Behl, A., Swami, G., Sircar, S.S., Bhatia, M.S., Banerjee, B.D., 2010. Relationship of possible stress-related biochemical markers to oxidative/antioxidative status in obsessive-compulsive disorder. *Neuropsychobiology* 61, 210-214.
- Ben-Shachar, D., Laifenfeld, D., 2004. Mitochondria, synaptic plasticity, and schizophrenia. *Int Rev Neurobiol* 59, 273-296.
- Benzel, I., Kew, J.N., Viknaraja, R., Kelly, F., de Belleruche, J., Hirsch, S., Sanderson, T.H., Maycox, P.R., 2008. Investigation of G72 (DAOA) expression in the human brain. *BMC Psychiatry* 8, 94.
- Beranova-Giorgianni, S., Zhao, Y., Desiderio, D.M., Giorgianni, F., 2006. Phosphoproteomic analysis of the human pituitary. *Pituitary* 9, 109-120.
- Berg, J.S., Cheney, R.E., 2002. Myosin-X is an unconventional myosin that undergoes intrafilopodial motility. *Nat Cell Biol* 4, 246-250.
- Bigeleisen, J., 1949. The validity of the use of tracers to follow chemical reactions. *Science* 110, 14-16.
- Billups, B., Forsythe, I.D., 2002. Presynaptic mitochondrial calcium sequestration influences transmission at mammalian central synapses. *J Neurosci* 22, 5840-5847.
- Bindschedler, L.V., Palmblad, M., Cramer, R., 2008. Hydroponic isotope labelling of entire plants (HILEP) for quantitative plant proteomics; an oxidative stress case study. *Phytochemistry* 69, 1962-1972.
- Biomarkers Definitions Working Group, Atkinson, A.J., Colburn, W.A., DeGruttola, V.G., DeMets, D.L., Downing, G.J., Hoth, D.F., Oates, J.A., Peck, C.C., Schooley, R.T., Spilker, B.A., Woodcock, J., Zeger, S.L., 2001. Biomarkers and surrogate endpoints: Preferred definitions and conceptual framework. *Clin Pharmacol Ther* 69, 89-95.
- Blundell, J., Tabuchi, K., Bolliger, M.F., Blaiss, C.A., Brose, N., Liu, X., Südhof, T.C., Powell, C.M., 2009. Increased anxiety-like behavior in mice lacking the inhibitory synapse cell adhesion molecule neuroligin 2. *Genes Brain Behav* 8, 114-126.
- Board, P.G., 2007. The use of glutathione transferase-knockout mice as pharmacological and toxicological models. *Expert Opin Drug Metab Toxicol* 3, 421-433.
- Bouayed, J., Rammal, H., Younos, C., Soulimani, R., 2007. Positive correlation between peripheral blood granulocyte oxidative status and level of anxiety in mice. *Eur J Pharmacol* 564, 146-149.
- Bozon, B., Kelly, A., Josselyn, S.A., Silva, A.J., Davis, S., Laroche, S., 2003. MAPK, CREB and zif268 are all required for the consolidation of recognition memory. *Philos Trans R Soc Lond B Biol Sci* 358, 805-814.
- Braithwaite, S.P., Adkisson, M., Leung, J., Nava, A., Masterson, B., Urfer, R., Oksenberg, D., Nikolich, K., 2006. Regulation of NMDA receptor trafficking and function by striatal-enriched tyrosine phosphatase (STEP). *Eur J Neurosci* 23, 2847-2856.
- Brandt, C., Grunze, H., Normann, C., Walden, J., 1998. Acetazolamide in the treatment of acute mania - A case report. *Neuropsychobiology* 38, 202-203.
- Breton, S., 2001. The cellular physiology of carbonic anhydrases. *JOP* 2, 159-164.
- Brunelli, S.A., 2005. Selective breeding for an infant phenotype: Rat pup ultrasonic vocalization (USV). *Behav Genet* 35, 53-65.
- Bukalo, O., Schachner, M., Dityatev, A., 2007. Hippocampal metaplasticity induced by deficiency in the extracellular matrix glycoprotein tenascin-R. *J Neurosci* 27, 6019-6028.



- Bunck, M., 2008. Behavioral phenotyping, gene expression profiles and cognitive aspects in a mouse model of trait anxiety. Dissertation, LMU Munich, Faculty of Biology.
- Bunck, M., Czibere, L., Horvath, C., Graf, C., Frank, E., Kessler, M.S., Murgatroyd, C., Muller-Myhsok, B., Gonik, M., Weber, P., Putz, B., Muigg, P., Panhuysen, M., Singewald, N., Bettecken, T., Deussing, J.M., Holsboer, F., Spengler, D., Landgraf, R., 2009. A hypomorphic vasopressin allele prevents anxiety-related behavior. *PLoS ONE* 4, e5129.
- Buschdorf, J.P., Li Chew, L., Zhang, B., Cao, Q., Liang, F.Y., Liou, Y.C., Zhou, Y.T., Low, B.C., 2006. Brain-specific BNIP-2-homology protein Caytaxin relocalises glutaminase to neurite terminals and reduces glutamate levels. *J Cell Sci* 119, 3337-3350.
- Bystritsky, A., 2006. Treatment-resistant anxiety disorders. *Mol Psychiatry* 11, 805-814.
- Calabresi, P., Gubellini, P., Picconi, B., Centonze, D., Pisani, A., Bonsi, P., Greengard, P., Hipskind, R.A., Borrelli, E., Bernardi, G., 2001. Inhibition of mitochondrial complex II induces a long-term potentiation of NMDA-mediated synaptic excitation in the striatum requiring endogenous dopamine. *J Neurosci* 21, 5110-5120.
- Cardno, A.G., Gottesman, I.I., 2000. Twin studies of schizophrenia: From bow-and-arrow concordances to star wars mx and functional genomics. *Am J Med Genet* 97, 12-17.
- Carlsson, A., 1978. Antipsychotic drugs, neurotransmitters, and schizophrenia. *Am J Psychiatry* 135, 165-173.
- Carter, C.S., Mintun, M., Nichols, T., Cohen, J.D., 1997. Anterior cingulate gyrus dysfunction and selective attention deficits in schizophrenia: [¹⁵O]H₂O PET study during single-trial Stroop task performance. *Am J Psychiatry* 154, 1670-1675.
- Chen, Q., Camara, A.K.S., Stowe, D.F., Hoppel, C.L., Lesnefsky, E.J., 2007. Modulation of electron transport protects cardiac mitochondria and decreases myocardial injury during ischemia and reperfusion. *Am J Physiol-Cell Physiol* 292, C137-C147.
- Chumakov, I., Blumenfeld, M., Guerassimenko, O., Cavarec, L., Palicio, M., Abderrahim, H., Bougueleret, L., Barry, C., Tanaka, H., La Rosa, P., Puech, A., Tahri, N., Cohen-Akenine, A., Delabrosse, S., Lissarrague, S., Picard, F.P., Maurice, K., Essioux, L., Millasseau, P., Grel, P., Debailleul, V., Simon, A.M., Caterina, D., Dufaure, I., Malekzadeh, K., Belova, M., Luan, J.J., Bouillot, M., Sambucy, J.L., Primas, G., Saumier, M., Boubkiri, N., Martin-Saumier, S., Nasroune, M., Peixoto, H., Delaye, A., Pinchot, V., Bastucci, M., Guillou, S., Chevillon, M., Sainz-Fuertes, R., Meguenni, S., Aurich-Costa, J., Cherif, D., Gimalac, A., Van Duijn, C., Gauvreau, D., Ouellette, G., Fortier, I., Raelson, J., Sherbatich, T., Riazanskaia, N., Rogaev, E., Raeymaekers, P., Aerssens, J., Konings, F., Luyten, W., Macciardi, F., Sham, P.C., Straub, R.E., Weinberger, D.R., Cohen, N., Cohen, D., 2002. Genetic and physiological data implicating the new human gene G72 and the gene for D-amino acid oxidase in schizophrenia. *Proc Natl Acad Sci U S A* 99, 13675-13680.
- Collins, M.O., Yu, L., Coba, M.P., Husi, H., Campuzano, I., Blackstock, W.P., Choudhary, J.S., Grant, S.G., 2005. Proteomic analysis of *in vivo* phosphorylated synaptic proteins. *J Biol Chem* 280, 5972-5982.
- Conrads, T.P., Alving, K., Veenstra, T.D., Belov, M.E., Anderson, G.A., Anderson, D.J., Lipton, M.S., Pasa-Tolic, L., Udseth, H.R., Chrisler, W.B., Thrall, B.D., Smith, R.D., 2001. Quantitative analysis of bacterial and mammalian proteomes using a combination of cysteine affinity tags and ¹⁵N-metabolic labeling. *Anal Chem* 73, 2132-2139.
- Coplan, J.D., Lydiard, R.B., 1998. Brain circuits in panic disorder. *Biol Psychiatry* 44, 1264-1276.
- Cox, B., Emili, A., 2006. Tissue subcellular fractionation and protein extraction for use in mass-spectrometry-based proteomics. *Nat Protoc* 1, 1872-1878.
- Coyle, J.T., 2006. Glutamate and schizophrenia: Beyond the dopamine hypothesis. *Cell Mol Neurobiol* 26, 365-384.



- Cryan, J.F., Holmes, A., 2005. The ascent of mouse: Advances in modelling human depression and anxiety. *Nat Rev Drug Discov* 4, 775-790.
- Cryan, J.F., Mombereau, C., Vassout, A., 2005. The tail suspension test as a model for assessing antidepressant activity: Review of pharmacological and genetic studies in mice. *Neurosci Biobehav Rev* 29, 571-625.
- Czibere, L., 2009. Assessing the complex nature of behavior: Sequence-based and transcriptomic analyses in a mouse model of extremes in trait anxiety. Dissertation, LMU Munich, Faculty of Biology.
- De Leenheer, A.P., Thienpont, L.M., 1992. Applications of isotope dilution-mass spectrometry in clinical chemistry, pharmacokinetics, and toxicology. *Mass Spectrom Rev* 11, 249-307.
- De Pinto, V.D., Palmieri, F., 1992. Transmembrane arrangement of mitochondrial porin or voltage-dependent anion channel (VDAC). *J Bioenerg Biomembr* 24, 21-26.
- Dennis, G., Jr., Sherman, B.T., Hosack, D.A., Yang, J., Gao, W., Lane, H.C., Lempicki, R.A., 2003. DAVID: Database for annotation, visualization, and integrated discovery. *Genome Biol* 4, P3.
- Detera-Wadleigh, S.D., McMahon, F.J., 2006. G72/G30 in schizophrenia and bipolar disorder: Review and meta-analysis. *Biol Psychiatry* 60, 106-114.
- Dettmer, K., Aronov, P.A., Hammock, B.D., 2007. Mass spectrometry-based metabolomics. *Mass Spectrom Rev* 26, 51-78.
- Díaz-Uriarte, R., Alvares de Andrés, S., 2006. Gene selection and classification of microarray data using random forest. *BMC Bioinformatics* 7, 3.
- Ditzen, C., Jastorff, A.M., Kessler, M.S., Bunck, M., Teplytska, L., Erhardt, A., Krömer, S.A., Varadarajulu, J., Targosz, B.S., Sayan-Ayata, E.F., Holsboer, F., Landgraf, R., Turck, C.W., 2006. Protein biomarkers in a mouse model of extremes in trait anxiety. *Mol Cell Proteomics* 5, 1914-1920.
- Ditzen, C., Varadarajulu, J., Czibere, L., Gonik, M., Targosz, B.S., Hamsch, B., Bettecken, T., Kessler, M.S., Frank, E., Bunck, M., Teplytska, L., Erhardt, A., Holsboer, F., Muller-Myhsok, B., Landgraf, R., Turck, C.W., 2010. Proteomic-based genotyping in a mouse model of trait anxiety exposes disease-relevant pathways. *Mol Psychiatry* 15, 702-711.
- Dong, M.Q., Venable, J.D., Au, N., Xu, T., Park, S.K., Cociorva, D., Johnson, J.R., Dillin, A., Yates, J.R., 3rd, 2007. Quantitative mass spectrometry identifies insulin signaling targets in *C. elegans*. *Science* 317, 660-663.
- Drevets, W.C., Savitz, J., 2008. The subgenual anterior cingulate cortex in mood disorders. *CNS Spectr* 13, 663-681.
- Du, J., McEwen, B., Manji, H.K., 2009. Glucocorticoid receptors modulate mitochondrial function: A novel mechanism for neuroprotection. *Commun Integr Biol* 2, 350-352.
- Ducottet, C., Belzung, C., 2004. Behaviour in the elevated plus-maze predicts coping after subchronic mild stress in mice. *Physiol Behav* 81, 417-426.
- Einat, H., Yuan, P., Manji, H.K., 2005. Increased anxiety-like behaviors and mitochondrial dysfunction in mice with targeted mutation of the Bcl-2 gene: Further support for the involvement of mitochondrial function in anxiety disorders. *Behav Brain Res* 165, 172-180.
- Eseh, R., Zimmerberg, B., 2005. Age-dependent effects of gestational and lactational iron deficiency on anxiety behavior in rats. *Behav Brain Res* 164, 214-221.



- Etkin, A., Wager, T.D., 2007. Functional neuroimaging of anxiety: A meta-analysis of emotional processing in PTSD, social anxiety disorder, and specific phobia. *Am J Psychiatry* 164, 1476-1488.
- Falconer, D.S., Mackay, T.F.C., 1996. Introduction to quantitative genetics, 4th ed., Longmans Green, Harlow, Essex, UK.
- Fava, M., Kendler, K.S., 2000. Major depressive disorder. *Neuron* 28, 335-341.
- Fey, S.J., Larsen, P.M., 2001. 2D or not 2D. Two-dimensional gel electrophoresis. *Curr Opin Chem Biol* 5, 26-33.
- Filiou, M.D., Bisle, B., Reckow, S., Teplytska, L., Maccarrone, G., Turck, C.W., 2010a. Profiling of mouse synaptosome proteome and phosphoproteome by IEF. *Electrophoresis* 31, 1294-1301.
- Filiou, M.D., Zhang, Y., Bisle, B., Frank, E., Kessler, M.S., Teplytska, L., Reckow, S., Haegler, K., Maccarrone, G., Hamsch, B., Landgraf, R., Turck, C.W., 2009. Stable isotope labeling of a mouse model reveals synaptic biomarkers for anxiety disorders. *Pharmacopsychiatry* 42, A37.
- Filiou, M.D., Zhang, Y., Teplytska, L., Frank, E., Kessler, M.S., Reckow, S., Maccarrone, G., Hamsch, B., Landgraf, R., Turck, C.W., 2010b. Biomarker discovery for psychiatric disorders by stable isotope metabolic labeling and quantitative proteomics. *Eur Psychiatry* 25, Suppl 1, 1464.
- Filiou, M.D., Zhang, Y., Teplytska, L., Reckow, S., Frank, E., Kessler, M.S., Maccarrone, G., Hamsch, B., Landgraf, R., Turck, C.W., 2010c. Biomarker discovery by stable isotope labeling and quantitative proteomics. *FASEB J* 24, 902.3.
- Fiori, L.M., Turecki, G., 2008. Implication of the polyamine system in mental disorders. *J Psychiatry Neurosci* 33, 102-110.
- Fleming, M.D., Campagna, D.R., Haslett, J.N., Trenor, C.C., 3rd, Andrews, N.C., 2001. A mutation in a mitochondrial transmembrane protein is responsible for the pleiotropic hematological and skeletal phenotype of flexed-tail (f/f) mice. *Genes Dev* 15, 652-657.
- Frank, E., Kessler, M.S., Filiou, M.D., Zhang, Y., Maccarrone, G., Reckow, S., Bunck, M., Heumann, H., Turck, C.W., Landgraf, R., Hamsch, B., 2009. Stable isotope metabolic labeling with a novel ¹⁵N-enriched bacteria diet for improved proteomic analyses of mouse models for psychopathologies. *PLoS ONE* 4, e7821.
- Freedman, R., 2003. Schizophrenia. *N Engl J Med* 349, 1738-1749.
- Freitag, S., Schachner, M., Morellini, F., 2003. Behavioral alterations in mice deficient for the extracellular matrix glycoprotein tenascin-R. *Behav Brain Res* 145, 189-207.
- Fujimoto, M., Uchida, S., Watanuki, T., Wakabayashi, Y., Otsuki, K., Matsubara, T., Suetsugi, M., Funato, H., Watanabe, Y., 2008. Reduced expression of glyoxalase-1 mRNA in mood disorder patients. *Neurosci Lett* 438, 196-199.
- Fulda, S., Galluzzi, L., Kroemer, G., 2010. Targeting mitochondria for cancer therapy. *Nat Rev Drug Discov* 9, 447-464.
- Gingrich, J.A., 2005. Oxidative stress is the new stress. *Nat Med* 11, 1281-1282.
- Gohil, V.M., Sheth, S.A., Nilsson, R., Wojtovich, A.P., Lee, J.H., Perocchi, F., Chen, W., Clish, C.B., Ayata, C., Brookes, P.S., Mootha, V.K., 2010. Nutrient-sensitized screening for drugs that shift energy metabolism from mitochondrial respiration to glycolysis. *Nat Biotechnol* 28, 249-255.
- Goldman-Wohl, D.S., Chan, E., Baird, D., Heintz, N., 1994. Kv3.3b: A novel Shaw type potassium channel expressed in terminally differentiated cerebellar Purkinje cells and deep cerebellar nuclei. *J Neurosci* 14, 511-522.



- Gorman, J.M., 1996. Comorbid depression and anxiety spectrum disorders. *Depress Anxiety* 4, 160-168.
- Gorman, J.M., 2002. Treatment of generalized anxiety disorder. *J Clin Psychiatry* 63, 17-23.
- Gouw, J.W., Tops, B.B., Mortensen, P., Heck, A.J., Krijgsveld, J., 2008. Optimizing identification and quantitation of ¹⁵N-labeled proteins in comparative proteomics. *Anal Chem* 80, 7796-7803.
- Gray, E.G., Whittaker, V.P., 1962. The isolation of nerve endings from brain: An electron-microscopic study of cell fragments derived by homogenization and centrifugation. *J Anat* 96, 79-88.
- Gross, C., Hen, R., 2004. The developmental origins of anxiety. *Nat Rev Neurosci* 5, 545-552.
- Gudmundsson, P., Skoog, I., Waern, M., Blennow, K., Zetterberg, H., Rosengren, L., Gustafson, D., 2010. Is there a CSF biomarker profile related to depression in elderly women? *Psychiatry Res* 176, 174-178.
- Gurevicius, K., Gureviciene, I., Valjakka, A., Schachner, M., Tanila, H., 2004. Enhanced cortical and hippocampal neuronal excitability in mice deficient in the extracellular matrix glycoprotein tenascin-R. *Mol Cell Neurosci* 25, 515-523.
- Haegler, K., Mueller, N.S., Maccarrone, G., Hunyadi-Gulyas, E., Webhofer, C., Filiou, M.D., Zhang, Y., Turck, C.W., 2009. QuantiSpec—Quantitative mass spectrometry data analysis of ¹⁵N-metabolically labeled proteins. *J Proteomics* 71, 601-608.
- Harrison, P.J., Weinberger, D.R., 2005. Schizophrenia genes, gene expression, and neuropathology: On the matter of their convergence. *Mol Psychiatry* 10, 40-68.
- Hartmann, H.J., Kaup, Y., Weser, U., 2003. Does ¹³C-or ¹⁵N-labeling affect Cu(I)-thiolate cluster arrangement in yeast copper-metallothionein? *Biometals* 16, 379-382.
- Hasler, G., Fromm, S., Alvarez, R.P., Luckenbaugh, D.A., Drevets, W.C., Grillon, C., 2007. Cerebral blood flow in immediate and sustained anxiety. *J Neurosci* 27, 6313-6319.
- Hayes, S.G., 1994. Acetazolamide in bipolar affective disorders. *Ann Clin Psychiatry* 6, 91-98.
- Hettema, J.M., Neale, M.C., Kendler, K.S., 2001. A review and meta-analysis of the genetic epidemiology of anxiety disorders. *Am J Psychiatry* 158, 1568-1578.
- Hettema, J.M., Prescott, C.A., Myers, J.M., Neale, M.C., Kendler, K.S., 2005. The structure of genetic and environmental risk factors for anxiety disorders in men and women. *Arch Gen Psychiatry* 62, 182-189.
- Hovatta, I., Tennant, R.S., Helton, R., Marr, R.A., Singer, O., Redwine, J.M., Ellison, J.A., Schadt, E.E., Verma, I.M., Lockhart, D.J., Barlow, C., 2005. Glyoxalase 1 and glutathione reductase 1 regulate anxiety in mice. *Nature* 438, 662-666.
- Huber, R., Spiegel, T., Buchner, M., Riepe, M.W., 2004. Graded reoxygenation with chemical inhibition of oxidative phosphorylation improves posthypoxic recovery in murine hippocampal slices. *J Neurosci Res* 75, 441-449.
- Hunter, A.J., Hendrikse, A.S., Renan, M.J., 2007. Can radiation-induced apoptosis be modulated by inhibitors of energy metabolism? *Int J Radiat Biol* 83, 105-114.
- Huttlin, E.L., Chen, X., Barrett-Wilt, G.A., Hegeman, A.D., Halberg, R.B., Harms, A.C., Newton, M.A., Dove, W.F., Sussman, M.R., 2009. Discovery and validation of colonic tumor-associated proteins via metabolic labeling and stable isotopic dilution. *Proc Natl Acad Sci U S A* 106, 17235-17240.



- Huttlin, E.L., Hegeman, A.D., Harms, A.C., Sussman, M.R., 2007. Comparison of full versus partial metabolic labeling for quantitative proteomics analysis in *Arabidopsis thaliana*. *Mol Cell Proteomics* 6, 860-881.
- Inoue, H., Hazama, H., Hamazoe, K., Ichikawa, M., Omura, F., Fukuma, E., Inoue, K., Umezawa, Y., 1984. Antipsychotic and prophylactic effects of acetazolamide (Diamox) on atypical psychosis. *Folia Psychiatr Neurol Jpn* 38, 425-436.
- Jacobi, F., Wittchen, H.U., Holting, C., Hofler, M., Pfister, H., Muller, N., Lieb, R., 2004. Prevalence, co-morbidity and correlates of mental disorders in the general population: Results from the German Health Interview and Examination Survey (GHS). *Psychol Med* 34, 597-611.
- Jeong, D.W., Kim, T.S., Cho, I.T., Kim, I.Y., 2004. Modification of glycolysis affects cell sensitivity to apoptosis induced by oxidative stress and mediated by mitochondria. *Biochem Biophys Res Commun* 313, 984-991.
- Jockusch, W.J., Speidel, D., Sigler, A., Sorensen, J.B., Varoqueaux, F., Rhee, J.S., Brose, N., 2007. CAPS-1 and CAPS-2 are essential synaptic vesicle priming proteins. *Cell* 131, 796-808.
- Kaddurah-Daouk, R., Kristal, B.S., Weinshilboum, R.M., 2008. Metabolomics: A global biochemical approach to drug response and disease. *Annu Rev Pharmacol Toxicol* 48, 653-683.
- Kageyama, G.H., Wongriley, M.T.T., 1982. Histochemical localization of cytochrome oxidase in the hippocampus: Correlation with specific neuronal types and afferent pathways. *Neuroscience* 7, 2337-2361.
- Kalueff, A.V., Wheaton, M., Murphy, D., 2007. What's wrong with my mouse model? Advances and strategies in animal modeling of anxiety and depression. *Behav Brain Res* 179, 1-18.
- Kanehisa, M., Goto, S., 2000. KEGG: Kyoto encyclopedia of genes and genomes. *Nucleic Acids Res* 28, 27-30.
- Kann, O., Kovacs, R., Heinemann, U., 2003. Metabotropic receptor-mediated Ca^{2+} signaling elevates mitochondrial Ca^{2+} and stimulates oxidative metabolism in hippocampal slice cultures. *J Neurophysiol* 90, 613-621.
- Karas, M., Bachmann, D., Hillenkamp, F., 1985. Influence of the wavelength in high-irradiance ultraviolet laser desorption mass spectrometry of organic molecules. *Anal Chem* 57, 2935-2939.
- Kato, T., 2006. The role of mitochondrial dysfunction in bipolar disorder. *Drug News Perspect* 19, 597-602.
- Kent, J.M., Mathew, S.J., Gorman, J.M., 2002. Molecular targets in the treatment of anxiety. *Biol Psychiatry* 52, 1008-1030.
- Kessler, M.S., Murgatroyd, C., Bunck, M., Czibere, L., Frank, E., Jacob, W., Horvath, C., Muigg, P., Holsboer, F., Singewald, N., Spengler, D., Landgraf, R., 2007. Diabetes insipidus and, partially, low anxiety-related behaviour are linked to a SNP-associated vasopressin deficit in LAB mice. *Eur J Neurosci* 26, 2857-2864.
- Kessler, R.C., Demler, O., Frank, R.G., Olfson, M., Pincus, H.A., Walters, E.E., Wang, P., Wells, K.B., Zaslavsky, A.M., 2005. Prevalence and treatment of mental disorders, 1990 to 2003. *N Engl J Med* 352, 2515-2523.
- Kierszniowska, S., Seiwert, B., Schulze, W.X., 2009a. Definition of *Arabidopsis* sterol-rich membrane microdomains by differential treatment with methyl-beta-cyclodextrin and quantitative proteomics. *Mol Cell Proteomics* 8, 612-623.
- Kierszniowska, S., Walther, D., Schulze, W.X., 2009b. Ratio-dependent significance thresholds in reciprocal ^{15}N -labeling experiments as a robust tool in detection of candidate proteins responding to biological treatment. *Proteomics* 9, 1916-1924.



- Kinter, M., Sherman, N.E., 2000. Protein sequencing and identification using tandem mass spectrometry, Wiley Interscience, New York, NY, USA.
- Kirkpatrick, B., Buchanan, R.W., Carpenter, W., 2001. A separate disease within the syndrome of schizophrenia. *Arch Gen Psychiatry* 58, 165-171.
- Krijgsveld, J., Ketting, R.F., Mahmoudi, T., Johansen, J., Artal-Sanz, M., Verrijzer, C.P., Plasterk, R.H., Heck, A.J., 2003. Metabolic labeling of *C. elegans* and *D. melanogaster* for quantitative proteomics. *Nat Biotechnol* 21, 927-931.
- Kroemer, G., Galluzzi, L., Brenner, C., 2007. Mitochondrial membrane permeabilization in cell death. *Physiol Rev* 87, 99-163.
- Krömer, S.A., Kessler, M.S., Milfay, D., Birg, I.N., Bunck, M., Czibere, L., Panhuysen, M., Putz, B., Deussing, J.M., Holsboer, F., Landgraf, R., Turck, C.W., 2005. Identification of glyoxalase-I as a protein marker in a mouse model of extremes in trait anxiety. *J Neurosci* 25, 4375-4384.
- Krüger, M., Moser, M., Ussar, S., Thievessen, I., Lubner, C.A., Forner, F., Schmidt, S., Zanivan, S., Fassler, R., Mann, M., 2008. SILAC mouse for quantitative proteomics uncovers kindlin-3 as an essential factor for red blood cell function. *Cell* 134, 353-364.
- Kuloglu, M., Atmaca, M., Tezcan, E., Gecici, O., Tunckol, H., Ustundag, B., 2002a. Antioxidant enzyme activities and malondialdehyde levels in patients with obsessive-compulsive disorder. *Neuropsychobiology* 46, 27-32.
- Kuloglu, M., Atmaca, M., Tezcan, E., Ustundag, B., Bulut, S., 2002b. Antioxidant enzyme and malondialdehyde levels in patients with panic disorder. *Neuropsychobiology* 46, 186-189.
- Kvajo, M., Dhillia, A., Swor, D.E., Karayiorgou, M., Gogos, J.A., 2008. Evidence implicating the candidate schizophrenia/bipolar disorder susceptibility gene G72 in mitochondrial function. *Mol Psychiatry* 13, 685-696.
- Landgraf, R., 2001. Neuropeptides and anxiety-related behavior. *Endocr J* 48, 517-533.
- Landgraf, R., Kessler, M.S., Bunck, M., Murgatroyd, C., Spengler, D., Zimbelmann, M., Nussbaumer, M., Czibere, L., Turck, C.W., Singewald, N., Rujescu, D., Frank, E., 2007. Candidate genes of anxiety-related behavior in HAB/LAB rats and mice: Focus on vasopressin and glyoxalase-I. *Neurosci Biobehav Rev* 31, 89-102.
- Landgraf, R., Wigger, A., 2002. High vs low anxiety-related behavior rats: An animal model of extremes in trait anxiety. *Behav Genet* 32, 301-314.
- Lanquar, V., Kuhn, L., Lelievre, F., Khafif, M., Espagne, C., Bruley, C., Barbier-Brygoo, H., Garin, J., Thomine, S., 2007. ¹⁵N-metabolic labeling for comparative plasma membrane proteomics in *Arabidopsis* cells. *Proteomics* 7, 750-754.
- LaRoche, S.M., Helmers, S.L., 2004. The new antiepileptic drugs: Scientific review. *JAMA* 291, 605-614.
- Leonardo, E.D., Hen, R., 2006. Genetics of affective and anxiety disorders. *Annu Rev Psychol* 57, 117-137.
- Levine, J., Cole, D.P., Chengappa, K.N., Gershon, S., 2001. Anxiety disorders and major depression, together or apart. *Depress Anxiety* 14, 94-104.
- Li, D., Collier, D.A., He, L., 2006. Meta-analysis shows strong positive association of the neuregulin 1 (NRG1) gene with schizophrenia. *Hum Mol Genet* 15, 1995-2002.
- Liao, L., McClatchy, D.B., Park, S.K., Xu, T., Lu, B., Yates, J.R., 3rd, 2008. Quantitative analysis of brain nuclear phosphoproteins identifies developmentally regulated phosphorylation events. *J Proteome Res* 7, 4743-4755.



- Liebsch, G., Linthorst, A.C., Neumann, I.D., Reul, J.M., Holsboer, F., Landgraf, R., 1998a. Behavioral, physiological, and neuroendocrine stress responses and differential sensitivity to diazepam in two Wistar rat lines selectively bred for high- and low-anxiety-related behavior. *Neuropsychopharmacology* 19, 381-396.
- Liebsch, G., Montkowski, A., Holsboer, F., Landgraf, R., 1998b. Behavioural profiles of two Wistar rat lines selectively bred for high or low anxiety-related behaviour. *Behav Brain Res* 94, 301-310.
- Lister, R.G., 1987. The use of a plus-maze to measure anxiety in the mouse. *Psychopharmacology (Berl)* 92, 180-185.
- Liu, Z., Fisher, R.A., 2004. RGS6 interacts with DMAP1 and DNMT1 and inhibits DMAP1 transcriptional repressor activity. *J Biol Chem* 279, 14120-14128.
- Lubec, G., Krapfenbauer, K., Fountoulakis, M., 2003. Proteomics in brain research: Potentials and limitations. *Prog Neurobiol* 69, 193-211.
- Luisetto, S., Basso, E., Petronilli, V., Bernardi, P., Forte, M., 2008. Enhancement of anxiety, facilitation of avoidance behavior, and occurrence of adult-onset obesity in mice lacking mitochondrial cyclophilin D. *Neuroscience* 155, 585-596.
- Maccarrone, G., Kolb, N., Teplytska, L., Birg, I., Zollinger, R., Holsboer, F., Turck, C.W., 2006. Phosphopeptide enrichment by IEF. *Electrophoresis* 27, 4585-4595.
- Macek, B., Gnad, F., Soufi, B., Kumar, C., Olsen, J.V., Mijakovic, I., Mann, M., 2008. Phosphoproteome analysis of *E. coli* reveals evolutionary conservation of bacterial Ser/Thr/Tyr phosphorylation. *Mol Cell Proteomics* 7, 299-307.
- Makarov, A., 2000. Electrostatic axially harmonic orbital trapping: A high-performance technique of mass analysis. *Anal Chem* 72, 1156-1162.
- Malenka, R.C., Nicoll, R.A., 1999. Long-term potentiation—a decade of progress? *Science* 285, 1870-1874.
- Matthiesen, R., Muttenda, K.E., Introduction to proteomics. In: Muttenda, R., 2007. *Mass spectrometry data analysis in proteomics*, Humana Press, Totowa, NJ, USA.
- Mattson, M.P., Partin, J., 1999. Evidence for mitochondrial control of neuronal polarity. *J Neurosci Res* 56, 8-20.
- McClatchy, D.B., Dong, M.Q., Wu, C.C., Venable, J.D., Yates, J.R., 3rd, 2007a. ¹⁵N metabolic labeling of mammalian tissue with slow protein turnover. *J Proteome Res* 6, 2005-2010.
- McClatchy, D.B., Liao, L.J., Park, S.K., Venable, J.D., Yates, J.R., 3rd, 2007b. Quantification of the synaptosomal proteome of the rat cerebellum during post-natal development. *Genome Res* 17, 1378-1388.
- McNaughton, N., 1997. Cognitive dysfunction resulting from hippocampal hyperactivity - A possible cause of anxiety disorder? *Pharmacol Biochem Behav* 56, 603-611.
- Melander, L., Saunders, W.H., 1980. *Reaction rates of isotopic molecules*. Wiley Interscience, New York, NY, USA.
- Milad, M.R., Rauch, S.L., 2007. The role of the orbitofrontal cortex in anxiety disorders. *Ann N Y Acad Sci* 1121, 546-561.
- Mohn, A.R., Gainetdinov, R.R., Caron, M.G., Koller, B.H., 1999. Mice with reduced NMDA receptor expression display behaviors related to schizophrenia. *Cell* 98, 427-436.
- Mothet, J.P., Parent, A.T., Wolosker, H., Brady, R.O., Jr., Linden, D.J., Ferris, C.D., Rogawski, M.A., Snyder, S.H., 2000. D-serine is an endogenous ligand for the glycine site of the N-methyl-D-aspartate receptor. *Proc Natl Acad Sci U S A* 97, 4926-4931.



- Mouse Genome Sequencing Consortium, Waterston, R.H., Lindblad-Toh, K., Birney, E., Rogers, J., Abril, J.F., Agarwal, P., Agarwala, R., Ainscough, R., Alexandersson, M., An, P., Antonarakis, S.E., Attwood, J., Baertsch, R., Bailey, J., Barlow, K., Beck, S., Berry, E., Birren, B., Bloom, T., Bork, P., Botcherby, M., Bray, N., Brent, M.R., Brown, D.G., Brown, S.D., Bult, C., Burton, J., Butler, J., Campbell, R.D., Carninci, P., Cawley, S., Chiaromonte, F., Chinwalla, A.T., Church, D.M., Clamp, M., Clee, C., Collins, F.S., Cook, L.L., Copley, R.R., Coulson, A., Couronne, O., Cuff, J., Curwen, V., Cutts, T., Daly, M., David, R., Davies, J., Delehaunty, K.D., Deri, J., Dermitzakis, E.T., Dewey, C., Dickens, N.J., Diekhans, M., Dodge, S., Dubchak, I., Dunn, D.M., Eddy, S.R., Elnitski, L., Emes, R.D., Eswara, P., Eyraes, E., Felsenfeld, A., Fewell, G.A., Flicek, P., Foley, K., Frankel, W.N., Fulton, L.A., Fulton, R.S., Furey, T.S., Gage, D., Gibbs, R.A., Glusman, G., Gnerre, S., Goldman, N., Goodstadt, L., Grafham, D., Graves, T.A., Green, E.D., Gregory, S., Guigo, R., Guyer, M., Hardison, R.C., Haussler, D., Hayashizaki, Y., Hillier, L.W., Hinrichs, A., Hlavina, W., Holzer, T., Hsu, F., Hua, A., Hubbard, T., Hunt, A., Jackson, I., Jaffe, D.B., Johnson, L.S., Jones, M., Jones, T.A., Joy, A., Kamal, M., Karlsson, E.K., Karolchik, D., Kasprzyk, A., Kawai, J., Keibler, E., Kells, C., Kent, W.J., Kirby, A., Kolbe, D.L., Korf, I., Kucherlapati, R.S., Kulbokas, E.J., Kulp, D., Landers, T., Leger, J.P., Leonard, S., Letunic, I., Levine, R., Li, J., Li, M., Lloyd, C., Lucas, S., Ma, B., Maglott, D.R., Mardis, E.R., Matthews, L., Mauceli, E., Mayer, J.H., McCarthy, M., McCombie, W.R., McLaren, S., McLay, K., McPherson, J.D., Meldrim, J., Meredith, B., Mesirov, J.P., Miller, W., Miner, T.L., Mongin, E., Montgomery, K.T., Morgan, M., Mott, R., Mullikin, J.C., Muzny, D.M., Nash, W.E., Nelson, J.O., Nhan, M.N., Nicol, R., Ning, Z., Nusbaum, C., O'Connor, M.J., Okazaki, Y., Oliver, K., Overton-Larty, E., Pachter, L., Parra, G., Pepin, K.H., Peterson, J., Pevzner, P., Plumb, R., Pohl, C.S., Poliakov, A., Ponce, T.C., Ponting, C.P., Potter, S., Quail, M., Reymond, A., Roe, B.A., Roskin, K.M., Rubin, E.M., Rust, A.G., Santos, R., Sapojnikov, V., Schultz, B., Schultz, J., Schwartz, M.S., Schwartz, S., Scott, C., Seaman, S., Searle, S., Sharpe, T., Sheridan, A., Shownkeen, R., Sims, S., Singer, J.B., Slater, G., Smit, A., Smith, D.R., Spencer, B., Stabenau, A., Stange-Thomann, N., Sugnet, C., Suyama, M., Tesler, G., Thompson, J., Torrents, D., Trevaskis, E., Tromp, J., Ucla, C., Ureta-Vidal, A., Vinson, J.P., Von Niederhausern, A.C., Wade, C.M., Wall, M., Weber, R.J., Weiss, R.B., Wendl, M.C., West, A.P., Wetterstrand, K., Wheeler, R., Whelan, S., Wierzbowski, J., Willey, D., Williams, S., Wilson, R.K., Winter, E., Worley, K.C., Wyman, D., Yang, S., Yang, S.P., Zdobnov, E.M., Zody, M.C., Lander, E.S., 2002. Initial sequencing and comparative analysis of the mouse genome. *Nature* 420, 520-562.
- Muigg, P., Hetzenauer, A., Hauer, G., Hauschild, M., Gaburro, S., Frank, E., Landgraf, R., Singewald, N., 2008. Impaired extinction of learned fear in rats selectively bred for high anxiety – evidence for altered neuronal processing in prefrontal-amygdala pathways. *Eur J Neurosci* 28, 2299-2309.
- Munton, R.P., Tweedie-Cullen, R., Livingstone-Zatchej, M., Weinandy, F., Waidelich, M., Longo, D., Gehrig, P., Potthast, F., Rutishauser, D., Gerrits, B., Panse, C., Schlapbach, R., Mansuy, I.M., 2007. Qualitative and quantitative analyses of protein phosphorylation in naive and stimulated mouse synaptosomal preparations. *Mol Cell Proteomics* 6, 283-293.
- Nemeroff, C.B., 2003. The role of GABA in the pathophysiology and treatment of anxiety disorders. *Psychopharmacol Bull* 37, 133-146.
- Neupert, W., 1997. Protein import into mitochondria. *Annu Rev Biochem* 66, 863-917.
- Nutt, D.J., 2005. Overview of diagnosis and drug treatments of anxiety disorders. *CNS Spectr* 10, 49-56.
- O'Farrell, P.H., 1975. High resolution two-dimensional electrophoresis of proteins. *J Biol Chem* 250, 4007-4021.
- Oda, Y., Huang, K., Cross, F.R., Cowburn, D., Chait, B.T., 1999. Accurate quantitation of protein expression and site-specific phosphorylation. *Proc Natl Acad Sci U S A* 96, 6591-6596.
- Ohl, F., 2005. Animal models of anxiety. *Handb Exp Pharmacol*, 35-69.
- Ong, S.E., Blagoev, B., Kratchmarova, I., Kristensen, D.B., Steen, H., Pandey, A., Mann, M., 2002. Stable isotope labeling by amino acids in cell culture, SILAC, as a simple and accurate approach to expression proteomics. *Mol Cell Proteomics* 1, 376-386.



- Ong, S.E., Mann, M., 2005. Mass spectrometry-based proteomics turns quantitative. *Nat Chem Biol* 1, 252-262.
- Otte, D.M., Bilkei-Gorzo, A., Filiou, M.D., Turck, C.W., Yilmaz, O., Holst, M.I., Schilling, K., Abou-Jamra, R., Schumacher, J., Benzel, I., Kunz, W.S., Beck, H., Zimmer, A., 2009. Behavioral changes in G72/G30 transgenic mice. *Eur Neuropsychopharmacol* 19, 339-348.
- Paige, L.A., Mitchell, M.W., Krishnan, K.R., Kaddurah-Daouk, R., Steffens, D.C., 2007. A preliminary metabolomic analysis of older adults with and without depression. *Int J Geriatr Psychiatry* 22, 418-423.
- Palmblad, M., Bindschedler, L.V., Cramer, R., 2007. Quantitative proteomics using uniform ¹⁵N-labeling, MASCOT, and the trans-proteomic pipeline. *Proteomics* 7, 3462-3469.
- Palmieri, F., 2004. The mitochondrial transporter family (SLC25): Physiological and pathological implications. *Pflugers Arch* 447, 689-709.
- Palminiello, S., Kida, E., Kaur, K., Walus, M., Wisniewski, K.E., Wierzbica-Bobrowicz, T., Rabe, A., Albertini, G., Golabek, A.A., 2008. Increased levels of carbonic anhydrase II in the developing Down syndrome brain. *Brain Res* 1190, 193-205.
- Pan, C., Kora, G., McDonald, W.H., Tabb, D.L., VerBerkmoes, N.C., Hurst, G.B., Pelletier, D.A., Samatova, N.F., Hettich, R.L., 2006a. ProRata: A quantitative proteomics program for accurate protein abundance ratio estimation with confidence interval evaluation. *Anal Chem* 78, 7121-7131.
- Pan, C., Kora, G., Tabb, D.L., Pelletier, D.A., McDonald, W.H., Hurst, G.B., Hettich, R.L., Samatova, N.F., 2006b. Robust estimation of peptide abundance ratios and rigorous scoring of their variability and bias in quantitative shotgun proteomics. *Anal Chem* 78, 7110-7120.
- Pan, C., Oda, Y., Lankford, P.K., Zhang, B., Samatova, N.F., Pelletier, D.A., Harwood, C.S., Hettich, R.L., 2008. Characterization of anaerobic catabolism of *p*-coumarate in *Rhodopseudomonas palustris* by integrating transcriptomics and quantitative proteomics. *Mol Cell Proteomics* 7, 938-948.
- Papakostas, G.I., 2009. Evidence for S-adenosyl-L-methionine (SAM-e) for the treatment of major depressive disorder. *J Clin Psychiatry* 70, Suppl 5, 18-22.
- Park, S.K., Venable, J.D., Xu, T., Yates, J.R., 3rd, 2008. A quantitative analysis software tool for mass spectrometry-based proteomics. *Nat Methods* 5, 319-322.
- Park, S.K., Yates, J.R., 3rd, 2010. Census for proteome quantification. *Curr Protoc Bioinformatics* Chapter 13, Unit 13.12.1-11.
- Paxinos, G., Franklin, K., 2001. The mouse brain in stereotaxic coordinates, 2nd ed., Academic Press, San Diego, CA, USA.
- Pellow, S., Chopin, P., File, S.E., Briley, M., 1985. Validation of open:closed arm entries in an elevated plus-maze as a measure of anxiety in the rat. *J Neurosci Methods* 14, 149-167.
- Pesheva, P., Spiess, E., Schachner, M., 1989. J1-160 and J1-180 are oligodendrocyte-secreted nonpermissive substrates for cell-adhesion. *J Cell Biol* 109, 1765-1778.
- Pocklington, A.J., Armstrong, J.D., Grant, S.G., 2006. Organization of brain complexity—synapse proteome form and function. *Brief Funct Genomic Proteomic* 5, 66-73.
- Politi, P., Minoretti, P., Falcone, C., Martinelli, V., Emanuele, E., 2006. Association analysis of the functional Ala111Glu polymorphism of the glyoxalase I gene in panic disorder. *Neurosci Lett* 396, 163-166.
- Politis, P.K., Makri, G., Thomaidou, D., Geissen, M., Rohrer, H., Matsas, R., 2007. BM88/CEND1 coordinates cell cycle exit and differentiation of neuronal precursors. *Proc Natl Acad Sci U S A* 104, 17861-17866.



- Quinones, M.P., Kaddurah-Daouk, R., 2009. Metabolomics tools for identifying biomarkers for neuropsychiatric diseases. *Neurobiol Dis* 35, 165-176.
- Rammal, H., Bouayed, J., Younos, C., Soulimani, R., 2008a. Evidence that oxidative stress is linked to anxiety-related behaviour in mice. *Brain Behav Immun* 22, 1156-1159.
- Rammal, H., Bouayed, J., Younos, C., Soulimani, R., 2008b. The impact of high anxiety level on the oxidative status of mouse peripheral blood lymphocytes, granulocytes and monocytes. *Eur J Pharmacol* 589, 173-175.
- Rapoport, J.L., Addington, A.M., Frangou, S., Psych, M.R., 2005. The neurodevelopmental model of schizophrenia: Update 2005. *Mol Psychiatry* 10, 434-449.
- Reinés, A., Cereseto, M., Ferrero, A., Bonavita, C., Wikinski, S., 2004. Neuronal cytoskeletal alterations in an experimental model of depression. *Neuroscience* 129, 529-538.
- Riepe, M.W., Esclaire, F., Kasischke, K., Schreiber, S., Nakase, H., Kempfski, O., Ludolph, A.C., Dirnagl, U., Hugon, J., 1997. Increased hypoxic tolerance by chemical inhibition of oxidative phosphorylation: "Chemical preconditioning". *J Cereb Blood Flow Metab* 17, 257-264.
- Rosen, J.B., Schulkin, J., 1998. From normal fear to pathological anxiety. *Psychol Rev* 105, 325-350.
- Saghatelyan, A.K., Dityatev, A., Schmidt, S., Schuster, T., Bartsch, U., Schachner, M., 2001. Reduced perisomatic inhibition, increased excitatory transmission, and impaired long-term potentiation in mice deficient for the extracellular matrix glycoprotein tenascin-R. *Mol Cell Neurosci* 17, 226-240.
- Schaff, J.E., Mbeunkui, F., Blackburn, K., Bird, D.M., Goshe, M.B., 2008. SILIP: A novel stable isotope labeling method for *in planta* quantitative proteomic analysis. *Plant J* 56, 840-854.
- Schmalzigaug, R., Rodriguiz, R.M., Phillips, L.E., Davidson, C.E., Wetsel, W.C., Premont, R.T., 2009. Anxiety-like behaviors in mice lacking GIT2. *Neurosci Lett* 451, 156-161.
- Schrimpf, S.P., Meskenaite, V., Brunner, E., Rutishauser, D., Walther, P., Eng, J., Aebersold, R., Sonderegger, P., 2005. Proteomic analysis of synaptosomes using isotope-coded affinity tags and mass spectrometry. *Proteomics* 5, 2531-2541.
- Schumacher, J., Laje, G., Abou Jamra, R., Becker, T., Muhleisen, T.W., Vasilescu, C., Mattheisen, M., Herms, S., Hoffmann, P., Hillmer, A.M., Georgi, A., Herold, C., Schulze, T.G., Propping, P., Rietschel, M., McMahon, F.J., Nothen, M.M., Cichon, S., 2009. The DISC locus and schizophrenia: Evidence from an association study in a central European sample and from a meta-analysis across different European populations. *Hum Mol Genet* 18, 2719-2727.
- Schwarz, E., Bahn, S., 2008. Biomarker discovery in psychiatric disorders. *Electrophoresis* 29, 2884-2890.
- Sies, H., Stahl, W., Sundquist, A.R., 1992. Antioxidant functions of vitamins. Vitamins E and C, beta-carotene, and other carotenoids. *Ann N Y Acad Sci* 669, 7-20.
- Siuzdak, G., 1996. Mass spectrometry for biotechnology. Academic Press, Boston, MA, USA.
- Smart, T.G., 1997. Regulation of excitatory and inhibitory neurotransmitter-gated ion channels by protein phosphorylation. *Curr Opin Neurobiol* 7, 358-367.
- Snyder, E.M., Nong, Y., Almeida, C.G., Paul, S., Moran, T., Choi, E.Y., Nairn, A.C., Salter, M.W., Lombroso, P.J., Gouras, G.K., Greengard, P., 2005. Regulation of NMDA receptor trafficking by amyloid-beta. *Nat Neurosci* 8, 1051-1058.
- Stefanova, N.A., Fursova, A.Z., Kolosova, N.G., 2010. Behavioral effects induced by mitochondria-targeted antioxidant SkQ1 in Wistar and senescence-accelerated OXYS Rats. *J Alzheimers Dis*, Jun 16, [Epub ahead of print].



- Stein, D.J., Westenberg, H.G.M., Liebowitz, M.R., 2002. Social anxiety disorder and generalized anxiety disorder: Serotonergic and dopaminergic neurocircuitry. *J Clin Psychiatry* 63, 12-19.
- Stork, C., Renshaw, P.F., 2005. Mitochondrial dysfunction in bipolar disorder: Evidence from magnetic resonance spectroscopy research. *Mol Psychiatry* 10, 900-919.
- Straub, R.E., Jiang, Y., MacLean, C.J., Ma, Y., Webb, B.T., Myakishev, M.V., Harris-Kerr, C., Wormley, B., Sadek, H., Kadambi, B., Cesare, A.J., Gibberman, A., Wang, X., O'Neill, F.A., Walsh, D., Kendler, K.S., 2002. Genetic variation in the 6p22.3 gene DTNBP1, the human ortholog of the mouse dysbindin gene, is associated with schizophrenia. *Am J Hum Genet* 71, 337-348.
- Südhof, T.C., 2008. Neuroligins and neurexins link synaptic function to cognitive disease. *Nature* 455, 903-911.
- Sunyer, B., Diao, W., Lubec, G., 2008. The role of post-translational modifications for learning and memory formation. *Electrophoresis* 29, 2593-2602.
- Sutton, F., Butler, E.T., 3rd, Smith, T.E., 1986. Isolation of the structural gene encoding a mutant form of *Escherichia coli* phosphoenolpyruvate carboxylase deficient in regulation by fructose 1,6-bisphosphate. Identification of an amino acid substitution in the mutant. *J Biol Chem* 261, 16078-16081.
- Szego, E.M., Janáky, T., Szabó, Z., Csorba, A., Kompagne, H., Müller, G., Lévy, G., Simor, A., Juhász, G., Kékesi, K.A., 2010. A mouse model of anxiety molecularly characterized by altered protein networks in the brain proteome. *Eur Neuropsychopharmacol* 20, 96-111.
- Tabb, D.L., McDonald, W.H., Yates, J.R., 3rd, 2002. DTASelect and Contrast: Tools for assembling and comparing protein identifications from shotgun proteomics. *J Proteome Res* 1, 21-26.
- Takahashi, M., Itakura, M., Kataoka, M., 2003. New aspects of neurotransmitter release and exocytosis: Regulation of neurotransmitter release by phosphorylation. *J Pharmacol Sci* 93, 41-45.
- Thornalley, P.J., 1993. The glyoxalase system in health and disease. *Mol Aspects Med* 14, 287-371.
- Trinidad, J.C., Specht, C.G., Thalhammer, A., Schoepfer, R., Burlingame, A.L., 2006. Comprehensive identification of phosphorylation sites in postsynaptic density preparations. *Mol Cell Proteomics* 5, 914-922.
- Turck, C.W., Maccarrone, G., Sayan-Ayata, E., Jacob, A.M., Ditzen, C., Kronsbein, H., Birg, I., Doertbudak, C.C., Haegler, K., Lebar, M., Teplytska, L., Kolb, N., Uwaje, N., Zollinger, R., 2005. The quest for brain disorder biomarkers. *J Med Invest* 52, Suppl, 231-235.
- Underwood, B.R., Broadhurst, D., Dunn, W.B., Ellis, D.I., Michell, A.W., Vacher, C., Mosedale, D.E., Kell, D.B., Barker, R.A., Grainger, D.J., Rubinsztein, D.C., 2006. Huntington disease patients and transgenic mice have similar pro-catabolic serum metabolite profiles. *Brain* 129, 877-886.
- Van Langenhove, A., 1986. Isotope effects: Definitions and consequences for pharmacologic studies. *J Clin Pharmacol* 26, 383-389.
- Vanden Berghe, P., Kenyon, J.L., Smith, T.K., 2002. Mitochondrial Ca²⁺ uptake regulates the excitability of myenteric neurons. *J Neurosci* 22, 6962-6971.
- Vaughn, A.E., Deshmukh, M., 2008. Glucose metabolism inhibits apoptosis in neurons and cancer cells by redox inactivation of cytochrome c. *Nat Cell Biol* 10, 1477-1483.
- Vestal, M.L., Cambell, J.M., Tandem time-of-flight mass spectrometry. In: Burlingame, A.L., 2005. *Methods in Enzymology*, vol. 402, Elsevier, Maryland Heights, MO, USA.



- Watson, D.G., Watterson, J.M., Lenox, R.H., 1998. Sodium valproate down-regulates the myristoylated alanine-rich C kinase substrate (MARCKS) in immortalized hippocampal cells: A property of protein kinase C-mediated mood stabilizers. *J Pharmacol Exp Ther* 285, 307-316.
- Whittaker, V.P., 1993. Thirty years of synaptosome research. *J Neurocytol* 22, 735-742.
- Williams, J.M., Thompson, V.L., Mason-Parker, S.E., Abraham, W.C., Tate, W.P., 1998. Synaptic activity-dependent modulation of mitochondrial gene expression in the rat hippocampus. *Brain Res Mol Brain Res* 60, 50-56.
- Williams, R., 4th, Lim, J.E., Harr, B., Wing, C., Walters, R., Distler, M.G., Teschke, M., Wu, C., Wiltshire, T., Su, A.I., Sokoloff, G., Tarantino, L.M., Borevitz, J.O., Palmer, A.A., 2009. A common and unstable copy number variant is associated with differences in *Glo1* expression and anxiety-like behavior. *PLoS ONE* 4, e4649.
- Witzmann, F.A., Arnold, R.J., Bai, F., Hrnairova, P., Kimpel, M.W., Mechref, Y.S., McBride, W.J., Novotny, M.V., Pedrick, N.M., Ringham, H.N., Simon, J.R., 2005. A proteomic survey of rat cerebral cortical synaptosomes. *Proteomics* 5, 2177-2201.
- Wood, S.J., Yücel, M., Pantelis, C., Berk, M., 2009. Neurobiology of schizophrenia spectrum disorders: The role of oxidative stress. *Ann Acad Med Singapore* 38, 396-401.
- World Health Organization, 2008. The global burden of disease: 2004 update. WHO Press, Geneva, Switzerland.
- Wu, C.C., MacCoss, M.J., Howell, K.E., Matthews, D.E., Yates, J.R., 3rd, 2004. Metabolic labeling of mammalian organisms with stable isotopes for quantitative proteomic analysis. *Anal Chem* 76, 4951-4959.
- Wu, L.J., Kim, S.S., Zhuo, M., 2008. Molecular targets of anxiety: From membrane to nucleus. *Neurochem Res* 33, 1925-1932.
- Yamanaka, K., Ogura, T., Niki, H., Hiraga, S., 1996. Identification of two new genes, *mukE* and *mukF*, involved in chromosome partitioning in *Escherichia coli*. *Mol Gen Genet* 250, 241-251.
- Yamashita, M., Fenn, J.B., 1984. Electrospray ion source. Another variation on the free-jet theme. *J Phys Chem* 88, 4451-4459.
- Yoshikumi, Y., Mashima, H., Ueda, N., Ohno, H., Suzuki, J., Tanaka, S., Hayashi, M., Sekine, N., Ohnishi, H., Yasuda, H., Iiri, T., Omata, M., Fujita, T., Kojima, I., 2005. Roles of CTPL/Sfxn3 and Sfxn family members in pancreatic islet. *J Cell Biochem* 95, 1157-1168.
- Zhang, H.Q., Berg, J.S., Li, Z.L., Wang, Y.L., Lang, P., Sousa, A.D., Bhaskar, A., Cheney, R.E., Stromblad, S., 2004. Myosin-X provides a motor-based link between integrins and the cytoskeleton. *Nat Cell Biol* 6, 523-531.
- Zhang, X.Y., Zhou, D.F., Qi, L.Y., Chen, S., Cao, L.Y., Chen, D.C., Xiu, M.H., Wang, F., Wu, G.Y., Lu, L., Kosten, T.A., Kosten, T.R., 2009a. Superoxide dismutase and cytokines in chronic patients with schizophrenia: Association with psychopathology and response to antipsychotics. *Psychopharmacology* 204, 177-184.
- Zhang, Y., Webhofer, C., Reckow, S., Filiou, M.D., Maccarrone, G., Turck, C.W., 2009b. A MS data search method for improved ¹⁵N-labeled protein identification. *Proteomics* 9, 4265-4270.
- Zhu, X.J., Wang, C.Z., Dai, P.G., Xie, Y., Song, N.N., Liu, Y., Du, Q.S., Mei, L., Ding, Y.Q., Xiong, W.C., 2007. Myosin X regulates netrin receptors and functions in axonal path-finding. *Nat Cell Biol* 9, 184-192.
- Zou, W., Tolstikov, V.M., 2009. Pattern recognition and pathway analysis with genetic algorithms in mass spectrometry based metabolomics. *Algorithms* 2, 638-666.



11 Appendixes

Appendix 1: Alphabetical list of the commercially available antibodies used

Antigen Name	Commercial source	Catalog No	Type
Car2	Santa Cruz Biotechnology	sc-17244	goat polyclonal
Crym	Santa Cruz Biotechnology	sc-22423	goat polyclonal
Gap43	Abcam	ab12274	rabbit polyclonal
Gria2	NeuroMab	73-067	mouse monoclonal
LacZ	Novus Biologicals	NB600-305	rabbit polyclonal
Mbp	Abcam	ab53294	rabbit monoclonal
Myh10	Santa Cruz Biotechnology	sc-47205	goat polyclonal
Nefm	Abcam	ab30309	rabbit polyclonal
PrkC	Santa Cruz Biotechnology	sc-10800	rabbit polyclonal
PSD95	Genetex	GTX12093	goat polyclonal
Sdhb	Abcam	ab14714	mouse monoclonal
Sfxn5	Abnova	PAB4481	rabbit polyclonal
Slc17a7	NeuroMab	75-066	mouse monoclonal
TnR (N-20)	Santa Cruz Biotechnology	sc-9874	goat polyclonal



Appendix 2: Bacteria-fed HAB/NAB/LAB animals used for quantitative proteomics analyses

¹⁴ N/ ¹⁵ N pair	EPM ^a	TST ^b	Cingulate cortex weight (mg)	Animal Weight (g)	EPM ^a	TST ^b	Cingulate cortex weight (mg)	Animal Weight (g)
Line comparison (¹⁴N HAB/¹⁵N NAB)	¹⁴N HAB				¹⁵N NAB			
1	2.66	143.8	28.3	24	26.86	59.6	25.8	26
2	4.10	99.7	23.7	29	25.20	40.7	31.4	25
3	5.10	75.0	38.3	28	30.90	92.1	43.5	21
Line comparison (¹⁴N LAB/¹⁵N NAB)	¹⁴N LAB				¹⁵N NAB			
1	65.65	0.0	32.7	25	24.36	122.4	34.2	23
2	79.72	1.2	37.2	24	25.24	43.8	46.2	23
3	77.18	0.0	49.0	22	20.56	73.1	42.5	24
¹⁵N isotope effect comparison (¹⁴N HAB/¹⁵N HAB)	¹⁴N HAB				¹⁵N HAB			
1	2.47	52.6	30.9	25	10.13	44.2	24.6	18
2	6.97	83.8	27.7	29	11.34	29.7	27.0	21
3	10.40	113.2	30.6	27	6.99	46.6	27.1	24

^a % of test time spent on the EPM open arms

^b total immobility time in sec during TST



Appendix 3: Phosphorylated peptides and proteins in whole mouse brain synaptosomes

Protein name ^a	Phosphopeptides identified	Phosphosites Identified ^b
Ablim1 RIKEN full-length enriched library, clone: F520009N11 product: Actin-binding LIM protein 1, full insert sequence	TLSPTPSAEGYQDVR	T1 T5
Ablim3 Actin-binding LIM protein 3	TSETSISPPGSSIGSPNR	S7 S11
Acly RIKEN full-length enriched library, clone: 4922505F07 product: ATP citrate lyase, full insert sequence	PAM*PQDSVPSR	S10
Adcy9 Adenylate cyclase type 9	GQGTASPGSVSDLAQTVK	T4 S6 S9 S11
Add1 Isoform 1 of Alpha-adducin	SPPDQSAVPNTPPSTPVK	S14 T15
Add2 Isoform 3 of Beta-adducin	TESVTSGPLSPEGSPSK	T5 S6 S10 S14 S16
Akap12 PKC binding protein SSeCKS	PLESPTSPVSNETTSSFK	T6 S10 T13
Akap5 similar to A-kinase anchor protein 5 isoform 1	SSAIQM*GTPELEK	T8
Als2 Isoform 2 of Alsln	TVVLTPTYSGEADALLPSLR	T1 T7 Y8 S9
Ank2 ankyrin 2, brain isoform 2	GSPIVQEPEEASEPK	S2
Ank2 ankyrin 2, brain isoform 3	ARSYIETETESR	S3 Y4
	SQVETEDLILKPGVVHVIDIR	S1
Aqp4 Isoform 2 of Aquaporin-4	GSYM*EVEDNRSQVETEDLILK	Y3 S11 T15
	SQVETEDLILK	S1
Atcay Caytaxin	LGAVEDSSPPSTLNLGSAHR	S8 S10
Bcas1 Breast carcinoma amplified sequence 1 homolog	TPSPPEPEPAGTAQK	T1
Bin1 Isoform 1 of Myc box-dependent-interacting protein 1	SPSPPPDGSPAATPEIR	S3
BM948371 similar to Brain-enriched guanylate kinase-associated protein isoform 1	RPSVDTPVTDVGFRLR	S3
	SQASEEESPVSPGRPR	S8 S11
Bsn Isoform 1 of Protein bassoon	YLGQGLQYGSFTDLR	Y8 S10 T12
Cadps Isoform 2 of Calcium-dependent secretion activator 1	PSSPSPSVVSEK	S5 S7 S10
Cartpt Isoform Long of Cocaine- and amphetamine-regulated transcript protein precursor	ALDIYSAVDDASHEK	S6 S12
Cend1 Cell cycle exit and neuronal differentiation protein 1	PAPTVAAPSSPDATSEPK	S10 S11 T15 S16
Chgb Secretogranin-1 precursor	SSYEGHPLSEER	S9
Clasp1 CLASP1 isoform 11	SRSDIDVNAAASAK ^c	S1 S3
Clasp2 protein		
	ALQSPEHHIDPIYEDR	S4
Ctnnd2 Isoform 1 of Catenin delta-2	TSTAPSSPGVDSVPLQR	S6
Cttn Src substrate cortactin	KQTPPASPSQPIEDRPPSSPIYEDAAPFK	T3 S7 S19 S20 Y23
D3Bwg0562e Plasticity related gene 1 protein	PGSSQLVHIPEETQENISTSPK	S18 T19
Dlg2 Isoform 1 of Discs large homolog 2	AISLEGEPR	S3
Dmnl2 Dmnl-like 2	NLASPEGLATLGLK	S4 T8
Dnajc5 protein	SLSTSGESLYHVLGLDK	S1 S3 T4 S5 S8
Dst Isoform 1 of Bullous pemphigoid antigen 1, isoforms 1/2/3/4	SVSVDMEKLOPLYETLR	T15
Ebag9 Receptor-binding cancer antigen expressed on SiSo cells (Fragment)	KLSGDQITLPTTVDYSSVPK	S3 T8
EG624619 similar to metaxin 3	FSGAPLKINIIDNTWR	T14
	GISQTNLITVTPEK	S3 T5 T9 T10 T12
Epb4.1l3 Isoform 1 of Band 4.1-like protein 3	VESTSVGSISPGGAK	S8 S10
	AEEATPVTALR	T5 T8
Epb4.9 Dematin	HLSAEDFSR	S3
Epn2 Isoform 1 of Epsin-2	GSSQPNLSTSYSEQEYGK	S3
Fbxo41 F-box only protein 41	RHSTEGEGDVSDVGSR	S3
Fcho2 RIKEN full-length enriched library, clone: C530046K19 product: Hypothetical protein, full insert sequence	PAHPNNLHHTMASLDELKVSIGNITLSPAVSR	S13 S20 T25 S27
Fxyd1 Phospholemman precursor	TGEPDEEEGTFRSSIR	T10 S13



Protein ^a	Phosphopeptides identified	Phosphosites Identified ^b
G3bp2 Isoform A of Ras GTPase-activating protein-binding protein 2	SATPPPAEPASLPQEPK	S1
Gabbr2 Ortholog of human G protein-coupled receptor 51 GPR51	DPIEDINSPEHIQR	S8
Gap43 Neuromodulin	EGDGSATTTDAAPATSPK	T14 S15
Gm996 Novel protein	SPAQAPEPAAEGLGR	S1
Gng3 Guanine nucleotide-binding protein G(I)/G(S)/G(O) gamma-3 subunit precursor	GETPVNSTM*SIGQAR	T3 S7 T8
Gpm6a Neuronal membrane glycoprotein M6-a	EEQELHDIHSTR	S10 T11
Gpr3711 Endothelin B receptor-like protein 2 precursor	PRESPLLPLGTPC	S4
	NSELVSPVKPER	S6
Gprin1 G protein-regulated inducer of neurite outgrowth 1	SPSAEAAAAPPPGPR	S1 S3
Iqsec1 Isoform 2 of IQ motif and Sec7 domain-containing protein 1	M*QFSFEGPEK ^c	S4
Iqsec2 IQ motif and Sec7 domain-containing protein 2		
Kbtbd11 Kbtbd11 protein	ASAAEGSEASPPSLR	S10
Kcnc3 Isoform KV3.3B of Potassium voltage-gated channel subfamily C member 3	SLSSIVGLSGVSLR	S1 S3
Kcnd2 Potassium voltage-gated channel subfamily D member 2	GSVQELSTIQIR	S2
Kcnma1 Isoform 1 of Calcium-activated potassium channel subunit alpha 1	RLEDEQPPTLSPK	S11
Klc1 64 kDa protein	KYDDDISPSEDK	Y2 S7 S9
Madd MAP-kinase activating death domain	SPTENVNTPVGK	T3
Magi2 Isoform 4 of Membrane-associated guanylate kinase, WW and PDZ domain-containing protein 2	IIPQEELNSPTSAPSSEK	S12
Mapt 76 kDa protein	SPVVSGDTSR	T8 S9
Marcks Myristoylated alanine-rich C-kinase substrate	GEATAERPGEA AVASSPSK	S15 S18
Mgea6 Cutaneous T-cell lymphoma-associated antigen 5 homolog	AFLSPPTLLEGPLR	S4
Mlf2 Myeloid leukemia factor 2	LAIQGPEDSPSR	S9
Mlt4 similar to Afadin	LPYLVELSPGR	S8
	SPFEIISPAPPEM*TGQR	S7 S11 T16
Mtap1a Isoform 1 of Microtubule-associated protein 1A	QLSPESLGLTQFGELSLGK	S3 S6 T9
	VPSAPGQESPVPDTK	S3 S9
	VLSPLRSPLLGSESPYEDFLSADSK	S3 S7 S13
	SVSPGVTVQAVVEEHCASPEEK	S17
Mtap1b Microtubule-associated protein 1B	DVSDERLSPAK	S8
	TPEEGGYSYEISEK	T1
	TGVIQTSTEQSFSK	T6 S7
	KETSPETSLIQDEVALK	S4 T7
Mtap2 Microtubule-associated protein 2	VDHGAEIITQSPSR	T9 S11 S13
	GSAQESLDTISPK	S11
Mtap4 Mtap4 protein	AAVGVGTGNDITTPPNK	T11 T12
Mtap6 microtubule-associated protein 6 isoform 1	AQSPLLPEPLK	S3
Nbea Isoform 3 of Protein neurobeachin	TPLENVPGNLSPIK	S11
Ncam1 Isoform N-CAM 180 of Neural cell adhesion molecule 1, 180 kDa isoform precursor	ASPAPTPTPAGAASPLA AVAAPATDAPQAK	S2 T6 T8 S14
Ncam2 Isoform Long of Neural cell adhesion molecule 2 precursor	NPPEAATAPASPK	S11
Ncbp1 Nuclear cap-binding protein subunit 1	ITNHEDGSPVNEPNETTLPTEPEK	S8
Ndr2 Isoform 1 of Protein NDRG2	SKATNDEIFSILK	S10
Nfasc Neurofascin precursor	TASLTSAA SIDGSR	T1 T5 S6 S9
Palm Isoform 1 of Paralemmin	PLQGSQTS LDGTIK	S5
	SETLVNAQQTPLGTPK	T10 T14
Pcsk1n ProSAAS precursor	ILTGSEPEAAPAPR	T3
Pde8b RIKEN full-length enriched library, clone: C630023C23 product: Similar to HIGH-AFFINITY CAMP-SPECIFIC AND IBMX-INSENSITIVE 3',5'-CYCLIC PHOSPHODIESTERASE 8B	ESIDVKSISR	S9



Protein ^a	Phosphopeptides identified	Phosphosites Identified ^b
Pdpk1 3-phosphoinositide-dependent protein kinase 1	ANSFVGTAQYVSPPELLTEK	S3 T7 Y10
Pex2 Isoform 3 of PEX5-related protein	NHSLEEEFER	S3
Pik4ca Phosphatidylinositol 4-kinase, catalytic, alpha polypeptide	TSSVSSISQVSPER	S8 S11
Pkp4 Isoform 1 of Plakophilin-4	VGSPLTLTDAQTR	S3
	SAVSPDLHITPIYEGR	S1
Plekha6 Pleckstrin homology domain-containing family A member 6	AYVPLESPPTVPPLPNESR	T10
Ppfia2 Liprin-alpha-2	VASVSLEGLNLR	S3 S5
Prkaca Isoform 2 of cAMP-dependent protein kinase, alpha-catalytic subunit	TWTLCGTPEYLAPEIILSK	T3 T7 Y10
Prkcb1 Protein kinase C beta type	HPPVLTTPDQEVIR	T6
Prkcc Protein kinase C gamma type	M*GPSSSPIPSPSPPTDSK	S10 S12 T16 S18
Prrt3 Proline-rich transmembrane protein 3 precursor	GSVGPAPSLSELDLRPPSPINLSR	S18
Psmc1 26S proteasome non-ATPase regulatory subunit 1	TVGTPIASVPGSTNTGTVPGSEK	T1 T4 S7
Psmc2 26S proteasome non-ATPase regulatory subunit 2	TPVQSQQPSATTPSGADEK	S9 T11 T12 S14
Ptprn Receptor-type tyrosine-protein phosphatase-like N precursor	AEDSSEGHEEEVLGGR	S5
Ptprn2 Receptor-type tyrosine-protein phosphatase N2 precursor	ADSVAGAIQSDPAEGSQESHGR	S10 S16 S19
Rab11fip5 Rab11 family-interacting protein 5	PLTAAPVEASPDRK	S10
Rgs6 Regulator of G-protein signaling 6	SVYGVTDDETQSQSPVHIPSQPIR	T6 T9 S11
Rtn4 Isoform 1 of Reticulon-4	RGSGSVDETLFALPAASEPVISSAEK	S5 T9
Rtn4 Isoform 2 of Reticulon-4	LPEDDEPPARPPAPAGASPLAEPAAAPPSTPAAPK	S18 S28 T29
Sgip1 Isoform 3 of SH3-containing GRB2-like protein 3-interacting protein 1	NLSSEEVAR	S3
Sgta Isoform 1 of Small glutamine-rich tetratricopeptide repeat-containing protein A	APDRTTPSEEDSAEAER	T5 S8
Shank2 Isoform 1 of SH3 and multiple ankyrin repeat domains protein 2	APSPVVSPTELSK	S7 S12
Slc6a5 Isoform a of Sodium- and chloride-dependent glycine transporter 2	SASTGAQTFQSADAR	T4 T8
Slc7a8 Large neutral amino acids transporter small subunit 2	NHPGSDTSPEAEASSGGGGVALK	S5 T7 S14 S15
Slc8a2 Sodium-calcium exchanger	GISALLNQNGDK	S3
Snap91 Isoform Long of Clathrin coat assembly protein AP180	PGNNEGSGAPSPLSK	S7
Sntb2 Beta-2-syntrophin	GPAGEASASPPVR	S7
Snx27 sorting nexin family member 27 isoform 1	SESGYGFNVR	S3
Sparcl1 SPARC-like protein 1 precursor	PSALNSEEETHEQSTEQDK	S6
Spnb2 Spectrin beta chain, brain 1	TLETAAQM*EGFLNR	T1 T4
Stx1b2 Syntaxin-1B2	SAKDSDDDEEVVHVDNR	S1 S5
Synj1 synaptojanin 1	TPGPPSSQGSFVDTQPAAQK	T1 S6 S7 S10
Tgoln2 Trans-Golgi network integral membrane protein 2 precursor	TESGETLAGDSDFLKPEK	T6 S11
Tjp2 Tight junction protein ZO-2	VQVAPLQGSPPSLSHDDR	S9 S13
Tnik Isoform 1 of Traf2 and NCK-interacting protein kinase (Fragment)	SEGSVPLPHEPSK	S1 S4
Ttc7b tetratricopeptide repeat domain 7B isoform 1	VEQALSEVASSLQSSAPK	S6 S10 S11 S14 S15
Vdac1 Isoform PI-VDAC1 of Voltage-dependent anion-selective channel protein 1	LTFDSSFSPNTGK	S5 S6 T11
Vps35 Vacuolar protein sorting-associated protein 35	RESPESEGIYEGIL	S3
- 16 kDa protein	IPESSELGSPTLTSAQK	S8 T10 T12 S13
- 35 kDa protein	HPSSQLAGPGVEGGEGTQK	S3 S4
- 39 kDa protein	GILAADESTGSIK	S8 T9 S11
1200015F23Rik Protein FAM82C	SHSLPNSLDYAQASER	S1 S3 S7
1700019D03Rik RIKEN full-length enriched library, clone: 2410136C24 product: Hypothetical protein, full insert sequence	TPSPGEQQVQVEVK	S3
6330569M22Rik Isoform 1 of Protein FAM40A	AASPPASASDLIEQQQK	S3 S7
6430548M08Rik Uncharacterized protein KIAA0513	TVTMT*ISPEDEQK	S6



- ^a proteins reported for the first time to be phosphorylated are indicated with a ***bold italic*** font
- ^b unambiguously assigned phosphosites are indicated with a **bold** font
- ^c phosphorylated peptide sequences belonging to two different proteins
- * methionine oxidation



Appendix 4: Differentially expressed proteins (>1.3 fold) in HAB/LAB cingulate cortex synaptosomes

Protein ID	HAB/LAB abundance ratio	HAB/LAB log ₂ ratio	log ₂ CI	Protein Name
IPI00112327	2.83	1.5	[0.7, 2.2]	Mtx1 Metaxin-1
IPI00130322	2.83	1.5	[0.8, 2.2]	Ndufa7 NADH dehydrogenase [ubiquinone] 1 alpha subcomplex subunit 7
IPI00130640	2.83	1.5	[1.1, 1.9]	Hrsp12 Ribonuclease UK114
IPI00113606	2.64	1.4	[0.6, 2.2]	Agk Isoform 1 of Acylglycerol kinase, mitochondrial precursor
IPI00116748	2.64	1.4	[1.1, 1.8]	Ndufa10 NADH dehydrogenase [ubiquinone] 1 alpha subcomplex subunit 10, mitochondrial precursor
IPI00226387	2.64	1.4	[0.5, 2.2]	Pgam5 Isoform 2 of Phosphoglycerate mutase family member 5 precursor
IPI00330754	2.64	1.4	[1.0, 1.8]	Bdh1 D-beta-hydroxybutyrate dehydrogenase, mitochondrial precursor
IPI00113869	2.46	1.3	[0.7, 1.9]	Bsg Isoform 2 of Basigin precursor
IPI00117300	2.46	1.3	[0.8, 1.7]	Ndufs5; BC002163 NADH dehydrogenase [ubiquinone] iron-sulfur protein 5
IPI00121288	2.46	1.3	[0.8, 1.7]	Ndufb10 NADH dehydrogenase [ubiquinone] 1 beta subcomplex subunit 10
IPI00131896	2.46	1.3	[0.9, 1.6]	Brp44 Brain protein 44
IPI00132050	2.46	1.3	[0.6, 2.0]	Ndufc2; LOC675851 NADH dehydrogenase [ubiquinone] 1 subunit C2
IPI00132623	2.46	1.3	[0.8, 1.8]	Ndufb9 NADH dehydrogenase [ubiquinone] 1 beta subcomplex subunit 9
IPI00133215	2.46	1.3	[0.8, 1.8]	Ndufb7 NADH dehydrogenase [ubiquinone] 1 beta subcomplex subunit 7
IPI00313475	2.46	1.3	[1.0, 1.6]	Atp5c1 ATP synthase subunit gamma, mitochondrial precursor
IPI00341322	2.46	1.3	[0.7, 2.0]	Ndufb6 NADH dehydrogenase [ubiquinone] 1 beta subcomplex subunit 6
IPI00453777	2.46	1.3	[0.9, 1.7]	Atp5d ATP synthase subunit delta, mitochondrial precursor
IPI00480233	2.46	1.3	[0.7, 2.0]	mt-Nd5 NADH dehydrogenase subunit 5
IPI00850053	2.46	1.3	[0.3, 2.3]	LOC100045547 similar to Calcium/calmodulin-dependent protein kinase type II gamma chain
IPI00110265	2.30	1.2	[0.8, 1.6]	Sirt2 Isoform 1 of NAD-dependent deacetylase sirtuin-2
IPI00118986	2.30	1.2	[0.9, 1.5]	LOC100047429; Atp5o ATP synthase subunit O, mitochondrial precursor
IPI00120212	2.30	1.2	[0.9, 1.5]	Ndufa9 NADH dehydrogenase [ubiquinone] 1 alpha subcomplex subunit 9, mitochondrial precursor
IPI00123712	2.30	1.2	[0.4, 1.9]	Timm23 Mitochondrial import inner membrane translocase subunit Tim23
IPI00127841	2.30	1.2	[0.8, 1.5]	Slc25a5 ADP/ATP translocase 2
IPI00128023	2.30	1.2	[0.8, 1.6]	Ndufs2 NADH dehydrogenase [ubiquinone] iron-sulfur protein 2, mitochondrial precursor
IPI00130460	2.30	1.2	[0.6, 1.8]	Ndufv1 NADH dehydrogenase [ubiquinone] flavoprotein 1, mitochondrial precursor
IPI00131176	2.30	1.2	[0.9, 1.5]	mt-Co2 Cytochrome c oxidase subunit 2
IPI00132531	2.30	1.2	[0.7, 1.7]	Ndufb5 NADH dehydrogenase [ubiquinone] 1 beta subcomplex subunit 5, mitochondrial precursor
IPI00133167	2.30	1.2	[0.3, 2.1]	ENSMUSG00000045886; LOC100047446; Magmas Mitochondrial import inner membrane translocase subunit Tim16
IPI00228150	2.30	1.2	[0.8, 1.5]	Immt Isoform 1 of Mitochondrial inner membrane protein
IPI00229008	2.30	1.2	[0.7, 1.7]	Ndufs4 NADH dehydrogenase [ubiquinone] iron-sulfur protein 4, mitochondrial precursor
IPI00230715	2.30	1.2	[0.9, 1.5]	Ndufa13 NADH dehydrogenase [ubiquinone] 1 alpha subcomplex subunit 13
IPI00266836	2.30	1.2	[0.4, 2.0]	1810026J23Rik Uncharacterized protein C19orf52 homolog
IPI00308162	2.30	1.2	[1.0, 1.4]	Slc25a12 Calcium-binding mitochondrial carrier protein Aralar1
IPI00308882	2.30	1.2	[1.0, 1.5]	Ndufs1 NADH-ubiquinone oxidoreductase 75 kDa subunit, mitochondrial precursor
IPI00341282	2.30	1.2	[0.8, 1.5]	Atp5f1 ATP synthase subunit b, mitochondrial precursor
IPI00344004	2.30	1.2	[0.9, 1.6]	Ndufa12 NADH dehydrogenase (ubiquinone) 1 alpha subcomplex, 12
IPI00109275	2.14	1.1	[0.8, 1.4]	Slc25a22 Mitochondrial glutamate carrier 1
IPI00110825	2.14	1.1	[0.6, 1.6]	Ndufc2 RIKEN full-length enriched library, clone: 2010300P09 product: 1810004I06RIK PROTEIN (SIMILAR TO NADH DEHYDROGENASE (UBIQUINONE) 1, SUBCOMPLEX UNKNOWN, 2) (14.5KD, B14.5B) homolog
IPI00111885	2.14	1.1	[0.8, 1.4]	Uqcrc1 Cytochrome b-c1 complex subunit 1, mitochondrial precursor
IPI00114246	2.14	1.1	[0.5, 1.7]	Ndufb11 NADH dehydrogenase [ubiquinone] 1 beta subcomplex subunit 11, mitochondrial precursor



Protein ID	HAB/LAB abundance ratio	HAB/LAB log ₂ ratio	log ₂ CI	Protein Name
IPI00115564	2.14	1.1	[0.9, 1.3]	Slc25a4 ADP/ATP translocase 1
IPI00116843	2.14	1.1	[0.7, 1.6]	ENSMUSG00000064363; mt-Nd4 NADH-ubiquinone oxidoreductase chain 4
IPI00119138	2.14	1.1	[0.8, 1.3]	Uqcrc2 Cytochrome b-c1 complex subunit 2, mitochondrial precursor
IPI00120232	2.14	1.1	[0.8, 1.5]	Ndufs7 NADH dehydrogenase [ubiquinone] iron-sulfur protein 7, mitochondrial precursor
IPI00121309	2.14	1.1	[0.8, 1.4]	Ndufs3 NADH dehydrogenase [ubiquinone] iron-sulfur protein 3, mitochondrial precursor
IPI00126917	2.14	1.1	[0.8, 1.4]	1700071K01Rik RIKEN full-length enriched library, clone: 1700071K01 product: Prohibitin (B-cell receptor associated protein 32) homolog
IPI00130280	2.14	1.1	[0.9, 1.3]	Atp5a1 ATP synthase subunit alpha, mitochondrial precursor
IPI00131177	2.14	1.1	[0.5, 1.7]	Letm1 Leucine zipper-EF-hand-containing transmembrane protein 1, mitochondrial precursor
IPI00132390	2.14	1.1	[0.7, 1.5]	Ndufb4; 100041273; 100042503 NADH dehydrogenase [ubiquinone] 1 beta subcomplex subunit 4
IPI00132728	2.14	1.1	[0.8, 1.4]	Cyc1 Isoform 1 of Cytochrome c1, heme protein, mitochondrial precursor
IPI00133240	2.14	1.1	[0.7, 1.5]	Uqcrcs1 Cytochrome b-c1 complex subunit Rieske, mitochondrial precursor
IPI00133403	2.14	1.1	[0.4, 1.8]	Ndufb3 NADH dehydrogenase [ubiquinone] 1 beta subcomplex subunit 3
IPI00133440	2.14	1.1	[0.8, 1.4]	Phb Prohibitin
IPI00136716	2.14	1.1	[0.7, 1.4]	Grm3 Metabotropic glutamate receptor 3 precursor
IPI00170093	2.14	1.1	[0.6, 1.5]	Ndufs8 NADH dehydrogenase [ubiquinone] iron-sulfur protein 8, mitochondrial precursor
IPI00221602	2.14	1.1	[0.7, 1.5]	Sfxn5 Sideroflexin-5
IPI00223092	2.14	1.1	[0.7, 1.5]	Hadha Trifunctional enzyme subunit alpha, mitochondrial precursor
IPI00230507	2.14	1.1	[0.9, 1.4]	Atp5h ATP synthase subunit d, mitochondrial
IPI00331182	2.14	1.1	[0.8, 1.4]	Gpd2 Glycerol phosphate dehydrogenase 2, mitochondrial
IPI00387430	2.14	1.1	[0.6, 1.6]	Ndufb8 NADH dehydrogenase [ubiquinone] 1 beta subcomplex subunit 8, mitochondrial precursor
IPI00468481	2.14	1.1	[1.0, 1.3]	Atp5b ATP synthase subunit beta, mitochondrial precursor
IPI00626928	2.14	1.1	[0.4, 1.9]	Tmem65 Transmembrane protein 65
IPI00109611	2.00	1	[0.4, 1.7]	2310056P07Rik E2-induced gene 5 protein homolog
IPI00111770	2.00	1	[0.6, 1.4]	Atp5k ATP synthase subunit e, mitochondrial
IPI00115089	2.00	1	[0.3, 1.6]	Entpd2 Isoform Long of Ectonucleoside triphosphate diphosphohydrolase 2
IPI00115949	2.00	1	[0.5, 1.4]	Cox7a2l; EG629383 Cox7a2l protein
IPI00116154	2.00	1	[0.4, 1.6]	Cox5b; OTTMUSG00000000426; LOC100045602; LOC100046079 cytochrome c oxidase, subunit Vb
IPI00120984	2.00	1	[0.7, 1.4]	Ndufa8 NADH dehydrogenase [ubiquinone] 1 alpha subcomplex subunit 8
IPI00121576	2.00	1	[0.6, 1.4]	Apoo Apolipoprotein O
IPI00125929	2.00	1	[0.6, 1.3]	Ndufa4 NADH dehydrogenase [ubiquinone] 1 alpha subcomplex subunit 4
IPI00128345	2.00	1	[0.6, 1.4]	Ndufs6 NADH dehydrogenase [ubiquinone] iron-sulfur protein 6, mitochondrial precursor
IPI00132347	2.00	1	[0.6, 1.3]	Uqcrcb RIKEN full-length enriched library, clone: 1500015I13 product: UBIQUINOL-CYTOCHROME C REDUCTASE BINDING PROTEIN homolog
IPI00133399	2.00	1	[0.6, 1.5]	Ndufa6 NADH dehydrogenase [ubiquinone] 1 alpha subcomplex subunit 6
IPI00227302	2.00	1	[0.7, 1.3]	Slc4a10 Solute carrier family 4, sodium bicarbonate co-transporter-like, member 10
IPI00229598	2.00	1	[0.7, 1.2]	Cnp Isoform CNP1 of 2',3'-cyclic-nucleotide 3'-phosphodiesterase
IPI00318645	2.00	1	[0.6, 1.4]	Ndufa11 NADH dehydrogenase (ubiquinone) 1 alpha subcomplex 11 isoform 3
IPI00321718	2.00	1	[0.7, 1.3]	Phb2 Prohibitin-2
IPI00331332	2.00	1	[0.7, 1.4]	Ndufa5 NADH dehydrogenase [ubiquinone] 1 alpha subcomplex subunit 5
IPI00338536	2.00	1	[0.6, 1.5]	Sdhb Succinate dehydrogenase [ubiquinone] iron-sulfur subunit, mitochondrial precursor
IPI00420244	2.00	1	[0.4, 1.5]	Slc1a1 Solute carrier family 1 (Neuronal/epithelial high affinity glutamate transporter, system Xag), member 1
IPI00113244	1.87	0.9	[0.3, 1.5]	Ttyh1 Isoform 1 of Protein tweety homolog 1
IPI00117978	1.87	0.9	[0.7, 1.2]	Cox4i1 Cytochrome c oxidase subunit 4 isoform 1, mitochondrial precursor
IPI00120076	1.87	0.9	[0.2, 1.6]	Ckmt2 Creatine kinase, sarcomeric mitochondrial precursor
IPI00120719	1.87	0.9	[0.6, 1.2]	Cox5a Cytochrome c oxidase subunit 5A, mitochondrial precursor



Protein ID	HAB/LAB abundance ratio	HAB/LAB log ₂ ratio	log ₂ CI	Protein Name
IPI00121419	1.87	0.9	[0.5, 1.4]	LOC631451; EG432822 hypothetical protein
IPI00121443	1.87	0.9	[0.5, 1.3]	Cox6a1 Cytochrome c oxidase polypeptide VIa
IPI00121534	1.87	0.9	[0.6, 1.3]	Car2 Carbonic anhydrase 2
IPI00124771	1.87	0.9	[0.7, 1.1]	Slc25a3 Phosphate carrier protein, mitochondrial precursor
IPI00132039	1.87	0.9	[0.5, 1.3]	Mtch2 Mitochondrial carrier homolog 2
IPI00133608	1.87	0.9	[0.2, 1.7]	Ociad1 Isoform 1 of OCIA domain-containing protein 1
IPI00169925	1.87	0.9	[0.4, 1.4]	Ndufv2 Isoform 1 of NADH dehydrogenase [ubiquinone] flavoprotein 2, mitochondrial precursor
IPI00225254	1.87	0.9	[0.3, 1.6]	Mtx2 Metaxin-2
IPI00225306	1.87	0.9	[0.3, 1.5]	Slc4a7 Isoform 1 of Sodium bicarbonate co-transporter 3
IPI00225390	1.87	0.9	[0.4, 1.3]	Cox6b1 Cytochrome c oxidase subunit VIb isoform 1
IPI00226140	1.87	0.9	[0.4, 1.4]	Maob Amine oxidase [flavin-containing] B
IPI00230289	1.87	0.9	[0.8, 1.0]	Slc1a2 Isoform Glt-1A of Excitatory amino acid transporter 2
IPI00230754	1.87	0.9	[0.7, 1.2]	Slc25a11 Mitochondrial 2-oxoglutarate/malate carrier protein
IPI00312174	1.87	0.9	[0.1, 1.7]	Ptges2 Prostaglandin E synthase 2
IPI00313390	1.87	0.9	[0.3, 1.6]	Chchd6 Coiled-coil-helix-coiled-coil-helix domain-containing protein 6
IPI00315325	1.87	0.9	[0.1, 1.7]	Timm22 Mitochondrial import inner membrane translocase subunit Tim22
IPI00319111	1.87	0.9	[0.3, 1.5]	Sdhc Succinate dehydrogenase cytochrome b560 subunit, mitochondrial precursor
IPI00331318	1.87	0.9	[0.2, 1.5]	Ppt1 Palmitoyl-protein thioesterase
IPI00112139	1.74	0.8	[0.3, 1.2]	Ociad2 OCIA domain-containing protein 2
IPI00114209	1.74	0.8	[0.4, 1.3]	Glud1 Glutamate dehydrogenase 1, mitochondrial precursor
IPI00115454	1.74	0.8	[0.4, 1.2]	Sfxn1 Sideroflexin-1
IPI00116558	1.74	0.8	[0.4, 1.3]	Rhog Rho-related GTP-binding protein RhoG precursor
IPI00123276	1.74	0.8	[0.1, 1.5]	Mosc2 MOSC domain-containing protein 2, mitochondrial precursor
IPI00124221	1.74	0.8	[0.2, 1.3]	Atp1b3 Sodium/potassium-transporting ATPase subunit beta-3
IPI00125460	1.74	0.8	[0.1, 1.5]	Atp5j; LOC674583 ATP synthase-coupling factor 6, mitochondrial precursor
IPI00126115	1.74	0.8	[0.5, 1.1]	Sfxn3 Isoform 1 of Sideroflexin-3
IPI00128296	1.74	0.8	[0.6, 1.1]	Ckmt1 Creatine kinase, ubiquitous mitochondrial precursor
IPI00128346	1.74	0.8	[0.4, 1.1]	Cisd1 CDGSH iron sulfur domain-containing protein 1
IPI00129395	1.74	0.8	[0.1, 1.5]	Slc7a5 Large neutral amino acids transporter small subunit 1
IPI00131771	1.74	0.8	[0.3, 1.3]	Cox6c Cytochrome c oxidase polypeptide VIc
IPI00132002	1.74	0.8	[0.5, 1.1]	Mgst3 Microsomal glutathione S-transferase 3
IPI00133562	1.74	0.8	[0.4, 1.3]	Chchd3 Coiled-coil-helix-coiled-coil-helix domain-containing protein 3, mitochondrial precursor
IPI00134131	1.74	0.8	[0.4, 1.3]	Scp2 Isoform SCPx of Non-specific lipid-transfer protein
IPI00153381	1.74	0.8	[0.1, 1.5]	1110020P15Rik Cytochrome b-c1 complex subunit 9
IPI00222419	1.74	0.8	[0.6, 1.1]	ENSMUSG00000058927; Cycs Cytochrome c, somatic
IPI00224210	1.74	0.8	[0.4, 1.3]	Uqcrcq Cytochrome b-c1 complex subunit 8
IPI00230351	1.74	0.8	[0.5, 1.2]	Sdha Succinate dehydrogenase [ubiquinone] flavoprotein subunit, mitochondrial precursor
IPI00315135	1.74	0.8	[0.3, 1.3]	Tomm22 Mitochondrial import receptor subunit TOM22 homolog
IPI00315302	1.74	0.8	[0.2, 1.4]	Ndufa2 NADH dehydrogenase [ubiquinone] 1 alpha subcomplex subunit 2
IPI00315908	1.74	0.8	[0.3, 1.3]	1700020C11Rik Mitochondrial 18 kDa protein
IPI00323442	1.74	0.8	[0.1, 1.5]	Slc4a8 Isoform 1 of Electroneutral sodium bicarbonate exchanger 1
IPI00344640	1.74	0.8	[0.4, 1.2]	Slc25a18 33 kDa protein
IPI00624653	1.74	0.8	[0.2, 1.4]	Usmg5 Up-regulated during skeletal muscle growth protein 5
IPI00122547	1.62	0.7	[0.4, 1.0]	Vdac2 Voltage-dependent anion-selective channel protein 2
IPI00122548	1.62	0.7	[0.4, 1.0]	Vdac3 Voltage-dependent anion channel 3
IPI00122549	1.62	0.7	[0.6, 0.9]	Vdac1 Isoform PI-VDAC1 of Voltage-dependent anion-selective channel protein 1
IPI00127558	1.62	0.7	[0.1, 1.3]	Acox1 Peroxisomal acyl-coenzyme A oxidase 1
IPI00227928	1.62	0.7	[0.4, 1.0]	Slc6a1 Sodium- and chloride-dependent GABA transporter 1
IPI00283611	1.62	0.7	[0.4, 1.0]	Hk1 Isoform HK1-SA of Hexokinase-1



Protein ID	HAB/LAB abundance ratio	HAB/LAB log ₂ ratio	log ₂ CI	Protein Name
IPI00311682	1.62	0.7	[0.6, 0.9]	Atp1a1 Sodium/potassium-transporting ATPase subunit alpha-1 precursor
IPI00454049	1.62	0.7	[0.2, 1.2]	Echs1 Enoyl-coenzyme A hydratase, mitochondrial precursor
IPI00465999	1.62	0.7	[0.1, 1.3]	Shank1 SH3 and multiple ankyrin repeat domains 1
IPI00117657	1.52	0.6	[0.3, 1.0]	Opa1 Isoform 1 of Dynamin-like 120 kDa protein, mitochondrial precursor
IPI00123540	1.52	0.6	[0.1, 1.0]	Tspan7 Tetraspanin-7
IPI00123744	1.52	0.6	[0.2, 1.0]	Cst3 Cystatin-C precursor
IPI00127713	1.52	0.6	[0.5, 0.8]	Atp2b2 Plasma membrane calcium-transporting ATPase 2
IPI00131472	1.52	0.6	[0.1, 1.2]	Gria3 Glutamate receptor 3 precursor
IPI00223325	1.52	0.6	[0.1, 1.1]	Gabbr1 Isoform 1A of Gamma-aminobutyric acid type B receptor subunit 1 precursor
IPI00322156	1.52	0.6	[0.1, 1.1]	Slc38a3 Sodium-coupled neutral amino acid transporter 3
IPI00380273	1.52	0.6	[0.2, 0.9]	Gja1 Gap junction protein
IPI00459279	1.52	0.6	[0.2, 1.1]	Qdpr Dihydropteridine reductase
IPI00465769	1.52	0.6	[0.4, 0.8]	Slc12a5 Isoform 2 of Solute carrier family 12 member 5
IPI00468685	1.52	0.6	[0.2, 1.0]	Gpr37i1 Endothelin B receptor-like protein 2 precursor
IPI00816921	1.52	0.6	[0.1, 1.1]	Map6d1 MAP6 domain-containing protein 1
IPI00114641	1.41	0.5	[0.2, 0.7]	Slc3a2 CD98 heavy chain
IPI00122094	1.41	0.5	[0.2, 0.8]	Dlg4 Isoform 2 of Disks large homolog 4
IPI00122826	1.41	0.5	[0.1, 0.9]	Cend1 Cell cycle exit and neuronal differentiation protein 1
IPI00124282	1.41	0.5	[0.1, 0.9]	Rala Ras-related protein Ral-A precursor
IPI00125147	1.41	0.5	[0.2, 0.9]	Mpp2 Isoform 1 of MAGUK p55 subfamily member 2
IPI00129268	1.41	0.5	[0.1, 0.9]	Gng3 Guanine nucleotide-binding protein G(l)/G(s)/G(o) subunit gamma-3 precursor
IPI00315794	1.41	0.5	[0.1, 0.9]	Cyb5b Cytochrome b5 type B precursor
IPI00420569	1.41	0.5	[0.3, 0.6]	Atp1a2 Sodium/potassium-transporting ATPase subunit alpha-2 precursor
IPI00420725	1.41	0.5	[0.3, 0.7]	Camk2a MKIAA0968 protein
IPI00114279	1.32	0.4	[0.2, 0.6]	Slc1a3 Excitatory amino acid transporter 1
IPI00119952	1.32	0.4	[0.2, 0.7]	Gpm6b Isoform 1 of Neuronal membrane glycoprotein M6-b
IPI00123390	1.32	0.4	[0.1, 0.8]	Acsl6 acyl-coenzyme A synthetase long-chain family member 6 isoform 1
IPI00123704	1.32	0.4	[0.1, 0.7]	Atp1b2 Sodium/potassium-transporting ATPase subunit beta-2
IPI00134093	1.32	0.4	[0.2, 0.6]	Bsn Isoform 1 of Protein bassoon
IPI00136134	1.32	0.4	[0.1, 0.7]	Ndr2 Isoform 1 of Protein NDRG2
IPI00136967	1.32	0.4	[0.1, 0.8]	Gria2 Isoform 1 of Glutamate receptor 2 precursor
IPI00162781	1.32	0.4	[0.1, 0.7]	Ahcy1 Putative adenosylhomocysteinase 2
IPI00230096	1.32	0.4	[0.2, 0.6]	Camk2a Isoform Alpha KAP of Calcium/calmodulin-dependent protein kinase type II alpha chain
IPI00265299	1.32	0.4	[0.1, 0.6]	Atp2b3 plasma membrane calcium ATPase 3
IPI00314749	1.32	0.4	[0.1, 0.6]	Slc4a4 Isoform 1 of Electrogenic sodium bicarbonate co-transporter 1
IPI00329927	1.32	0.4	[0.2, 0.7]	Nfasc Neurofascin precursor
IPI00338983	1.32	0.4	[0.1, 0.7]	Cntnap1 Contactin-associated protein 1 precursor
IPI00396743	1.32	0.4	[0.1, 0.7]	P140 Isoform 1 of p130Cas-associated protein
IPI00463589	1.32	0.4	[0.1, 0.6]	Atp2b4 Plasma membrane Ca ²⁺ transporting ATPase 4 splice variant a
IPI00113112	0.76	-0.4	[-0.7, -0.2]	Rab3b Ras-related protein Rab-3B
IPI00114375	0.76	-0.4	[-0.5, -0.2]	Dpysl2 Dihydropyrimidinase-related protein 2
IPI00115157	0.76	-0.4	[-0.7, -0.1]	Snca Isoform 1 of Alpha-synuclein
IPI00116498	0.76	-0.4	[-0.5, -0.2]	Ywhaz 14-3-3 protein zeta/delta
IPI00117910	0.76	-0.4	[-0.6, -0.1]	Prdx2 Peroxiredoxin-2
IPI00118384	0.76	-0.4	[-0.6, -0.2]	Ywhae 14-3-3 protein epsilon
IPI00119458	0.76	-0.4	[-0.6, -0.2]	Aldoc Fructose-bisphosphate aldolase C
IPI00120415	0.76	-0.4	[-0.7, -0.1]	Rtn4 Isoform 3 of Reticulon-4
IPI00122565	0.76	-0.4	[-0.7, -0.1]	Gdi2 Isoform 1 of Rab GDP dissociation inhibitor beta
IPI00122684	0.76	-0.4	[-0.7, -0.3]	Eno2 Enolase
IPI00124444	0.76	-0.4	[-0.7, -0.1]	Pfkfb Isoform 1 of 6-phosphofruktokinase type C



Protein ID	HAB/LAB abundance ratio	HAB/LAB log ₂ ratio	log ₂ CI	Protein Name
IPI00130589	0.76	-0.4	[-0.7, -0.1]	Sod1 Superoxide dismutase
IPI00135730	0.76	-0.4	[-0.6, -0.2]	Arf2 ADP-ribosylation factor 2
IPI00221613	0.76	-0.4	[-0.7, -0.1]	Arf1 ADP-ribosylation factor 1
IPI00227235	0.76	-0.4	[-0.8, -0.1]	Ank2 RIKEN full-length enriched library, clone: A930028N13 product: Similar to Ankyrin-2, full insert sequence (Fragment)
IPI00227805	0.76	-0.4	[-0.7, -0.1]	Pfn2 Isoform 2 of Profilin-2
IPI00229080	0.76	-0.4	[-0.6, -0.1]	Hsp90ab1 Heat shock protein 84b
IPI00229510	0.76	-0.4	[-0.6, -0.2]	Ldhb L-lactate dehydrogenase B chain
IPI00312527	0.76	-0.4	[-0.6, -0.1]	Crmp1 Crmp1 protein
IPI00319320	0.76	-0.4	[-0.8, -0.1]	Nckap1 Isoform 1 of Nck-associated protein 1
IPI00330804	0.76	-0.4	[-0.6, -0.1]	Hsp90aa1 Heat shock protein HSP 90-alpha
IPI00338604	0.76	-0.4	[-0.7, -0.1]	Myh10 Myosin, heavy polypeptide 10, non-muscle
IPI00343557	0.76	-0.4	[-0.8, -0.1]	Mapre3 Microtubule-associated protein RP/EB family member 3
IPI00407130	0.76	-0.4	[-0.6, -0.2]	Pkm2 Isoform M2 of Pyruvate kinase isozymes M1/M2
IPI00462072	0.76	-0.4	[-0.7, -0.2]	EG433182; Eno1; LOC100044223 Alpha-enolase
IPI00555069	0.76	-0.4	[-0.6, -0.1]	Pgk1 Phosphoglycerate kinase 1
IPI00605677	0.76	-0.4	[-0.6, -0.1]	Dmxl2 Dmx-like 2
IPI00626790	0.76	-0.4	[-0.6, -0.1]	Glul Glutamine synthetase
IPI00108330	0.71	-0.5	[-0.8, -0.1]	Cnrip1 Uncharacterized protein C2orf32 homolog
IPI00109142	0.71	-0.5	[-0.9, -0.1]	Esd S-formylglutathione hydrolase
IPI00114352	0.71	-0.5	[-0.9, -0.1]	Bin1 Isoform 1 of Myc box-dependent-interacting protein 1
IPI00117264	0.71	-0.5	[-0.9, -0.1]	Park7 Protein DJ-1
IPI00122069	0.71	-0.5	[-0.8, -0.1]	Prkcc Protein kinase C gamma type
IPI00122349	0.71	-0.5	[-0.8, -0.1]	Dpysl3 Dihydropyrimidinase-related protein 3
IPI00123613	0.71	-0.5	[-0.8, -0.2]	Pacsin1 Protein kinase C and casein kinase substrate in neurons protein 1
IPI00132575	0.71	-0.5	[-0.9, -0.1]	Cotl1 Coactosin-like protein
IPI00133224	0.71	-0.5	[-0.9, -0.1]	Fxyd6 Isoform 1 of FXVD domain-containing ion transport regulator 6 precursor
IPI00137331	0.71	-0.5	[-0.9, -0.2]	Cap1 Adenylyl cyclase-associated protein 1
IPI00137730	0.71	-0.5	[-0.9, -0.2]	Pebp1 Phosphatidylethanolamine-binding protein 1
IPI00172221	0.71	-0.5	[-0.7, -0.2]	Dnm1l Isoform 2 of Dynamin-1-like protein
IPI00187407	0.71	-0.5	[-1.0, -0.1]	Cops8 COP9 signalosome complex subunit 8
IPI00224740	0.71	-0.5	[-0.8, -0.2]	Pfn1 Profilin-1
IPI00227898	0.71	-0.5	[-0.9, -0.1]	Prkcb1 Protein kinase C beta type
IPI00228583	0.71	-0.5	[-0.9, -0.1]	Mtpn Myotrophin
IPI00228633	0.71	-0.5	[-0.8, -0.3]	Gpi1 Glucose-6-phosphate isomerase
IPI00229534	0.71	-0.5	[-0.9, -0.1]	Marcks Myristoylated alanine-rich C-kinase substrate
IPI00263822	0.71	-0.5	[-1.0, -0.1]	Prkacb Isoform 1 of cAMP-dependent protein kinase catalytic subunit beta
IPI00310240	0.71	-0.5	[-0.9, -0.1]	Anxa6 annexin A6 isoform b
IPI00313151	0.71	-0.5	[-0.8, -0.1]	Dpysl4 Isoform 1 of Dihydropyrimidinase-related protein 4
IPI00314191	0.71	-0.5	[-0.9, -0.1]	Cbr1 Carbonyl reductase [NADPH] 1
IPI00314748	0.71	-0.5	[-0.9, -0.2]	Wdr1 WD repeat-containing protein 1
IPI00322312	0.71	-0.5	[-0.8, -0.1]	Arhgdia Rho GDP-dissociation inhibitor 1
IPI00323179	0.71	-0.5	[-0.8, -0.2]	Gdi1 Rab GDP dissociation inhibitor alpha
IPI00395193	0.71	-0.5	[-0.8, -0.2]	Rtn1 Reticulon-1
IPI00467833	0.71	-0.5	[-0.7, -0.3]	Tpi1 Triosephosphate isomerase
IPI00471372	0.71	-0.5	[-0.9, -0.1]	Wasf1 Wiskott-Aldrich syndrome protein family member 1
IPI00890117	0.71	-0.5	[-0.9, -0.1]	Cfl1 Cofilin-1
IPI00108189	0.66	-0.6	[-1.0, -0.3]	Hint1 Histidine triad nucleotide-binding protein 1
IPI00112776	0.66	-0.6	[-1.0, -0.1]	Atp8a1 Probable phospholipid-transporting ATPase IA
IPI00113214	0.66	-0.6	[-1.0, -0.1]	Usp5 Ubiquitin carboxyl-terminal hydrolase 5
IPI00130920	0.66	-0.6	[-0.8, -0.3]	Mtap1b Microtubule-associated protein 1B
IPI00133713	0.66	-0.6	[-1.2, -0.1]	Dtd1 Isoform 1 of D-tyrosyl-tRNA (Tyr) deacylase 1



Protein ID	HAB/LAB abundance ratio	HAB/LAB log ₂ ratio	log ₂ CI	Protein Name
IPI00154004	0.66	-0.6	[-0.9, -0.3]	LOC100046081; Otub1 Ubiquitin thioesterase OTUB1
IPI00169448	0.66	-0.6	[-1.2, -0.1]	Ube2m NEDD8-conjugating enzyme Ubc12
IPI00221788	0.66	-0.6	[-0.9, -0.3]	Hpcal4 Hippocalcin-like protein 4
IPI00230034	0.66	-0.6	[-1.1, -0.1]	Ddt D-dopachrome decarboxylase
IPI00266899	0.66	-0.6	[-1.0, -0.1]	Fkbp1a FK506-binding protein 1A
IPI00308885	0.66	-0.6	[-0.9, -0.2]	Hspd1 Isoform 1 of 60 kDa heat shock protein, mitochondrial precursor
IPI00313962	0.66	-0.6	[-0.9, -0.4]	Uchl1 Ubiquitin carboxyl-terminal hydrolase isozyme L1
IPI00319994	0.66	-0.6	[-0.8, -0.4]	Ldha L-lactate dehydrogenase A chain
IPI00331066	0.66	-0.6	[-1.0, -0.1]	Calb1 Calbindin
IPI00331299	0.66	-0.6	[-1.0, -0.3]	Ncdn Isoform 1 of Neurochondrin
IPI00331704	0.66	-0.6	[-0.9, -0.2]	Eno2 Gamma-enolase
IPI00387232	0.66	-0.6	[-1.2, -0.1]	Nsf1c Isoform 3 of NSFL1 cofactor p47
IPI00387312	0.66	-0.6	[-1.1, -0.2]	Pfkl phosphofructokinase, liver, B-type
IPI00469987	0.66	-0.6	[-1.0, -0.2]	Gda Guanine deaminase
IPI00119663	0.62	-0.7	[-1.1, -0.4]	Mapk1 Mitogen-activated protein kinase 1
IPI00121378	0.62	-0.7	[-1.1, -0.3]	Alcam CD166 antigen precursor
IPI00130000	0.62	-0.7	[-1.2, -0.2]	Npepps Puromycin-sensitive aminopeptidase
IPI00133557	0.62	-0.7	[-1.2, -0.2]	Tppp3 Tubulin polymerization-promoting protein family member 3
IPI00120346	0.57	-0.8	[-1.5, -0.2]	Rab27b Ras-related protein Rab-27B
IPI00131548	0.57	-0.8	[-1.5, -0.1]	Prosc Proline synthetase co-transcribed bacterial homolog protein
IPI00222044	0.57	-0.8	[-1.3, -0.2]	D12Erd553e Protein FAM49A
IPI00228828	0.57	-0.8	[-1.5, -0.1]	Guk1 RIKEN full-length enriched library, clone: 1110048P09 product: Guanylate kinase 1, full insert sequence
IPI00118654	0.54	-0.9	[-1.3, -0.4]	Pdpx Pyridoxal phosphate phosphatase
IPI00134373	0.54	-0.9	[-1.5, -0.3]	Ly6h RIKEN full-length enriched library, clone: B230215I21 product: Lymphocyte antigen 6 complex, locus H, full insert sequence
IPI00283511	0.54	-0.9	[-1.2, -0.5]	Pdxx Pyridoxal kinase
IPI00330477	0.54	-0.9	[-1.7, -0.1]	Epn1 Isoform 2 of Epsin-1
IPI00408626	0.54	-0.9	[-1.5, -0.2]	Tpd52 Tumor protein D52
IPI00318522	0.50	-1	[-1.8, -0.2]	Gad2 Glutamate decarboxylase 2
IPI00466610	0.50	-1	[-1.5, -0.4]	Map2k1 Dual specificity mitogen-activated protein kinase kinase 1
IPI00129319	0.47	-1.1	[-1.6, -0.5]	Ppp1r7 Protein phosphatase 1 regulatory subunit 7
IPI00135231	0.47	-1.1	[-1.9, -0.3]	Idh1 RIKEN full-length enriched library, clone: E030024J03 product: Isocitrate dehydrogenase 1 (NADP ⁺), soluble, full insert sequence
IPI00380799	0.47	-1.1	[-1.4, -0.7]	Pde2a RIKEN full-length enriched library, clone: K230012M18 product: Phosphodiesterase 2A, cGMP-stimulated, full insert sequence
IPI00128973	0.44	-1.2	[-1.6, -0.8]	Gap43 Neuromodulin
IPI00624192	0.44	-1.2	[-1.6, -0.8]	Dpysl5 Dihydropyrimidinase-related protein 5
IPI00129451	0.41	-1.3	[-2.1, -0.5]	Cpne6 Copine-6
IPI00120030	0.27	-1.9	[-2.4, -1.4]	Crym Mu-crystallin homolog
IPI00135604	0.27	-1.9	[-2.7, -1.1]	Pcsk1n ProSAAS precursor
IPI00321734	0.16	-2.6	[-3.0, -2.1]	Glo1 Lactoylglutathione lyase

Proteins whose differential expression was validated by Western blot are indicated with a

bold italic font.



Appendix 5: Differentially expressed proteins (>1.3 fold) in ¹⁴N HAB/¹⁵N HAB cingulate cortex synaptosomes

Protein ID	¹⁵ N HAB/ ¹⁴ N HAB abundance ratio	¹⁵ N HAB/ ¹⁴ N HAB log ₂ ratio	log ₂ CI	Protein Name
IPI00122486	1.41	0.5	[0.3, 0.7]	Camkv CaM kinase-like vesicle-associated protein
IPI00408378	1.32	0.4	[0.5, 0.2]	Ywhaq Isoform 1 of 14-3-3 protein theta
IPI00227392	1.32	0.4	[0.2, 0.6]	Ywhah 14-3-3 protein eta
IPI00230418	1.32	0.4	[0.3, 0.5]	Vsnl1 Visinin-like protein 1
IPI00109061	0.76	-0.4	[-0.6, -0.3]	Tubb2b Tubulin beta-2B chain
IPI00131618	0.76	-0.4	[-0.5, -0.2]	Stx1a Syntaxin-1A
IPI00114279	0.76	-0.4	[-0.5, -0.3]	Slc1a3 Excitatory amino acid transporter 1
IPI00130187	0.76	-0.4	[-0.6, -0.3]	Atp6v0a1 Isoform A1-II of Vacuolar proton translocating ATPase 116 kDa subunit a isoform 1
IPI00230289	0.71	-0.5	[-0.6, -0.4]	Slc1a2 Isoform Glt-1A of Excitatory amino acid transporter 2
IPI00312527	0.71	-0.5	[-0.7, -0.3]	Crmp1 Crmp1 protein
IPI00420569	0.71	-0.5	[-0.6, -0.4]	Atp1a2 Sodium/potassium-transporting ATPase subunit alpha-2 precursor
IPI00314749	0.66	-0.6	[-0.7, -0.4]	Slc4a4 Isoform 1 of Electrogenic sodium bicarbonate co-transporter 1
IPI00114641	0.66	-0.6	[-0.7, -0.4]	Slc3a2 CD98 heavy chain
IPI00122094	0.66	-0.6	[-0.8, -0.4]	Dlg4 Isoform 2 of Disks large homolog 4
IPI00136867	0.62	-0.7	[-1.0, -0.5]	Slc6a11 Sodium- and chloride-dependent GABA transporter 4
IPI00222419	0.62	-0.7	[-0.9, -0.6]	ENSMUSG00000058927; Cycs Cytochrome c, somatic
IPI00122549	0.57	-0.8	[-0.9, -0.6]	Vdac1 Isoform PI-VDAC1 of Voltage-dependent anion-selective channel protein 1
IPI00663736	0.57	-0.8	[-1.0, -0.6]	Syngap1 similar to SynGAP-a
IPI00109109	0.57	-0.8	[-1.1, -0.6]	Sod2 Superoxide dismutase [Mn], mitochondrial precursor
IPI00465999	0.57	-0.8	[-1.1, -0.5]	Shank1 SH3 and multiple ankyrin repeat domains 1
IPI00330754	0.57	-0.8	[-1.1, -0.6]	Bdh1 D-beta-hydroxybutyrate dehydrogenase, mitochondrial precursor
IPI00321718	0.54	-0.9	[-1.1, -0.7]	Phb2 Prohibitin-2
IPI00132653	0.54	-0.9	[-1.3, -0.5]	Oxct1 Succinyl-coenzyme A: 3-ketoacid-coenzyme A transferase 1, mitochondrial precursor
IPI00323592	0.54	-0.9	[-1.1, -0.7]	Mdh2 Malate dehydrogenase, mitochondrial precursor
IPI00117312	0.54	-0.9	[-1.1, -0.7]	Got2 Aspartate aminotransferase, mitochondrial precursor
IPI00113141	0.54	-0.9	[-1.1, -0.6]	Cs Citrate synthase, mitochondrial precursor
IPI00137460	0.54	-0.9	[-1.4, -0.4]	Armc10 Isoform 2 of Armadillo repeat-containing protein 10
IPI00116074	0.54	-0.9	[-1.1, -0.7]	Aco2 Aconitate hydratase, mitochondrial precursor
IPI00122548	0.50	-1	[-1.2, -0.7]	Vdac3 Voltage-dependent anion channel 3
IPI00464317	0.50	-1	[-1.3, -0.8]	Gls glutaminase isoform 1
IPI00230241	0.50	-1	[-1.5, -0.5]	Atp5e ATP synthase subunit epsilon, mitochondrial
IPI00154054	0.50	-1	[-1.3, -0.7]	Acat1 Acetyl-coenzyme A acetyltransferase, mitochondrial precursor
IPI00323800	0.47	-1.1	[-1.5, -0.7]	Nefm Neurofilament medium polypeptide
IPI00230394	0.47	-1.1	[-1.5, -0.8]	Lmnb1 Lamin-B1
IPI00126635	0.47	-1.1	[-1.5, -0.8]	Idh3b Tumor-related protein
IPI00133903	0.47	-1.1	[-1.7, -0.6]	Hspa9 Stress-70 protein, mitochondrial precursor
IPI00112126	0.47	-1.1	[-1.6, -0.5]	1810027O10Rik UPF0451 protein C17orf61 homolog precursor
IPI00308885	0.44	-1.2	[-1.5, -0.9]	Hspd1 Isoform 1 of 60 kDa heat shock protein, mitochondrial precursor



Protein ID	¹⁵ N HAB/ ¹⁴ N HAB abundance ratio	¹⁵ N HAB/ ¹⁴ N HAB log ₂ ratio	log ₂ CI	Protein Name
IPI00459725	0.44	-1.2	[-1.5, -0.9]	Idh3a Isoform 1 of Isocitrate dehydrogenase NAD] subunit alpha, mitochondrial precursor
IPI00114342	0.41	-1.3	[-1.9, -0.7]	Hk2 Hexokinase-2
IPI00120045	0.41	-1.3	[-1.5, -1.0]	EG628438; Hspe1-rs1 CPN10-like protein
IPI00624192	0.41	-1.3	[-1.6, -1.0]	Dpysl5 Dihydropyrimidinase-related protein 5
IPI00122349	0.41	-1.3	[-1.6, -1.0]	Dpysl3 Dihydropyrimidinase-related protein 3
IPI00134809	0.41	-1.3	[-1.9, -0.7]	Dlst Isoform 1 of Dihydrolipoyllysine-residue succinyltransferase component of 2- oxoglutarate dehydrogenase complex, mitochondrial precursor
IPI00153660	0.41	-1.3	[-1.9, -0.8]	Dlat Dihydrolipoyllysine-residue acetyltransferase component of pyruvate dehydrogenase complex, mitochondrial precursor
IPI00329998	0.38	-1.4	[-1.6, -1.3]	- 11 kDa protein
IPI00274407	0.35	-1.5	[-2.1, -0.9]	Tufm Isoform 1 of Elongation factor Tu, mitochondrial precursor
IPI00331564	0.33	-1.6	[-2.1, -1.1]	Dld Dihydrolipoyl dehydrogenase
<i>IPI00227126</i>	<i>0.31</i>	<i>-1.7</i>	<i>[-2.0, -1.5]</i>	<i>Tnr Isoform 1 of Tenascin-R precursor</i>

Proteins whose differential expression was validated by Western blot are indicated with a ***bold italic*** font.



12 Acknowledgments

First of all, I would like to express my deep gratitude to Prof. Chris Turck for giving me the opportunity to work in his group in an innovative field that bridges proteomics technologies and behavioral biology. I am really thankful for his helpful guidance and support, for him always having his door open for discussions, advice and problem solving, for entrusting me with a number of exciting projects and showing interest for my work and for giving me the freedom to develop and pursue my own ideas.

I am very grateful to Prof. Rainer Landgraf not only for taking over my supervision at the LMU and being a member of my thesis advisory committee but also for giving me the chance to work with the HAB/NAB/LAB animal model, his constructive feedback, insightful suggestions, support and motivation throughout my PhD studies.

My sincere thanks to Prof. George Boyan for his kind willingness to be the second reviewer of my thesis.

I would like to thank my external thesis committee advisor Prof. Manuel Graeber at the Brain and Mind Research Institute at the University of Sydney for being an inspiring mentor and always being willing to offer advice and help.

I thank the Director of our Institute, Prof. Florian Holsboer for ensuring financial support for our projects. Funding from the Federal Ministry of Education and Research (BMBF) is also gratefully acknowledged.

For her invaluable support with mass spectrometry, her unconfined help concerning all sorts of questions, manuscript preparation and troubleshooting as well as her whole-hearted encouragement throughout my PhD studies, I am indebted to Dr. Giuseppina Maccarrone.

I am thankful to all present and past members of the Proteomics and Biomarkers group for creating an exceptionally pleasant working environment. A big thanks to Larysa Teplytska for being a great help in the lab. Thanks to Yaoyang Zhang for sharing the ups and downs of the $^{14}\text{N}/^{15}\text{N}$ project with me, Stefan Reckow and Philipp Gormanns for help with bioinformatics, Maria Lebar and Christiane Rewerts for the excellent organization of our lab, Christian Webhofer for the nice team work, Dr. Jeeva Varadarajulu for guidance with cell culture, Dr.



Daniel Martins-de-Souza and Dr. Claudia Ditzen for fruitful discussions and Dr. Birgit Bisle for help with mass spectrometry.

Special thanks to all present and past members of the Behavioral Neuroendocrinology group, particularly Dr. Lisa Frank, Dr. Melanie Kessler, Dr. Boris Hambsch, Markus Nussbaumer, Dr. Ludwig Czibere, Dr. Mirjam Bunck and Alana Knapman for a wonderful collaboration all these years and for always being eager to share their knowledge and provide valuable advice.

Thanks to Prof. Andreas Zimmer, Dr. David Otte and Öznur Yilmaz for welcoming me warmly during our collaboration projects in Bonn and providing me with useful insights into the G72/G30 animal model. Thanks to Dr. Vladimir Tolstikov and the Metabolomics Core personnel of UC Davis for metabolomics measurements. I am also grateful to Dr. Alexandros Yassouridis for statistical analysis and for patiently explaining exploratory statistics to me.

For organizing a great International Max Planck Research School, I would especially like to thank Dr. Hans-Joerg Schaeffer and Maxi Reif.

Thanks to Carola Hetzel, Vesna Cerovac, Albin Varga and the Animal Facility team, the Ergotherapy Department and everyone in our Institute that ensures on a daily basis our work-related well-being.

Finally, a warm thanks to all the people that made these years in Munich an exciting experience and so many thanks to my beloved parents, Dimitris and Zoi, for everything!



13 Curriculum Vitae

Personal information

Name Michaela Filiou
Date of birth July 9th, 1982
Nationality Greek

Education

10/2006 - present **PhD, International Max Planck Research School,
Proteomics and Biomarkers, Max Planck Institute of Psychiatry,
Munich, Germany**
PhD Thesis *Biomarker discovery for psychiatric disorders: Insights from quantitative proteomics studies in animal models*

10/2005 - 09/2006 **MSc, Human Molecular Genetics, Imperial College, London, UK**
MSc Thesis *DNAJ/HSP40 chaperone family: Expression in Parkinson's disease* **Grade A**

07/2004 - 08/2004 Internship, Medical Microbiology, Hellenic Pasteur Institute, Athens, Greece

09/2000 - 06/2005 **BSc (Hons), Biological Applications and Technologies,
University of Ioannina, Ioannina, Greece** **Grade 'Excellent' 8.71/10**
BSc Thesis *Duplications of 15q11-q13 in children with developmental delay* **Grade 10/10**

Awards-scholarships

2010 ASBMB Postgraduate travel award (Experimental Biology 2010, USA)
2009 DAAD and ASMS travel scholarships (57th ASMS, USA)
2008, 2009, 2010 DGPF travel scholarships (Proteomics Summer School, Italy; Proteomic Forum, Germany; 4th EUPA Meeting, Portugal)
2005 - 2006 Georgios Stavros Foundation scholarship for MSc studies
2005 Valedictorian of the Faculty of Biological Applications and Technologies
2003, 2004, 2005 Onassis Foundation scholarships (Onassis Foundation Lecture Series)
2000 - 2002 State Scholarships Foundation scholarship
(awarded to the top 1% students of each year, based on academic excellence)



Invited talks

Filiou, M.D., Proteomics and metabolomics analysis for biomarker discovery in a trait anxiety mouse model, 3rd NGFN Meeting, 25-27 November 2010, Berlin, Germany

Filiou, M.D., ¹⁵N isotope effect during metabolic labeling of Escherichia coli proteins, 4th EUPA Meeting, 23-27 October 2010, Estoril, Portugal (Young Investigator Award Session)

Filiou, M.D., Biomarker discovery using ¹⁵N metabolic labeling and an Orbitrap mass spectrometer, 1st Greek Orbitrap Users Workshop, 9 October 2010, Heraklion, Greece

Language skills

English	Fluent (Certificate of Proficiency, University of Cambridge)
German	Fluent (Kleines Deutsches Sprachdiplom, Goethe Institut)
French	Fluent (Diplôme Approfondi de Langue Française, Institut Français)
Spanish	Working knowledge (Certificado Inicial, Instituto Cervantes)
Greek	Mother tongue



14 Publications

1. Durrenberger, P.F., **Filiou, M.D.**, Moran, L.B., Michael, G.J., Novoselov, S., Cheetham, M.E., Clark, P., Pearce, R.K., Graeber, M.B., 2009. DnaJB6 is present in the core of Lewy bodies and is highly up-regulated in parkinsonian astrocytes. *J Neurosci Res* 87, 238-245.
2. Otte, D.M., Bilkei-Gorzó, A., **Filiou, M.D.**, Turck, C.W., Yilmaz, Ö., Holst, M.I., Schilling, K., Abou-Jamra, R., Schumacher, J., Benzel, I., Kunz, W.S., Beck, H., Zimmer, A., 2009. Behavioral changes in G72/G30 transgenic mice. *Eur Neuropsychopharmacol* 19, 339-348. #
3. Frank, E., Kessler, M.S., **Filiou, M.D.**, Zhang, Y., Maccarrone, G., Reckow, S., Bunck, M., Heumann, H., Turck, C.W., Landgraf, R., Hamsch, B., 2009. Stable isotope metabolic labeling with a novel ¹⁵N-enriched bacteria diet for improved proteomic analyses of mouse models for psychopathologies. *PLoS ONE* 4, e7821. #
4. Zhang, Y., Webhofer, C., Reckow, S., **Filiou, M.D.**, Maccarrone, G., Turck, C.W., 2009. A MS data search method for improved ¹⁵N-labeled protein identification. *Proteomics* 9, 4265-4270.
5. Haegler, K., Mueller, N.S., Maccarrone, G., Hunyadi-Gulyas, E., Webhofer, C., **Filiou, M.D.**, Zhang, Y., Turck, C.W., 2009. QuantiSpec – Quantitative mass spectrometry data analysis of ¹⁵N-metabolically labeled proteins. *J Proteomics* 71, 601-608.
6. **Filiou, M.D.**, Bisle, B., Reckow, S., Teplytska, L., Maccarrone, G., Turck, C.W., 2010. Profiling of mouse synaptosome proteome and phosphoproteome by IEF. *Electrophoresis* 31, 1294-1301. #
7. **Filiou, M.D.**, Turck, C.W., Martins-de-Souza, D., 2010. Quantitative proteomics for investigating psychiatric disorders. *Prot Clin Applications. Dec 6 Epub ahead of print.* #
8. **Filiou, M.D.**, Zhang, Y., Teplytska, L., Reckow, S., Gormanns, P., Maccarrone, G., Frank, E., Kessler, M.S., Hamsch, B., Nussbaumer, M., Bunck, M., Lebar, M., Yassouridis, A., Holsboer, F., Landgraf, R., Turck, C.W., (*submitted*). Biomarker and pathway discovery in a trait anxiety mouse model: Evidence for mitochondrial implication. #
9. Zhang, Y., **Filiou, M.D.**, Reckow, S., Webhofer, C., Gormanns, P., Maccarrone, G., Frank, E., Kessler, M.S., Hamsch, B., Landgraf, R., Turck, C.W., (*submitted*). Proteomic and metabolomic analyses of brain and plasma from a trait anxiety mouse model. #



10. Otte, D.M., Albayram, Ö., Guerrero, C., Kudin, A., Sommersberg, B., **Filiou, M.D.**, Turck, C.W., Yilmaz, Ö., Bilkei-Gorzó, A., Kunz, W.S., Beck, H., Zimmer, A., (*submitted*). Mitochondrial dysfunctions and synaptic deficits in G72/G30 transgenic mice. #
11. **Filiou, M.D.**, Varadarajulu, J., Teplytska, L., Reckow, S., Maccarrone, G., Turck, C.W., (*in preparation*). Altered *Escherichia coli* protein expression caused by a ¹⁵N isotope effect during metabolic labeling. #
12. **Filiou, M.D.**, Otte, D.M., Teplytska, L., Yilmaz, Ö., Zimmer, A., Turck, C.W., (*in preparation*). Biomarker discovery in G72/G30 mice by ¹⁵N metabolic labeling and quantitative proteomics.
13. **Filiou, M.D.**, Conti, D., Michael, G.J., Gentleman, S.M., Dawn, D.C., Graeber, M.B., Moran, L.B., (*in preparation*). Cortical involvement in Parkinson's disease: Evidence from expression profiling.
14. **Filiou, M.D.***, Webhofer, C.*, Zhang, Y.*, Bisle, B., Teplytska, L., Frank, E., Kessler, M.S., Hamsch, B., Maccarrone, G., Landgraf, R., Turck, C.W., (*in preparation*). Protein correlates of a ¹⁵N stable isotope behavioral effect in a mouse model of trait anxiety. *equal contribution, alphabetical order #

parts of the thesis are included in these publications

Book chapters

1. **Filiou, M.D.**, Turck, C.W., Psychiatric disorder biomarker discovery using quantitative proteomics (*submitted*). In: Psychiatric Disorders Methods and Protocols, Humana Press, Totowa, NJ, USA.
2. **Filiou, M.D.**, Turck, C.W., General overview: biomarkers in neuroscience research (*in preparation*). In: International Review of Neurobiology, Academic Press, San Diego, CA, USA.



Published Conference Abstracts

(To date, 31 contributions in conference abstracts)

1. **Filiou, M.D.**, Zhang, Y., Teplytska, L., Reckow, S., Frank, E., Kessler, M.S., Maccarrone, G., Hamsch, B., Landgraf, R., Turck, C.W., 2010. Biomarker discovery by stable isotope labeling and quantitative proteomics. *FASEB J* 24, 902.3.
Experimental Biology 2010, 23-28 May 2010, Anaheim, CA, USA
2. **Filiou, M.D.**, Zhang, Y., Teplytska, L., Frank, E., Kessler, M.S., Reckow, S., Maccarrone, G., Hamsch, B., Landgraf, R., Turck, C.W., 2010. Biomarker discovery for psychiatric disorders by stable isotope metabolic labeling and quantitative proteomics. *Eur Psychiatry* 25, S1, 1464.
18th European Congress of Psychiatry, 27 February-2 March 2010, Munich, Germany
3. **Filiou, M.D.**, Zhang, Y., Bisle, B., Frank, E., Kessler, M.S., Teplytska, L., Reckow, S., Haegler, K., Maccarrone, G., Hamsch, B., Landgraf, R., Turck, C.W., 2009. Stable isotope labeling of a mouse model reveals synaptic biomarkers for anxiety disorders. *Pharmacopsychiatry* 42, A37.
26th AGNP Symposium, 7-10 October 2009, Munich, Germany
4. Turck, C.W., Landgraf, R., Ditzen, C., Frank, E., Kessler, M., **Filiou, M.D.**, Zhang, Y., Bisle, B., Haegler, K., Webhofer, C., Hamsch, B., 2008. The quest for affective disorder biomarkers. *Int J Neuropsychopharmacol* 11, 81.
XXVI CINP Congress, 13-17 July 2008, Munich, Germany
5. Kessler, M.S.*, Frank, E.*, **Filiou, M.D.***, Zhang, Y.*, Haegler, K., Maccarrone, G., Hamsch, B., Landgraf, R., Turck, C.W., 2007. ¹⁵N metabolic labeling of high and low anxiety-related behavior HAB/LAB mice. *Pharmacopsychiatry* 40, A126.
*equal contribution
25th AGNP Symposium, 3-6 October 2007, Munich, Germany
6. Durrenberger, P.F., **Filiou, M.D.**, Moran, L.B., Pearce, R.K.B., Graeber, M.B., 2007. The DnaJ/HSP40 chaperone family: Involvement in Parkinson's disease. *Neuropathol Appl Neurobiol* 33, 255-256.
108th Meeting of the British Neuropathological Society, 10-12 January 2007, London, UK

Declaration/Erklärung

Hiermit versichere ich, dass ich die vorliegende Arbeit selbstständig und nur mit den angegebenen Quellen und Hilfsmitteln angefertigt habe. Alle Ausführungen, die wörtlich oder sinngemäß übernommen wurden, sind als solche gekennzeichnet. Auch habe ich nicht anderweitig versucht, eine Dissertation einzureichen oder mich der Doktorprüfung zu unterziehen.

München, 23 Juli 2010

A handwritten signature in black ink, consisting of stylized, cursive letters that appear to be 'MF'.

Michaela Filiou